Integrated CO_2 Capture and Electrochemical Conversion

Burgers, I.A.E.

DOI
10.4233/uuid:be8c345a-ae4d-43c1-9327-53435c594501

Publication date
2025

Document Version
Final published version

Citation (APA)
Burgers, I. A. E. (2025). *Integrated CO_2 Capture and Electrochemical Conversion*. [Dissertation (TU Delft), Delft University of Technology]. https://doi.org/10.4233/uuid:be8c345a-ae4d-43c1-9327-53435c594501

Large concentrations of anthropogenic CO_2 emissions in our atmosphere are causing a severe thread on our planet. This forces us to move away from fossil fuels and find sustainable alternatives. Research has been exploring ways to remove CO_2 from the atmosphere and investigating different pathways to reduce and reuse these carbon emissions. Electrochemical conversion of CO_2 is a promising way forward, where CO_2 can be converted into different chemicals by applying electricity. A circular carbon economy can be established in which CO_2 serves as a resource instead of a waste gas.

This dissertation explores the technical feasibility of integrating CO_2 capture with electrochemical conversion. Through experimental investigation, the performance of the electrochemical conversion of CO_2 is explored. Furthermore, this dissertation provides a perspective on the feasibility of the proposed integrated capture and electrochemical conversion process.

Integrated CO_2 Capture and Electrochemical Conversion

I.A.E. Burgers

Integrated CO_2 Capture and Electrochemical Conversion

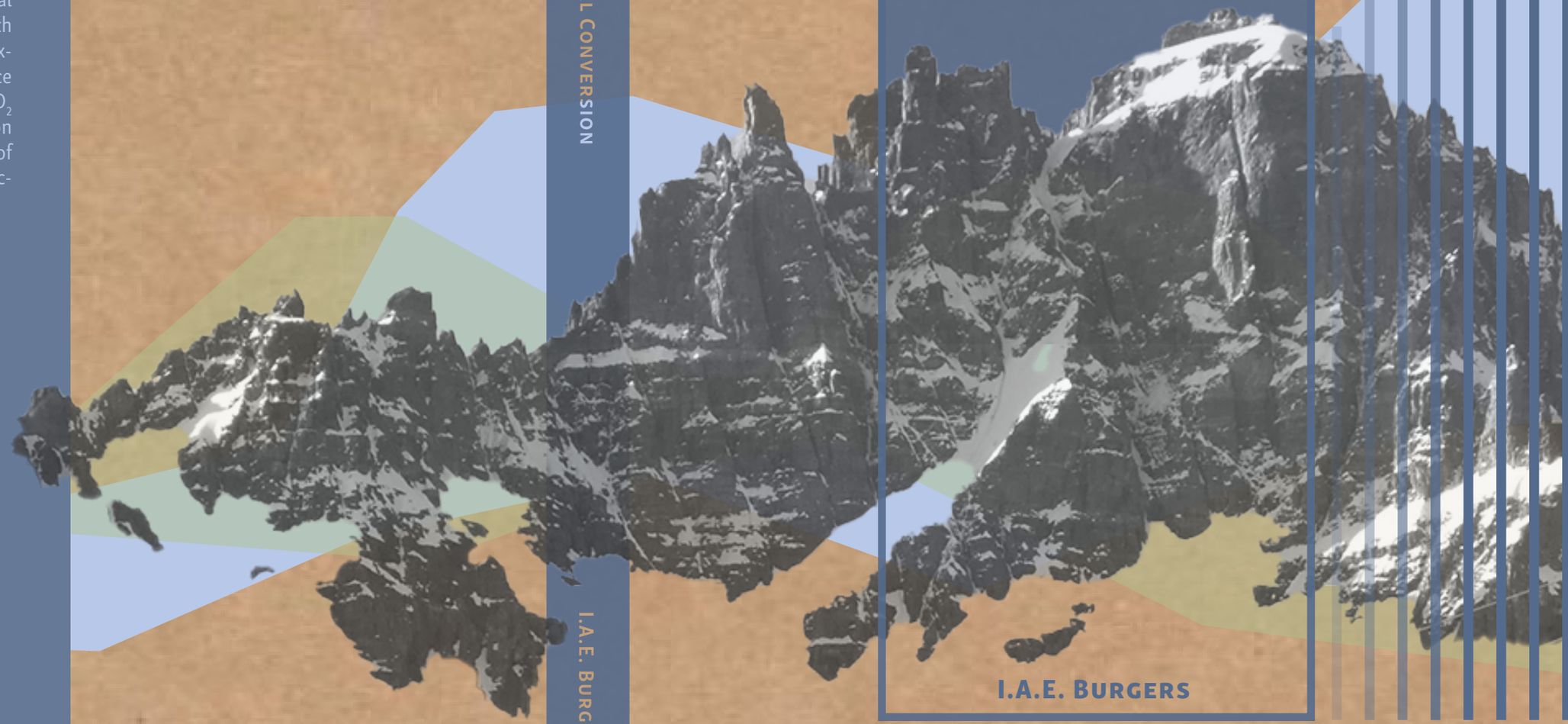

I.A.E. Burgers

Integrated CO_2 Capture and Electrochemical Conversion

Iris Apollonia Elisabeth Burgers

Integrated CO_2 Capture and Electrochemical Conversion

Dissertation

for the purpose of obtaining the degree of doctor
at Delft University of Technology
by the authority of the Rector Magnificus prof. dr. ir. T.H.J.J. van der Hagen,
Chair of the Board for Doctorates
to be defended publicly on
Monday the 26$^{\text{th}}$ of May 2025 at 12:30 o'clock

by

Iris Apollonia Elisabeth BURGERS

Master of Science in Mechnical Engineering,
Delft University of Technology, the Netherlands
born in Eindhoven, the Netherlands.

This dissertation has been approved by the promotors.

Composition of the doctoral committee:

Rector Magnificus	chairperson
Prof. dr. ir. E.L.V. Goetheer	Delft University of Technology, promotor
Dr. R. Kortlever	Delft University of Technology, promotor

Independent members:

Prof. dr. ir. W. de Jong	Delft University of Technology
Prof. dr. ir. D.W.F. Brilman	University of Twente
Dr. ir. D.A. Vermaas	Delft University of Technology
Dr. A.C. Garcia	Universiteit van Amsterdam

Reserve member:

Prof. dr. R. Pecnik	Delft University of Technology

Keywords: Electrochemistry | Bicarbonate Conversion | CO_2 Capture | Integrated System Design | Organic CO_2 Reduction

Printed by: Ridderprint | www.ridderprint.nl

An electronic version of this dissertation is available at

https://repository.tudelft.nl/

The final chapter is ours to write. We know what we need to do.
What happens next is up to us.

— *David Attenborough*

Summary

In a future where society can no longer rely on fossil resources, a transition towards renewable energy and production pathways is required. This involves the development of renewable energy sources, such as solar and wind power, and the production of chemicals that are currently fossil-based through different pathways. CO_2 is a potential carbon source that can be used for the production of valuable chemicals by, for example, electrochemical CO_2 reduction. In this way, a circular carbon economy is created where CO_2 serves as a resource for carbon based products that is captured and reused.

This dissertation explores the integration of CO_2 capture with the electrochemical conversion of CO_2. By integrating the capture and conversion step, solvent regeneration is achieved by the electrochemical conversion, replacing the energy intensive thermal regeneration that is typically used in CO_2 capture systems. Two different CO_2 capture routes are considered using physical or reactive absorption. The first route studies the physical absorption of CO_2 using a non-aqueous capture solvent. The second route investigates the use of reactive absorption using a (bi)carbonate solvent.

This dissertation is divided into three parts. The first two parts focus on electrochemical CO_2 conversion in different CO_2 capture solvents, whereas the last part studies the integrated process design. Part I examines electrochemical CO_2 reduction on a Cu electrode using propylene carbonate as physical absorption solvent. The product selectivity towards C_{2+} products is investigated by varying water concentrations, operating temperature, and salt ions used in the non-aqueous electrolyte. Part II explores bicarbonate electrolysis towards CO, using (bi)carbonate as reactive absorption solvent. The overall system stability and the product selectivity, specifically at a more alkaline electrolyte pH, are studied. Part III delves into the integrated process design and discusses the feasibility and challenges related to the proposed system.

Part I: CO_2 reduction in organic solvent
Chapter 2 investigates the product selectivity of CO_2 reduction on a Cu electrode using a propylene carbonate electrolyte. The major products detected are H_2, CO, and formic acid, with no C_{2+} products detected. Organic solvents are known to suppress the H_2 evolution reaction, because of the lack of water and protons present. However, due to the aqueous anolyte used, water diffuses through the membrane

to the catholyte, increasing its water content. This results in large concentration of H_2 produced. By exchanging the aqueous anolyte with a non-aqueous anolyte, the H_2 production can be partially suppressed, while simultaneously increasing CO formation.

Chapter 3 focuses on the salts used in the propylene carbonate solvent. Several different salt combinations, varying both the cation and the anion, were tested. The salt present in the propylene carbonate electrolyte has a significant influence on the product selectivity of CO_2 reduction on a Cu electrode. The use of a larger cation, with a weaker hydration shell, led to the largest amount of C_2H_4 produced. The highest Faradaic efficiency towards C_2H_4 of 22% was achieved using 0.7 M THACl in propylene carbonate.

Part II: Electrolytic bicarbonate reduction

Chapter 4 studies the overall product stability of a bicarbonate electrolyser. The Faradaic efficiency towards CO (FE_{CO}) decreased by 30% within the first three hours of operation. During the experiment, the electrolyte is recirculated and CO_2 is consumed, increasing the electrolyte pH. An increase in electrolyte pH causes a decrease in the product selectivity towards CO. Furthermore, the metal trace ion impurities present in the (bi)carbonate electrolyte strongly influence the overall stability. This was avoided by complexing trace metal ion impurities using ethylenediaminetetraacetic acid (EDTA).

Chapter 5 investigates the performance of a bicarbonate electrolyser at an increased electrolyte pH. The performance in terms of FE_{CO} and solvent regeneration were investigated. At an increased operating temperature of 60 °C, an improved solvent regeneration could be achieved. However, this leads to a decrease in FE_{CO} and overall product stability. By increasing the catalyst loading and adding EDTA to the electrolyte, both the selectivity towards CO and the overall stability were significantly improved.

Part III: Integrated capture and conversion

Chapter 6 studies at the integration of direct air capture, using a solid adsorption and liquid desorption step, with electrolytic bicarbonate electrolysis. An experimental proof-of-concept is accomplished and provides an initial insight into the feasibility of integrating direct air capture with electrochemical conversion. These results are accompanied by a simplified process model. The regeneration of the capture solvent by electrochemical conversion is limited to a lower pH range. At a more alkaline solvent pH, the electrolyser performance decreases, whereas a highly alkaline capture solvent is preferred for the capture of CO_2 from the air, due to the low partial pressure of CO_2.

Chapter 7 provides a perspective on the feasibility of integrating post-combustion carbonate capture with bicarbonate electrolysis using flue gas with higher partial pressures of CO_2. Increasing the operating temperature and pressure can improve the capture step and the system integration, as flue gas is typically at higher partial pressure and temperature. The performance of the bicarbonate electrolyser at ele-

vated pressure (5 bar) and temperature (60 °C) is shown to improve the overall solvent regeneration. The feasibility of the integration of CO_2 capture and electrochemical conversion is concluded to be highest when using flue gas with high partial pressures of CO_2.

In summary, this dissertation offers a diverse perspective on the feasibility of integrating CO_2 capture and electrochemical conversion. It explores the performance of the electrochemical conversion of CO_2 using two different solvents and it provides a perspective on the feasibility of integrating reactive absorption of CO_2 with bicarbonate reduction.

Samenvatting

In een toekomst waar de samenleving niet langer afhankelijk kan zijn van fossiele grondstoffen is een transitie naar hernieuwbare energiebronnen en productiemethode vereist. Dit omvat de ontwikkeling van hernieuwbare energiebronnen, zoals zonne- en windenergie, en de productie van chemicaliën, die op dit moment van fossiele brandstof gemaakt worden, via andere wegen. CO_2 is een potentiële koolstofbron die kan worden gebruikt voor de productie van waardevolle chemicaliën door bijvoorbeeld elektrochemische CO_2 reductie. Op deze manier kan er een circulaire koolstofeconomie gecreëerd worden waarin CO_2 dient als grondstof en wordt afgevangen en hergebruikt.

Dit proefschrift onderzoekt de integratie van CO_2 afvangen met electrochemische conversie van CO_2. Door het afvangen en omvormen van CO_2 te integreren wordt de regeneratie van de absorptievloeistof bereikt met de elektrochemische conversie en kan de energie-intensieve thermische regeneratie die doorgaans gebruikt wordt in CO_2 afvangsystemen vermeden worden. Twee verschillende routes voor het afvangen van CO_2 worden onderzocht waarin gebruik gemaakt wordt van fysieke of reactieve absorptie. De eerste route bestudeert de fysieke absorptie van CO_2 met behulp van een niet-waterige absorptievloeistof. De tweede route onderzoekt het gebruik van een reactieve absorptie met behulp van een (bi)carbonaatoplossing.

Dit proefschrift is verdeeld in drie delen. De eerste twee delen richten zich op de electrochemische CO_2 conversie met behulp van verschillende CO_2 absorptievloeistoffen. Deel I onderzoekt de electrochemische CO_2 reductie op een Cu elektrode in propyleencarbonaat als fysische absorptievloeistof. De productselectiviteit naar C_{2+} producten wordt onderzocht door te kijken naar de waterconcentratie, temperatuur en de gebruikte zoutionen in de niet-waterige elektrolyt. Deel II onderzoekt de elektrolytische bicarbonaatreductie naar CO, met behulp van (bi)carbonaat als reactieve absorptievloeistof. De algehele systeemstabiliteit en de productselectiviteit, met name bij meer alkalische elektrolyt pH, worden bestudeerd. Deel III duikt in het geïntegreerde procesontwerp en bespreekt de haalbaarheid en de uitdagingen met betrekking tot het voorgestelde systeem.

Deel I: CO_2 reductie in organisch oplosmiddel
Hoofdstuk 2 onderzoekt de productselectiviteit van de CO_2 reductie op een Cu elektrode in propyleencarbonaat elektrolyt. De belangrijkste gedetecteerde producten zijn H_2, CO en mierenzuur, en bijna geen detecteerbare C_{2+} producten. Organische

oplosmiddelen staan erom bekend de H_2 evolutiereactie te onderdrukken, vanwege het gebrek aan aanwezige protonen. Echter, vanwege het gebruik van een waterig anolyte, diffundeert er water door het membraan naar het katholyt, waardoor de waterconcentratie toeneemt. Dit resulteert in een grote concentratie geproduceerde H_2. Door de waterige anolyte te vervangen door een niet-waterige anolyt kan de H_2 productie gedeeltelijk worden onderdrukt, waardoor tegelijkertijd de CO productie toeneemt.

Hoofdstuk 3 richt zich op het ionzout dat wordt gebruikt in combinatie met propyleencarbonaat. Er werden verschillende zoutcombinaties getest, waarbij zowel het kation als het anion gevarieerd werd. Het gebruikte zout in de propyleencarbonaat elektrolyt heeft een belangrijke invloed op de productselectiviteit van de CO_2 reductiereactie op een Cu elektrode. Het gebruik van een groter kation, met een zwakkere hydratatieschil, bleek de grootste hoeveelheid C_2H_4 te produceren. De hoogste Faraday-efficiëntie naar C_2H_4 van 22% werd bereikt gebruik makend van 0.7 M THACl in propyleencarbonaat.

Deel II: Elektrolytische bicarbonaatreductie

Hoofdstuk 4 bestudeert de algehele productstabiliteit van de bicarbonaatelektrolyser. Een daling in de Faraday-efficiëntie naar CO (FE_{CO}) van 30% werd waargenomen binnen de eerste drie uur van operatie. De afname in productselectiviteit is gedeeltelijk gerelateerd aan de verandering in de pH van het elektrolyt vanwege het recirculeren van de vloeistof gedurende het experiment. De toenemende pH van het elektrolyt verlaagt de FE_{CO}. Verder werd geconcludeerd dat de sporen van metaalionenverontreinigingen die aanwezig zijn in het gebruikte (bi)carbonaatzout de algehele stabiliteit sterk beïnvloedden, doordat deze het actieve elektrode oppervlakte voor de CO_2 reductiereactie blokkeren. Dit werd voorkomen door de sporen van metaalionen te complexeren met behulp van ethyleendiaminetetra-azijnzuur (EDTA).

Hoofdstuk 5 onderzoekt de bicarbonaatelektrolyser bij meer alkalische elektrolyt pH. De prestatie in termen van de FE_{CO} en regeneratie van de absorptievloeistof werden onderzocht. Er werd vastgesteld dat bij een verhoogde temperatuur van 60 °C een verbeterde regeneratie kan worden bereikt. Dit leidt echter tot een afname in FE_{CO} en de algehele productstabiliteit. Door de hoeveelheid katalysator te verhogen en EDTA toe te voegen aan het elektrolyt, werden zowel de selectiviteit naar CO als de algehele stabiliteit aanzienlijk verbeterd.

Deel III: Geïntegreerde afvang en conversie

Hoofdstuk 6 bekijkt de integratie van CO_2 afvangen uit de lucht met behulp van een vaste adsorptie- en vloeistofdesorptiestap, met elektrolytische bicarbonaatelektrolyse. Een experimentele proof-of-concept is voltooid en biedt een eerste inzicht in de haalbaarheid van het integreren van CO_2 afvangen uit de lucht met elektrochemische conversie. Deze resultaten worden vergezeld door een vereenvoudigd procesmodel. De regeneratie van de desorptievloeistof door elektrochemische conversie is beperkt tot een lager pH bereik. Bij meer alkalische vloeistoffen neemt de prestatie van de elektrolyser af, terwijl een zeer alkalische oplossing meer CO_2 uit de lucht kan afvangen, vanwege de lage partiele druk van CO_2 in de lucht.

Hoofdstuk 7 biedt een perspectief op de haalbaarheid van het integreren van CO_2 afvangen na verbranding met bicarbonaatelektrolyse gebruikmakend van rookgassen met een hogere partiele druk van CO_2. Het verhogen van de temperatuur en druk kan de CO_2 afvangstap en de systeemintegratie verbeteren, aangezien rookgas doorgaans een hogere partiële druk van CO_2 en temperatuur heeft. De prestaties van de bicarbonaatelektrolyser bij verhoogde drukken (5 bar) en temperatuur (60 °C) blijken de algehele regeneratie van de oplossing te verbeteren. De haalbaarheid van de integratie van CO_2 afvang met elektrochemische conversie is het hoogst bij gebruik van rookgas met hoge partiële drukken van CO_2.

Samenvattend biedt dit proefschrift een divers perspectief op de haalbaarheid van het integreren van CO_2 afvangen met elektrochemische conversie. Het onderzoekt de prestaties van de elektrochemische conversie van CO_2 met behulp van verschillende absorptievloeistoffen en biedt een perspectief op de haalbaarheid van het integreren van reactieve absorptie van CO_2 met elektrolytische bicarbonaatreductie.

Contents

Chapter 1

Introduction

Chapter 1

1.1 Background

Climate change and its effects on global weather patterns and average temperatures poses a severe thread on our planet.[1,2] The main driver of climate change is the increase of anthropogenic green house gas (GHG) concentrations, in particular carbon dioxide (CO_2), in our atmosphere.[3] Since the industrialization in the 1800s, the concentration of atmospheric CO_2 has increased from 280 to 425 parts per million (ppm) as of 2024 (see Figure 1.1).[4] The use of fossil fuels for transportation and the production of energy are the root cause for the increased CO_2 emissions. An increased concentration of CO_2 traps the heat near the Earth's surface, increasing global temperatures which causes climate change.[5]

The impact of climate change is already clearly visible in the change in weather conditions across the globe.[2] Europe is facing warmer summers, combined with heavy rainfall or prolonged droughts. Warmer winters disrupt the total number of snow days and cause the glacier ice to melt at an alarming rate.[7] Likewise, sub-Saharan Africa is facing a rise in average temperatures combined with frequent extreme heat waves. Precipitation patterns are changing, causing a distinct decline in rainfall in southern Africa and an increase in east Africa.[8] This eminently affects rainfed agricultural systems and the livelihoods of many who depend on them, leading to higher risks of in-

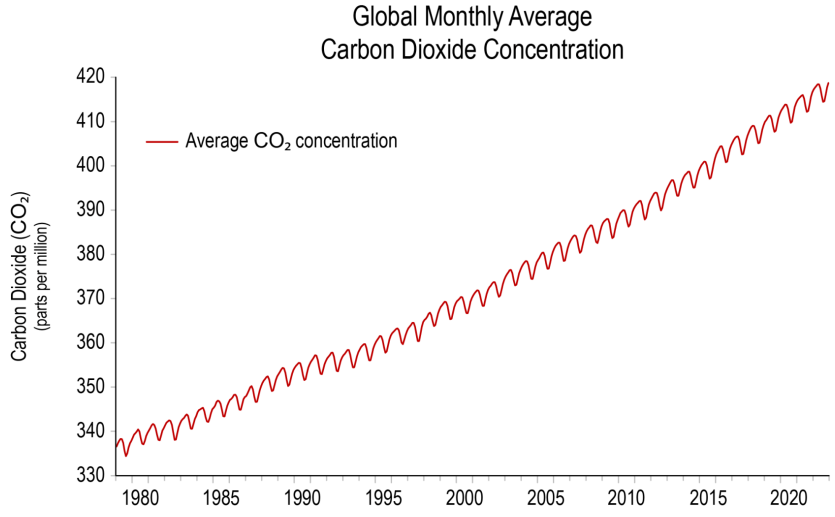

Figure 1.1: Concentrations of CO_2 in the atmosphere measured at Mauna Loa Observatory, Hawaii.[6] Seasonal oscillations of atmospheric CO_2 are measured, however a clear upwards trend is observed over the years.

fectious diseases and famines.[8] As a global effort to combat climate change, the Paris agreement was adopted in 2015. This was the first universal, legally-binding, intergovernmental treaty on climate change. The main goal, as defined by the agreement, is to limit global temperature rise to well below 2 °C above pre-industrial levels.[9] In order to achieve this, the reduction and removal of anthropogenic emissions of CO_2 is crucial.[10] This involves phasing out the use of fossil fuels, adopting renewable energy and feedstock usage, improving energy efficiencies, and reducing energy consumption.[10,11] Furthermore, this requires the removal of the already expelled CO_2 from our atmosphere, known as carbon capture.

1.2 Carbon Capture and Utilization

Alongside the reduction of emissions, the UN Intergovernmental Panel on Climate Change (IPCC) highlights the need for carbon dioxide removal (CDR) technologies, specifically in energy and industry sectors, to achieve net-zero emission goals.[3] CDR technologies include carbon capture either from point sources, such as flue gas stream, or directly from the air. The carbon can subsequently be transported and stored in geological or ocean reservoirs or stored in products e.g. minerals. This is also known as carbon capture and storage (CCS).[12] The main drawback of CCS is that it requires large storage locations, which are not available everywhere. It is, however, a necessary technology, both during the transition of fossil fuels to renewable energy alternatives and thereafter, to reduce the total amounts of CO_2 in our atmosphere and prevent the global temperature to rise above 2 °C.[9,12] The utilization of CO_2 entails producing a carbon product from the captured CO_2. In this way, a circular CO_2 economy can be established, replacing the need for fossil fuels and feedstocks. However, current technologies still require large amounts of energy to convert the captured carbon into products. This section discusses the existing capture and utilization technologies.

1.2.1 Carbon Capture

Capturing CO_2 is a highly necessary method to reduce the excess amount of anthropogenic CO_2 in our atmosphere. The main three approaches to carbon capture from point sources are: post-combustion capture, pre-combustion capture, and oxy-fuel capture.[13] Post-combustion carbon capture is performed after the final combustion step in industrial processes, in which the exhaust gas contains low CO_2 concentrations (4-14 v%). The implementation of post-combustion carbon captures is relatively easy, since no changes to the existing process have to be made. Pre-combustion capture removes the CO_2 from fuels before combustion by oxygen and/or steam reforming, creating a mixture of purely CO_2 and H_2.[13] H_2 is then separated from the CO_2 and combusted with air. Higher CO_2 concentrations are obtained, making the separation process easier. However, large investment costs are associated with pre-combustion CO_2 capture.[14] Lastly, oxy-fuel combustion utilizes oxygen instead of air for the combustion process, resulting in an exhaust gas of CO_2 and water. By condensing the

water, the CO_2 can be separated and removed. Combustion with oxygen requires a large energy consumption and is an expensive process.[13]

Multiple technologies can be used for the separation of CO_2 from the different gas streams. There are three leading technologies which can be classified as adsorption, absorption, and membrane separation.[15] Adsorption uses a solid sorbent to physically adsorb a molecule in either gaseous or liquid phase. Regeneration of the adsorbent is achieved by applying heat (temperature swing adsorption) or reducing the pressure (pressure swing adsorption).[15] The high selectivity of the adsorbents makes adsorption suitable for the separation of CO_2 from gas streams with low partial pressures of CO_2.[16,17] Membrane separation is based on diffusion of gas molecules across the membrane, driven by the differences in partial pressure of the components on either side of the membrane. Therefore, membrane separation is less suitable for gas streams with low CO_2 concentrations, such as in post-combustion gas streams.[16] Furthermore, the durability of the membranes is poor, affecting the performance of the membrane.[18] Absorption uses a liquid solvent to capture gaseous CO_2 and can be divided into physical absorption and reactive absorption. The physical absorption of a gas molecule to an absorbent material is achieved by van der Waals bonding and dissolution of the gas in the liquid, whereas in reactive absorption CO_2 forms a chemical bond with the absorbent material. Reactive absorption is highly selective and is therefore typically employed in capture processes with low partial pressures of CO_2. Furthermore, reactive absorption can easily be scaled and is a relatively easy process to work with. Absorption solvents, can be regenerated by applying heat or elevating the pressure, similar to solid adsorbents. Currently, monoethanolamine (MEA) based solvents are most frequently used for CO_2 capture.[16,19,20] The kinetics of MEA are very rapid, however, a high regeneration energy (around 3.2-4.2 GJ/tonne CO_2) is required and the solution is very corrosive.[20] Reactive absorption is regarded as the most mature capture method for post-combustion CO_2 capture, as it has good long-term stability, low regeneration costs, and is relatively inexpensive.[18] Therefore, CO_2 capture with reactive absorption will be used in this thesis.

Several commercial projects are currently running worldwide. One of the largest operational carbon capture projects in the Netherlands is situated at AVR in Duiven. AVR is a waste processing plant that has installed a CO_2 capture plant with a capture capacity of 100 kt CO_2 /year.[21] Next to already commercially running projects, there is also still a lot of research ongoing to improve CO_2 capture technology both at small lab scale and larger industrial scale. In Norway the Technology Centre Mongstad facilitates as a large testing facility for CO_2 capture technologies and is leading in connecting science and industrial applications.[22]

Next to carbon capture from point sources at industrial plants, the removal of CO_2 directly from the air is inevitable to achieve net zero emissions to be below the 2 °C target.[23,24] DAC is typically achieved by adsorption using a solid sorbent material engineered to selectively bind with CO_2. Due to the relatively low partial pressure of CO_2 in the atmosphere, significant quantities of air need to be processed to saturate the sorbent material. Typically, heat is used to release the capture CO_2 from the sorbent material. The first large-scale DAC plant commissioned by Climeworks

in Iceland in 2021, captures 4 kt CO_2/year.[25] Currently, Climeworks is building a second much larger facility, which aims to capture up to 36 kt CO_2 /year.

1.2.2 Carbon Utilization

The utilization of captured CO_2 has the prospect of creating a circular carbon economy. Currently, the largest consumer of CO_2 is the fertilizer industry, to produce urea from ammonia, followed by oil companies, using the CO_2 for enhanced oil recovery. Furthermore, CO_2 is used in the food and beverage industry and in greenhouses for stimulating plant growth.[26] New emerging technologies look into converting the captured CO_2 into fuels, chemicals, and building materials.[27] Different utilization routes include, amongst others, electrochemical or photocatalytic reduction of CO_2 , and thermochemical conversion of CO_2.[28] Thermochemical conversion processes such as pyrolysis, gasification, and hydrogenation are typically used for the conversion of biomass into different energy carriers.[29] These processes are energy intensive methods as they require high temperatures and pressures. Photocatalytic and electrochemical conversion are both processes that can convert CO_2 into value-added chemicals, such as CO, methane (CH_4), ethylene (C_2H_4) and ethanol (C_2H_5OH).[30–33] Photocatalytic conversion uses sunlight, whereas electrochemical conversion requires an external applied energy source to initiate the reduction of CO_2. Electrochemical CO_2 conversion has shown great potential to produce a wide range of chemicals and is therefore the main focus of this thesis.[27,34] In the next section, the fundamentals of electrochemical CO_2 reduction will be explained in more detail.

Electrochemical CO_2 reduction (CO_2R) is a promising method where captured CO_2 can be used as a building block to create value-added chemicals.[31–33] An external (renewable) energy supply is required to initiate the reaction as it is non-spontaneous. In Figure 1.2, a schematic representation of a typical electrochemical cell is depicted. An electrochemical cell consists of two electrode, a positively charged anode and negatively charged cathode, an anolyte, catholyte, and a membrane to separate the two compartments. The CO_2 reduction reaction (CO_2RR) takes place at the interface between the electrode and the electrolyte, within the electric double layer.[35]

The electrochemical reaction consists of two half reactions, taking place at the anode and cathode simultaneously. At the anode, the oxygen evolution reaction (OER) takes place, whereas at the cathode, the CO_2 reduction reaction (CO_2RR) occurs (see Table 1.1). The anodic reaction supplies the electrons and protons for the cathodic reaction. The electrons are transported by an external electrical circuit and the membrane transports the protons between the two electrolytes. In Table 1.1, several half reactions for the CO_2 reduction are listed as well as the hydrogen evolution reaction (HER).[36] The HER is a competing site reaction taking place at the catalyst surface and is difficult to suppress when doing CO_2R in aqueous electrolytes. Different CO_2 reduction products can be obtained, depending on the catalyst used. For the conversion of CO_2 into higher hydrocarbons, more electrons and intermediate reaction steps are required. The choice of the electrode material has a strong effect on which reaction pathway is used and which products are formed. Silver (Ag) and gold (Au)

electrodes are largely used for the formation of CO, whereas copper (Cu) is the only material that can produce hydrocarbons with decent selectivity. Cu is able to bind CO* to its surface with the right binding energy, allowing it to react further to form hydrocarbons.[37] Many possible reaction pathways have been formulated and extensively discussed in literature.[36,38–40]

To improve the CO_2 reduction reaction, a lot of research is focused on the catalyst design.[41] Changing the electrode morphology, by for example creating nanowires or nano cubes, increases the reactive surface area and enhances the mass transfer ki-

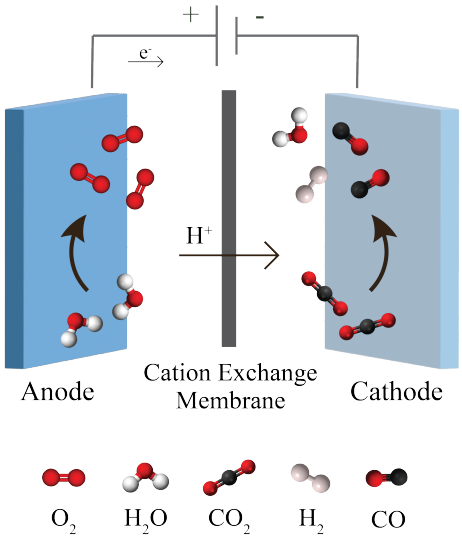

Figure 1.2: Schematic depiction of a typical electrochemical cell for the reduction of CO_2R to CO on a Ag electrode.

Table 1.1: Electrochemical half reactions for the reduction of CO_2R to several hydrocarbon products and their respective standard equilibrium potentials.[36]

Half Cell Reactions	**E_0 [V vs. RHE]**
$2\ H_2O \rightarrow O_2 + 4\ H^+ + 4e^-$ (OER)	1.23
$2\ H^+ + 2e^- \rightarrow H_2$ (HER)	0
$CO_2 + 2\ H_2 + 2e^- \rightarrow CO + H_2O$	-0.10
$CO_2 + 6\ H_2 + 6e^- \rightarrow CH_3OH + H_2O$	0.03
$CO_2 + 8\ H_2 + 8e^- \rightarrow CH_4 + 2\ H_2O$	0.17
$2\ CO_2 + 12\ H_2 + 12e^- \rightarrow C_2H_4 + 4\ H_2O$	0.08
$2\ CO_2 + 12\ H_2 + 12e^- \rightarrow C_2H_5OH + 3\ H_2O$	0.09
$3\ CO_2 + 18\ H_2 + 18e^- \rightarrow C_3H_7OH + 5\ H_2O$	0.10

netics.[42] However, next to the electrode design, the electrolyte also plays a crucial role.[35,43] Commonly, aqueous electrolytes are used in electrochemical CO_2 reduction systems. The main disadvantage of aqueous electrolytes is the low CO_2 solubility, which is only 34 mM at standard temperature and pressure.[44] This limits the total amount of CO_2 that can react at the electrode surface and facilitates the competing HER. The catalytic selectivity can be controlled by the local pH at the electrode surface. Both the CO_2RR and the HER produce OH^-, which significantly increases the pH close to the electrode surface as compared to the bulk electrolyte pH.[43] Since the HER is a pH dependent reaction, this reaction can be suppressed by controlling the local pH at the electrode. Furthermore, the nature of the cations and anions present in the electrolyte have an effect on the reaction kinetics of the CO_2RR. Larger cations, with larger hydration shells, tend to improve the selectivity of the CO_2RR on Cu towards C_{2+} products.[45]

Furthermore, there are different electrochemical cell configurations used for different types of systems. Two frequently used electrochemical cell configurations are the membrane electrode assembly (MEA) cell and the gas diffusion electrode (GDE) flow cell.[32] In a MEA cell, the electrodes are directly deposited on the membrane, limiting the total cell resistance. GDE flow cells operate with a gaseous CO_2 feed, compared to dissolved CO_2 , in a separate compartment. The GDE prevents the liquid from entering the gas compartment, whereas the CO_2 is transported to the catalyst interface. This increases the CO_2 concentration on the catalyst, decreasing the mass transport limitations and improving the current densities.

1.3 Integrated System Design

The capture of post-combustion CO_2 by absorption, as described previously in Section 1.2.1 is a promising method to remove the anthropogenic CO_2 from the atmosphere. In Figure 1.3, a typical absorption process is depicted. First, CO_2 is captured by the absorption solvent in the capture column. Then, the CO_2 rich solvent is collected at the bottom of the absorber column and subsequently sent to the stripper column for the regeneration step. By applying heat, the captured CO_2 is released and leaves the column at the top and the CO_2 lean solvent is recycled back to the absorber column to start a new capture cycle.[20] The main drawback of CO_2 capture by absorption is the energy intensive desorption process, as it requires large amounts of thermal energy to regenerate the capture solvent.[46,47] Furthermore, it produces pure CO_2 as a product which subsequently must be stored or further processed, both of which are expensive processes.

Therefore, this thesis will focus on the integration of post-combustion carbon capture with the electrochemical CO_2 reduction to produce value-added chemicals. This novel integrated system design replaces the stripper column with an electrochemical process, eliminating the energy intensive desorption step and making the process more efficient.[46–50] In Figure 1.4, a schematic diagram of an integrated carbon capture and electrochemical conversion process is shown.

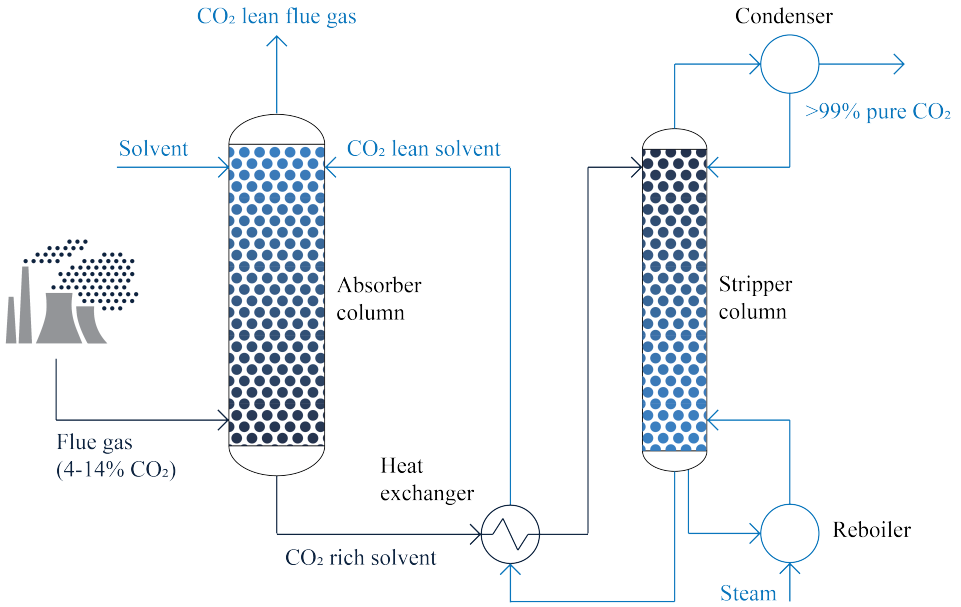

Figure 1.3: Liquid solvent based CO_2 capture system, using an absorber column for the CO_2 capture followed by a stripper column which removes the CO_2 from the solvent due to the increased temperature.

This thesis investigates two different approaches for the integration of carbon capture and electrochemical conversion. The first system is based on the capture of CO_2 by physical absorption using organic solvents. Non-aqueous electrolytes have higher CO_2 solubility (5 to 8-fold compared to aqueous solvents[51]) and can suppress the HER, due to the low amount of protons present.[43,44] The CO_2 rich solvent can therefore directly be used in an electrochemical cell for the CO_2 reduction to value-added chemicals. In Section 1.3.1 the main challenges related to organic CO_2 reduction will be discussed.

Secondly, an integrated system based on reactive absorption is investigated. This process uses a pH swing to capture and release the CO_2 by making use of the acid-base equilibrium reaction between CO_2 and carbonate (see Equation 1.1). An alkaline carbonate solution captures the CO_2 in the form of bicarbonate.[52,53] This process is also known as the Benfield process, which has been widely used for the purification of synthesis gases.[52] The process has the advantage of low solvent costs, low degradation, and low corrosion. The main disadvantage of CO_2 capture using a carbonate solvent is the slow reaction rate.[53] However, this can be overcome by operating at higher pressure and temperature or by the addition of promotors.

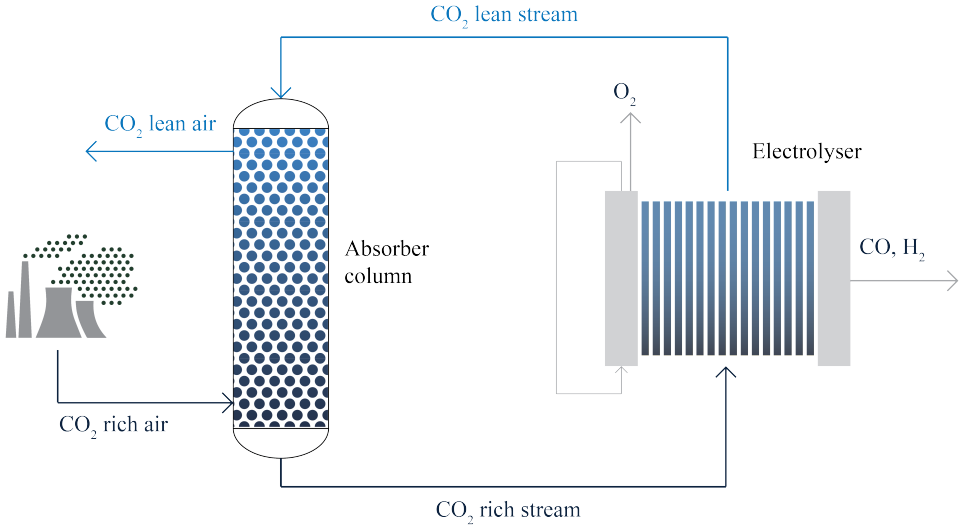

Figure 1.4: Integrated capture and conversion system in which the CO_2 is capture in an absorber column and subsequently removed and converted in an electrolyser stack. The CO_2 lean solvent produced in the electrolyser is recycled back to the absorber column for the next cycle and the CO_2 reduction products are separated.

$$\text{Equilibrium reaction:} \quad CO_2(g) + CO_3^{2-} + H_2O \rightleftharpoons 2HCO_3^- \tag{1.1}$$

The bicarbonate rich capture solution is used in the bicarbonate electrolyser. This method does not use dissolved CO_2 and is therefore not limited by the CO_2 solubility in the solvent. Hori and Suzuki [54] were the first to effectively convert bicarbonate into formate in 1983. In the next subsections, both systems will be elaborated in more detail.

1.3.1 Organic Solvent Based Electrolysis

CO_2 reduction using non-aqueous electrolytes can potentially improve the overall efficiency of the CO_2RR, due to the increased CO_2 solubility and suppression of the HER. [43,44] Frequently used non-aqueous electrolytes are acetonitrile (ACN), methanol, dimethylformamide (DMF), and propylene carbonate (PC). There are several studies that show promising results for the reduction of CO_2 to CO on Au electrodes, using various organic solvents. [55–57] Furthermore, several studies have explored the CO_2 reduction to other 2-electron products such as formate and oxalate, using i.e. Pb, Ag, and Pt electrodes. [58–60] Relatively little research focuses on the CO_2 reduction towards

hydrocarbons in organic solvents.[51,61] Kumar et al.[51] investigated multiple organic solvents (DMF, n-methyl-2-pyrrolidone (NMP), and ACN, using 0.1 M tetrabutylammonium hexafluorophosphate ($TBAPF_6$) and quantified the product distribution of the CO_2 reduction on a Cu electrode. For all three organic solvents, negligible quantities of hydrocarbons were measured. The major product detected for DMF and NMP was oxalate, and hydrogen and formate for AN. Similarly, Deacon-Price et al.[61] concluded for CO_2 reduction on a Cu electrode using a 0.1 M tetraethylammonium chloride (TEACl) in ACN solvent, only small amounts of hydrocarbons were formed and CO served as the major product.

A possible reason for the lack of hydrocarbons being formed in the organic solvent is the limited amount of protons present, which are required for the CO_2RR. Therefore, several studies have suggested the addition of small amounts of water to the non-aqueous electrolyte.[55,56] Furthermore, the effect of the cations and anions of the salt dissolved in the organic solvents is less explored compared to aqueous solvents.[57,62] It is unclear how the salt effects to product distribution of the CO_2 reduction reaction, which is an interesting path for future research.

1.3.2 Bicarbonate Electrolysis

Bicarbonate electrolysis is another promising technique to convert CO_2 into value-added chemicals. In Figure 1.5 a schematic depiction of a bicarbonate electrolyser is shown. In the bicarbonate electrolyser, the carbon dioxide is supplied in the form of bicarbonate (HCO_3^-). CO_2 is liberated from bicarbonate by making use of the acid-base equilibrium reaction between bicarbonate and CO_2 (see Equation 1.1). A bicarbonate electrolyser uses a bipolar membrane (BPM), which splits water into OH^- and H^+. By facing the cathodic side towards the cathode compartment, H^+ ions are provided for the CO_2 liberation (Equation 1.2 and 1.3). Subsequentially, the liberated CO_2 is reduced on the catalyst surface (see Table 1.1).

$$\text{CO}_2 \text{ liberation:} \quad \text{H}^+ + \text{HCO}_3^- \rightleftharpoons \text{CO}_2 + \text{H}_2\text{O} \tag{1.2}$$

$$2\text{H}^+ + \text{CO}_3^{2-} \rightleftharpoons \text{CO}_2 + \text{H}_2\text{O} \tag{1.3}$$

Most of the research on bicarbonate electrolysis has been performed by the Berlinguette group. They have published multiple studies on bicarbonate electrolysis towards CO, using a Ag GDE.[63–65] Initial faradaic efficiencies towards CO (FE_{CO}) achieved were around 40% at 100 mA/cm^2 and standard temperature and pressure.[63] A maximum of 82% FE_{CO} at 100 mA/cm^2 was achieved for an optimally designed electrode, made using both physical vapour deposition (PVD) and spray coating of Ag nanoparticles.[64] The best performance of the bicarbonate electrolyser system thus far was obtained at an elevated pressure of 4 bar. A maximum of 95% FE_{CO} at 100 mA/cm^2 was reached, due to the increase in CO_2 solubility.[65]

To use bicarbonate electrolysis on a larger scale, the product stability is of significant importance. However, in most currently published work, the product stability of

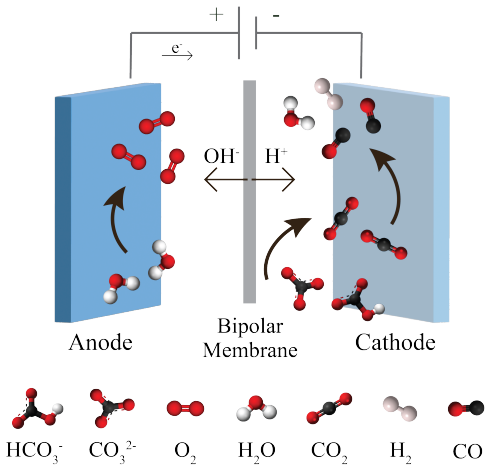

Figure 1.5: Schematic depiction of a bicarbonate electrolyser.

the bicarbonate electrolyser remains unclear. A brief mention on the stability of the bicarbonate system is made in the work by Lees et al.[64] in which the performance over an eight hour window is examined. A clear decline in product selectivity as function of time is observed, which is directly related by the authors to the increase of the pH in the bicarbonate solution as CO_2 is being used for the CO_2 reduction reaction. The stability of the bicarbonate electrolyser for a constant inlet pH remains unclear. Furthermore, the total CO_2 utilization is an important parameter to consider to evaluate the performance of the bicarbonate electrolyser. The CO_2 is supplied in the form of bicarbonate, therefore, the amount of CO_2 that is actually being liberated and converted in the system is crucial and directly related to the outlet pH of the electrolyte. A high CO_2 utilization is crucial for the integration of CO_2 capture with electrochemical conversion.

Several studies have discussed the potential of an integrated capture and conversion system using a (bi)carbonate solvent, however, most research has focused on the bicarbonate electrolyser only. Li et al.[66] demonstrated an integrated capture and conversion system at lab-scale. The CO_2 capture was simply achieved by purging the CO_2 through a KOH solution in a bottle. Subsequently, the (bi)carbonate rich solution was pumped to the electrolyser with a BPM where it was converted into syngas with a ratio of 2:1 (H_2:CO). Later work by Xiao et al.[67] used the same capture setup, and a slightly modified electrolyser using a cation exchange membrane (CEM) and a TiO_2 adlayer on the catalyst to improve the overall carbon efficiency. Furthermore, a recent study by Kim et al.[48] demonstrated a coupled capture and conversion system to convert CO_2 into syngas with a ratio of 1.7:1 (H_2:CO). A packed bed capture column was used for the capture of CO_2. The solvent stream was directly coupled to

the bicarbonate electrolyser to convert the captured CO_2 into syngas. Based on this study, the electrolyte pH was identified as a key parameter for an effective integration of this system.

For the successful integration of a capture and conversion system using a (bi)carbonate solvent, it is crucial to obtain the right operating conditions for both the capture and conversion step.[68] The capture step requires a high inlet pH for efficient CO_2 capture, whereas the bicarbonate electrolyser performs optimally at near-neutral pH conditions. If the electrolyser cannot regenerate the (bi)carbonate solvent to the required alkaline inlet conditions for the capture step, the sizing of the capture column must be increased accordingly to capture an equal amount of CO_2. Therefore, more research into the regeneration of the solvent by the electrolyser is required. Furthermore, a better understanding of how the electrolyser performs at sub-optimal pH inlet conditions and how this can be improved is highly necessary.

Lastly, several studies have investigated the techno-economics of a potential integrated system.[47,69,70] The main benefit of an integrated system approach are the energy saving and reduction in carbon emissions.[47,69] However, currently the high cell potentials and low FEs are limiting the successful integration at an economically relevant scale. Moreover, most research has been conducted at lab-scale electrolysers only, making the uncertainties of the techno-economic assessments high.[71] It is essential to understand how these key parameters can be improved in order to accelerate the technological development of this promising integrated system design and contribute to sustainable development.

1.4 Outline

This dissertation aims at addressing the main challenges and opportunities for an integrated capture and conversion process, of which the scope is depicted in Figure 1.6. The thesis focuses on the electrochemical conversion of CO_2 using two different electrochemical systems. The first system is an electrochemical system using an organic electrolyte (route A). The organic solvent can be used as a physical CO_2 capture solution for higher partial pressure gas streams. It has a high CO_2 solubility and can be used directly in an electrochemical cell. The second electrochemical system is a bicarbonate electrolyser where the captured CO_2 is provided to the electrochemical system in the form of (bi)carbonate (route B).

This thesis is divided into three parts. Part I focuses on the CO_2 reduction in organic electrolyte (route A). Specifically, in this part, the reduction of CO_2 on a copper electrode in a propylene carbonate electrolyte is studied. **Chapter 2** investigates the effect on the product distribution when adding small amounts of water to the non-aqueous electrolyte as well as the effect of temperature. Then, in **Chapter 3**, the salt used in aprotic solvents is systematically evaluated to better understand its effect on the product distribution.

In Part II, the bicarbonate electrolyser is discussed (route B). **Chapter 4** explores the stability of the bicarbonate electrolyser and how this can be improved. Further-

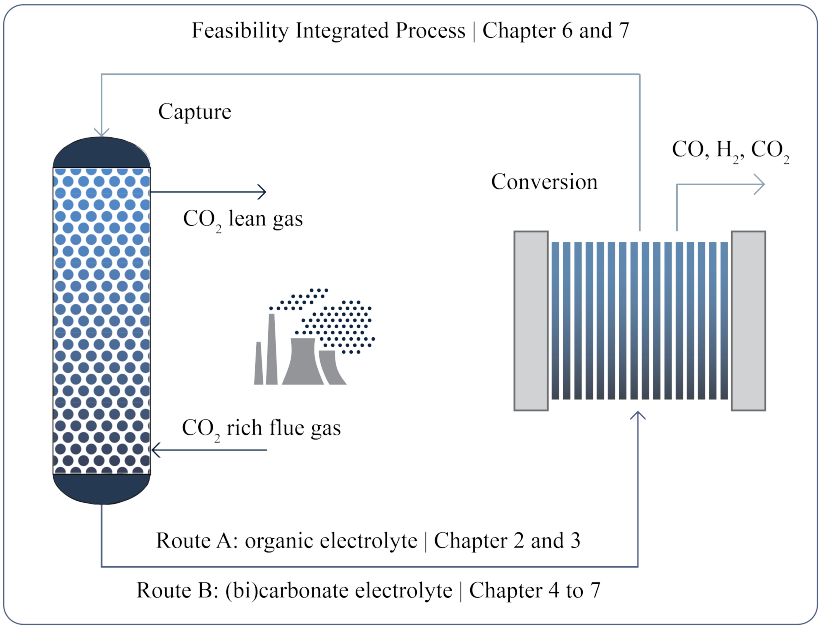

Figure 1.6: Schematic representation of the scope of this dissertation.

more, the effect of the electrolyte pH and the impurities present in the solvent on the stability are investigated. **Chapter 5** further explores the effect of the electrolyte pH, specifically how the performance of the bicarbonate electrolyser can be improved at increased pH inlet conditions. Moreover, the trade-off between efficient capture and efficient electrochemical conversion for an integrated process is discussed.

Lasty, Part III discusses the integrated capture and conversion process. In **Chapter 6** a novel integrated direct air capture and electrochemical conversion process is examined, in which a solid and liquid sorbent are combined. Lastly, in **Chapter 7** the feasibility of integrated flue gas capture using a carbonate capture process combined with a bicarbonate electrolyser is discussed and a comprehensive perspective on the process integration is provided.

Chapter 2

Electrochemical CO_2 Reduction on Copper in Propylene Carbonate Influence of Water Content

This chapter has been published as: Burgers, I., Pérez-Gallent, E., Goetheer, E., & Kortlever, R. (2023). Electrochemical CO_2 Reduction on Copper in Propylene Carbonate: Influence of Water Content and Temperature on the Product Distribution. *Energy Technology, 11(8).*

Abstract

Aqueous electrolytes are most commonly used for the CO_2 reduction reaction (CO_2RR), but suffer from a low CO_2 solubility that limits the reaction. Electrochemical CO_2 reduction in nonaqueous electrolytes can provide a solution, due to the higher CO_2 solubility of organic solvent-based electrolytes. Herein, the product distribution of the electrochemical CO_2 reduction on polycrystalline Cu in 0.7 M tetraethylammonium chloride in propylene carbonate with different water additions (0, 10, and 90 v%), and for different operating conditions (10, 25, 40, and 60 °C), is investigated. It is found that CO_2 reduction on Cu in a propylene carbonate solution results in H_2, CO, and formic acid formation only, even though Cu is known to produce C_{2+} products such as ethylene and ethanol in aqueous electrolytes. Increasing the operating temperature increases the CO_2RR kinetics and shows an improvement in CO formation and decrease in H_2 formation. However, increasing the operating temperature also increases water transport through the membrane, resulting in an increase of H_2 formation over time when operating at 60 °C.

2.1 Introduction

Currently most of our fuels and chemicals are produced from fossil feedstock, resulting in large amounts of CO_2 emissions from these processes which create a great threat on our environment. With decreasing renewable electricity prices and increasing availability of renewable electricity, the production of fuels and chemicals using electrochemistry becomes more interesting.[72] In the electrochemical reduction of CO_2, electricity is used to convert CO_2 into value-added chemicals.[32,33,38] With the intermittent production of renewable electricity, the CO_2 reduction reaction (CO_2RR) can provide a means for long-term and large-scale storage of renewable energy in chemical bonds as well as a way to close the carbon cycle.[73,74]

The choice of electrode material is key in electrochemical CO_2 reduction, as it determines which products are formed in the reduction reaction and the overall selectivity toward these products. Therefore, most studies on CO_2 reduction have focused on the design of selective and efficient catalysts and on obtaining insights in the possible reaction pathways for the different products.[33,39,41,42,44,75] However, there are many more important factors that influence the CO_2RR, such as the electrolyte choice, including, for instance, cation and anion effects and operating conditions such as the local pH, pressure, and temperature.[43,44,76,77] Typically, aqueous electrolytes are used for CO_2RR. Unfortunately, the solubility of CO_2 in water is very low ($\sim$34mM).[36,39,44] This significantly limits the amount of CO_2 present in the electrolyte and thereby limits the CO_2RR due to the limited mass transport of CO_2 to the electrode surface. Furthermore, the large amount of water present facilitates the hydrogen evolution reaction (HER), an undesired side reaction competing with CO_2 reduction in the same potential window.[43]

One possible way to increase the CO_2 solubility and limit the HER is using organic solvents.[43,44,78,79] There are a limited number of studies that investigate the reduction of CO_2 in organic solvents. Most studies have focused on electrolytes based on acetonitrile (ACN), methanol, propylene carbonate (PC), dimethyl sulfoxide (DMSO), and dimethylformamide (DMF).[39,44,76] The main CO_2RR products observed in organic solvents are oxalic acid, CO, and carbonate (CO_3^{2-}).[39,44] Oxalic acid is formed through the dimerization of two free CO_2 radicals in aprotic conditions. In the absence of water, CO and CO_3^{2-} are formed through a disproportionation reaction of a CO_2^- radical and CO_2. The formation of formic acid is only possible in the presence of water, by protonation of a CO_2^- radical and electron transfer.[39,44] Although most organic solvents are capable of suppressing the HER, the current densities for CO_2 reduction are typically low, due to a lack of protons available for the reduction reaction. Therefore, several studies have suggested that CO_2 reduction in organic solvents can be significantly enhanced by adding small amounts of water, acting as a proton donor.[55,56]

Rudnev et al.[55] demonstrated a strong promoting effect of water in ACN for the reduction of CO_2 on gold. Water is thought to serve as a proton donor, reducing the overpotential at which CO_2 reduction is taking place. However, this study only performed cyclic voltammetry (CV) experiments. Therefore, it is still unclear what

effect water additions have on the product distribution of the CO_2RR. A previous study by Shi et al.[56] studied the effect of adding 6.8 wt% water to PC for the reduction of CO_2 to CO on a gold cathode. PC was chosen as the preferred organic electrolyte as it has a large electrochemical operating window, high CO_2 solubility (134mM), and is nontoxic.[44,56] This study observed a decrease in the reduction potential during potentiostatic electrolysis, confirming that water acts as a catalyst for the CO_2RR toward CO. However, the authors did not measure the water concentration after electrolysis, nor did they investigate different water concentrations. Therefore, it is still unclear how and if the water concentration in the catholyte is influencing the product distribution. Furthermore, a recent study by Boor et al.[59] investigated CO_2 reduction to oxalic acid on a lead electrode in a propylene carbonate electrolyte. The influence of the water content was investigated and the authors concluded that an increase in water concentration decreases the oxalic acid formation and increases byproduct formation (e.g., formate, glycolic acid, and glyoxylic acid). Currently, most studies investigating CO_2 reduction in organic solvents with water additions do not quantify the products formed during the reduction reaction. Therefore, there is a need for more studies reporting the product distribution of CO_2RR in organic solvents with the addition of small amounts of water.

Although most experimental studies are performed at ambient temperature and pressure, industrial electrochemical processes typically operate at elevated temperatures up to 80 °C.[80] The main sources of heat generation are the applied overpotential and the resistive losses generated within the electrolyzer stack. Only a few studies have investigated the effect of temperature on the CO_2 reduction performance and product distribution.[65,81–86] In general, increasing the temperature improves the ionic conductivity of the membrane and the electrocatalytic activity, but also enhances the membrane's chemical degradation processes and decreases CO_2 solubility.[86,87] The earliest work on the effect of temperature on the CO_2RR dates back to 1986, by Hori and coworkers,[81] who studied CO_2RR on a Cu electrode in a 0.5 M $KHCO_3$ solution at 5 mA/cm^2 in a temperature range from 0 to 40 °C. The amount of methane (CH_4) was found to decrease by increasing the temperature to 40 °C, whereas hydrogen (H_2), carbonmonoxide (CO), and ethylene (C_2H_4) production increased. A similar trend was observed by Ahn et al.[85], using a polycrystalline copper electrode in a 0.1 M $KHCO_3$ solution at -1.60 V versus Ag/AgCl to study the reduction of CO_2 between 2 and 42 °C. A shift in selectivity from ethylene and formate to methane was observed when decreasing the temperature. The large amount of H_2 formation at higher temperatures is attributed to the decrease in dissolved CO_2. In addition, a recent systematic study performed by Vos et al.[86] concluded that at elevated temperatures the increase in kinetics of CO_2RR is counteracted by the decrease in CO_2 solubility. The effect of temperature on CO_2RR so far has mainly been investigated in aqueous systems, with a limited amount of studies looking at the effect of temperature in nonaqueous electrolytes. Studies using nonaqueous electrolytes focus mainly on methanol or acetonitrile electrolytes at temperatures around 243 K, based on the Rectisol method, to increase the methane formation.[88–93] Additionally, Boor et al.[59] studied CO_2 reduction to oxalic acid on a Pb electrode at 55 and 75 °C, using a PC

electrolyte. They achieved the highest oxalic acid selectivities and current densities at 55 °C, due to the decrease in CO_2 solubility at higher temperatures. To the best of our knowledge, there are no studies that have investigated the effect of temperature on CO_2 reduction on a copper electrode using a nonaqueous electrolyte.

Here, we report on the product distribution of CO_2 reduction on a Cu electrode using 0.7 M TEACl in PC electrolyte. We investigate the effect of adding small amounts of water to the electrolyte and the effect of the operating temperature on the resulting product distribution.

2.2 Results and Discussion

2.2.1 Cyclic Voltammetry

To determine the potential window for CO_2 reduction on a Cu electrode in a 0.7 M TEACl in PC solution with varying concentrations of water (0, 10, and 90 v% water), CV experiments were performed in the presence and absence of CO_2. Figure 2.1 shows the voltammograms with solid lines representing the argon (Ar)-saturated solutions,

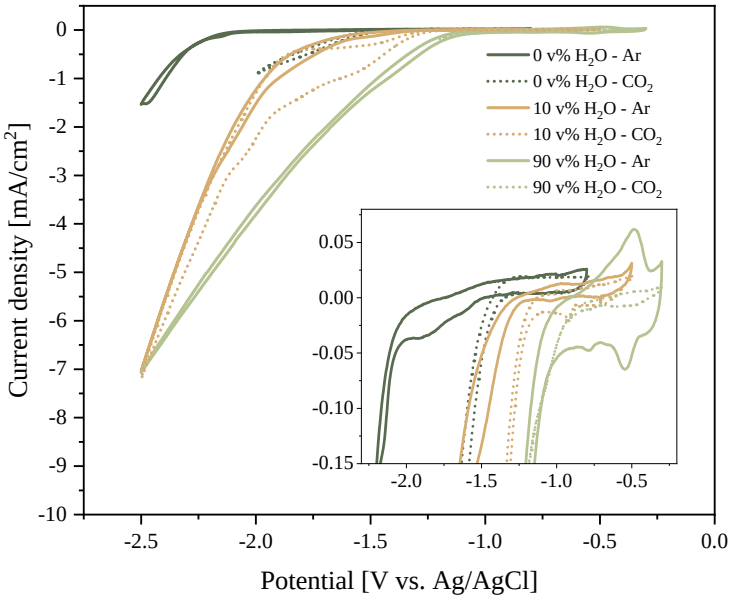

Figure 2.1: Cyclic voltammograms of a polycrystalline Cu electrode in a argon saturated (-) and CO_2 saturated (···) propylene carbonate with 0.7 M TEACl solution, with 0, 10, and 90 v% water addition, recorded at a scan rate of 20 mVs^{-1}. The insert displays a zoom-in between -0.25 V until -2.25 V vs. Ag/AgCl.

whereas the dotted lines represent the CO_2-saturated solutions. It is of importance to note that upon addition of water to the PC solvent, the CO_2 solubility will decrease. However, upon an addition of 10 v% of water, the CO_2 solubility is expected to only be slightly lower than for a pure PC electrolyte. Therefore, the decrease in dissolved CO_2 is expected to have a rather limited effect on the CO_2RR.

Figure 2.1 shows that in an Ar atmosphere a reductive current is observed with an onset potential of -2.1 V versus Ag/AgCl (solid green line) when there is no water added to the electrolyte. This suggests that at potentials of -2.1 V versus Ag/AgCl and lower, either PC or the supporting electrolyte salts (TEACl) decomposes. Upon adding 10 v% water to the electrolyte (solid orange line), the onset potential of the reductive current shifted to less negative potentials (-1.4 V vs. Ag/AgCl). Moreover, the slope of the reduction current increases at -2.0 V versus Ag/AgCl. We hypothesize that the first reductive current is related to H_2 formation, while the second reductive current is related to the reduction of the organic solvent. Increasing the water concentration shift of the onset potential of the reductive current to -1.1 V versus Ag/AgCl. This current is assumed to be associated with H_2O reduction.

When the electrolyte with 0 v% water is saturated with CO_2 (dotted green line), there is a reductive current observed with an onset potential of -1.4 V versus Ag/AgCl that is associated with CO_2RR. When 10 v% water is added to the electrolyte (dotted orange line), a current associated with CO_2 reduction was observed with an onset potential of -1.2 V versus Ag/AgCl. The onset potential for the CO_2-saturated electrolyte with 90 v% water (dotted blue line) is equal to the onset potential of the Ar-saturated solution (-1.1 V vs. Ag/AgCl) and no clear reduction current related to CO_2 reduction is observed.

From the voltammograms, a minimum and maximum cathode potential was selected to be applied in the chronoamperometry studies. A minimum potential of -1.6 V versus Ag/AgCl is chosen and the maximum applied potential is limited to -2.0 V versus Ag/AgCl to prevent decomposition of the electrolyte.

2.2.2 Chronoamperometry: The Effect of Water

Chronoamperometry (CA) studies for CO_2 reduction on Cu in a 0.7 M TEACl in PC electrolyte with 0, 10 and 90 v% water were performed for 1 hour, with the aim of determining the product distribution of CO_2RR. The water concentration was limited to 10 v% due to solubility limit of water in PC, as with higher water concentrations the electrolyte behaves as a two-phase system. During these measurements, gaseous products were analyzed with an inline gas chromatograph, while liquid samples were taken from the electrolyte after the measurements to measure the liquid products formed.

Figure 2.2 shows the faradaic efficiencies of all the products detected during CO_2RR on Cu with different concentrations of water added to the 0.7 M TEACl in PC solution at three different potentials: -1.6 V versus Ag/AgCl, -1.8 V versus Ag/AgCl, and -2.0 V versus Ag/AgCl. All faradaic efficiencies are averaged over the last 20 min of the experiment when the measured current was stable. For all three water concentrations,

three main products were detected: hydrogen (H_2), carbon monoxide (CO), and formic acid (HCOOH). Besides these products, trace amounts of methane (CH_4) and ethylene (C_2H_4) were detected. The CO_2RR on Cu in a 0.7 M TEACl in PC electrolyte without added water does not form any methane or ethylene. Instead, formic acid is formed as major product next to H_2. The formic acid concentration decreased with increasing the water concentration from 0 to 10 v%. When the water content in the catholyte increases from 10 to 90 v%, the system starts behaving more as an aqueous system and therefore the product selectivity is shifted toward H_2 and CO formation at all three applied potentials. However, ethylene is not detected and only small amounts of CH_4 are observed with an applied potential of -2.0 V versus Ag/AgCl (see Figure 2.2(c)). The catholyte with 90 v% water in PC was expected to perform similarly as an aqueous system. Even with 90 v% water present, no ethylene or other hydrocarbons are formed, which suggests that the presence of PC is somehow limiting the CO_2RR to hydrocarbons.

As expected, H_2 formation increases when increasing the water concentration for all three potentials. Even in the electrolyte with 0 v% water addition, a large amount of H_2 is formed. It is important to note that 0 v% water content refers to the freshly prepared electrolyte, where no water was added to it. However, during electrolysis, water from the aqueous anolyte diffuses through the membrane to the catholyte, due to the water concentration gradient and due to electro-osmotic drag.[94] The effect of the electro-osmotic drag is increased as the applied potential increases. Moreover, the Nafion membrane is stored in water for activation and therefore can also slightly contribute to an increase in water concentration after electrolysis. The water content after electrolysis was measured with coulometric Karl–Fisher (KF) titration (see Figure A.3). After electrolysis, the water content of the electrolyte with 0 v% water addition increased from 0.2 v% to around 4 v%, whereas the water content of

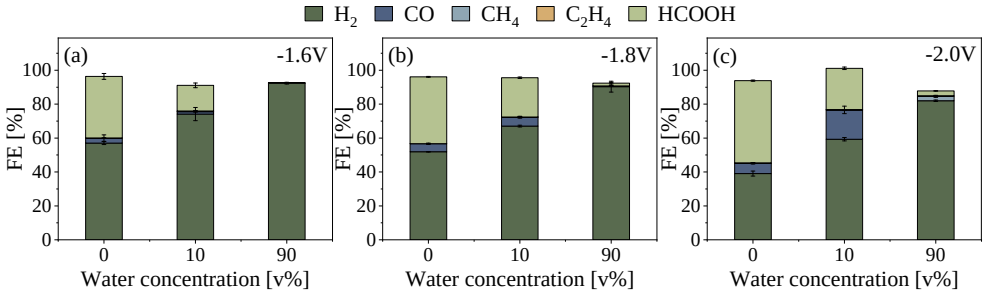

Figure 2.2: Chronoamperometry (CA) on a Cu electrode in 0.7 M TEACl in PC electrolyte at different potentials as a function of electrolyte water additions (0, 10, and 90 v% water). Faradaic efficiencies for (a) CA at -1.6 V vs. Ag/AgCl, (b) CA at -1.8 V vs. Ag/AgCl, and (c) CA at -2.0 V vs. Ag/AgCl. Error bars indicate differences between duplicate easurements.

the electrolytes with 10 and 90 v% water added remain the same. Nonetheless, for both electrolytes with 0 and 10 v% water addition, there is a decreasing trend in H_2 production when the applied potential is increased, whereas an increase in CO production is observed.

To eliminate the water present in the entire system, the anolyte was replaced with a nonaqueous solution, equal to the composition of the catholyte, and a chronoamperometry experiment was performed. In Figure 2.3, the CA results at -2.0 V versus Ag/AgCl are presented for a system with: (a) 0.7 M TEACl in PC with 0 v% water added as catholyte and anolyte (C:0|A:0), (b) 0.7 M TEACl in PC with 0 v% water added as catholyte and an aqueous anolyte (C:0|A:100), and (c) 0.7 M TEACl in PC with 10 v% water added and aqueous anolyte (C:10|A:100). The current obtained when using 0.7 M TEACl in PC as anolyte and catholyte (light green line in Figure 2.3(a)) is lower in comparison to using an aqueous anolyte (dark green and blue line). The products detected for chronoamperometry measurements with a PC-based catholyte and anolyte are mainly formic acid, H_2, and CO, and small amounts of ethylene (Figure 2.3(b)) with formic acid as the main product formed. Furthermore, the amount of CO formed without water present in the catholyte and anolyte is similar to the amount of CO formed when using 10 v% water in a PC catholyte and an aqueous anolyte.

The total amount of water measured after 1 hour of electrolysis is represented in Figure 2.3(c). Without water additions to the anolyte or catholyte, the total amount of water measured in the catholyte is around 1.3 v% (Figure 2.3(c) C:0|A:0). The blank catholyte contains around 0.2 v% water, which means that there is still water

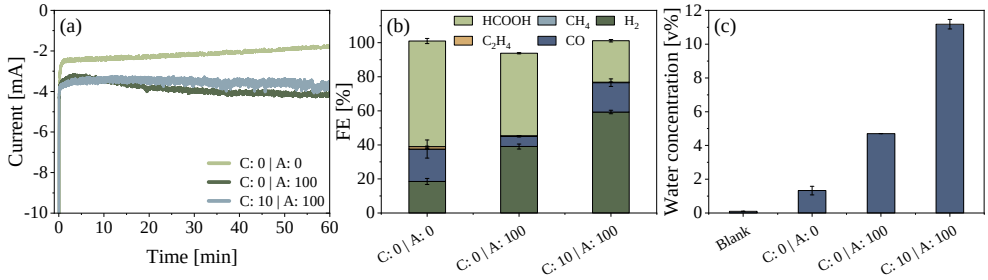

Figure 2.3: Chronoamperometry at -2.0 V vs. Ag/AgCl on a Cu electrode comparing (i) 0.7 M TEACl in PC with 0% water added as catholyte and anolyte (C:0|A:0), (ii) 0.7 M TEACl in PC with 0% water added as catholyte and an aqueous anolyte (0.5M H_2SO_4) (C:0| A:100), and (iii) 0.7 M TEACl in PC with 10 v% water added and aqueous anolyte (C:10|A:100). (a) Current density, (b) faradaic efficiencies , and (c) water concentrations before (blank) and after 1 hour of CA for the three different electrolyte combinations. Error bars indicate differences between duplicate measurements.

entering the catholyte. The source of the water must be due to the use of a wet Nafion membrane, which needs to be activated in water. There is a direct relation between the amount of H_2 produced and the water concentration at the end of electrolysis: reducing the water concentration results in a reduced amount of H_2 produced. The suppression of the HER under the studied conditions did however not improve the CO_2RR selectivity toward hydrocarbon products, but only toward the CO and formic acid.

There are a limited amount of studies of CO_2 reduction in nonaqueous systems that use a Cu electrode.[89,90,93] These studies used methanol as electrolyte and operated at temperatures below 273 K. Murugananthan et al.[93] showed the best faradaic efficiency toward CH_4 of 37.5% at -4 V versus Ag quasi reference electrode at 243 K by increasing the pressure to 4 bar. In this work, the electrolysis is performed at different operating conditions and with PC instead of methanol, making it difficult to compare results and understand why in this study hydrocarbons where detectedwhile here this is not the case. For Cu electrodes in aqueous systems, it is known that faradaic efficiencies toward ethylene and ethanol in a 0.1 M $KHCO_3$ electrolyte range up to 30% and 10%, respectively, depending on the applied potential.[40,95,96] We expect that the interaction of the solvent and the electrode in the double layer influences the binding strength of the different intermediates.

Figure 2.4 illustrates the different pathways in CO_2RR. The yellow path represents the formation of formate. In blue, the reaction pathway toward CO is presented. Due to the higher CO solubility in PC compared to water, it is expected that in PC electrolytes CO will desorb more readily from the surface.[97,98] This results in a lower

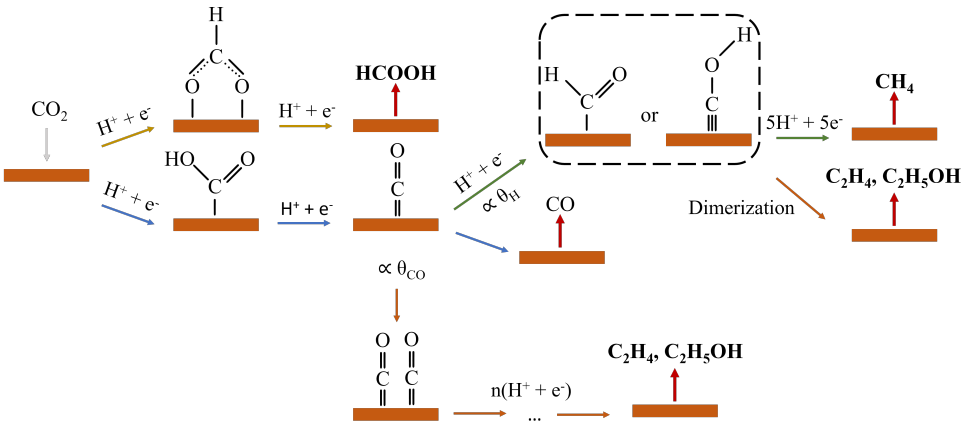

Figure 2.4: Schematic of different possible pathways for electrocatalytic CO_2 reduction. The yellow pathway leads to formate, blue pathway to CO, orange pathway toward multi-carbon products, and green path way to methane production.

CO coverage on the copper electrode and thus prevents CO–CO dimerization and the further reduction of CO to hydrocarbons such as ethylene and ethanol (pathway in in orange), which could explain why hydrocarbons are not formed in our system. Furthermore, if there is enough adsorbed hydrogen present on the surface, further reduction of CO to CH_4 is possible (pathway in green).[39,99] However, due to the lack of water present in our system, the amount of adsorbed hydrogen on the surface is expected to be limited and this will in turn limit CH_4 formation. Finally, dimerization of the C_1 intermediates can also result in the formation of multicarbon products. This pathway will however also be limited due to the relatively lower coverage of hydrogen on the surface.

In aqueous systems, it is well known that alkali metal cations have a large impact on the selectivity and activity of the CO_2RR.[36,38,45,100] Therefore, an initial chronoamperometry experiment was performed with 0.1 M $KClO_4$ in PC at -1.8 V (see Figure A.5). Due to solubility limitations of alkali metal salts in PC, it was not possible to perform a one-on-one comparison. More details can be found in Appendix A. The use of an alkali cation did not increase the amount hydrocarbon products and only resulted in the formation of H_2. This indicates that alkali metal cations do not affect the CO_2RR in nonaqueous systems the same way as in aqueous systems.

One other possible way of increasing the selectivity toward ethylene is by increasing the operating temperature.[81,85] Therefore, the next section will further explore the effect of operating temperature on the reduction of CO_2 on Cu in a 0.7 M TEACl/PC electrolyte.

2.2.3 Chronoamperometry: The Effect of Temperature

The effect of temperature during CO_2RR on Cu electrodes in PC-based electrolytes was studied using a slightly adapted flow-cell design (see Figure A.1). The cell was heated using a water bath and the temperature was kept constant throughout the electrolysis experiment. 1 hour electrolysis experiments at -1.8 V versus Ag/AgCl were performed at 10, 25, 40, and 60 °C, using a 0.7 M TEACl in PC catholyte and aqueous anolyte (0.5 M H_2SO_4). The results are shown in Figure 2.5. The electrolysis results at 25 °C represent the same data as presented in Figure 2.2(c) for 0 v% water added to the organic electrolyte. An increase of the electrolyte temperature results in a decrease in ohmic losses, as the conductivity of the electrolyte and membrane increases.[84,86] This results in a higher current response at -1.8 V versus Ag/AgCl as the operating temperature increases, ranging from -2 mA/cm^2 at 10 °C to -6 mA/cm^2 at 60 °C (see Figure 2.5(a)).

Figure 2.5(b) shows that decreasing the temperature to 10 °C results in the formation of only H_2 and formic acid whereas at temperatures higher than 10 °C CO and traces of CH_4 and C_2H_4 were detected. Several studies concluded that decreasing the temperature also increases CH_4 formation in both aqueous and nonaqueous systems.[85,88–93] However, at 10 °C in 0.7 M TEACl in PC, no CH_4 was detected as CO_2RR product on a Cu electrode. The previously mentioned studies using nonaque-

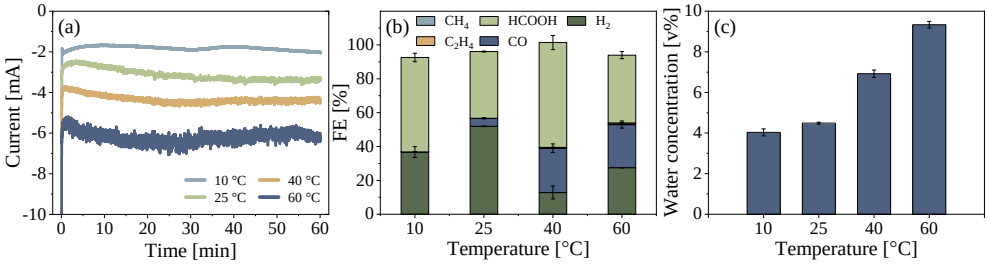

Figure 2.5: (a) Current density, (b) faradaic efficiency, and (c) water concentration after 1 hour of chronoamperometry measurements on Cu electrode in a 0.7 M TEACl in propylene carbonate solution containing 0 v% water at -1.8 V vs. Ag/AgCl at different temperatures. Error bars indicate differences between duplicate measurements.

ous systems all used methanol-based electrolytes, which is a protic solvent. Since PC is aprotic, we anticipate that there are not enough protons present to form CH_4 and thus no increase in CH_4 formation at lower operating temperatures is observed in our system. The total faradaic efficiency towards H_2 at 10 °C slightly decreased to 37% as compared to 52% when operating at 25 °C. Previous studies confirm that the H_2 production decreases with decreasing operating temperatures.[81–83,85] However, in our experiments the faradaic efficiency toward H_2 also decreases at elevated temperatures, with a decrease to 13% at 40 °C and to 27% at 60 °C.

Interestingly, the faradaic efficiency toward formic acid increased from 40% at 25 °C to 62% at 40 °C, but then decreased again to 40% at 60 °C. Furthermore, an increase in CO formation of 5% and 26% was observed when increasing the temperature from 25 to 40 °C and 60 °C respectively. Earlier studies on temperature effects showed that the increase in temperature resulted in an increase in reaction kinetics, but also in a decrease of CO_2 solubility.[86] However, as described by Vos et al.,[86] in aqueous systems, the increased reaction kinetics obtained when operating at higher operating conditions are not severely counteracted by the decrease in CO_2 solubility. Analogues to an aqueous system, this is expected to be similar in a PC electrolyte. The increased kinetics will lead to a higher formation rate of CO_2RR products, which is indeed observed in the partial current density toward CO for different operating temperatures (see Figure A.7). At 60 °C ethylene was detected, albeit in very small amounts ($FE_{C_2H_4} = 0.76\%$). This suggests that the reaction kinetics can be improved toward ethylene when increasing the temperature further, which is similar for aqueous systems.[81] It is however not feasible to operate the Nafion membrane at higher temperatures, as the conductivity of the membrane significantly reduces above 80 °C.[101]

The total amount of water measured after electrolysis for each operating temperature is presented in Figure 2.5(c). The total amount of water measured increases with increasing operating temperature, as the permeability of the membrane increases at

higher temperatures.[87] Therefore, more water was transported through the membrane from the anolyte to the catholyte during the experiment, resulting in the highest water concentration of around 9 v% water when CO_2 electrolysis was conducted at 60 °C. This increase in water concentration in the catholyte at higher operating temperatures contributes to an increase in H_2 formation. All faradaic efficiencies presented in Figure 2.5 are averaged over the last 20 minutes of the experiment when the measured current was stable. However, the product distribution over time, specifically at 60 °C, showed a clear trend where the H_2 concentration continuously increases and CO and C_2H_4 concentrations start to decrease (see Figure A.6). When running the CA for longer than 1 hour at 60 °C, H_2 formation is expected to keep increasing as water will continue to be transported through the membrane. A similar trend was observed in terms of product distribution for experiments performed at 40 °C. However, the trend was less pronounced as compared to the results of electrolysis at 60 °C.

2.2.4 Morphology Characterization

Scanning electron microscopy (SEM) was used to study the morphology changes of the copper foil before and after electrolysis at different operating temperatures. As expected, the surface undergoes structural transformations during electrolysis because of the reactions taking place.[102] Figure 2.6(a,b,d) shows an increased surface roughening when operating the cell at 60 °C as compared to 25 °C (see Figure A.8). More and larger height differences were observed as well as more agglomeration and reshaping of the copper surface.

Furthermore, a black layer was observed on the copper surface after electrolysis at 60 °C (see Figure 2.6(c)). Energy-dispersive X-ray spectroscopy (EDS) results showed that in this black layer an increase in C atoms and O atoms occurred compared to the rest of the electrode surface. At the rest of the surface, the composition of the Cu electrode is equal to the composition of the Cu electrode after electrolysis at 25 °C (see Table A.1). Earlier work in aqueous solutions reported a similar poisoning process, where a thin black graphitic carbon layer was formed on the Cu electrode.[82] In the blank tests with Ar instead of CO_2 under the same conditions, no products or black layer were detected,meaning that the used electrolyte was stable. This strongly indicates that the observed graphitic layer is formed as a consequence of intermediates of CO_2 decomposing on the electrode, similarly to aqueous systems. The graphitic carbon is expected to form via a side reaction, in which CO_2 is reduced through formate to graphitic carbon. It is therefore expected that the black layer has a significant role in the loss of the cathode performance in the CO_2 reduction at 60 °C, which was observed at the end of the 1 hour electrolysis experiment (see Figure A.6).

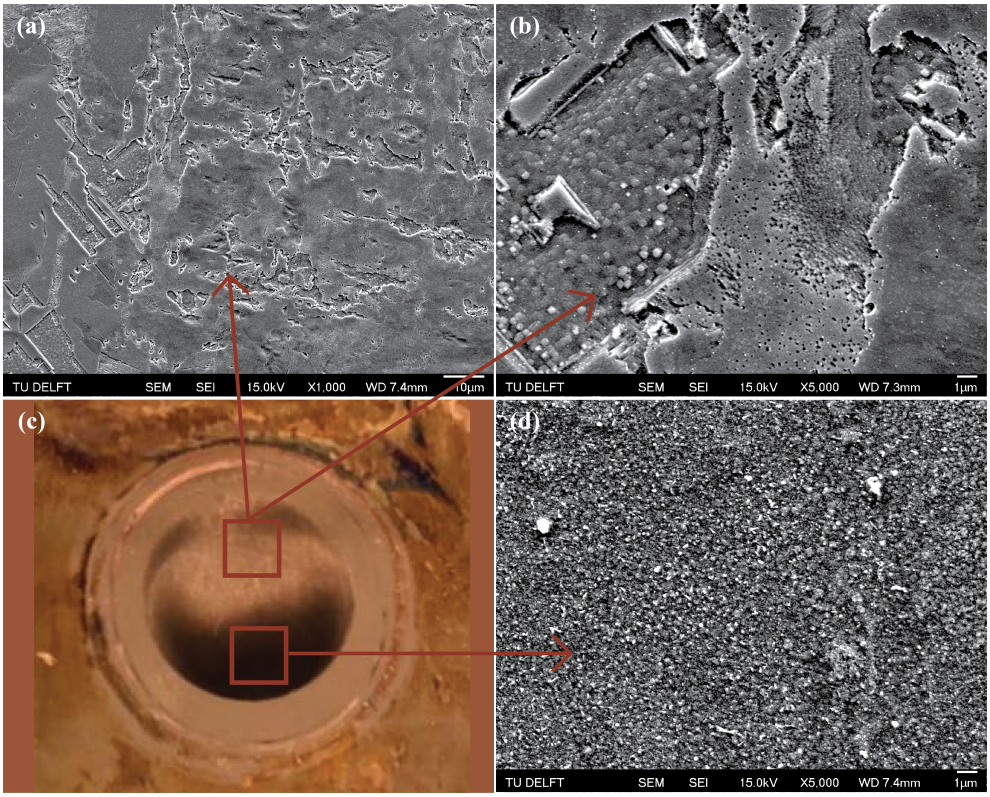

Figure 2.6: SEM images of the Cu electrode after chronoamperometry at -1.8 V for in a 0.7 M in propylene carbonate solution with 0 v% water additions, at 60 °C at a magnification of (a) 1000x, (b) 5000x, and (d) 5000x. In (c) a picture of the electrode after electrolysis at 60 °C is shown, which clearly shows the change in surface colour.

2.3 Conclusion

Electrochemical CO_2 reduction on Cu electrodes in a 0.7 M TEACl in propylene carbonate catholyte has shown to produce mainly H_2, CO, and formic acid. It remains unclear what mechanism is preventing the reduction of CO_2 to hydrocarbon products on a Cu electrode when employing a PC electrolyte in comparison with CO_2RR in aqueous media. The influence on the product distribution during CO_2RR when increasing the water concentration in PC electrolyte was studied. Increasing the water content of the organic catholyte from 0 to 10 v% enhanced the formation of H_2 and CO while formic acid production decreased. Due to the aqueous nature of the anolyte used, water was transported through the membrane, and thus even when no additional water was added to the PC catholyte; around 4 v% water was measured in the catholyte after electrolysis which promoted H_2 production. By eliminating the aqueous anolyte and replacing it with a nonaqueous solvent, the HER can be suppressed further. As a result, an increase in formic acid and CO formation was observed. Furthermore, the effect of the operating temperatures on the CO_2RR in a PC-based electrolyte was studied and it was observed that increasing the operating temperature increased the CO formation. However, due to the increased temperature, the amount of water transported through the membrane also increased. Particularly at 60 °C, this resulted in an increasing trend of H_2 formation and a decreasing trend in CO and C_2H_4 formation. Finally, SEM images showed that the stability of the Cu electrode was reduced at higher operating temperatures, as shown by surface roughening which occurred after electrolysis at 60 °C as compared to electrolysis at 25 °C.

Chapter 3

The Effect of Salts on the CO_2 Reduction Product Distribution in an Aprotic Electrolyte

This chapter has been published as: Burgers, I., Wortmann, B., Garcia, A. C., Deacon-Price, C., Pérez-Gallent, E., Goetheer, E., & Kortlever, R. (2024). The Effect of Salts on the CO_2 Reduction Product Distribution in an Aprotic Electrolyte. *ChemPhysChem*.

Abstract

Electrochemical CO_2 reduction in non-aqueous solvents is promising due to the increased CO_2 solubility of organic-based electrolytes compared to aqueous electrolytes. Here the effect of nine different salts in propylene carbonate (PC) on the CO_2 reduction product distribution of polycrystalline Cu is investigated. Three different cations (tetraethylammonium (TEA), tetrabutylammonium (TBA), and tetrahexylammonium (THA)) and three different anions (chloride (Cl), tetrafluoroborate (BF_4), and hexafluorophosphate (PF_6)) were used. Chronoamperometry and in-situ FTIR measurements show that the size of the cation has a crucial role in the selectivity. A more hydrophobic surface is obtained when employing a larger cation with a weaker hydration shell. This stabilizes the $CO_2^{\cdot-}$ radical and promotes the formation of ethylene. CO_2 reduction in 0.7 M THACl/PC shows the highest hydrocarbon formation. Lastly, we hypothesize that the hydrocarbon formation pathway is not through C-C coupling, as the CO solubility in PC is very high, but through the dimerization of the COH intermediate.

3.1 Introduction

Electrochemical CO_2 reduction is a promising sustainable pathway to convert flue gas into renewable fuels and chemicals by using renewable electricity.[33,38,95] The CO_2 reduction reaction (CO_2RR) typically requires mild operating conditions and produces a variety of C_1-C_3 products.[38,39] However, the reaction still suffers from large overpotentials, low current densities and a limited product selectivity.[34,36,76]

In CO_2 reduction research, most commonly aqueous electrolytes are deployed.[44] However, organic solvents are a promising alternative.[43,44] The main advantages of using organic solvent are the relatively higher CO_2 solubility compared to aqueous systems and the limited amounts of protons present, hence limiting the formation of H_2 by the hydrogen evolution reaction.[43,44,76] Frequently used organic solvents in CO_2 reduction include acetonitrile (ACN), propylene carbonate (PC), and dimethylformamide (DMF).[44] Several recent studies have explored CO_2 reduction on Au electrodes using various organic solvents.[55–57,103] For 2-electron reduction products, such as CO, formate, and oxalate, promising results have been obtained on i.e. Pb, Ag and Pt electrodes.[58–60] Nonetheless, there is a relatively low amount of research conducted on the utilization of Cu electrodes, that are able to form hydrocarbons, in organic solvents.[51,61,104] All of these studies conclude that no hydrocarbons are formed while using a Cu electrode in aprotic solvent. Hydrocarbons are only observed when the aprotic electrolyte is altered with a proton donor such as phenol.[105]

Kumar et al.[51] quantified the product distribution of CO_2 reduction on a Cu electrode in dimethylformamide (DMF), n-methyl-2- pyrrolidone (NMP), and acetonitrile (ACN), using 0.1 M tetrabutylammonium hexafluorophosphate ($TBAPF_6$) as electrolyte. Different potential windows for the different solvents were used, investigating the difference in product distribution between -1.4 and -1.8 V vs. Ag/AgCl. For all three organic solvents, negligible amounts of hydrocarbons were detected. In DMF and NMP, the major product formed was oxalate, whereas hydrogen and formate were the main products found in ACN. The addition of water to the different organic solvents only increased the formation of hydrogen and formate with negligible hydrocarbon production. Hence, this study concludes that aqueous systems are the preferred solvent for the formation of hydrocarbons on a Cu electrode. No clear reasoning was given for the suppressed formation of hydrocarbons in organic solvent.

Deacon-Price et al.[61] recently studied the solvent effect in CO_2 reduction on a nanostructured Cu electrode and compared this to a polycrystalline Cu electrode. A 0.1 M tetraethylammonium chloride (TEACl) in ACN was used as electrolyte, and CO_2 reduction was performed at -2.0 V vs. Ag/Ag^+. A small amount of hydrocarbons were observed, whereas the major product was CO. It is interesting to note that this differs from the observations of Kumar et al., who mainly observed formate production. As the only difference in these systems was the salt used, this indicates that the choice of cations and anions in organic solvents can have a significant effect on the product distribution. The addition of water to the organic solvent led to a slight increase in formate production and a minor increasing trend in hydrocarbon formation with increasing water concentration (up to 1000 mM). Kumar et al.[51]

investigated much larger water concentrations, hence they do observe an increase in hydrogen formation when increasing the water concentration (up to 5% (v/v)). To better understand the competition between the hydrogen evolution reaction (HER) and CO_2 reaction mechanism on the electrode surface, in-situ FTIR measurements were performed. This revealed that the presence of CO_2 completely suppressed the OH bending of water and lowered the OH stretching intensity, inhibiting the formation of hydrogen. However, the addition of water does not have any effect on the selectivity or activity of the CO_2RR. Furthermore, it is hypothesized that CO desorption in acetonitrile is easier than in aqueous media. Hence the major product measured by the GC was found to be CO, as it detaches from the surface before a CC bond can be formed, which is a crucial step in the pathway to hydrocarbons.

Lastly, in our previous work[104] the product distribution of CO_2 reduction using a Cu electrode in 0.7 M TEACl in PC as solvent was studied. As expected, negligible amounts of hydrocarbons were detected. The addition of water mainly increased the hydrogen formation. Increasing the operating temperature to 40 and 60 °C suppressed the hydrogen formation and increased the CO production. It was hypothesized that the hydrocarbon formation was suppressed due to the higher solubility of CO in PC compared to aqueous solvents leading to a low CO coverage on the catalyst surface and thus limiting C-C coupling.

We hypothesize that to further understand why previous studies for CO_2 reduction in non-aqueous electrolytes observe little to no hydrocarbons, the role of the electrolyte salt and its interaction with the catalytic surface needs to be better understood. The effect of the cation size on the selectivity of CO_2 reduction on Cu electrodes in aqueous systems was already discussed in early studies from Murata and Hori.[45] Smaller, strongly hydrated cations do not adsorb as easily on the electrode surface as larger cations. This changes the potential in the outer Helmholtz plane (OHP), hence effecting the selectivity of the CO_2 reduction. It is well known that the larger cations, such as Cs^+, lead to a higher selectivity towards hydrocarbons, compared to a smaller cations like Li^+.[36,43,106–108] Furthermore, the anions are also known to have an effect on the selectivity, due to their buffering capacity and can serve as proton donors.[44] Different studies have shown that the presence of halide anions, such as Cl^-, Br^-, and I^-, has an effect on the Cu surface structure, and tend to steer the selectivity of the CO_2 reduction on Cu electrodes towards C_{2+} products.[36,43,109]

The effect of cations and anions for CO_2 reduction in organic solvents is less well understood. A study by Berto et al.[57] compared the onset potential (obtained by cyclic voltammetry) for different NR_4^+ salts with varying alkyl chains. The onset potentials for all salts were very similar, hence they concluded that the cation did not have an catalytic role on the CO_2 reduction and that the NR_4^+ does not have an electrostatic interaction with CO_2 nor with the electrode surface area. This study did not further investigate the effect of the salts on the product distribution during CO_2 reduction. Furthermore, Gomes et al.[62] studied different tetrabutylammonium (TBA) salts in 1,2 dimethoxyethane (DME) and dimethyl sulfoxide (DMSO) for CO_2 reduction on a Cu electrode. They showed that ion pair formation in DME is depen-

dent on the anion type, whereas this is not the case for DMSO. Moreover, a decrease of ion pair formation increased the CO_2 current density and CO faradaic efficiency. Recent work by König et al.[110] investigated the diffusion coefficients of CO_2 in aprotic solvents and found that both the CO_2 mass transport and the electrolyte solvent have an important effect on the product distribution towards CO or oxalate. Besides these studies, there is a limited amount of research available on the effect of the cation and anion on the product distribution for CO_2 reduction on a Cu electrode.

In this study, a screening of the CO_2 reduction performance of a copper electrode using several different organic salts dissolved in PC is reported. The product distribution was measured during 1 hour chronoamperometry (CA) experiments at -2.0 V vs. Ag/AgCl. Both the anion and the cation were varied, creating 9 different salt combinations. The length of the cation chain was increased from tetraethylammonium (TEA), to tetrabutylammonium (TBA), and tetrahexylammonium (THA). The anion was varied by using chloride (Cl), tetrafluoroborate (BF_4), and hexafluorophosphate (PF_6). We show that the size of the salt, both cation and anion, plays a major role in the observed product distribution. With insitu FTIR measurements the interaction of the salt, the PC and the catalytic surface were further investigated.

3.2 Results and Discussion

3.2.1 Electrolytic Performance

Figure 3.1 shows the faradaic efficiencies of products formed during 1 hour chronoamperometry (CA) experiments at -2.0 V vs. Ag/AgCl using a Cu electrode and the 9 different PC electrolytes. The investigated potential of -2.0 V vs. Ag/AgCl was chosen based on the optimum found in our earlier work on the CO_2 reduction product distribution in a TEACl/PC electrolyte.[104] All experiments were performed in a small H-cell, which was deemed most appropriate to understand the mechanistic effects, with inline gas chromatography (GC) for the gas product analysis, and a constant salt concentration of 0.7 M. The results are grouped per anion, with the x-axis as a function of the varying cations. Figure B.1 in Appendix B shows the results grouped per cation. Furthermore, Figure B.5 shows the water concentration before and after electrolysis for each measured salt is presented. The salts naturally adsorb water from the atmosphere, hence it is difficult to start with a dry electrolyte without performing extra preparation steps. Therefore, the water concentration of the fresh electrolyte is measured to understand the starting conditions for the CA experiments. Due to the aqueous anolyte (0.5 M H_2SO_4), protons will diffuse through the Nafion membrane during the experiment. The water concentration is measured again after the electrolysis, to quantify the diffusion of water. By measuring the gaseous product distribution over time, we can understand the effect of the water in our system.

Figure 3.1 illustrates a notable disparity in the formation of hydrocarbon products across the nine tested salts. In the case of TEA as cation, the CO_2 reduction products are consistently limited to CO and formate, irrespective of the anion employed.

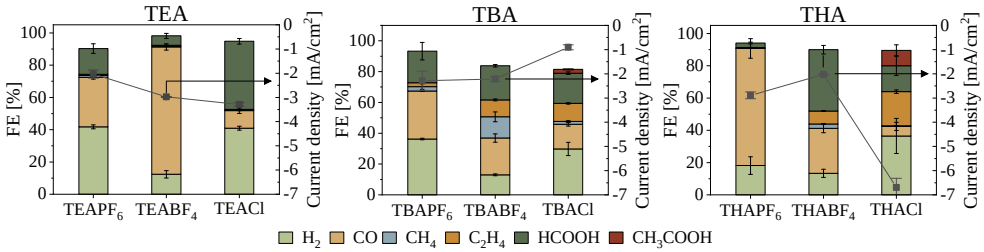

Figure 3.1: Faradaic efficiencies of CO_2 reduction products during 1 hour chronoamperometry (CA) on a Cu electrode using PC electrolytes with different salts at -2.0 V vs. Ag/AgCl. All experiments were performed with 0.7 M salt concentrations. The results are grouped per anion used, with error bars indicating differences between duplicate measurements.

Hydrogen was also detected as result of the residual water and proton reduction reaction.[111] Notably, the use of THACl yields the highest ethylene production (typical measured peak concentration of 165 ppm), while $TBABF_4$ results in the highest methane yield (typical measured peak concentrations of 80 ppm). We hypothesize that the adsorption of the organic cations on the electrode surface increases the hydrophobicity of the surface, where the hydrophobicity of the surface increases with increasing alkyl chain lengths of the cation. Such a hydrophobic catalyst surface allows for limited available space for H^+ to adsorb. Ethylene formation is favored in environments with low H^+ availability, hence negligible amounts of ethylene were formed when using TEA salts, and the largest amount of ethylene was measured when using THA (22% $FE_{C_2H_4}$). The faradaic efficiency towards ethylene in THACl/PC is comparable to aqueous based electrolytes, where the observed faradaic efficiency towards ethylene is commonly around 30%.[36,40,96] Methane formation is favored with a higher H^+ coverage.[36] Therefore, the faradaic efficiency of methane was higher for the TBA salts than for the THA salts. However, since for the TBA and THA cations there was only ethylene production when combined with BF_4^- or Cl^- anions, the production of hydrocarbons cannot solely be dependent on the size of the cation.

When looking at the anion effect, the systems with salts using PF_6^- as anion showed negligible or no hydrocarbons production. BF_4^- anions only showed decent amounts of methane and ethylene when combined with a larger cation, such as TBA and THA. Clanions showed a similar trend, where hydrocarbons were observed when TBACl or THACl was used in the PC solvent during CO_2 reduction. When using TBACl and THACl, some acetic acid was measured, which was not detected when using any of the other salts. However, with THACl no methane was measured suggesting that with THACl the C_1 pathway forming methane is suppressed in favor of the C_2 pathway. Furthermore, the salts with a Cl^- anion show the highest water concentration in the electrolyte, whereas the salts with PF_6^- anion have the lowest water concentration

in the electrolyte (see Figure B.5). Cl^- based salts are better soluble in water than the organic based BF_4 and PF_6 salts, which can explain the larger amount of water present in the solvents using Cl^- salts. The high concentrations of water when Cl^- anions were used can explain why more formate was formed, in comparison to the PF_6^- and BF_4^- anions. Despite this, an increased formate faradaic efficiency was only observed with TEACl and TBACl and not with the THACl.

Additionally, chronoamperometry experiments with a nonaqueous catholyte and anolyte were conducted to confirm that the observed change in product distribution is mainly due to the salt used and not due to the unregulated water concentration caused by diffusion through the membrane. However, due to the Nafion membrane used which is activated and stored in water, the water in the system cannot be completely eliminated. TEACl and THACl salts were tested, using a PC electrolyte as anolyte and catholyte. Figure B.4 shows the faradaic efficiencies of the CO_2 reduction products. Comparable results were obtained, confirming that the nature of the salt present in the electrolyte is indeed controlling the selectivity of the CO_2RR and controlling whether ethylene is produced. Moreover, as a decrease in ethylene faradaic efficiency is observed when using a PC based anolyte, caused by the lower concentration of water (see Figure B.6) as proton donor which is required in non-aqueous electrolytes to obtain significant amounts of ethylene.

3.2.2 In-situ FTIR Spectroscopy

To better comprehend how the cations and anions interact with the catalytic surface during CO_2 reduction, in-situ FTIR measurements were performed. Figure 3.2 shows the spectra at -2.4 V vs. Ag/AgCl for both Ar and CO_2 saturated conditions. The full spectra can be found in the Supporting Information (Figure B.7 and Figure B.8). This potential was chosen as it clearly shows the different bands for all measured conditions. The effect of the anion on the CO_2 reduction product distribution is tested by investigating $THAPF_6$/PC, $THABF_4$/PC, and THACl/PC, and the effect of the cation by comparing TEACl/PC, TBACl/PC, and THACl/PC. In Figure 3.2(a) a negative band is observed at 2335 cm^{-1}, which corresponds to CO_2 being consumed during the CO_2 reduction reaction.[61,111] A relatively larger negative band is indicative for a higher CO_2 consumption, which corresponds well to the total partial current density for CO_2 reduction for the different salts (see Figure B.2 and Figure B.8).

Furthermore, at 1276 cm^{-1} a growing positive band is observed (see Figure 3.2(a)) which is attributed to bicarbonate formation.[112] The bands in between 1673-1605 cm^{-1} are likely related to the carbonate concentration at the surface.[111] It is hypothesized that the increase in (bi)carbonate at the surface is related to an increased hydrocarbon production, because an increase in the amount of (bi)carbonates indicates a higher local alkalinity at the surface.[44] Comparing to the product distribution (as given in Figure 3.1), the largest amount of hydrocarbons were produced when using THACl, which directly corresponds to the highest intensity of the bands around the carbonate and bicarbonate wavelength. The least amount of hydrocarbons were formed when using $THAPF_6$. In the spectrum of CO_2 saturated 0.7 M $THAPF_6$/PC

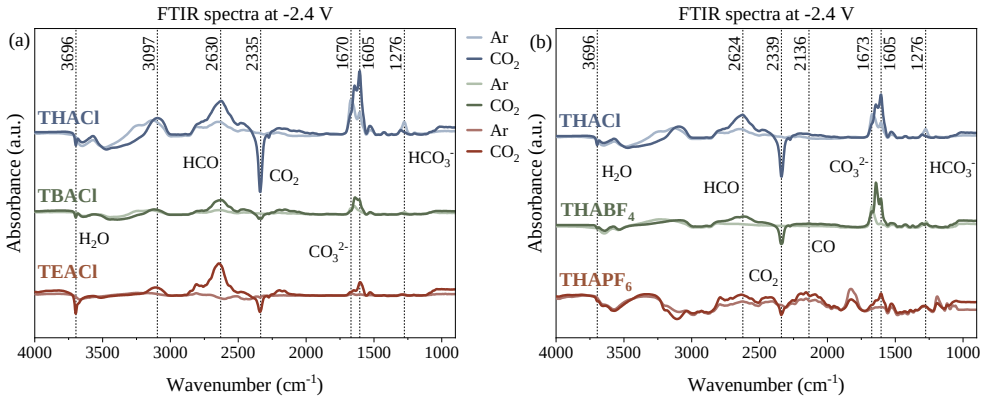

Figure 3.2: FTIR spectra at -2.4 V vs. Ag/AgCl for the different salts (0.7 M) dissolved in PC, for Ar and CO_2 saturated conditions, using a Cu electrode. (a) Spectra for electrolytes using THACl, TBACl, and TEACl in PC. (b) Spectra for electrolytes using THACl, $THABF_4$, and $THAPF_6$ in PC.

(dark orange line in Figure 3.2(b)), there is very little to no band present at these wavenumbers.

Furthermore, the Ar saturated spectra (see Figure B.7), also show (bi)carbonate bands. It is assumed that in the FTIR blank control experiments (using an Ar saturated electrolyte), these bands correspond to the degradation of propylene carbonate, forming (bi)carbonate at these negative potentials. Due to the high OH^- concentration on the surface, the alkaline pH catalyzes the chemical degradation process of propylene carbonate into (bi)carbonate.[113] Hence, in the FTIR spectrum, the breakdown of PC is already visible at a lower potential compared to the onset potential measured in the blank CV experiments (see Figure B.9 and Figure B.10).

There are multiple pathways through which hydrocarbons can be formed. The first is through the C_1 pathway, where *COH is a key intermediate.[36,39] Dimerization of intermediates in this pathway leads to the production of both methane and C_2 products. Second, a C-C bond can be formed through the C_2 pathway, where two adsorbed *CO(H) molecules dimerize. There has been discussion regarding the exact dimerization reaction, as both *CO and *COH have been identified as reactants for this dimerization.[114,115] Typically, a band corresponding to adsorbed *CO is expected around 2136 cm^{-1}, however such a band is not observed in any of the spectra.. This can be due to the limited sensitivity of FTIR for measuring adsorbed *CO on a Cu electrode surface. A similar observation was made by Deacon-Price et al.,[61] where they studied CO_2 reduction in acetonitrile. Additionally, they observed a higher FE_{CO}, which was detected by gas chromatograph, in comparison to an aqueous solvent, suggesting indeed that CO do not adsorb strong on Cu surface in less protic solvent.

In contrast, a clear band is observed around 2630 cm^{-1}, that is attributed to a *COH intermediate. The presence of this intermediate on the surface suggests that the reaction pathway to form hydrocarbons is either via the C_1 pathway, where dimerization of intermediates occurs to form ethylene, or through the dimerization of *COH intermediates, possibly with co-adsorbed CO.

Lastly, the negative bonds at 3696 cm^{-1} are related to OH stretching of the water present in the electrolytes. The salts with Cl^- anions contained the most amount of water, which correlates with the intensity of the negative band related to OH^- stretching. There is no negative band observed near 1628 cm^{-1}, which typically corresponds to OH^- bending of water.[61] However, the total amount of water present at the end of the FTIR measurement will be comparable to the water concentration measured before electrolysis, since no water crossover from the anolyte can happen during the experiment. Furthermore, this band is overlapping with the (bi)carbonate bands, which could also be the reason why this is not clearly visible.

3.3 Conclusion

This study shows that the electrolyte, and more concretely the type of salt used, plays a crucial role in determining the product distribution during CO_2 reduction in propylene carbonate. We conclude that the size of the cation strongly effects the product formation. A larger cation, with an increasing alkyl chain length, creates an increasingly hydrophobic surface which promotes the formation of ethylene. Hence, using THACl/PC results in the highest ethylene formation. Furthermore, based on the FTIR results, we conclude that a higher (bi)carbonate concentration near the electrode surface is related to a higher hydrocarbon production. The differences in (bi)carbonate concentration at the surface is related to the local pH at the electrode. This affects the observed product distribution, as a higher local pH promotes C_{2+} hydrocarbon production. The observed concentration of (bi)carbonate at the surface is highly dependent on the dissolved salt in the electrolyte. The THACl salt shows the highest amount of (bi)carbonate at the surface, which indeed corresponds to the highest amount of hydrocarbons formed during the CA experiments. Lastly, we hypothesize that the reaction pathway for hydrocarbon formation in a PC electrolyte occurs dominantly through the *COH intermediate, either through the C_1 or C_2 pathways, irrespective of the salt used. This is supported by FTIR spectra where a large band corresponding to COH was measured. Hence, the salt has a major role in the product selectivity of CO_2 reduction in PC. The highest amount of ethylene (22% $FE_{C_2H_4}$) was achieved using 0.7 M THACl in PC.

Chapter 4

The Effect of Electrolyte pH and Impurities on the Stability of Electrolytic Bicarbonate Conversion

This chapter has been published as: Burgers, I., Jónasson, J., Goetheer, E., & Kortlever, R. (2024). The Effect of Electrolyte pH and Impurities on the Stability of Electrolytic Bicarbonate Conversion. *ChemSusChem*.

Abstract

Electrolytic bicarbonate conversion holds the promise to integrate carbon capture directly with electrochemical conversion. Most research has focused on improving the faradaic efficiencies of the system, however, the stability of the system has not been thoroughly addressed. Here, we find that the bulk electrolyte pH has a large effect on the selectivity, where a higher pH results in a lower selectivity. However, the bulk electrolyte pH has no effect on the stability of the system. A decrease in CO selectivity of 30% was observed within the first three hours of operation in an optimized system with 3 M $KHCO_3$ and gap between the membrane and electrode. Singlepass electrolyte experiments at various constant pH values (8.5, 9.0, 9.5, and 10.0), show that only at a pH of 10 the CO selectivity was stable during three hours, reaching a faradaic efficiency toward CO of only 18% as compared to an initial 55% at pH 8.5. Trace metal impurities present in the electrolyte were found to be the cause of the decrease in stability as these deposit on the electrode surface. By complexing the trace metal ions with ethylenediaminetetraacetic acid (EDTA), the metal deposition was avoided and a stable CO selectivity was obtained.

4.1 Introduction

The electrochemical CO_2 reduction reaction (CO_2RR) is a promising method for using renewable electricity to convert waste CO_2 gas into value-added chemicals such as CO or hydrocarbons.[33,38,41] Most research focuses on gas-fed electrolyser systems, where a pure CO_2 gas input is required. However, these systems are still far from commercial applications, due to limitations such as low single-pass conversion efficiency, loss of CO_2 to carbon species, and low carbon utilization.[69,116–119]

To supply a pure CO_2 gas feed to the electrolyser, a CO_2 capture process is required to concentrate CO_2 either from the air or from a flue gas stream. This can be achieved by a liquid absorption, such as amine based capture solvents, or solid adsorption sorbent, such as activated carbon.[24,120,121] The regeneration of the capture solvent requires an energy intensive thermal regeneration process, which reduces the economic feasibility of a CO_2 electrolyser.[122,123] One potential method to eliminate the energy-intensive regeneration step is by directly using a CO_2 rich capture solvent as input to the electrolyser. This can be achieved by using an alkaline capture solvent which forms (bi)carbonate when reacting with CO_2. The (bi)carbonate rich solvent can be directly used in an electrolyser, where the CO_2 is first liberated in the acidic environment near the bipolar membrane (Equations 4.1 and 4.2) and subsequently reduced on the catalyst surface (Equation 4.3).[63,66] The main advantage of this electrolyser system is that it can provide a high concentration of CO_2 near the catalyst surface as compared to systems using dissolved CO_2.[63,64] Furthermore, due to the production of OH^- as byproduct during CO_2 reduction, the (bi)carbonate capture solvent is regenerated and can theoretically be recycled back to the capture column (Equation 4.4).

$$\text{CO}_2\text{ liberation:}\quad \mathrm{H^+ + HCO_3^- \rightleftharpoons CO_2 + H_2O} \tag{4.1}$$

$$\mathrm{2H^+ + CO_3^{2-} \rightleftharpoons CO_2 + H_2O} \tag{4.2}$$

$$\text{CO}_2\text{ reduction:}\quad \mathrm{CO_2 + H_2O + 2e^- \longrightarrow CO + 2OH^-} \tag{4.3}$$

$$\text{Capture reaction:}\quad \mathrm{CO_2(}g\mathrm{) + CO_3^{2-} + H_2O \rightleftharpoons 2HCO_3^-} \tag{4.4}$$

Currently, most research conducted in the field of the electrolysis of bicarbonate solutions, also referred to as bicarbonate electrolysis, has focused on improving the faradaic efficiency of the system. Berlinguette and co-workers have published several studies on the bicarbonate electrolyser, using a Ag gas diffusion electrode (GDE) for the production of CO.[63,64,124] The electrolyser typically uses a 3 M $KHCO_3$ catholyte, 1 M KOH anolyte, and a bipolar membrane to supply a constant H^+ flux to the cathode compartment. A porous carbon support layer spray-coated with Ag nanoparticles and Ni foam served as cathode and anode, respectively. An initial faradaic efficiency towards CO (FE_{CO}) of around 40% was reached at 100 mA/cm^2.[63]

An in-depth electrode design analysis was performed by the same group, looking into different deposition techniques such as spray-coating, physical vapor deposition, and a combination of these two methods.[64] Their optimized GDE, a combination of

a 500 nm thick Ag layer, deposited using physical vapor deposition (PVD), and a spray coated Ag layer, resulted in a reported FE_{CO} of 82% at 100 mA/cm^2, which was confirmed by personal communication to be the initial faradaic efficiency after 5 minutes of operation.[125] Furthermore, the use of a free standing porous Ag electrode was compared with a Ag GDE.[65] An initial FE_{CO} of around 60% was reached using a porous electrode at ambient conditions and 100 mA/cm^2. Despite the decrease in performance of the porous electrode compared to the Ag GDE, a porous electrode was argued to be better than a GDE due to the higher durability and easy handling.[65] Increasing the pressure up to 4 bar resulted in a significant increase in FE towards CO up to 95% at 100 mA/cm^2, due to the increased solubility of CO_2.[65] However, the stability of the bicarbonate electrolysis system was not discussed in detail.

Carbonate reduction, as opposed to bicarbonate reduction, using a Ag GDE was investigated by Li et al.[66] The performance of a carbonate electrolyser was studied with different concentrations of K_2CO_3 (0.1 to 2 M) as catholyte. At a concentration of 2 M K_2CO_3 and current density of 100 mA/cm^2, a FE_{CO} of approximately 30% was obtained. Recently, Xiao et al.[67] demonstrated that by physically separating the catalyst and the membrane with a thin TiO_2 layer (25 μm) on top of the catalyst, the FE_{CO} increases from around 10% to 46% at 200 mA/cm^2 for a system using a 2 M K_2CO_3 catholyte at a pH between 10 and 11. Similarly, a study by Lee et al.[126] further investigated the effect of a spacing between the membrane and catalyst to improve the pH gradient in the system. They modelled the local pH as a function of the distance between the membrane and the electrode surface for a carbonate electrolyser. Interestingly, they found that in a zero-gap configuration, the pH at the membrane does not reach acidic conditions. When introducing a spacing of 135 μm, the pH at the membrane decreases to around 3 at 200 mA/cm^2, providing the right conditions for the in-situ generation of CO_2 inside the system.

The above mentioned results seem very promising for using a bicarbonate electrolyser in an integrated capture and conversion system. However, as mentioned before, the stability of all of these systems remains unclear and is often overlooked in the current literature. Lees et al.[64] briefly discuss the decrease of the FE_{CO} over time and conduct an 8 hour experiment where the 3 M $KHCO_3$ electrolyte was refreshed every three hours, showing a temporary recovery of the CO faradaic efficiency to the initial efficiency of around 40% after refreshing the electrolyte. Furthermore, the Ag loading on the electrode before and after electrolysis measured by XRF was within 2% difference. Additionally, they performed a control experiment in which they acidified the recirculating electrolyte by adding 4 M H_2SO_4 after every 2 hours of operation during an 8 hour experiment, such that the electrolyte pH remains around 8.5. In this case, the FE_{CO} does not completely recover to the initial 40% and an overall decreasing CO selectivity is measured over time. This is explained by a depletion of the carbon present in the electrolyte. Therefore, it is suggested by Lees et al.,[64] that the increase in pH and decrease in carbon concentration is the main cause for the decrease in the product selectivity over time.

This work focuses on quantifying and understanding the changes in CO selectivity in a bicarbonate electrolyser as function of time. To understand the role of the

electrolyte pH on the stability of the system, several experiments with recirculated electrolytes and single-pass electrolytes at a various bulk pH conditions were studied. The bulk pH strongly effects the overall FE_{CO}, where a more alkaline electrolyte results in a lower FE_{CO}. However, the bulk pH does not control the stability of the system. Instead, the deposition of trace metal ion impurities which are present in the high concentration electrolyte salt are found as the main cause for the decrease in selectivity. By complexing these trace metal ions with ethylenediaminetetraacetic acid (EDTA), the metal deposition was avoided and a stable CO selectivity was obtained.

4.2 Results and Discussion

4.2.1 Improving In-situ CO_2 Liberation

Initial bicarbonate electrolysis experiments were conducted using a zero-gap configuration and recirculating electrolytes leading to an initial FE_{CO} of around 40% (see Figure 4.1(b). This obtained result is similar to previously reported values.[63,64,66] To improve the in-situ CO_2 liberation, a spacing between the membrane and electrode was introduced, as suggested previously by Lee et al.[126] for carbonate reduction, using a mixed cellulose ester (MCE) membrane. It was shown that the spacing improved the pH gradient between the membrane and the electrode, creating an acidic pH for

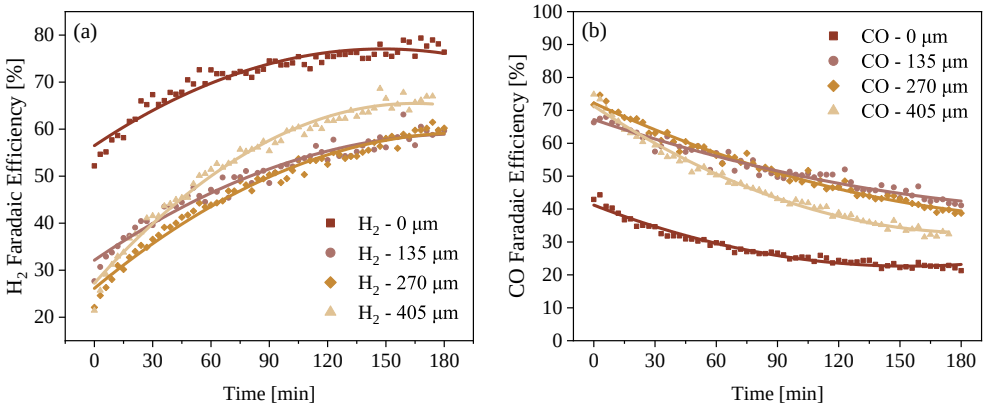

Figure 4.1: Bicarbonate electrolysis experiments at 100 mA/cm^2 using a Ag spray-coated cathode and recirculating 3 M $KHCO_3$ catholyte (70 mL) and 1 M KOH (140 mL). Faradaic efficiencies of (a) H_2 and (b) CO over time, for different distances between the membrane and the catalyst layer. All data points are average values of duplicate measurements with an average error of ± 3.2% and total FE of >98%. The lines represent polynomial fitting of the data for a better representation of the stability trend over time.

CO_2 liberation at the membrane, while maintaining an alkaline pH for CO_2 reduction at the cathode. Lee et al.[126] showed an optimal increase in C_{2+} selectivity when using a spacing of 135 μm in a carbonate electrolyte with a pH in the range of 10 to 11. To understand how this translates to a bicarbonate electrolysis system with a lower pH, three different gap dimensions (135, 270, and 405 μm) were tested in the bicarbonate electrolyser system (pH 8.2 $\pm$ 2). In Figure 4.1 the faradaic efficiencies of H_2 and CO for the four different conditions are presented as a function of time. The measured cell potential was 3.6 $\pm$ 0.1 V for all experiments. We find that by introducing a spacer in between the bipolar membrane and electrode the faradaic efficiencies towards CO are significantly improved. Initially, around 70% FE_{CO} was achieved with all three spacing dimensions, compared to only 40% for the zero-gap configuration. The highest reported initial FE_{CO} is 82%, which was achieved by using an optimized electrode consisting of a 500 nm Ag PVD layer on both sides of the electrode and a spray coated Ag layer on the side facing the membrane.[64] Our results show that the use of a spacer results in a similar initial FE_{CO}, while using a simple electrode preparation with significantly less Ag loading, making it more economical.

As can be seen in Figure 4.1, the product selectivity decreased significantly during the 3 hour experiment for all four tested spacings. For the zero-gap configuration, a FE_{CO} of only 25% is reached after three hours of operation. Using a spacer did not prevent the decrease in FE_{CO}. The stability of the system with a gap of 135 μm and 270 μm is very comparable. When the introduced spacing is increased to 405 μm, the decrease in FE_{CO} over time is more significant as compared to all other configurations, due to the increased rate of in-situ CO_2 capture over the longer distance in between the membrane and electrode.[67,126] In summary, the typically reported faradaic efficiencies in the literature are the initial values, which do not accurately represent the behaviour of the system. Even though the FE_{CO} can be increased by introducing a spacer, with a spacing of 135 μm performing best, the observed significant decreases in FE_{CO} over time are undesirable for continuous operation of a bicarbonate electrolyser and should therefore be explored further.

4.2.2 Longer Term Stability

The results obtained in the three hour bicarbonate electrolyser experiments suggest that the product distribution was reaching stability near the end of the experiments. In order to better characterize the longer-term stability, 15 hour experiments were conducted. In Figure 4.2 and Figure C.4, the faradaic efficiencies of H_2 and CO are represented as a function of time, as well as the bulk pH over time for a zero-gap configuration and for a spacing between the electrode and membrane of 135 μm. Similar to the 3 hour experiments, recirculating electrolytes were used in the 15 hour experiments. Due to the longer duration of the experiments, the volumes of the catholyte and anolyte were increased to 1 L and 0.5 L, respectively, to ensure that the (bi)carbonate and KOH concentrations were maintained relatively constant. The pH was measured at the outlet of the electrolyser, and represents the bulk pH of the catholyte. The results shown in Figure 4.2 demonstrate that the FE_{CO} does

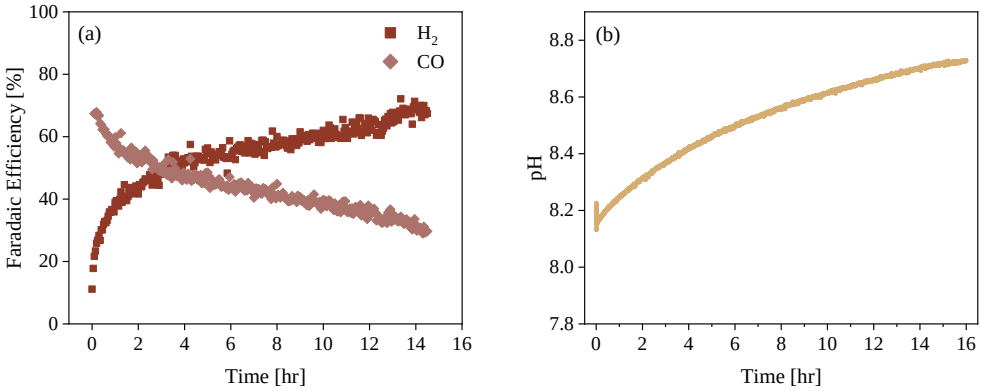

Figure 4.2: Long term stability of bicarbonate electrolyser at 100 mA/cm^2 using a Ag spray-coated cathode and recirculating 3 M $KHCO_3$ catholyte (1 L) and 1 M KOH anolyte (0.5 L). (a) Faradaic efficiencies over time towards H_2 and CO for a configuration with a spacing between the electrode and membrane of 135 μm. (b) The change in electrolyte bulk pH over time. All results are average values of duplicate measurements with an average error of ± 3% and total FE of >98%.

not stabilize over 15 hours of operation. The change in selectivity is larger in the beginning, and slows down near the end of the 15 hours. The pH of the 1 L catholyte increases steadily from around 8.1 to 8.7 after 15 hours of operation. The steady decrease after the first 2 hours can be related to the steady increase in pH of the bulk electrolyte. A very similar observation was made by Lees et al.[64] in which the pH increased in just 2 hours from 8.5 to 9 for a bicarbonate electrolyser using only 125 mL of catholyte and comparable electrode surface area. Similarly, at a higher pH, the FE_{CO} dropped from 40% to 30% faradaic efficiency. However, the larger initial change in selectivity during the first 2 hours of the experiment is not expected to be caused by the change in bulk pH, as the selectivity decrease is much faster than the measured gradual rise in pH. To confirm this hypothesis, a series of singlepass electrolyte experiments were conducted.

4.2.3 The Effect of pH on CO Selectivity

As suggested previously,[64] the increase in pH and decrease in FE_{CO} suggests that the pH is affecting the selectivity of the CO_2RR and competing hydrogen evolution reaction (HER). Therefore, a set of single-pass catholyte experiments were conducted with a different inlet pH, while maintaining a constant 3 M K^+ concentration. Four different (bi)carbonate electrolytes with a pH of 8.5, 9.0, 9.5, and 10.0 were evaluated in the bicarbonate electrolyser, using a gap of 135 μm at a constant current of 100 mA/cm^2. The anolyte was recirculated, as no changes in pH were observed

and this is thus not limiting the anodic reaction. In Figure 4.3(a), the FE_{CO} for the four different inlet pH conditions are presented as a function of time. These results clearly demonstrate that a constant inlet pH does not result in a constant product output, indicating that there are more factors contributing to the decrease in FE_{CO} of the bicarbonate electrolyser system. It can however clearly be observed that an increase in pH decreases the selectivity towards CO production. At a pH of 8.5, the initial FE_{CO} reaches 55%, whereas for a pH of 9.0, 9.5, and 10.0 the FE_{CO} initially reaches 50%, 31%, and 18%, respectively. Interestingly, at a constant catholyte pH of 10.0, a relatively stable faradaic efficiency towards CO is observed. At a lower pH of 8.5, the concentration of unreacted CO_2 at the outlet is close to 30 000 ppm,

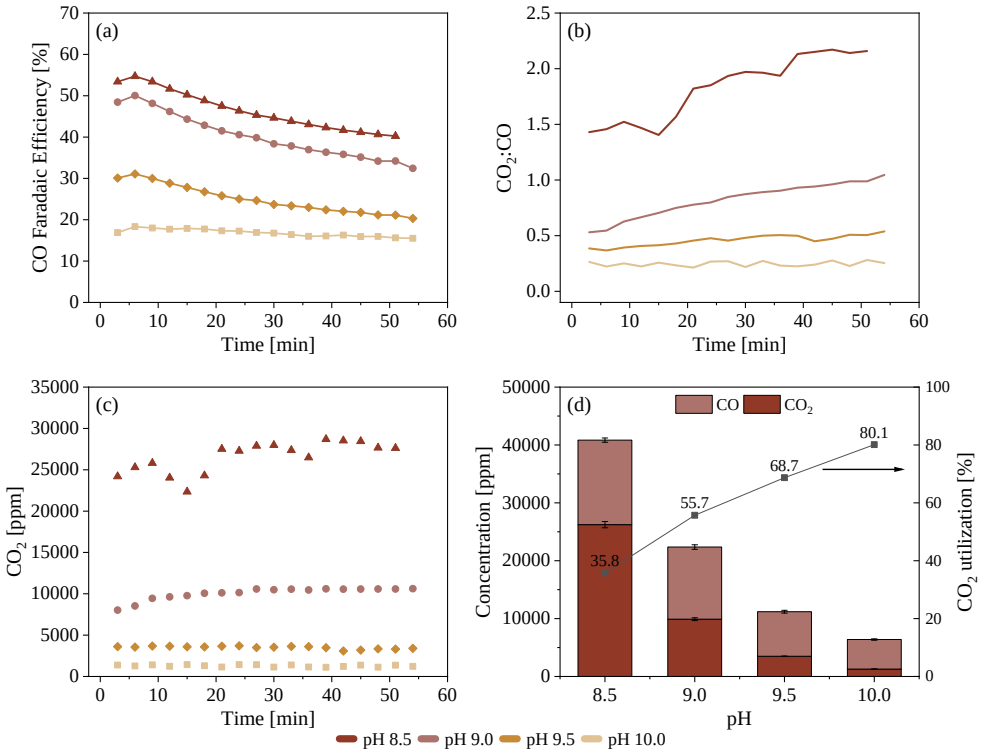

Figure 4.3: The effect of constant pH inlet conditions for a pH of 8.5, 9.0, 9.5, and 10.0 in a bicarbonate electrolyser using a Ag spray-coated cathode at a constant applied current of 100 mA/cm^2, and a fixed spacing of 135 μm between the membrane and the cathode. (a) Faradaic efficiencies towards CO, (b) CO_2:CO ratio over time, (c) total CO_2 concentration measured at outlet of the electrolyser in ppm, (d) total concentration carbon at the outlet of the electrolyser (CO products and CO_2 unreacted) in ppm and the CO_2 utilization ratio.

as can be seen in Figure 4.3(c). At a pH of 9.0, the concentration significantly decreases to only 10 000 ppm. At a pH of 9.5 and 10.0, the concentration of unreacted CO_2 in the outlet is approximately 2500 and 1300 ppm, respectively. The lower CO_2 concentration at a higher pH is due to the higher concentration of carbonate. CO_2 liberation from carbonate requires 2 protons instead of 1 proton required for CO_2 liberation from bicarbonate (Equation 4.1 and 4.2), making CO_2 liberation from carbonate more sluggish. Furthermore, the CO_2 reabsorption rate is higher at higher pH. These results are in line with unreacted CO_2 concentrations reported in earlier studies[63,64] The CO_2:CO ratio, reported in Figure 4.3(b), demonstrates that unreacted CO_2 concentration rises as CO production decreases over time. Furthermore, the cell potential was 3.6 ± 0.1 V for all four different pH conditions and remained stable over time. The average CO_2 utilization ratio was calculated based on the average CO and CO_2 concentrations measured at the outlet. The CO_2 utilization ratio was calculated using Equation 5.5 and represented in Figure 4.3(d).

$$\text{CO}_2 \text{ utilization ratio} = \frac{[\text{CO}]}{[\text{CO}_2]_{\text{unconverted}} + [\text{CO}]} \times 100\% \tag{4.5}$$

There is a very clear trend visible, showing an increased CO_2 utilization ratio at higher electrolyte pH. A utilization of 80was achieved at pH 10.0, compared to only 36% at pH 8.5. The CO_2 utilization ratio previously reported for carbon composite electrodes using 3 M $KHCO_3$ (pH 8) at 100 mA/cm^2 is around 20%–30%.[64] The higher CO_2 utilization ratio stems from the increased CO_2 reabsorption to form (bi)carbonates at higher pH concentrations, and not from the increase in CO_2 conversion to CO.

The results presented here contradict the hypothesis that a constant inlet pH of the catholyte will provide a constant product selectivity as suggested earlier.[64] Although there is a clear dependency of the FE_{CO} on the inlet pH, with a higher pH leading to a lower FE_{CO}, for all inlet pH values a similar decline in FE_{CO} over time is observed compared to the experiment with recycled electrolytes. Therefore, we hypothesize that the decline in FE_{CO} during experiments must stem from changes of the electrode. However, scanning electron microscopy (SEM) images (Figure C.6) showed no visible degradation of the catalyst surface. Additionally, through inductively coupled plasma spectroscopy (ICP) analysis (Table C.1), no Ag catalyst traces were found in the electrolyte post electrolysis, but very low quantities of Fe, Na and Cl were detected. Previous studies in CO_2 electroreduction have suggested that catalyst deactivation can occur due to the deposition of trace metal ions or organic impurities in the electrolyte.[127–129] By complexing these trace metal ion impurities with EDTA, the metal deposition can be suppressed.[129] Two control experiment using 0.02 M EDTA were performed. First, 15 hour experiments with 1 L of 3 M $KHCO_3$ recirculating electrolyte, and second a single-pass experiment using a 3 M $KHCO_3/K_2CO_3$ catholyte at a constant inlet pH 9 for 6 hours were conducted. The results were compared to the initial measurements wherein no EDTA was used and are presented in Figure 4.4. For the longer term experiment a linear decrease of FE_{CO} over time

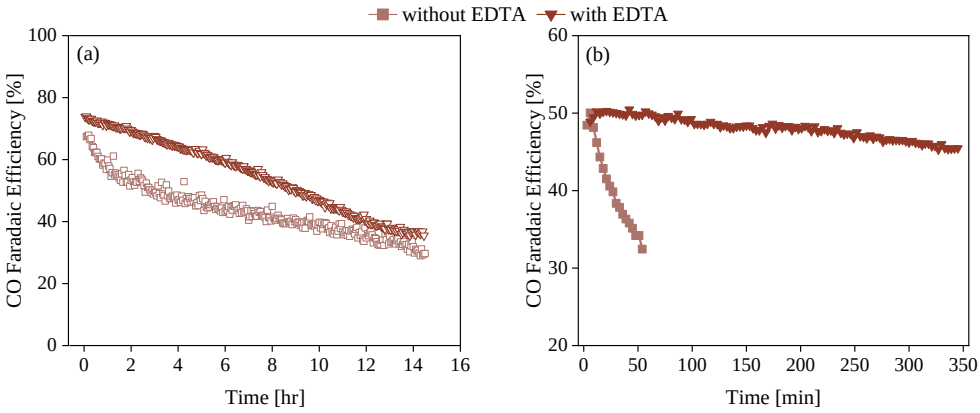

Figure 4.4: Stability experiments using 0.02 M EDTA at 100 mA/cm^2 using a Ag spray-coated cathode. Faradaic efficiency towards CO are shown comparing with and without the addition of EDTA for (a) longer-term 15 hour run using recirculating electrolyte, and (b) single-pass electrolyte at pH 9.

is observed. The larger initial drop at the start of the 15 hour experiment in which no EDTA was added is therefore very likely related to the deposition of trace metal impurities on the surface. The total decrease of the FE_{CO} for the experiment in which EDTA was used is larger than for the experiment in which no EDTA was used. It is hypothesized that this is related to the change in pH over time, which was measured to be larger for the experiment in which EDTA was added (see Figure C.5). A significant improvement in the CO selectivity over time is observed for the single-pass electrolyte control experiment. A total decrease of 5% FE_{CO} over 6 hours is measured. This confirms that the decline in FE_{CO} when recirculating the electrolyte is related to the pH and EDTA can significantly improve the stability of the system by removing metal trace impurities from the electrolyte and protecting the electrode active surface area. Due to the very low concentration of the impurities in the electrolyte salt (see Table C.2), it is difficult to measure the impurities on the electrode surface using X-ray photoelectron spectroscopy (XPS). Wuttig et al.[129] managed to measure the impurities by using a rotating disk electrode to increase the rate of diffusion-limited metal deposition. However, for the electrode used in this study, it is not feasible to measure the concentration of the impurities at the surface. Next to metal impurities such as Fe, other impurities such as Ca^{2+} and Mg^{2+} can also affect the stability of the electrolysis system at a larger scale. It is known from water electrolysis literature that Ca^{2+} and Mg^{2+} ions can adhere to the membrane, lowering the conductivity, or cathode surface, limiting the access to the electrode active sites.[130–132] A fundamental understanding of the electrode stability is highly desirable, including understanding the destabilization mechanisms for CO_2 reduction systems, caused by electrocatalytic

degradation and changes in the catalyst microenvironment evolution during long-term operation. [102,133,134]

4.3 Conclusion

In this study, the product selectivity of a bicarbonate electrolyser as a function of time as well as the role of the electrolyte pH has been evaluated. We observed that the product selectivity of the bicarbonate electrolyser at a fixed current density is not stable over time. Introducing a spacing between the membrane and the catalyst improves the product selectivity of the CO_2RR towards CO, however it does not improve the stability of the system. A decrease in FE_{CO} of 30% during the first three hours of operation is observed. Longer-term experiments of 15 hours show a continuous decrease in the product selectivity, related to the steady increase of the recirculated electrolyte bulk pH. It is found that the bulk electrolyte pH has a large effect on the overall selectivity, where a more alkaline pH lowers the selectivity towards CO. However, the bulk electrolyte pH was found to have no effect on the stability of the system. Electrolytes of four different pH values (8.5, 9.0, 9.5, and 10.0) were tested in a single-pass configuration. At a pH of 10.0, the product selectivity towards CO was constant over time, reaching a FE_{CO} of 18% compared to an initial 55% at pH 8.5. The total amount of CO_2 liberated at higher pH conditions is significantly lower, hence less CO_2 is available for the CO_2RR. This does improve the CO_2 utilization ratio of the system, which is only 36% at a pH of 8.5 compared to 80% at pH 10.0. Finally, a stable FE_{CO} selectivity was obtained by using EDTA to complex the trace metal ion impurities present in the electrolyte salt and prevent its deposition on the electrode surface. A significant improvement in stability was measured, with a small drop of 4% FE_{CO} during 6 hour operation.

Chapter 5

Enhancing the Electrolysis of a Bicarbonate Electrolyte at Increased Alkaline Conditions for Effective System Integration

This chapter has been submitted for publication.

Abstract

The integration of carbon capture and utilization technology is a promising approach towards creating a circular carbon economy. By capturing CO_2 in an alkaline solvent, a bicarbonate rich solvent is formed, which can serve as a feed for a bicarbonate electrolyser. In this way, the captured CO_2 is directly converting into value added chemicals using electrochemically CO_2 reduction and the energy intensive solvent regeneration step can be avoided. However, the performance of the bicarbonate electrolyser decreases as the electrolyte pH becomes more alkaline, limiting the feasibility of a deep electrochemical regeneration. Therefore, in this study, the performance of the bicarbonate electrolyser is investigated for more alkaline electrolytes (testing at pH 8, 9, and 10). It is shown that increasing the operating temperature (from ambient to 40 and 60 °C) decreases the faradaic efficiency towards CO (FE_{CO}) and CO_2 utilization, whereas it increases the total amount of released CO_2. However, the FE_{CO} and CO_2 utilization at 60 °C is improved by increasing the catalyst Ag loading as well as by adding 0.02 M EDTA to the electrolyte. Finally, a FE_{CO} of 53% at pH 9 is achieved with a CO_2 utilization of 52% at 60 °C. A similar improvement is achieved at electrolyte pH 8 and 10. These results are a promising next step for a successful integration of carbon capture and utilization using a bicarbonate electrolyser.

5.1 Introduction

The removal of anthropogenic CO_2 from our atmosphere is of great importance to mitigate climate change. Several mature capture technologies exist, such as reactive absorption for post-combustion carbon capture using amine based solvents.[16,19,20] Typically, a thermal regeneration step is performed to remove captured CO_2 from the solvent, which is highly energy intensive.[123,135,136] Next to carbon capture, CO_2 utilization will be crucial to replace the need for fossil fuels and to create a circular carbon economy. Electrochemical CO_2 reduction is a promising method to convert waste CO_2 into value-added chemicals such as CO, CH_4, and C_2H_4.[33,38] Currently, most research on CO_2 electrolysis focuses on gas-fed electrolysers, using a pure CO_2 input gas stream.

A promising method to eliminate the energy intensive regeneration step of CO_2 capture processes is integrating the carbon capture with direct utilization of the CO_2 rich solvent in an electrolyser.[50,137] This can be achieved by capturing the CO_2 in an alkaline capture solvent that reacts with the CO_2 to form a bicarbonate rich solvent (Equation 5.1). The (bi)carbonate solvent is then used in an electrolyser, where it undergoes two subsequent reactions. First, the CO_2 is liberated from the (bi)carbonate (Equation 5.2 and 5.3) near a bipolar membrane. Second, the CO_2 is converted at the cathode surface into value-added chemicals such as CO (Equation 5.4). The OH^- formed as byproduct of the CO_2 reduction reaction (CO_2RR) regenerates the (bi)carbonate capture solvent, such that it can be recycled back to the capture column for a new capture cycle.

$$\text{Capture reaction:} \quad CO_2(g) + CO_3^{2-} + H_2O \rightleftharpoons 2HCO_3^- \tag{5.1}$$

$$CO_2 \text{ liberation:} \quad H^+ + HCO_3^- \rightleftharpoons CO_2 + H_2O \tag{5.2}$$

$$2H^+ + CO_3^{2-} \rightleftharpoons CO_2 + H_2O \tag{5.3}$$

$$CO_2 \text{ reduction:} \quad CO_2 + H_2O + 2e^- \longrightarrow CO + 2OH^- \tag{5.4}$$

Recently, the electrolysis of bicarbonate solutions, commonly referred to as bicarbonate electrolysis, has attracted significant attention.[63,64,66,138] The bicarbonate electrolyser can provide a high CO_2 concentration near the catalyst surface compared to systems using dissolved CO_2, due to the in-situ CO_2 liberation that occurs near the electrode surface.[63,64] Currently, most research focuses on bicarbonate electrolysis using a near neutral catholyte with a pH of around 8 – 8.5. For instance, Lees et al.[64] achieved a faradaic efficiency towards CO (FE_{CO}) of 82% at 100 mA/cm^2 using a 3 M $KHCO_3$ and an optimized Ag GDE.

However, for the integration of a bicarbonate electrolyser with an alkaline capture step, the connecting liquid streams must be suitable for the operating conditions of both separate systems. For typical industrial potassium carbonate capture processes, alkaline inlet conditions (pH around 12) are required, while the pH remains greater than 9 at the outlet.[52,139] In contrast, bicarbonate electrolysis currently performs

best at lower pH values of around 8.5. In our recent work, a systematic investigation of the effect of pH on FE_{CO} was performed.[138] This showed that at a more alkaline electrolyte pH, the FE_{CO} decreases whereas the CO_2 utilization increases. In this case, the CO_2 utilization is defined as the amount of CO produced as a fraction of the sum of the CO and the liberated CO_2 that remains unconverted.

$$CO_2 \text{ utilization ratio} = \frac{[CO]}{[CO_2]_{\text{unconverted}} + [CO]} \times 100\% \tag{5.5}$$

This implies that a deep regeneration of the solvent with a bicarbonate electrolyser is challenging. This was further stressed recently by Almajed et al.[68], who highlighted the importance of understanding if and how the electrolyser can regenerate the capture solvent such that it can be recycled for a subsequent capture step.

An increase in selectivity of CO_2R towards CO in a bicarbonate electrolyser at more alkaline electrolyte pH can potentially be achieved by increasing the operating temperature and pressure or optimizing the catalyst and electrode. Zhang et al.[65] demonstrated that increasing the operating temperature from 20 to 70 °C at 100 mA/cm^2 leads to an increase in FE_{CO} from 59% to 78%, respectively. Furthermore, Xiao et al.[67] show an increased FE_{CO} of 46% in a carbonate electrolyte (pH between 10-11) at 200 mA/cm^2 using a Ag catalyst with a 25 μm thick TiO_2 layer, as compared to around 10% without added layer. The TiO_2 layer separates the membrane and electrode to achieve an optimal pH gradient. Moreover, they observe a different optimum flow rate at different current densities, articulating the importance of the flow rate on the product selectivity. At higher flow rates, it is hypothesized that more mixing will take place in the space between the electrode and bipolar membrane, decreasing the pH gradient. This will limit the total CO_2 liberation and hence the CO selectivity.

In this study, it is investigated how the product selectivity toward CO can be maintained at a higher electrolyte pH. The effect of the operating temperature is investigated for 3 different electrolyte pH conditions (8, 9, and 10). The electrolyte pH in the electrolyser was limited to 10 as only very limited amounts of CO were detected at this pH during initial measurements. Increasing the operating temperature can both increase the reaction kinetics and the CO_2 liberation.[81,140] However, it is still unclear how the operating temperature effects the FE_{CO} at different electrolyte pH conditions. Therefore, electrochemical experiments at constant current density and different temperatures (ambient, 40 and 60 °C) were conducted for all three electrolyte pH. It was found that at higher operating temperatures the FE_{CO} and the CO_2 utilization decreases, with larger concentrations of unreacted CO_2 measured in the outlet gas flow. The CO_2 utilization at higher operating temperatures is improved by increasing the Ag loading of the catalyst and by adding ethylenediaminetetraacetic acid (EDTA) to the electrolyte. This leads to a significant improvement from 30% to 53% FE_{CO} at pH 9 with a CO_2 utilization of 52% at 60 °C.

5.2 Results and Discussion

5.2.1 Changing the Operating Temperature for Different Electrolyte pH

Thus far, most work on bicarbonate electrolysis has used a 3 M $KHCO_3$ electrolyte.[63–65] However, as discussed previously by Almajed and co-workers[68], the composition of the electrolyte is an important parameter that effects the electrolyser performance. Therefore, in this study, initial testing was performed with varying electrolyte compositions to better understand electrolyte effects on the bicarbonate electrolyser performance. Electrolytes with a constant pH 9 and varying K^+ concentrations were prepared and tested, as can be seen in Figure D.4. The initial FE_{CO} is highest at a concentration of 1.5 M K^+ and more stable over time when compared to other K^+ concentrations. Moreover, the relatively largest CO_2 liberation can be obtained by the electrolyser when using 1.5 M K^+ electrolyte, as can be seen by the total CO and CO_2 concentration measured at the output of the electrolyser (see Figures D.6(a)). Therefore, this study used a constant K^+ concentration of 1.5 M K^+ throughout, while changing the pH of the electrolyte when comparing electrolyser performance at different conditions.

As discussed in our previous work[138], the electrolyte pH significantly influences the FE_{CO}. At a more alkaline electrolyte pH, the FE_{CO} decreases. For an effective integration of carbon capture and utilization, it is important to understand how the performance of the bicarbonate electrolyser can be improved at more alkaline electrolyte pH. One potential parameter to improve FE_{CO} is to increase the operating temperature, as temperature is known to increase the reaction kinetics and the CO_2 liberation.[65] In Figure 5.1, the FE_{CO} measured during 1 hour chronopotentiometry

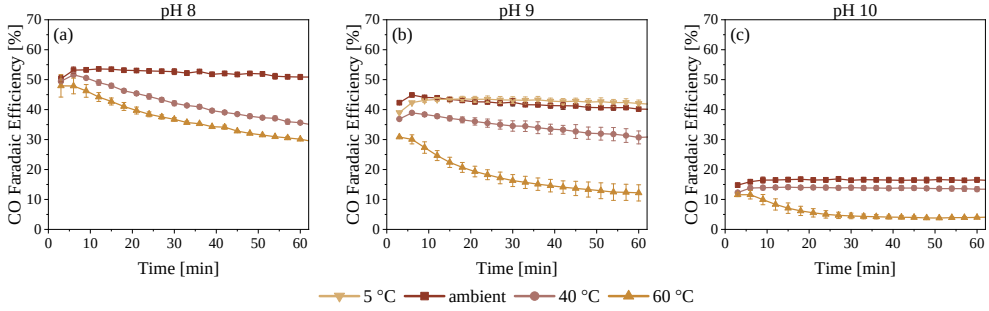

Figure 5.1: Bicarbonate electrolysis at constant current of 100 mA/cm^2 using a Ag spray-coated cathode and recirculating 1.5 M K^+ catholyte and 1 M KOH anolyte. FE_{CO} over time for varying operating temperature and three electrolyte pH conditions (a) pH 8, (b) pH 9, and (c) pH 10. Error bars indicated for duplicate measurements with a maximum error of ± 5% and a total FE of 90 ± 5%.

(CP) experiments at 100 mA/cm^2 is plotted as a function of time. The effect of the operating temperature for the 3 different electrolyte pH conditions using a 1.5 M K^+ concentration is shown. Overall, increasing the operating temperature decreases the FE_{CO} for all 3 pH conditions. Moreover, at higher temperatures, e.g. 60 °C, the overall stability of the electrochemical conversion towards CO decreases.

The effect of temperature is relatively small at pH 8, where the initial FE_{CO} is approximately 50% for all three operating temperatures. However, over time the difference in CO selectivity increases. Specifically, the product selectivity strongly decreases over time for higher operating temperatures resulting in a FE_{CO} of only 30% after 1 hour of operation at 60 °C. Similarly at pH 10, the differences in initial FE_{CO} at varying temperatures are relatively small. The initial FE_{CO} at ambient conditions is approximately 17%, which remains stable during the 1 hour experiment. At an operating temperature of 60 °C, the selectivity towards CO decreases from 11% to only 4% after 1 hour of operation. At pH 9 a larger difference in FE_{CO} is observed between the varying operating temperatures. At ambient conditions, the initial FE_{CO} reaches around 45% whereas the initial FE_{CO} is 39% and 30% at 40 °C and 60 °C, respectively. One extra temperature of 5 °C was added at pH 9, which shows a similar however slightly more stable selectivity towards CO as compared to ambient conditions.

In addition, the operating temperature plays an important role in the CO_2 liberation that occurs within the cell. By liberating more CO_2 at higher temperatures, the pH of the electrolyte will be increased. This is necessary for an effective integration of a capture and conversion process, such that the outflow of the electrolyser can meet the alkaline pH requirements necessary for the capture column. Furthermore, operating the conversion at higher temperatures is beneficial for the systems heat integration. In Figure D.7 and D.8, the total amount of unreacted CO_2 measured in the outflow of the electrolyser and the CO_2:CO ratio is shown for all temperatures and different electrolyte pH conditions as a function of time. At higher operating temperatures of 60 °C, the total amount of liberated CO_2 in the outflow of the electrolyser is significantly higher for all three pH conditions. However, under the current electrolyser operating conditions, not all of the liberated CO_2 is converted into CO. This is clearly shown by the CO_2 utilization as presented in Figure D.9. A clear decrease in CO_2 utilization as a function of increasing operating temperatures is observed for all electrolyte pH.

It is important to note that a previous study by Zhang et al.[65] showed an increase in FE_{CO} with increasing operating temperature for a porous Ag electrode and a 3 M $KHCO_3$ catholyte. The authors observed a large increase in FE_{CO} at higher operating temperatures, which is contradicting with the results observed in this study. It must be pointed out that the electrode used by Zhang et al. is very different in structure as compared to the Ag spray coated GDE used in this work. The total active surface area of the catalyst of the porous Ag is larger, which can play a crucial role in the increase in CO_2 reduction products. These results, combined with our observation that the CO_2 utilization decreases with increasing temperatures, are a clear indication that the optimal electrode structure is different for differing operating temperatures.

5.2.2 Improving CO_2 Utilization at Higher Temperatures

A standard electrolyte of 1.5 M K^+ at pH 9 and 60 °C was used to investigate how the CO_2 utilization and FE_{CO} can be improved, as these are relevant industrial operating conditions. First, the total Ag loading on the catalyst was increased from 1 to 6 and 12 mg/cm^2. In Figure 5.2(a), the FE_{CO} over time are presented for 1 hour CP experiments at 100 mA/cm^2. A significant increase in FE_{CO} was obtained for a Ag loading of 12 mg/cm^2 as well as a more stable product selectivity. It is hypothesized that since a larger amount of catalyst is available, more of the liberated CO_2 can be converted. However, increasing the Ag catalyst loading can not indefinitely increase the FE_{CO}. A control experiment with an increased Ag loading of 23 mg/cm^2 Ag was tested as can be seen in Figure D.10(a). A comparable selectivity towards CO is measured for 23 and 12 mg/cm^2 Ag.

In our previous study[138], the metal trace impurities present in the electrolyte salt were shown to play a crucial role in the stability of the bicarbonate electrolyser. Likewise, EDTA was added to the electrolyte in this study. In Figure 5.2(b) the FE_{CO} over time for 0.02 M EDTA addition to the electrolyte is compared to the base case electrolyte at 60 °C. Interestingly, the addition of 0.02 M EDTA significantly improves the FE_{CO}. It is of importance to not that adding EDTA to the electrolyte acidifies the solution. Therefore, a control experiment was performed for 0.02 M EDTA which was correct to pH 9 by adding 0.08 M KOH. As expected, this slightly lowers the FE_{CO} and serves a more accurate comparison. It is important to note

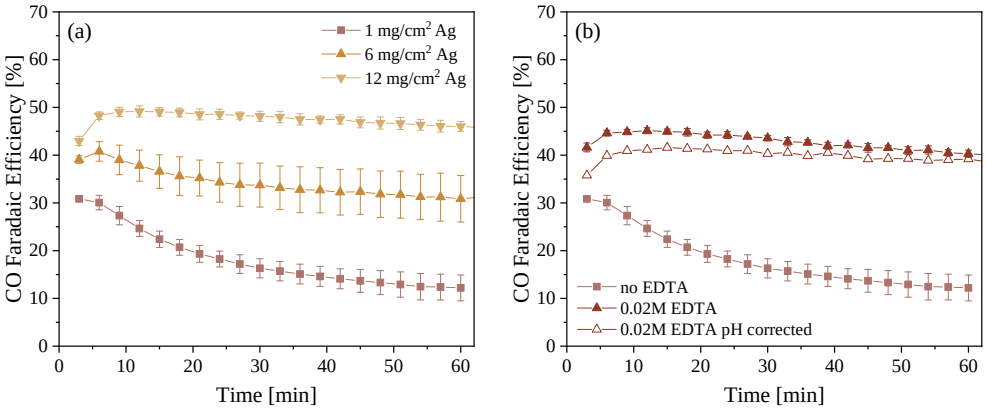

Figure 5.2: Performance of bicarbonate electrolysis at constant current of 100 mA/cm^2 and operating temperature of 60 °C using a Ag spray-coated cathode and recirculating 1.5 M K^+ catholyte at pH 9 and 1 M KOH anolyte. FE_{CO} over time for (a) changing catalyst Ag loading, and (b) increasing concentration of EDTA added to the electrolyte using catalyst loading of 1 mg/cm^2. Error bars indicated for duplicate measurements with a maximum error of ± 5% and a total FE of 90 ± 5%.

that the addition of 0.02 M EDTA to the electrolyte at ambient conditions does not improve the FE_{CO} significantly (see Figure D.11(b)). Moreover, an increase in overall stability of the electrochemical conversion toward CO is observed, as expected from previous work.[138]

Furthermore, as shown in Figure D.10(b), the addition of a higher concentration of 0.08 M EDTA further improves the FE_{CO}, however it decreases the overall stability. By adding a larger concentration of EDTA, the change in pH of the electrolyte is even larger. Therefore, initially more CO_2 is liberated and converted, but the stability of the system therefore drops. This trend is also observed for a lower pH electrolyte as presented in Figure 5.1(a). Next to that, a control experiment using a solid-supported iminodiacetate resin (Chelex) was performed to purify the electrolyte (see Figure D.10).[129] This resulted in a similar initial FE_{CO} as compared to using 0.02 M EDTA.

In Figure 5.3(a), the CO_2 and CO concentrations as well as the CO_2 utilization are compared for different Ag loadings and operating temperatures. As previously described, the CO_2 utilization decreases significantly when the operating temperature is increased. Increasing the Ag loading from 1 to 12 mg/cm^2 Ag at 60 °C shows an increase in the CO_2 utilization from 28% to 48%, respectively. To better understand how the Ag loading effects the CO_2 utilization, a control experiment with 12 mg/cm^2 Ag loading at ambient conditions was conducted. Figure D.11(a) shows that for 12 mg/cm^2 Ag loading at ambient conditions, the FE_{CO} does not significantly increase as compared to 1 mg/cm^2 Ag at ambient conditions. This is contrary to the trend that was observed at elevated temperatures of 60 °C. This is expected to be related

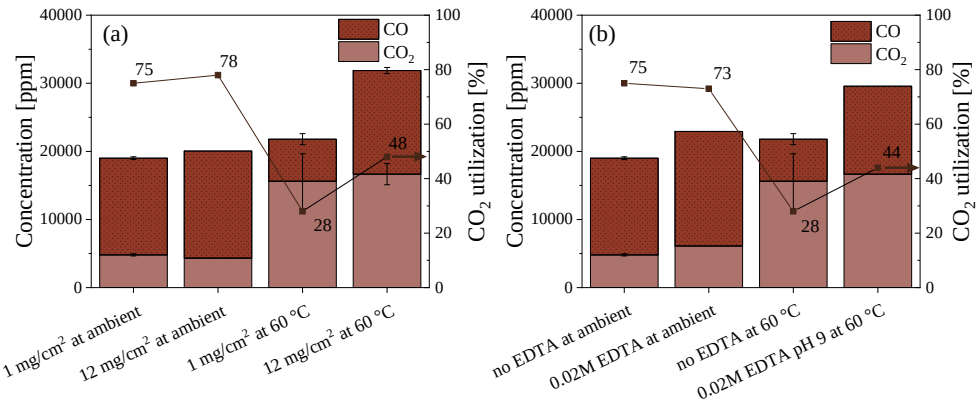

Figure 5.3: Measured CO_2 and CO concentration at the outlet of the bicarbonate electrolyser and calculated CO_2 utilization. Results presented at ambient temperature and 60 °C for (a) changing catalyst Ag loading of 1 and 12 mg/cm^2, and (b) increasing concentration of EDTA added to the electrolyte.

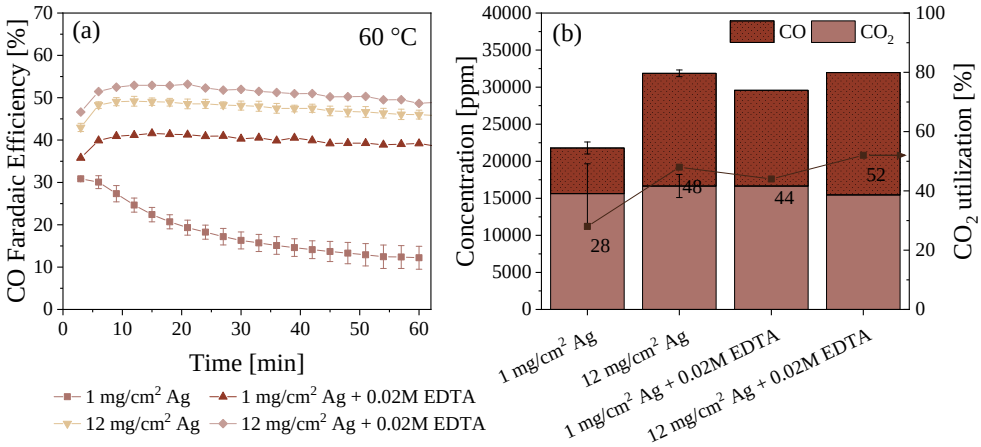

Figure 5.4: Performance of bicarbonate electrolysis at constant current of 100 mA/cm^2 and operating temperature of 60 °C using a Ag spray-coated cathode and recirculating 1.5 M K^+ catholyte at pH 9 and 1 M KOH anolyte. Comparing results for using different Ag loadings and increasing concentrations of EDTA added to the electrolyte. Presenting (a) FE_{CO} over time and (b) measured CO_2 and CO concentration at the outlet of the bicarbonate electrolyser and calculated CO_2 utilization. Error bars indicated for duplicate measurements with a maximum error of ± 5% and a total FE of 90 ± 5%.

to the increase in CO_2 liberation at elevated operating temperatures, which is not achieved at ambient conditions (see Figure 5.3(a)). Therefore, an increase in CO_2 conversion is only achieved for an increased Ag loading at 60 °C.

A similar comparison in CO_2 and CO concentration as well as CO_2 utilization was made for the addition of EDTA at ambient temperature and 60 °C, as can be seen in Figure 5.3(b). The CO_2 utilization at 60 °C improves from 28% to 44% for no and 0.02 M EDTA addition, respectively. No change in CO_2 utilization was observed at ambient conditions for no and 0.02 M EDTA addition to the electrolyte. Finally, a combination of a higher Ag loading (12 mg/cm^2) and 0.02 M EDTA (pH corrected) was tested using a 1.5 M K^+ electrolyte at pH 9, for which the results are presented in Figure 5.4. A further increase in FE_{CO} to 53% is observed as well as an increased CO_2 utilization rate of 52%. Surprisingly, the FE_{CO} exceeds the selectivity at ambient conditions using a 1 mg/cm^2 Ag electrode (see Figure 5.1(b)) and a relatively stable product selectivity is maintained during the 1 hour CP experiment.

The results presented above show the improvements obtained for the bicarbonate electrolyser using an electrolyte at pH 9. To understand how these improvements translate to both lower and higher electrolyte pH, the bicarbonate electrolyser was tested under similar conditions for electrolytes at pH 8 and 10. The results of the

optimized condition (using a 12 mg/cm^2 Ag loading catalyst and 0.02 M EDTA addition to the electrolyte) at 60 °C were compared to the base case conditions (using a 1 mg/cm^2 Ag loading without EDTA addition) at 60 °C, for all three pH. The results are presented in Figure D.13. A similar improvement in FE_{CO}, both in selectivity and stability, is observed for all three tested electrolyte pH. Moreover, an increase in CO_2 utilization is obtained.

By improving the FE_{CO} and increasing the total CO_2 liberation, the possibility of a successful integration of carbon capture and conversion is increased. However, the main challenge will remain at the electrolyser. It has proven difficult, based on the presented results, to release large concentrations of CO_2 at higher electrolyte pH. On the one hand, the electrolyser performance will decrease as the electrolyte pH increases, and the product output of the electrolyser will therefore consist of more H_2 and less CO. On the other hand, lowering the electrolyte pH inlet for the capture will decrease the capture efficiency and hence increase the sizing of the absorber column. Future work will focus on what the optimal pH swing of the recycling stream is, such that both the capture and the electrolyser can work efficiently.

5.3 Conclusion

In this study, the performance of the bicarbonate electrolyser at more alkaline electrolyte conditions was investigated using three electrolyte pH (8, 9, and 10). Firstly, the effect of higher operating temperatures on the performance of the bicarbonate electrolyser was tested at ambient conditions, 40 and 60 °C. It was found that the total amount of unconverted CO_2 in the outlet gas flow of the electrolyser increased significantly with increasing temperature. Consequently, at elevated operating temperatures, the FE_{CO} as well as the total CO_2 utilization decreased. Furthermore, the overall stability of the electrochemical conversion toward CO decreased significantly with increasing operating temperature. This effect was most notable for an electrolyte with pH 9. Therefore, an electrolyte with pH 9 was used for further investigation.

An increased CO_2 liberation in combination with an increased CO_2 utilization is beneficial for a more effective integration of carbon capture and conversion and improved heat integration. Therefore, the performance of the bicarbonate electrolyser was tested at 60 °C for different operating conditions to improve both the FE_{CO} and the CO_2 utilization. It was found that by increasing the Ag loading of the catalyst from 1 to 12 mg/cm^2, an improved CO_2 utilization and FE_{CO} as well as a more stable product selectivity was observed. Additionally, it was found that the addition of 0.02 M EDTA to the electrolyte created a similar improvement on both the CO_2 utilization and FE_{CO}. Finally, a combination of a higher Ag loading (12 mg/cm^2) and the addition of 0.02 M EDTA to the electrolyte was tested. This combination resulted in the best performance with an increase in FE_{CO} from 18% to 53% and a CO_2 utilization increase from 28% to 52% at electrolyte pH 9 and operating temperature 60 °C. A similar improvement, both in FE_{CO} and CO_2 utilization, was measured for electrolytes at pH 8 and 10 operated at 60 °C.

These results are a promising next step for a successful integration of carbon capture and utilization using a bicarbonate electrolyser. With an increase in CO_2 removal from the electrolyte, a deeper regeneration can be obtained, which is beneficial for the performance of the alkaline capture step. Future work will further investigate what an optimal pH swing could be for a feasible system integration, such that both the capture and the conversion process perform efficiently.

Chapter 6

A Dual Sorbent Direct Air Capture System with Integrated Electrochemical Conversion

This chapter has been submitted for publication.

Abstract

Direct air capture and CO_2 conversion will play a vital role in a future circular carbon economy. Here, we propose a novel system for integrated CO_2 capture and conversion through the combined use of solid and liquid sorbents, and demonstrates its technical feasibility. CO_2 is initially captured from the air using an amine-functionalised solid sorbent that is regenerated by rinsing with an aqueous carbonate-rich solution. The resulting bicarbonate-rich solution is fed to an electrolyser converting the bicarbonate electrolyte to syngas. Through our experiments, we demonstrate that the dual-sorbent system is capable of capture from air, as well as solid sorbent regeneration and CO_2 conversion. We use a simplified process model based on experimental results to explore the effects of scaling the components of the proposed system. We find that that the pH-swing between the rich and lean solutions is a dominant design parameter, which is almost exclusively governed by the electrolyser sizing. A small pH swing results in an improved electrolyser performance and beneficial syngas composition, whereas a large pH swing results in efficient solid sorbent use and decreased water loss. Our results further highlight the fundamental trade-offs that are present when designing integrated capture and conversion systems.

6.1 Introduction

Direct Air Capture (DAC) of carbon dioxide is expected to play a vital role in humanities roadmap to a net-zero CO_2 economy[141]; both as CO_2 removal technology and as carbon source for sustainable products. Efficiently capturing CO_2 from a stream as dilute as ambient air (≈425 ppm[142]) presents a formidable engineering challenge. Since its introduction by Klaus Lackner in 1999[143], a plethora of process routes for DAC have been suggested. The currently most prevalent ones are the amine-functionalised solid sorbent process as developed by, among others, Gebald[144] and Wurzbacher[145] and commercialised by Climeworks[146] and Global Thermostat[147], and liquid-based alkali scrubbing processes such as those developed by e.g., Zeman and Lackner[143] and Keith[148] and commercialised by Carbon Engineering.[149] Both processes offer unique advantages and disadvantages. However, large barriers remain for the gigatonne-scale implementation of DAC, most notably its high costs (≥1 000 $/tonne[150]) and energy demands (>500 kJ/mol.[151])

In the solid sorbent process, the incoming air is contacted with an amine functionalised porous material (e.g. cellulose or silica-based), on which CO_2 is adsorbed through the formation of carbamates and bicarbonates. A combination of elevated temperature (≥ 120 °C), reduced pressure (≥ 30 mbar) and optionally steam purging (Steam-assisted Temperature Vacuum Swing Adsorption, S-TVSA) can be used to release CO_2 and regenerate the sorbent. The major energy demand (up to 76%[152]) in this DAC process is associated with the thermal cycling of the sorbent, considering the combined effect of the large thermal capacity of the contactor, and the energy spent on evaporation of the adsorbed water. Furthermore, the elevated temperatures are associated with accelerated degradation of the sorbent, limiting its lifetime (1-3 years) and forming a major cost-driver.[153]

Contrarily, in the alkali scrubbing process the air is contacted with a sodium or potassium hydroxide solution in a cooling tower-like structure. The resulting carbonate solution is causticized with calcium hydroxide to regenerate the capture solution and form calcium carbonate crystals, which are calcined to release the CO_2. Finally, a steam slaking step converts the formed calcium oxide to calcium hydroxide, and closes the calcium loop. A major drawback of this process is the high temperature required for the calcining process (≈ 900 °C)[68], which is currently only achieved through combustion of natural gas. Such a fossil fuel-dependency is clearly undesirable in a carbon-neutral economy. Additionally, the direct contact of the capture solution and large volumes of air leads to evaporation of the solvent and thus loss of water from the system. Water losses can reach up to 20 tonne water per tonne CO_2.[154] With half of earth's population predicted to face severe water stress by 2030[155], losses should be minimised to conserve this critical resource.

Various steps can be taken to alleviate these challenges in DAC. The calcium loop with calcining step can be replaced by an electrochemical pH-swing to release the CO_2. This concept was for example demonstrated by Shu et al.[156], who employed a H_2-recycling electrochemical system to generate the sodium hydroxide solution and achieved a energy consumption of 374 kJ/mol CO_2. Sabatino et al.[157] modelled a

similar system using bipolar membrane electrodialysis instead, and predicted a minimum energy consumption of 236 kJ/mol CO_2. In experiments of the same process, Eisaman et al.[158] demonstrated values in a similar range.

Rather then only releasing the CO_2, electrolysis can be used to simultaneously release and convert CO_2 from a (bi)carbonate solution. This concept has been demonstrated extensively in for instance our own lab[138] and other research groups.[50,63,159] For bicarbonate electrolysis to CO, the smallest of C-products, Li et al. have demonstrated a faradaic efficiency (FE) of 82% at 100 mA/cm^2 and a cell voltage of 3.5 to 3.8 V, corresponding to an energy consumption of 859 kJ/mol CO produced.[64] Integration of the capture and conversion steps provides the added benefit of producing valuable products, potentially at a lower energy penalty than separate capture and conversion processes, e.g. through heat integration.[160] Simultaneously, process integration constrains the design space, leading to trade-offs that must be carefully considered.[161] This was highlighted by Almajed et al.[68] in a recent letter, who marked the pH-mismatch between the capture ($13.70 \leq$ pH ≤ 14.00) and conversion ($10.40 \leq$ pH ≤ 11.15) steps as one of the largest challenges for the integration of DAC and bicarbonate electrolysis.

Shu et al. proposed a dual sorbent system, where CO_2 is initially captured on an amine-functionalised solid, which is then rinsed with a sodium hydroxide solution to remove the CO_2, while the resulting bicarbonate solution is regenerated electrochemically.[162] This eliminates the thermal cycling of the solid sorbent and the associated energy penalty and sorbent degradation, while also avoiding the direct contact between the air and the alkali solution, reducing the resulting water loss by 63%. It should be noted that in this process, CO_2 is merely released as a pure stream and is not converted into higher-value products.

In this work, we demonstrate the integration of a dual sorbent system with bicarbonate electrolysis for direct air capture of CO_2 and conversion to CO. This process combines the aforementioned advantages of no thermal cycling and low water loss, while the use of an intermate amine-sorbent works to close the pH-gap between the capture and conversion steps. In Section 6.2, we outline the process and our set-up. In Section 6.3 we discuss our experimental results and use them in a simplified process model to explore the scaling of the integrated system. We demonstrate that the loaded solid sorbent can be regenerated with the electrolyser outlet stream. We also show how the electrolyser performance is strongly pH dependent and how this influences the capture step and the overall process. Finally, we provide a perspective on how this technology can further developed and contribute to sustainable development goals.

6.2 Process Outline

Figure 6.1 shows the process flow diagram of our proposed system for the integrated direct air capture (DAC) and electrochemical conversion using combined solid and liquid sorbents. Firstly, the CO_2 is captured by adsorption using an amine-functionalized solid sorbent. This sorbent provides a chemical adsorption mechanism with a large adsorption capacity, rapid kinetics, and stability under the relevant DAC conditions.[163] In this study, LEWATIT® VP OC 1065 is used, a commercially available, primary amine-functionalised sorbent frequently employed in DAC studies.[151,164] It forms a carbamate species with the captured CO_2 according to Equation 6.1,

$$2\mathrm{RNH_2} + \mathrm{CO_2} \rightleftharpoons \mathrm{RNH_3^+} + \mathrm{RNHCOO^-} \tag{6.1}$$

In this system, a mixture of (humidified) N_2 and CO_2 (425 ppm) was blown over the solid sorbent in the adsorber column until breakthrough was achieved. The outlet flow of the column was directly connected to a CO_2 gas analyser continuously measuring

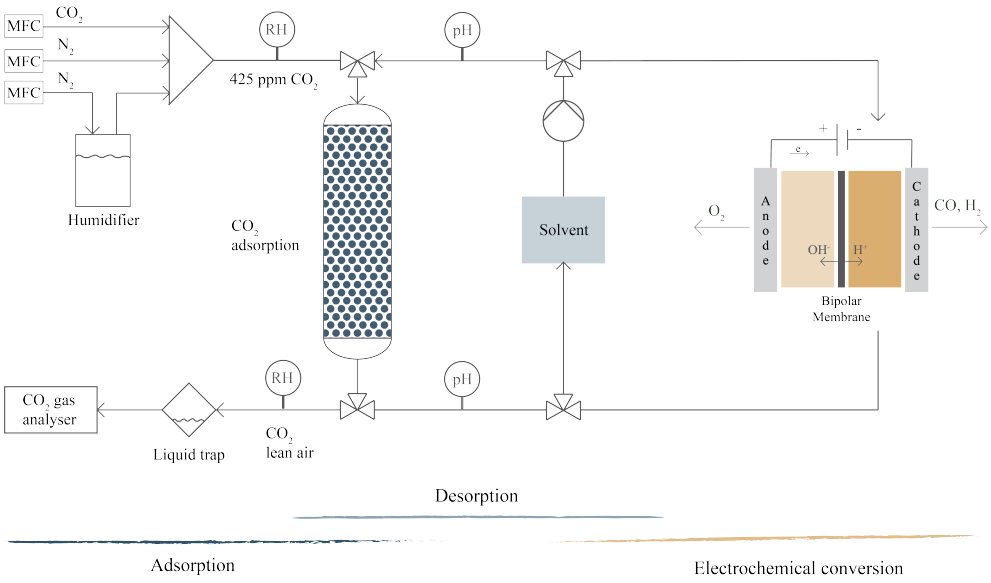

Figure 6.1: Process flow diagram of integrated DAC and electrochemical conversion. Through the various process steps, different parts of the system are active. During adsorption, simulated air is fed to the column, with its outlet connected to the CO_2 gas analyser. During desorption, the solvent is recirculated over the column. For the conversion step, the loaded solvent is recirculated through the electrochemical cell, with the gaseous output connected to a gas chromatograph.

the CO_2 concentration. Both before and after the column, the relative humidity of the air was monitored (see Figure E.1(a)).

An alkaline 0.5 M K_2CO_3 solution was used to rinse the saturated sorbent (see Figure E.1(b)). In this step, the adsorbed carbamate is hydrolysed and released from the resin to form $KHCO_3$, regenerating the sorbent according to Equation 6.2 and 6.3.[165] Though mechanistic studies for similar systems exist (e.g. Said et al.[165], Matsuzaki et al.[166]), the exact mechanism through which LEWATIT® VP OC 1065 is regenerated by the (bi)carbonate solution is unknown and is a subject for further study.

$$RNH_3^+ : HCO_3^- + K_2CO_3 \rightleftharpoons RNH_2 + 2KHCO_3 \tag{6.2}$$

$$RNHCOO^- + RNH_3^+ + H_2O \rightleftharpoons RNH_3^+ : HCO_3^- + RNH_2 \tag{6.3}$$

Secondly, the regeneration of the liquid capture solvent is achieved by electrochemical conversion of the solution using a bicarbonate electrolyser (see Figure E.2 and E.3). In the electrolyser, the CO_2 is first liberated in situ by the acidic environment close to the bipolar membrane (Equation 6.4 and 6.5). Next, the liberated CO_2 is reduced on the Ag catalyst (Equation 6.6).

$$\text{CO_2 liberation:} \quad H^+ + HCO_3^- \rightleftharpoons CO_2 + H_2O \tag{6.4}$$

$$2H^+ + CO_3^{2-} \rightleftharpoons CO_2 + H_2O \tag{6.5}$$

$$\text{CO_2 reduction:} \quad CO_2 + H_2O + 2e^- \longrightarrow CO + 2OH^- \tag{6.6}$$

The bipolar membrane provides a constant flux of H^+ to the cathodic compartment, creating the acidic environment required for the CO_2 liberation. This results in a higher local CO_2 concentrations near the catalyst surface as compared to system using dissolved CO_2, as the these systems are limited by the CO_2 solubility in water.[63,64] By removing the CO_2 from the solution, the pH is increased such that it can be recycled back to the capture step for a new cycle of resin regeneration. In Figure E.4, the full experimental setup that was used is depicted.

6.3 Results and Discussion

6.3.1 Experimental Results

The integrated capture and conversion process was tested consecutively for the direct air capture, both adsorption and desorption, and the conversion process. In Figure 6.2(a), the breakthrough curve for the amine-functionalized solid sorbent is presented for the initial dry sorbent (orange line) and the carbonate rinsed sorbent (yellow line). Breakthrough was obtained after 5-6 hours with a total capture capacity of 0.91 mmol CO_2/g sorbent using a fresh batch of the solid sorbent, in good correspondence with previous literature data.[164] After regeneration by rinsing with a carbonate solution, the measured breakthrough capacity was 0.87 mmol CO_2/g, indicating the sorbent bed maintained its absorption capacity. However, after regeneration, a significant decrease in the adsorption rate was observed. We observe that the particle bed remains saturated with liquid after draining due to the small particle size and resulting strong capillary forces, and then dries over the course of the adsorption time. Therefore, we hypothesize that the CO_2 mass transfer is slowed down due to the liquid blocking the pores. This effect increases the adsorption time for the second and any consecutive cycle.

Initial desorption experiments show a minimal decrease in pH of the solvent, due to the relatively low mass of CO_2 capture in the lab-scale capture column (using a total of 20 g of LEWATIT® VP OC 1065 sorbent). The optimal operating conditions for the bicarbonate electrolyser are at a near-neutral pH of around 8.5.[138] Therefore, the

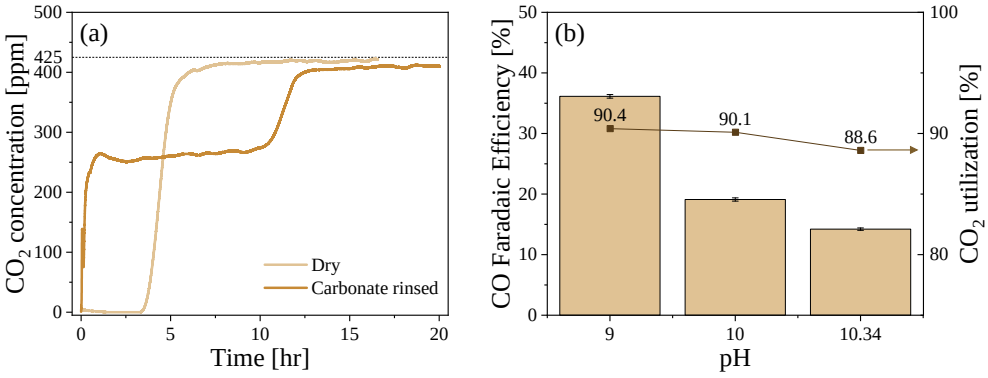

Figure 6.2: Experimental results for the integrated capture and conversion process. (a) Breakthrough curves for the fresh and dry adsorbent (orange line) and carbonate rinsed sorbents (yellow line). Electrolyser performance using the obtained electrolyte after desorption (pH 10.3) and electrolyte at pH 9 and 10 presented in (b) faradaic efficiency towards CO as a function of inlet pH (bars), as well as the CO_2 utilization (markers).

same solvent was ran through multiple desorption cycles, obtaining a progressively lower solvent pH each cycle. In Figure E.5(a) the dissolved inorganic carbon (DIC) concentration and pH of the solvent are presented as a function of four adsorption-desorption cycles. As the pH decreases, the CO_2 capture capacity of the solvent decreases, leading to a less deep regeneration of the solid sorbents with each cycle and simultaneously reducing the capture capacity of the solid sorbents. The solvent initially had a pH of 11.9 and dissolved inorganic carbon (DIC) concentration of 0.49 M. After the four cycles, the pH decreased to 10.3 and the DIC concentration increased to 0.74 M.

The final capture solution obtained after four adsorption-desorption cycles with a pH of 10.3 was then used directly as input for the electrochemical conversion in the bicarbonate electrolyser. The performance of the bicarbonate electrolyser, shown in Figure 6.2(b), is highly dependent on the electrolyte pH, therefore two other solvent pH points were included to highlight the change in performance as a function of pH. A faradaic efficiency (FE) towards CO of 14% is obtained at an inlet pH of 10.3, resulting in an energy consumption of 5383 kJ/mol CO produced and a voltage efficiency of 39.2% (see Section E.3 for calculation). The performance can be improved to 36% FE_{CO} (2131 kJ/mol CO, 41% voltage efficiency) by decreasing the pH to 9. The total output gas flow of the electrolyser includes a mixture of CO, H_2,and unconverted CO_2, creating a relevant syngas mixture. In Figure E.5(b), the total concentrations of CO and CO_2 measured at the outlet of the electrolyser are presented as a function of pH. These values were used to calculate the CO_2 utilization. Here, the CO_2 utilization is defined as the fraction of CO over the sum of CO and CO_2.[138] The utilization of CO_2 is approximately 90% for all three tested solvent pH. Therefore, the concentration of unconverted CO_2 in the outlet is limited.

6.3.2 Model Results

Next, we used our experimental electrochemical results obtained as input for a simplified process model. These calculations evaluate the process conditions at steady state, when the capture and conversion steps are in equilibrium with each other. They are based on the chemical equilibria between the dissolved and adsorbed carbon species during sorbent regeneration, and the electrolyser performance metrics (faradaic efficiency and CO_2 utilisation) observed in our experiments. We used these calculations to assess how the integrated system performs when the relative sizing of the capture and conversion devices are altered. A detailed description of the model calculations and parameters used is provided in Section E.4.

Here, we present our model results as a function of the normalised electrode area and normalised solid sorbent mass. The horizontal axis represents the electrode area available per volumetric liquid flow rate, and should be interpreted analogous to the electrolyser size or the residence time of the liquid in the device. The vertical axis represents the liquid-solid ratio during the regeneration step, and should be interpreted as the adsorption column size relative to the liquid flow. Our experimental conditions correspond to the central point in each figure ($A_e/\phi_V = 9$ s/mm, M_s/V_l

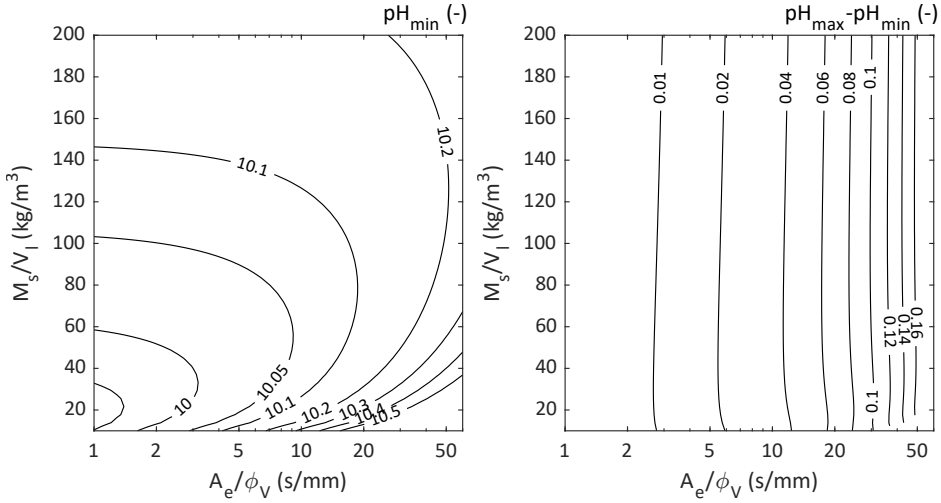

(a) (b)

Figure 6.3: Calculated results of pH of (bi)carbonate-rich solution (pH_{min}), (a) and pH-difference between (bi)carbonate-rich and (bi)carbonate-lean solutions (pH_{max} - pH_{min}), (b) as function of electrolyser size (A_e/ϕ_V, electrode area per volumetric solvent flow rate) and column size (M_s/V_l, sorbent mass per solvent volume). Results were obtained from the model described in the Section E.4.

= 100 kg/m^3).

Figure 6.3(a) shows the pH of the (bi)carbonate rich solution at the adsorber outlet. We observe almost semicircular isolines; for a constant electrode area, increasing the sorbent mass first decreases the outlet pH to a minimum value, then increases the pH again. For a small sorbent mass, the solvent pH is limited by the availability of CO_2 on the loaded sorbent. The lowest pH at the electrolyser inlet is achieved when the capture and conversion steps are carefully balanced. When the column is further over-sized, the sorbent working capacity (Figure 6.4(a)) is limited by regeneration in the electrolyser, again raising the pH and resulting in a decrease of electrolyser performance. The achievable pH swing between the rich and lean solutions (Figure 6.3(b)) is governed almost exclusively by the electrolyser sizing and is mostly invariant to the sorbent mass.

The most efficient use of the sorbent (Figure 6.4(a)) is found at a large electrode area, capable of achieving a large pH swing. For a small electrode area, the regeneration efficiency (fraction of adsorbed CO_2 removed from the sorbent during regeneration) can be as low as 1%, whereas a large electrode area can boost the regeneration efficiency as high as 60%, comparable to TVSA processes.[151] However, the high regeneration efficiency comes at the cost of decreased electrolyser productivity (Figure 6.4(b)). As described in previously, the electrolyser performance strongly

depends on the electrolyte pH. An excessively large electrode area results in a diminishing faradaic efficiency and CO_2 conversion, corresponding to a decreasing CO content in the product stream, both from increasing H_2 production and decreasing CO_2 conversion (Figure E.7). Combined, these effects confirm that careful balancing between capture and conversion steps is needed to make efficient use of the equipment.

Figure 6.5(a) shows the solvent productivity, which is governed by the (bi)carbonate-lean and rich stream pH values. It is largely determined by the pH swing between them, and therefore only dependent on electrode area. A notable exception is found for the combination of a large electrode area and small sorbent mass, in which case the solvent productivity decreases sharply. The high pH under these conditions places the process in a window where little bicarbonate-carbonate interconversion occurs, leading to a decreased uptake/liberation capacity and, by consequence, poor electrolyser performance.

One of the potential advantages of the presented process is a lower water loss compared to liquid-DAC, as it avoids direct contact between the solvent and air streams. In our experiments, we observed a water loss equal to the entire interstitial volume of the adsorber column. Applying this to our model, Figure 6.5(b) shows that in the current unoptimized column design, water loss is significantly higher than

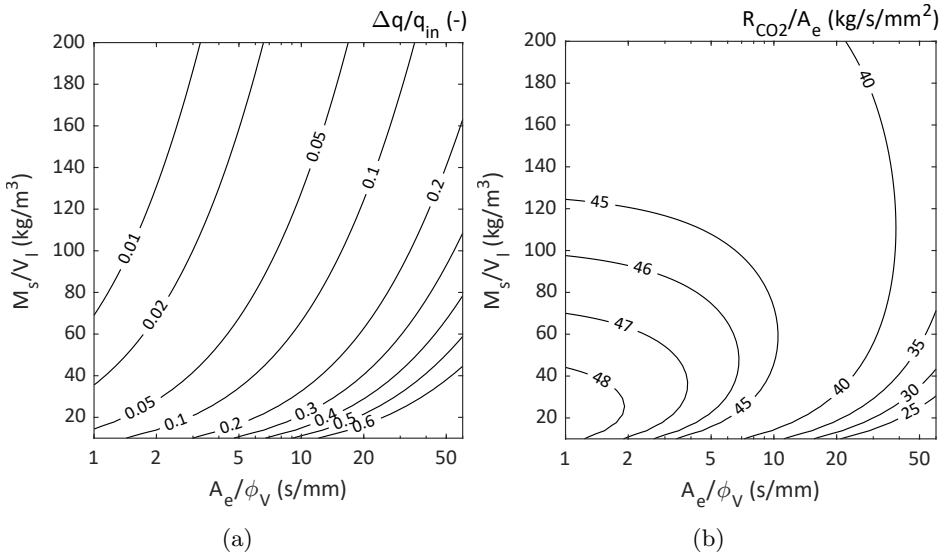

Figure 6.4: Calculated results of regeneration efficiency ($\Delta q/q_{in}$, loading difference before and after regeneration over initial loading, (a) and electrolyser productivity (R_{CO_2}/A_e, CO_2 capture mass rate over electrode area, (b) as function of electrolyser size (A_e/ϕ_V, electrode area per volumetric solvent flow rate) and column size (M_s/V_l, sorbent mass per solvent volume). Results were obtained from the model described in Section E.4.

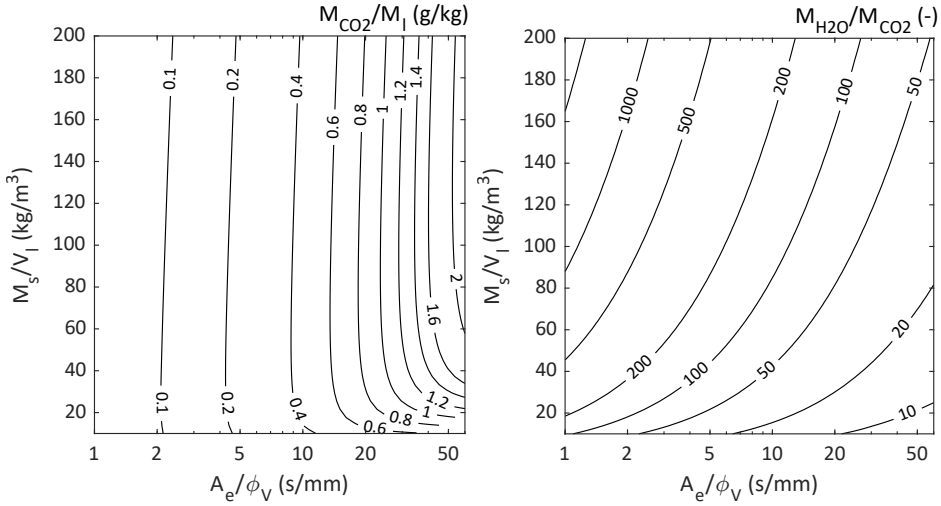

(a) (b)

Figure 6.5: Calculated results of solvent productivity (M_{CO_2}/M_l, CO_2 capture mass rate per solvent mass flow rate), (a) and water loss (M_{H_2O}/M_{CO_2}, water mass per CO_2 mass), (b) as function of electrolyser size (A_e/ϕ_V, electrode area per volumetric solvent flow rate) and column size (M_s/V_l, sorbent mass per solvent volume). Results were obtained from the model described in Section E.4.

in liquid-DAC, by a factor ≈8. By changing the sizing of adsorption and conversion steps, it can be reduced to 10-20 kg/kg, comparable to liquid-DAC.[154] The minimum water loss is found at maximum sorbent utilisation, meaning the sorbent goes through fewer regeneration cycles per kg CO_2 captured.

6.3.3 Future Perspective

The proposed novel integration of direct air capture using a dual sorbent system with the electrochemical conversion in a bicarbonate electrolyser is a promising yet challenging method. As previously discussed by Almajed et al.[68], the most challenging part of integrated carbon capture and conversion is the coupling of the electrolyte streams at a pH conditions that is suitable for both systems. The electrolyser product selectivity decreases with an increasing electrolyte pH, whereas the CO_2 capture capacity increases for an increased electrolyte pH. The integrated nature of the process provides a constrained design space.[161] A trade-off between an optimal capture and conversion conditions is therefore inevitable.

In the presented study, the electrolyser produces a mixture of CO, H_2, and unconverted CO_2, creating a syngas. The ratio in which this gas mixture is obtained determines the application of the syngas and therefore the relevance of the product.

Typically, a 2:1 H_2:CO syngas ratio is required for Fischer-Tropsch synthesis of long-chain hydrocarbon products, such as synthetic fuels.[167] Correction of the product gas composition can be achieved through for instance a high-temperature reverse water-gas shift step. However, preferable over adjusting the syngas ratio, we believe it is crucial to improve the performance of the electrolyser, specifically at a higher pH. By improving the FE at a higher pH, the pH swing can be enlarged, allowing for a more efficient use of the sorbent by consequence. We therefore see a role for the further development of electrocatalysts for bicarbonate reduction. Additionally, increasing the operating temperature is expected to improve the electrolyser performance as the CO_2 liberation from the (bi)carbonate solvent is enhanced and the reaction kinetics increased.[65]

One of the additional potential benefits of the proposed system is the decrease of water loss by elimination of direct contact between the liquid solvent and the air. However, our present results instead show a remarkably higher water loss, roughly 8 times higher than liquid-DAC. We have identified that this can be reduced to levels comparable to liquid-DAC by adjusting the electrolyser sizing. However, more importantly than sizing, the water loss can be reduced through improved column design. In our experiments and calculations, the water loss was equal to the static liquid holdup in the column after regeneration. Without any additional purging or drying steps, this is the water volume evaporated to the atmosphere during the subsequent adsorption cycle. In our current column design using commercial LEWATIT® VP OC 1065 sorbent, we observed the static holdup to be equal to the entire interstitial volume (37% of the column volume), due to the small particle size (≈ 500 µm[168]) and resulting strong capillary forces. In contrast, structured packings for trickle columns, such as the Mellapak Y packing often employed in liquid-DAC set-ups[169], can have a static holdup as low as 3%.[170] We envision that water loss can be reduced up to an additional factor 10 by optimising the sorbent material and shape (increasing particle size and contact angle) and operating procedure.

Lastly, one parameter left untouched in our analysis is the type of solid sorbent material used. Our choice was based on a commercially available ion exchange resin (LEWATIT® VP OC 1065), functionalised with benzylamine groups (pKa = 9.34[171]). Choosing a material with a lower pKa will likely result in a lower absorption capacity, but will also allow for a deeper regeneration at lower pH. This once again underlines the fundamental trade-off between the capture and conversion steps.

6.4 Conclusion

In this work, we have demonstrated a novel dual-sorbent system for integrated Direct Air Capture and conversion of CO_2 for the production of syngas from ambient air and (renewable) electricity. Through the combination of a solid, amine-functionalised sorbent and an alkalic solvent, this system is able to bridge the pH-gap between the capture and conversion steps found in single-sorbent systems.[68] Based on our experimental and model results, we conclude that the proposed system is technically feasible and capable of producing syngas with limited (<13 mol%) CO_2 content, albeit at relatively high (H_2:CO ≈ 4-5) syngas ratios. The pH swing between the capture and conversion steps is a vital design parameter, and is mainly governed by the electrolyser sizing. A large pH swing results in diminishing electrolyser productivity through decreased faradaic efficiency and CO_2 utilisation. Conversely, a small pH swing results in inefficient use of the solid sorbent and excessive water loss. As such, a careful trade-off between these opposite effects must be made when considering the design of this integrated capture-conversion process. We identified the electrolyser faradaic efficiency at high pH (>9) as the main constricting factor for the process performance, highlighting a focus area for future electrocatalysis development. Furthermore, to reduce water losses to feasible levels, it is vital to revisit the packing design and minimise capillary effects.

Chapter 7

Perspective on Integrated Carbon Capture and Conversion Systems

This chapter is in preparation for submission.

Abstract

This final chapter on the feasibility of integrating carbon capture and bicarbonate electrolysis discusses the hurdles related to carbonate capture and bicarbonate electrolysis and provides insight into possible optimization options. The main challenges are related to the slow reaction kinetics of the carbonate capture system and the decrease in electrochemical CO_2 conversion in more alkaline electrolytes. The capture performance can be improved by increasing the operating temperature and pressure, as this increases the reaction kinetics. The effect of temperature and pressure on the performance of the bicarbonate electrolyse have, until now, been discussed separately. Therefore, in this chapter, a bicarbonate electrolyser is tested at elevated temperatures (60 °C) and pressure (5 bar) at varying electrolyte pH values. Experimental results show that increasing the temperature and pressure only improves the FE_{CO} when using an electrolyte pH above 10. At a lower electrolyte pH, increasing the pressure does not improve the FE_{CO}. Overall, significant reductions of the cell potential and improvements of the FE_{CO} at higher electrolyte pH are crucial challenges that need to be overcome in order for the system to be feasible.

7.1 Introduction

In the recent literature there is a significant interest in using bicarbonate electrolysis to integrate CO_2 capture and conversion. In this thesis, bicarbonate electrolysis has been discussed extensively in Chapters 4 to 6. Bicarbonate electrolysis performance was discussed in terms of (i) the stability toward CO production during electrolysis and (ii) the effect of electrolyte pH conditions. The performance of the bicarbonate electrolyser significantly decreases as the electrolyte pH increases, making the integration with a capture system more challenging. The possibility of integrating a bicarbonate electrolyser with a direct air capture system by using a dual sorbent system was investigated. Here, the performance of the bicarbonate electrolyser is the dominating design parameter as this controls the CO_2 capture capacity in the following cycle.

For instance, Almajed et al.[68] examined the integration of a direct air capture (DAC) with a bicarbonate electrolyser by using mass-balance, microkinetic, and multiphysics modelling. They conclude that the accumulation of bicarbonate in the solvent stream, caused by the inability of the electrolyser to convert enough bicarbonate into products, leads to a decrease in capture efficiency in the capture column. Therefore, the sizing of the capture column significantly increases in contactor volume to achieve sufficient carbon capture. The authors suggest to add an external pH adjustment step after both the capture and conversion process. However, the economic feasibility of an integrated system with external pH correction processes is questionable.

Moreover, Gutierrez-Sanchez et al.[159] performed a proof-of-concept study for the integration of a DAC system with electrochemical conversion of CO_2 to formate. A $FE_{formate}$ of 16% was achieved at 50 mA/cm^2. Furthermore, Kim et al.[172] investigated the integration of carbon capture and conversion using a bicarbonate electrolyser in a small scale lab setup. They designed a packed-bed capture column for the reactive absorption of CO_2 in a carbonate rich solution coupled to a bicarbonate electrolyser. A simulated flue gas stream of 20% CO_2 and 80% N_2 at 1000 sccm was used in combination with a 1.0 M K_2CO_3 capture solution at 100 mL/min (gas/liquid volume ratio of 10). The solvent was circulated between the electrolyser and capture column continuously. At the start of the experiment, the solvent pH was around 11 and the performance of the bicarbonate electrolyser was limited to only 5% faradaic efficiency towards CO (FE_{CO}) at 100 mA/cm^2. After 23 hours of recirculating the solvent, the pH dropped to around 9 and the FE_{CO} increased to 35%. The addition of 0.1 M piperazine and glycine both helped in increasing the capture rates by 4 and 2 times for piperazine and glycine, respectively. However, the use of 0.5 M piperazine suppressed the FE_{CO} to 5%, whereas when using 0.5 M glycine the FE_{CO} remained around 25%. A capture efficiency of only 1.5% is obtained when doping the 1.0 M K_2CO_3 solvent with 0.1 M glycine and using a simulated flue gas stream of 20% CO_2 at 1000 sccm. The capture efficiency of the unpromoted solvent is not reported.

Based on this, two main challenges can be identified for the integration of capture and conversion systems. First, the reaction kinetics of carbonate capture are slow and promoters such as the tested piperazine and glycine, can only marginally im-

prove this. Second, the electrolyser performance at more alkaline solvent conditions decreases significantly, and therefore no deep regeneration of the capture solvent can be achieved. This limits the capture capacity when recycling the solvent back to the capture column.

In this chapter, these challenges are addressed and quantified. Firstly, the reaction kinetics of the carbonate capture system are discussed and how they can be improved by using different types of promotors or higher operating temperature and pressure based on the literature available. Secondly, the performance of the electrolyser at elevated temperatures and pressure is investigated experimentally. Increased operating temperatures can improve the CO_2 liberation and CO_2 utilization. Pressure is known the increase the CO_2 solubility and is therefore expected to improve the electrolyser performance, specifically at more alkaline electrolyte pH. Then, based on these improvements, the feasibility of an integrated system design is discussed. Finally, the findings are compared to the current non-integrated system design for capture and conversion in terms of energy requirements.

7.2 Enhancing CO_2 Capture Efficiency

In Figure 7.1, the results of explorative carbonate capture experiments are presented. A hollow fiber membrane contactor (2.5 x 8 Extra-Flow Membrane Contactor with X50 membrane fiber, LiquiCel) was usedg in counter flow mode. The liquid flow rate was kept constant at 50 mL/min, in line with the electrolyte flow rate used in the bicarbonate electrolysis experiments. The gas flow rate was varied to obtain for a high CO_2 capture efficiency (>80%). A simulated flue gas mixture of 20% CO_2 with N_2 was used as input gas. Two capture solvents were used: 1 M KOH and 1 M K_2CO_3. The reaction kinetics for CO_2 capture using K_2CO_3 solution are significantly slower compared to KOH solvents.[52,53] Therefore, the gas flow rates used for capturing CO_2 with a K_2CO_3 rich solution are much lower to ensure enough contact time between the gas and liquid as compared to KOH. A decrease in pH from 12.4 to 10 is obtained using a KOH capture solvent while maintaining a capture efficiency of 83%. When using a 1 M K_2CO_3 solvent, the initial pH was 10.8 and decreased to 10.6 in order to maintain a capture efficiency of 84%.

These results confirm that the capture of CO_2 with a carbonate rich solution is limited by the CO_2 concentration in the gas flow. The molar flux of CO_2 transported through the membrane area increases with an increasing G/L ratio, whereas the capture efficiency decreases. In industry, this results in taller absorber columns to achieve a high absorption efficiency by increasing the gas-liquid contact time, resulting in high capital investment costs.[52,173] Therefore, research has focused on finding different methods to increase the kinetics by using promotors. Monoethanolamine (MEA), piperazine (PZ), boric acid, and carbonic anhydrase (CA) are the most widely studied promoters in carbonate solutions. Other methods that have shown improved reaction kinetics are by increasing the operating temperature and pressure.

MEA is a widely used solvent for CO_2 capture due to its fast kinetics, large absorp-

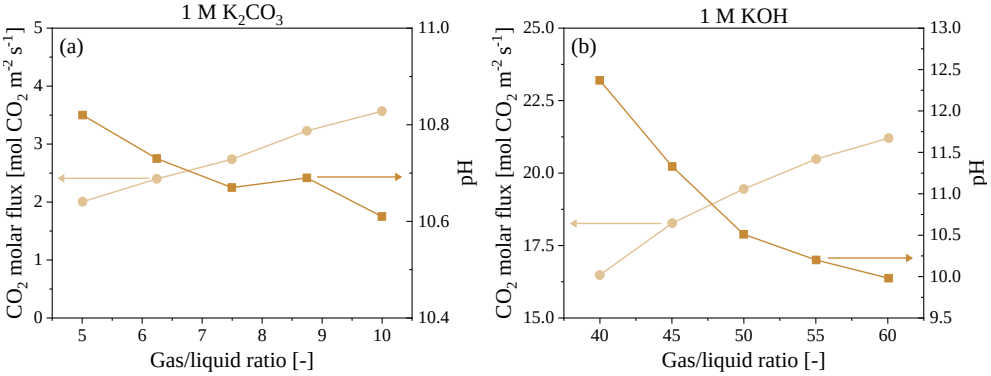

Figure 7.1: CO_2 molar flux [mol CO_2 $m^{-2}s^{-1}$] (circles) and solvent pH (squares) of carbonate capture system using a hollow fibre membrane contactor for (a) 1 M K_2CO_3 and (b) 1 M KOH solvent. The gas flow rate is varied during the experiment, whereas the liquid flow rate is fixed at 50 mL/min passing through the system in single-pass.

tion capacity, and good selectivity. However, MEA is also known to cause corrosion and degradation. Therefore, several studies have used a mixture of carbonate and MEA, because of the slow reaction kinetics of carbonate, and shown improved capture performance.[139,174] Piperazine (PZ) is a amine promotor that is comparable to MEA in performance. It has low degradation and corrosion properties and a good promoting performance.[52] The solubility of PZ is limited, therefore precipitation issues have been observed that cause a decrease in capture efficiency and an increase in potential operational issues.[52] Promotors such as boric acid have the advantage of being environmentally friendly and affordable. However, adding an acid to the carbonate solutions reduces the solvent pH. Therefore, the capture capacity of the solvent decreases as the OH^- concentration decreases.[173,175] Lastly, carbonic anhydrase has been shown to improve the CO_2 absorption, however, only at low temperatures (298 K).[52,176] Increasing the operating temperature will lead to the denaturation of the enzyme, diminishing the promoting properties.

In a recent study by Fink et al.[177] the influence of using a carbon capture solution containing carbonic anhydrase (CA) in an electrochemical flow cell was investigated. It was shown that the presence of CA decreased the faradaic efficiency towards CO (FE_{CO}) to 16%, in comparison to 56% when using a bicarbonate solution without CA at 100 mA/cm^2. This is due to deactivation of the electrode surface by CA. This demonstrates a major challenge for using promotors in the carbonate capture system when integrating with electrochemical conversion systems. Furthermore, it is hypothesized that the in-situ liberated CO_2 inside the bicarbonate electrolyser is again captured by the promotor, limiting the CO_2 available for the CO_2RR. A possible solution could be to remove the promotors from the carbonate solution prior

to feeding the solvent to the electrochemical cell. This can be achieved by using a selective membrane to remove the promotor from the solvent after the capture step.[178] In this way, the promotor maintains in the capture cycle without disrupting the electrochemical conversion process.

Next to adding promotors to the carbonate capture solvent, the reaction kinetics can also be enhanced by increasing the operating temperature, which is also known as the hot potassium carbonate (Benfield) process.[52] Operating at higher temperatures increases the carbonate solubility and improves the absorption of CO_2.[53,139] Capsol[179] has developed a commercial hot potassium carbonate capture technology and build units capturing over 200,000 tons of CO_2 per year, operating their process at 8-20 bar and 110-120 °C and a gas/liquid mass ratio of 0.1.[180] With their technology, a reduction in energy cost for the capture of CO_2 of 12.5% is achieved.

When integrating bicarbonate electrolysis with a hot potassium carbonate capture process, the electrolyser is ideally operated at the same temperature and pressure. In Chapter 5, it was shown that the performance of the electrolyser can be improved in terms of CO_2 liberation and CO_2 utilization when increasing the temperature to 60 °C. A previous study by Zhang et al.[65] investigated the effect of temperature and pressure separately. However, the combined effect of temperature and pressure has not yet been studied. Therefore, in this chapter, the experimental performance of the bicarbonate electrolyser at a combined high temperature (60 °C) and pressure (5 bar) is investigated. The results are discussed in the next section.

7.3 Bicarbonate Electrolyser Performance at Industrially Relevant Operating Conditions

In Figure 7.2, the faradaic efficiency towards CO (FE_{CO}) over time is presented for varying operating conditions and electrolyte pH. All experiments were conducted for 1 hour at a constant current density of 100 mA/cm^2 and operating temperature of 60 °C. The electrolyte pH was varied to 8, 9, 10, and 11 while maintaining a constant K^+ concentration of 1.5 M.

Figure 7.2(a) compares the electrolyser performance at different pH using a 1 mg/cm^2 Ag electrode and a 12 mg/cm^2 Ag electrode with 0.02 M EDTA added to the electrolyte. The increased Ag loading increases the active sites of the electrode available for the in-situ liberated CO_2 to be converted, whereas EDTA complexes the metal trace impurities present in the electrolyte. Consequently, the metal trace impurities cannot deposit on the electrode surface. In this way, a significant improvement in product selectivity is obtained for all measured electrolyte pH values. At pH 8, the selectivity increases from an initial FE_{CO} of 47% to 65%. However, the selectivity decreases slightly over time for both electrode conditions with a final FE_{CO} of 54% when using 12 mg/cm^2 and 0.02 M EDTA. This is expected to be due to the increase in electrolyte pH as CO_2 is being used during the experiment, since a volume of only 200 mL is continuously recirculated through the electrolyser. A similar improvement is observed for electrolyte with pH 9, for which the initial FE_{CO} of 30% increased to

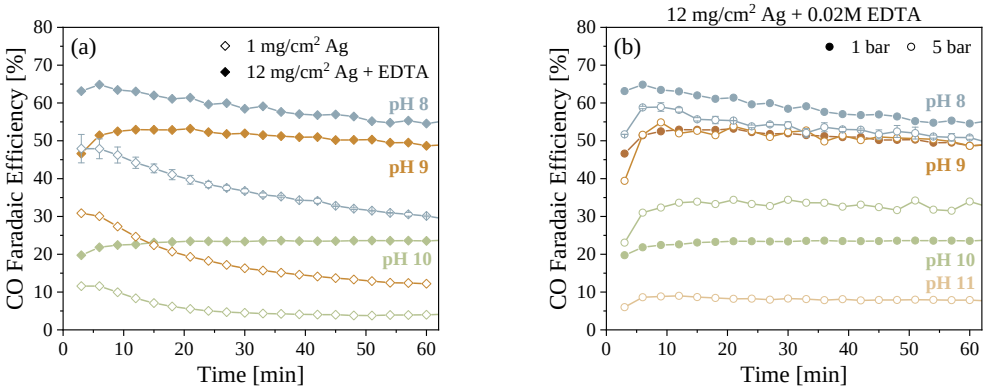

Figure 7.2: Product selectivity towards CO over time for bicarbonate electrolysis at 100 mA/cm^2 and 60 °C using a Ag spray-coated electrode and recirculating 1.5 M K^+ catholyte at varying pH for (a) 1 mg/cm^2 Ag (open diamonds) electrode and 12 mg/cm^2 Ag electrode with 0.02 M EDTA addition to the electrolyte (closed diamonds), and (b) 12 mg/cm^2 Ag electrode with 0.02 M EDTA addition to the electrolyte at 1 bar (closed circles) and 5 bar (open circles). Error bars indicate duplicated measurements with a maximum error of ± 5%.

53%. Again, a more stable product selectivity is obtained when increasing the Ag loading and adding EDTA to the electrolyte. Furthermore, at electrolyte pH 10 the FE_{CO} improved to 23% with a constant product selectivity over time.

Figure 7.2(b) shows the effect of the operating pressure on the performance of the bicarbonate electrolyser. The most optimal electrolyser configuration (12 mg/cm^2 Ag loading and 0.02 M EDTA addition to the electrolyte) was tested at 5 bar for an electrolyte pH of 8, 9, 10, and 11. Increasing the operating pressure increases the CO_2 solubility which enhances the CO_2 reduction reaction. It is observed that at a more alkaline pH of 10, the effect of pressure has a significant impact on the FE_{CO}. An increase in FE_{CO} from 23% at 1 bar to 34% at 5 bar was achieved. When increasing the pH to 11, the effect of pressure is very limited. At ambient conditions, the FE_{CO} obtained when using an electrolyte at pH 11 is only 8% (see Figure F.2) and the total CO_2 utilization is 93% (see Figure F.3). Therefore, increasing the pressure does not improve the performance, since there is not enough in-situ liberation of CO_2 happening at these alkaline conditions. Hence, the solubility of CO_2 can also not be improved further.

Interestingly, at a lower electrolyte pH of 8 and 9, the effect of pressure is minimal as well. No change in FE_{CO} was observed for pH 9 and at pH 8 a small decrease was measured. This indicates that the availability of CO_2 near the electrode surface is not limiting at a lower electrolyte pH. Figure 7.3 shows the total CO and CO_2 concentrations at the outlet of the electrolyser and the calculated CO_2 utilization as

defined by Equation 7.1

$$\text{CO}_2 \text{ utilization ratio} = \frac{[\text{CO}]}{[\text{CO}_2]_{\text{unconverted}} + [\text{CO}]} \times 100\% \tag{7.1}$$

As expected, there is a minimal change in the CO and CO_2 concentrations and CO_2 utilization is for both electrolyte pH 8 and 9 when compared the operation at 1 bar and 5 bar. At pH 10, an increase in total CO_2 liberation is measured as well as an increase in CO_2 utilization. For pH 11, the CO_2 liberation is very low, resulting in a total CO_2 utilization of 97%.

The results obtained in this study at higher operating pressures are contradicting with the results previously reported by Zhang et al.[65] They observed a strong increase in FE_{CO} when increasing the pressure from 55% at 1 bar to 95% at 4 bar. The electrolyte concentration used by Zhang et al. was 3 M $KHCO_3$ instead of 1.5 M K^+ that was used in this study. Therefore, a control experiment was performed using a similar electrolyte, operated at 5 bar (see Figure F.2). No significant differences in performance are observed in comparison to the electrolytes at 1.5 M $KHCO_3$. Therefore, the difference is performance can be related to the electrode used. In our experiments, a spray-coated Ag GDE electrode is used, whereas Zhang et al.[65] used a porous electrode. It is expected that the flow behaviour inside the electrode and in between the membrane and electrode is very different, resulting in a different pH gradient. This affects the CO_2 liberation and CO_2 available for the CO_2 reduction reaction at the catalyst surface. Nevertheless, the differences in performance are very large. Therefore, further investigation into the effect of operating temperature and pressure for the electrolytic reduction of bicarbonate is required.

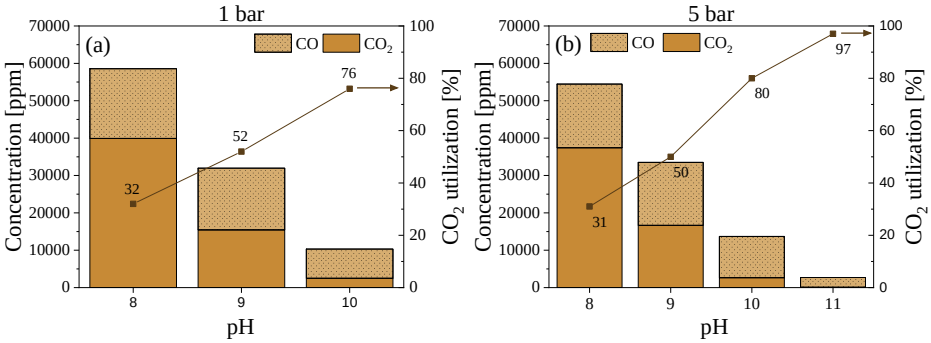

Figure 7.3: Concentration of CO and CO_2 at the electrolyser gas outlet measured during the electrolysis of bicarbonate electrolyte at 60 °C using 1.5 M K^+ at varying pH and constant current of 100 mA/cm^2 and the calculated CO_2 utilization using a 12 mg/cm^2 electrode and 0.02 M EDTA addition to the electrolyte at (a) 1 bar and (b) 5 bar.

7.4 Perspective

Effective regeneration of the solvent to achieve optimal operating conditions for both the capture step and conversion step is the biggest challenge when integrating a carbonate capture system with an electrochemical conversion. An improved electrolyser performance was achieved at higher operating temperature (60 °C) and pressure (5 bar), with larger CO_2 liberation as well as CO_2 utilization, while maintaining a reasonable FE_{CO}. However, it is yet unclear whether these improvements sufficiently improve the solvent regeneration to make the system integration feasible.

The electrolyte pH is the dominating parameter that defines the efficiency of the integrated process. When operating at an alkaline pH, the capture capacity is high, whereas the FE_{CO} obtained in the bicarbonate electrolyser is low. The optimum switches when the electrolyte pH is near neutral, where a high CO_2 conversion (FE_{CO}) is obtained and a low capture capacity. In Figure 7.4, these opposing operating performances are visualized as a function of electrolyte inlet pH. With these conditions in mind, three operating scenarios for an integrated capture and conversion system are proposed.

In the first scenario, the electrolyser performance is maximized and the electrolyte pH used remains within a range of 8 to 10. This results in a favourable H_2:CO product ratio, while penalizing the capture capacity. Consequently, this would result in a relatively large capture column and increased use of solvent. A second scenario would be to maximize the capture fraction and operate only at more alkaline pH range between 9 and 11. Under these circumstances, the H_2:CO ratio and the electricity costs for the electrolyser will be high. Additionally, in a third scenario, a pH mid-range could be chosen between for instance pH 9 to 10. This would result in sub-optimal performance for both the capture capacity and the conversion efficiency. A more detailed techno-economical analysis should be performed to understand the trade-offs for each of these scenarios and the consequences on the overall system performance. An important parameter that should be included in this analysis is the CO_2 concentration of flue gas stream used, , as the capture efficiency decreases due

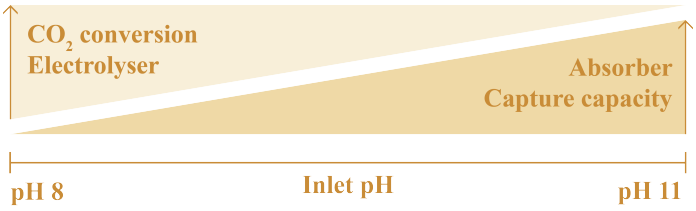

Figure 7.4: Schematic representation of the operating performance of the bicarbonate electrolyser in terms of FE_{CO} and the carbonate capture system in terms of capture capacity as a function of solvent pH.

to the limited CO_2 concentration. If the capture capacity can be improved by using a different CO_2 source stream, such as high CO_2 concentration biogas, it is expected that a more feasible integrated process can be obtained.

Next to improving the FE_{CO} at more alkaline conditions, it is also possible to make use of these alkaline conditions to produce C_{2+} products such as C_2H_4 or ethanol. Several studies have investigated carbonate electrolysis, achieving $FE_{C_2H_4}$ of 34% at 300 mA/cm^2.[126] A possible system design could include multiple electrolyser stacks each operating at a specific pH range. This would allow for using different electrodes at different electrolyte pH to produce a wider range of products. This will, however, require extra down stream separation processing. This is not desirable as it will significantly affect the capital costs, but also the recyclability of the solvent. The build up of product such as ethanol and methanol that remain in the solution will be stripped out in the capture process. Therefore, the most likely pathway for an integrated CO_2 capture and electrochemical conversion process is for higher CO_2 concentration flue gas streams focusing on producing CO. The obtained product stream of CO and H_2 can directly be used for the production of for example methanol.

The bicarbonate electrolyser shown in this work has an energy consumption in the range of 500 to 4000 kJ/mol CO produced, where a more alkaline electrolyte pH results in a higher energy consumption (see Table F.1). The energy consumption significantly increases as the electrolyte pH increases to more alkaline conditions, resulting in a decrease in FE_{CO} and increase in cell potential. This is comparable to what has been reported in the literature for bicarbonate electrolysers performing at near neutral pH conditions achieving FE_{CO} of 82% at 100 mA/cm^2 and a cell voltage of 3.5 to 3.8 V, resulting in 416 kJ/mol CO produced.[64] Comparatively, conventional CO production through electrolysis approximately requires 240 kJ/mol CO produced assuming a FE_{CO} of 90% and cell potential of 3 V.[181]

In order to put the energy requirement into perspective, a comparison with a non-integrated system is made. CO_2 capture with an electrical regeneration is assumed, using an electrochemical cell to perform a pH swing.[162,182] The liberated CO_2 is subsequently converted into CO using the reverse water gas shift reaction (see Section F.3). This results in a total of around 5.5 MJ/kg CO_2 captured required. For comparison, a more conventional regeneration using thermal energy requires approximately 3.6 MJ/kg CO_2 captured, which is equivalent to an electric energy of about 1.2 MJ/kg CO_2 captured. This would further lower the total energy required for a non-integrated system to around 2.2 MJ/kg CO_2 captured. An integrated CO_2 capture and conversion system, based on the experimental results obtained in this study, requires 11 to 90 MJ/kg CO_2 captured (where a more alkaline electrolyte results in a larger energy consumption). This significant difference highlights the importance of improving the energy efficiency of the bicarbonate electrolyser. A cell potential of around 2.6 V, as compared to 3.65 V in the current system, is required to compete with the assumed non-integrated CO_2 capture and conversion system. Therefore, future research should focus on reducing the electrochemical cell potential under at industrially relevant current density.

In literature, several studies have investigated the techno-economic feasibility of

electrochemical CO_2 reduction using a bicarbonate electrolyser.[70,183–186] Moreno-Gonzales et al.[70] found that syngas production through integrated carbonate capture and conversion is ∼50% more expensive than conventional gaseous electrolysis routes. Here, the cost for renewable electricity has the biggest impact on the cost price.[70,184] Current bicarbonate electrolysers operate at high cell potentials, making the electrolysers not commercially viable. Similarly, Salvatore et al.[187] reported that cell potentials below 2 V are required for commercial applications of electrolysers. Current bicarbonate electrolyser operate at a cell potential of 3.5 to 4 V. A recent study by Venkataraman et al.[183] investigated the process and techno-economic feasibility of ethylene produced in a carbonate electrolyser for the production of C_2H_4. A similar result was found, indicating that a carbonate electrolyser can only be more feasible than conventional CO_2 electrolysis with significant reductions the cell potential and increased product selectivity.

7.5 Conclusion

In conclusion, the integration of CO_2 capture and electrochemical conversion is a promising pathway. However, key challenges have to be overcome to make the integrated system a feasible system at industrially relevant scale. First and foremost, further research is required into decreasing the overall cell potential of the bicarbonate electrolyser at industrially relevant current densities. The energy requirement of an integrated system is a two-fold higher than for a non-integrated system. This requires significant improvements in the cell potential, ideally reaching a cell potential below 2.6 V. Furthermore, the CO_2 reduction selectivity towards CO has to be improved significantly at more alkaline pH conditions. Next to that, trade-offs between the optimum operation of the capture system and electrochemical conversion system will have to be made. Therefore, a detailed techno-economic analysis is required to find the optimum operating window in terms of the electrolyte pH used and CO_2 concentration in the flue gas.

Chapter 8

Conclusions & Recommendations

Chapter 8

8.1 Conclusions

To mitigate the effect of climate change, new technologies to remove CO_2 from the atmosphere as well as technologies that can produce carbon based products out of CO_2 are required. With these technologies a circular carbon economy can be established, in which CO_2 is reused, reduced and removed from the atmosphere. This thesis investigates two different pathways to integrate carbon capture and electrochemical conversion to CO and C_{2+} products, using physical and reactive absorption. Route A explores the use of the non-aqueous electrolyte propylene carbonate and route B the use of a (bi)carbonate electrolyte.

In Part I, the use of propylene carbonate as an organic electrolyte was studied. Non-aqueous solvents have a larger CO_2 solubility compared to aqueous solvents. Therefore, a larger concentration of CO_2 can be captured with an organic electrolyte and the mass transport of CO_2 to the electrode surface can be improved in the electrochemical cell. In Chapter 2, the use of propylene carbonate with 0.7 M TEACl in combination with a polycrystalline Cu electrode was investigated for the formation of C_2H_4. However, mainly H_2, CO, and formic acid were measured and no was C_2H_4 detected. The lack of water and protons present in non-aqueous electrolyte is often discussed to limit the current densities of the CO_2 reduction reaction as H^+ is required. However, by adding 10 v% water, the formation of H_2 and CO increased while decreasing formic acid formation. Due to the aqueous nature of the anolyte (0.5 M H_2SO_4), water diffused through the membrane to the catholyte, therefore increasing the water concentration, and increasing the H_2 formation. Therefore, the anolyte was replaced with a similar non-aqueous electrolyte as the catholyte, to suppress the water crossover and control the water concentration in the catholyte. This resulted in the suppression of H_2 formation and an increase in CO and formic acid selectivity. Water remained present in the electrolyte in small concentrations, mostly due to the water present in the membrane used. Furthermore, the effect of the operating temperature was studied. This showed that an increase in temperature increases the CO selectivity. However, increasing the temperature also increases the water diffusion through the membrane, resulting in a larger concentration of H_2 formed at 60 °C. Replacing the anolyte or increasing the operating temperature did not result in the formation of C_2H_4. In Chapter 3, It was shown that the size of the cation plays a crucial role in the product selectivity. The effect of the salt dissolved in the electrolyte was studied, by varying both the cation and anion. When using a larger cation with a weaker hydration shell, a more hydrophobic surface is obtained. Therefore, using 0.7 M THACl in PC and a Cu electrode resulted in the largest concentration of C_2H_4 (22% $FE_{C_2H_4}$).

In Part II, the use of a (bi)carbonate electrolyte was studied in Chapters 4 and 5. By using a (bi)carbonate electrolyte, carbonate capture can be directly integrated with electrolytic bicarbonate reduction, making use of the acid-base equilibrium reaction between CO_2 and carbonate. Contrary to conventional electrolysis systems, when using a bicarbonate electrolyser, there is no gaseous CO_2 supplied to the electrolyser. Instead, the CO_2 is liberated inside the electrolyser in the acid layer near

the bipolar membrane. In Chapter 4, it was shown that increasing the distance between the electrode and membrane improves the pH gradient within the electrolyser, facilitating the right conditions for both the CO_2 liberation near the membrane and CO_2 reduction at the electrode. However, a significant decrease in FE_{CO} of 30% was observed in the first 3 hours of continuous operation at a constant current. It was found that both the increasing electrolyte pH and the trace metal impurities present in the electrolyte caused this decrease in selectivity. A set of single-pass electrolyte experiments were conducted, identifying the FE_{CO} for bicarbonate electrolysis at a pH 8 to 10. As the electrolyte pH becomes more alkaline, the FE_{CO} decreases, limiting the electrochemical regeneration of the solvent. In Chapter 5, the CO_2 liberation and utilization were improved by increasing the operating temperature (60 °C) and increasing the Ag loading of the catalyst. Furthermore, a complexing agent (EDTA) was used to complex the trace metal ion impurities present in the electrolyte, to avoid the deposition of these metals on the catalyst surface. This significantly improved the overall stability of the bicarbonate electrolyser, as was shown in Chapter 4 in a single pass electrolyte experiment using EDTA. A small decrease of only 4% in FE_{CO} after 6 hours of operation was measured. Similarly, in Chapter 5, the FE_{CO} measured when operating at 60 °C was constant over time when adding EDTA to the electrolyte.

In the final Part III of this thesis, the feasibility of integrating the bicarbonate electrolyser with carbon capture are evaluated. In Chapter 6, a DAC system using a solid adsorption and liquid desorption is coupled with a bicarbonate electrolyser. Experimental validation for the solid adsorption, liquid desorption, and electrochemical conversion are presented, demonstrating a proof-of-concept. The pH swing between the CO_2 rich and CO_2 lean solvent is identified as the dominant design parameter and is almost exclusively controlled by the electrolyser sizing. This is caused by the decrease in electrolyser performance at more alkaline electrolyte conditions, limiting the regeneration of the solvent. Consequently, using a small pH swing results in inefficient solid sorbent use and excessive water loss.

Finally, in Chapter 7, a perspective on the feasibility of post-combustion carbonate capture with bicarbonate electrolysis is evaluated. The electrolyte pH is identified as the dominant parameter in identifying the efficiency of an integrated system, as it controls the capture and conversion efficiency. As previously discussed in Chapter 5, the CO_2 liberation and FE_{CO} can be improved at elevated operating temperatures by increasing the Ag loading and adding EDTA to the electrolyte. In Chapter 7, it is shown that an increase in operating pressure to 5 bar can further improve the FE_{CO} at more alkaline electrolyte pH, which improves the deep regeneration of the solvent. A flue gas stream with high CO_2 partial pressures will result in the most feasible integration of CO_2 capture and electrochemical conversion.

8.2 Recommendations

Based on the findings discussed in this thesis, the following recommendations for future research are given:

- Electrochemical CO_2 reduction on a Cu electrode in non-aqueous solvents does not effectively produce C_{2+} products, as compared to aqueous systems. In Chapter 3, the use of a large cation with a weak hydration shell showed that the selectivity of CO_2 reduction towards C_2H_4 could be significantly improved. However, it remains unclear what exactly happens on the electrode surface and what is preventing the reduction of CO_2 to hydrocarbons. It is therefore recommended to better understand the mechanistic pathways that occur on the surface of the electrode by using operando techniques, such as Raman. Furthermore, computational techniques such as density function theory (DFT) could be used. Moreover, the current densities achieved for CO_2 reduction in non-aqueous solvents are currently very low. Therefore, future research should focus on achieving significant improvements on the current density and product selectivity for industrially relevant applications.

- In bicarbonate electrolysis, where a bipolar membrane is used, a large cell potential is attained. Future research should focus on improving the cell potential under industrially relevant conditions for a feasible application. Furthermore, the faradaic efficiencies as well as CO_2 liberation, specifically at a more alkaline electrolyte pH, should be improved for deeper electrolyte regeneration. This could be achieved by for instance improving the catalyst utilization or by increasing the operating pressure. Ideally, the capture and conversion process operate at the same temperature and pressure, reducing the need for compressors and heat integration. Additionally, the stability of the bicarbonate electrolyser for long term operation should be investigated for industrial applications.

- A detailed model of the integrated carbonate capture and bicarbonate conversion system, based on the obtained experimental results, is recommended to evaluate the current feasibility of the system and to better understand what challenges are remaining. Moreover, a techno-economic evaluation of the integrated system, including an optimized heat integration, for different scenarios with varying pH ranges is recommended.

- In this thesis, bicarbonate electrolysis towards CO was investigated. CO is valuable product, both on its own and as a syngas to produce other carbon based molecules. However, future research should investigate the possible pathways for producing C_{2+} products by bicarbonate electrolysis. This could be achieved by directly converting bicarbonate to C_{2+} products, as already shown in several studies, or by converting the CO to C_{2+} products in a second CO electrolyser. Most likely, a second capture step is then required in between the first and second electrolyser, to remove the unconverted CO_2.

- Lastly, future research could investigate other potential integration methods for CO_2 capture and conversion. As shown in this thesis, the bicarbonate electrolyser currently cannot effectively regenerate the solvent. Therefore, a comparison with non-integrated system using a gas-fed electrolyser would be interesting in future research.

Appendix A

Supporting Information to Chapter 2

Appendix A

A.1 Experimental Section

A.1.1 Electrode Surface Area Preparation

Copper foil (Aldrich 99.999%, 1 mm thickness, 2.5 cm x 2.5 cm) was used as working electrode. Initial sanding (up to grain size 2000) and polishing (up to 1 μm grade diamond paste) of the copper electrode were done to make sure no visible scratches were present on the copper. Prior to each experiment, electropolishing of the copper in phosphoric acid (85% in H_2O, Aldrich) at 2.1 V versus a graphite rod as counter electrode was performed for 3 min, based on Kuhl et al.[40] SEM and EDS were used to characterize the electrode surface before and after electrolysis.

A.1.2 Electrochemical Cell

All experiments were performed in a two-compartment batch electrolyzer, based on the design of Lobaccaro et al.[140] CO_2 was continuously bubbled at 8 mL min^{-1} through the catholyte during the chronoamperometry experiments. The anolyte used was a 0.5 M aqueous H_2SO_4 (except otherwise stated) and the catholyte 0.7 M tetraethylammonium chloride (TEACl) in propylene carbonate (PC) with different concentrations of water (0, 10 and 90 v%). To prevent any contamination, the cell was stored in 20% v/v nitric acid and rinsed with MilliQ water before use.

Furthermore, a platinum counter electrode (MaTeck 99.99%, 0.1mm thickness, 2.5 cm x 2.5 cm) and a leak-free Ag/AgCl reference electrode (Innovative Instruments LF-1-45) were used. A cation exchange membrane (Nafion-117) separated the anolyte and catholyte compartments. A potentiostat (SP-200, BioLogic) was used to perform the CV and chronoamperometry experiments.

The two-compartment electrochemical cell was modified for the high temperature experiments (see Figure A.1). The back plates were replaced with aluminum back plates, which were heated using a water bath. The heated back plates were indirectly in contact with the electrodes and thus heating the electrolyte. An electrically insulating rubber gasket was placed in between the aluminum back plates and the electrodes, to prevent electricity passing through. The temperature of the anolyte was continuously measured during the experiment and kept constant. The thermocouple interfered with the measured current signal by the reference electrode; therefore it was not possible to measure the catholyte temperature during electrolysis. However, the anolyte and catholyte temperatures can be presumed to be equal. The chronoamperometry experiment was started as the soon as the anolyte was at the desired temperature.

A.1.3 Gas and Liquid Product Analysis

The compact H-cell was coupled to a gas chromatograph (Compact GC 4.0, Interscience) equipped with two thermal conductivity detectors and one flame ionization detector that measured the gaseous products formed in the cathode compartment with 2 min intervals during experiments. At the end of the experiment, samples of the electrolytes were analyzed using a high-pressure liquid chromatograph (HPLC) (1290 Infinity II, Agilent). For HPLC analysis, 5 μL of the catholyte solution was injected on two Aminex HPX-87H columns (Biorad) placed in series. The columns were heated to 60 °C, using an eluent containing 1mM H_2SO_4 in ultrapure water and a refractive index detector (RID) for the detection of products. Coulometric KF (Metrohm 756 KF Coulometer) was used for the water content measurement before and after the experiment.

A.2 Electrochemical Setup for High Temperature Experiments

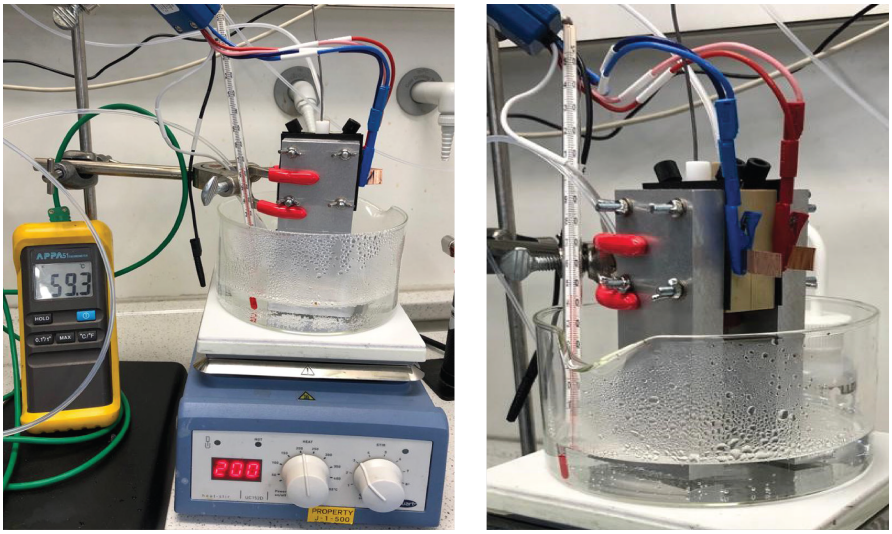

Figure A.1: Modified batch cell for the electrolysis at different operating temperatures.

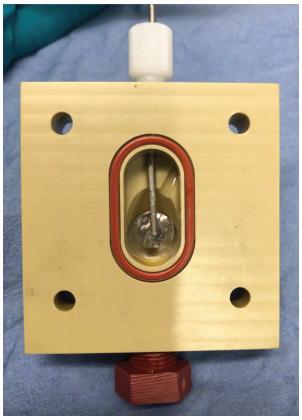

Figure A.2: Thermocouple positioned in anolyte compartment to measure the electrolyte temperature during the chronoamperometry experiment.

A.3 Effect of Water

In Figure A.3 the water concentrations measured with coulometric Karl Fischer titration are presented for each electrolyte water concentration. The blank measurements represents the water concentration of the electrolyte before electrolysis. There is around 0.2 w% of water present in the propylene carbonate at the start of the electrolysis experiment.

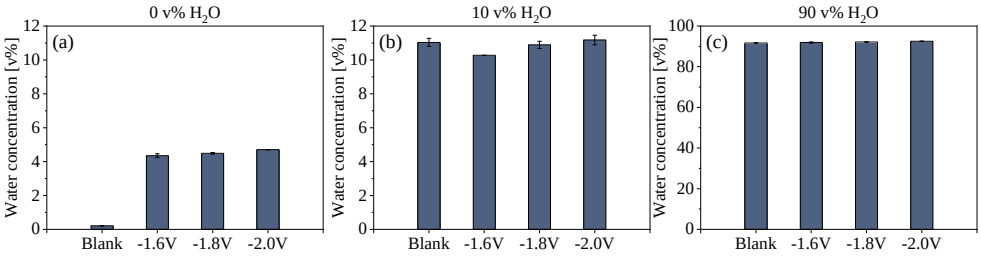

Figure A.3: Water concentrations before and after CA at different potentials, for propylene carbonate with (a) 0 v% H_2O, (b) 10 v% H_2O, and (c) 90 v% H_2O.

A.4 Effect of Water Concentration – Product Distribution over Time

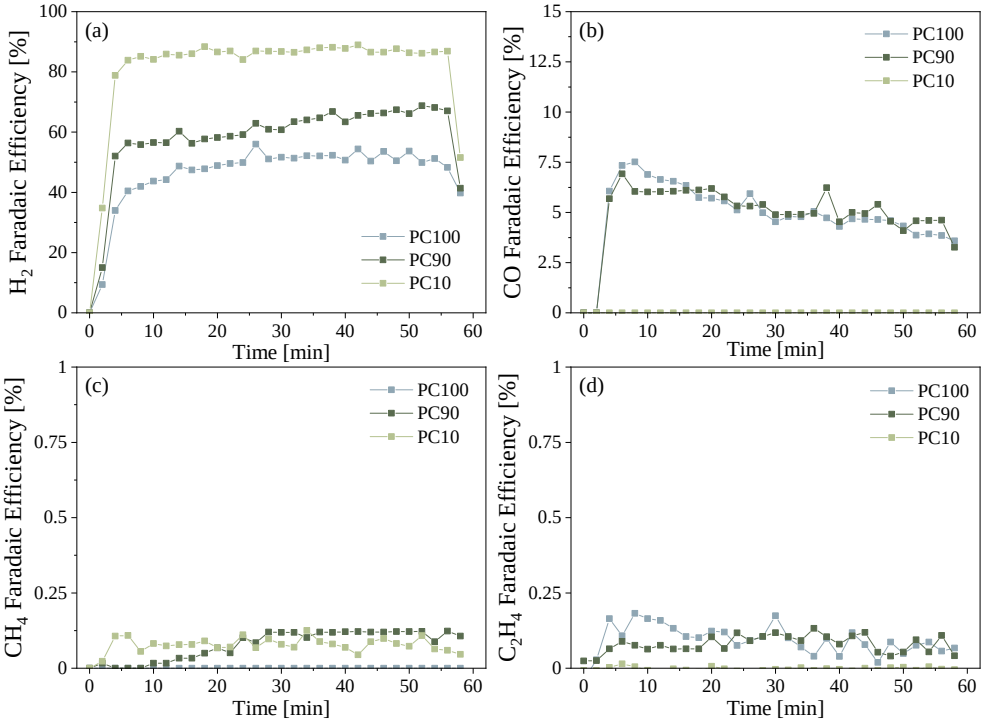

Figure A.4: Product distribution as a function of time for different water concentrations in PC electrolyte, measured for 1 hour chronoamperometry experiment on copper electrode at -1.8 V vs. Ag/AgCl. Faradaic efficiency presented for (a) hydrogen, (b) carbon monoxide, (c) methane, and (d) ethylene.

A.5 Effect of Salt on Product Distribution

Due to solubility limitations of alkali metal salts in PC, it was not possible to perform a one on one comparison. Therefore, the 0.1 M $KClO_4$ was dissolved in PC90. However, when using 0.1 M TEACl, the addition of 10 v% water to PC results in a two-phase system. Therefore, the comparison was made with 0.1 M TEACl in pure PC, 0.7M TEACl in PC with 10 v% water, and 0.7 M TEACl in pure PC.

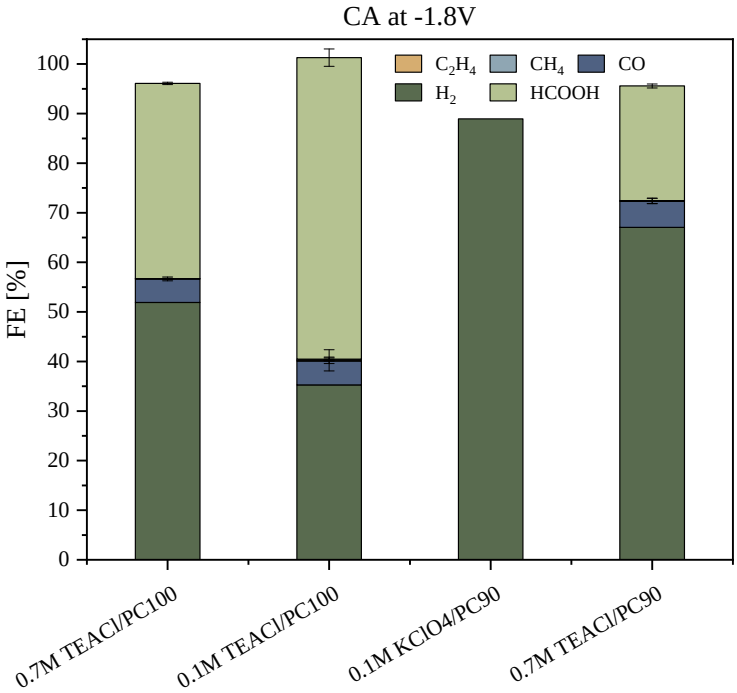

Figure A.5: Faradaic efficiencies for (a) 0.7 M TEACl in PC100, (b) 0.1 M TEACl in PC100, (c) 0.1 M KClO4 in PC90, and (d) 0.7 M TEACl in PC90 electrolyte, measured for 1 hour chronoamperometry experiment on copper electrode at -1.8 V vs. Ag/AgCl.

A.6 Effect of Temperature – Product Distribution over Time

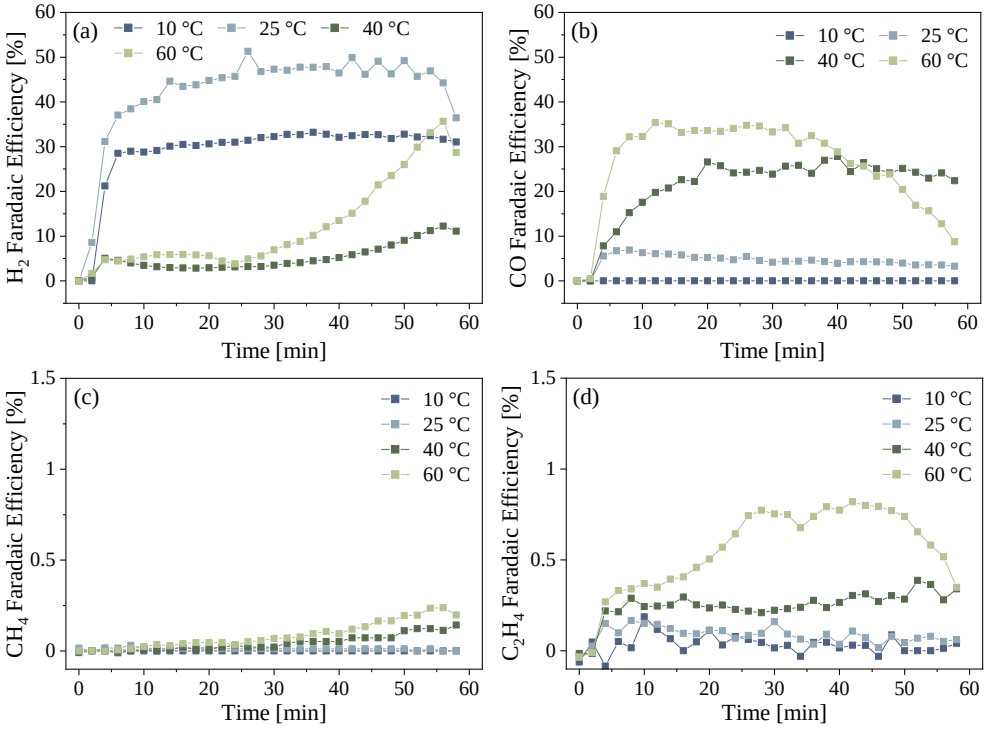

Figure A.6: Product distribution as a function of time for different operating temperatures, measured for 1 hour chronoamperometry experiment on a copper electrode at -1.8 V vs. Ag/AgCl with propylene carbonate electrolyte containing 0 v% H_2O. Faradaic efficiency presented for (a) hydrogen, (b) carbon monoxide, (c) methane, and (d) ethylene.

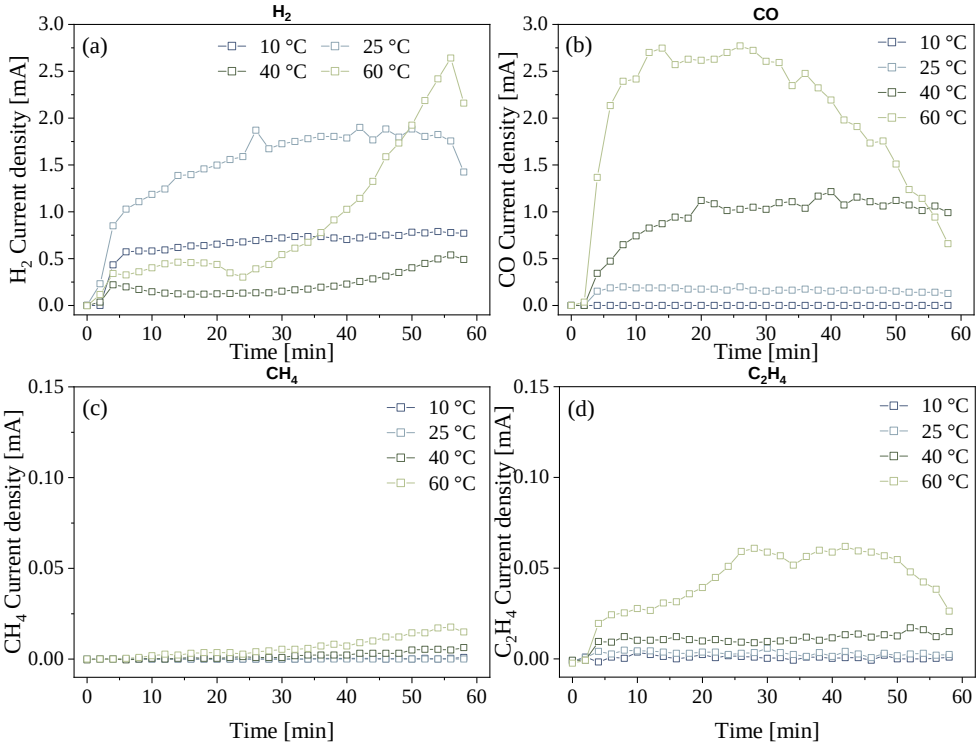

Figure A.7: Partial current densities as a function of time for different operating temperatures, measured for 1 hour chronoamperometry experiment on a copper electrode at -1.8 V vs. Ag/AgCl with propylene carbonate electrolyte containing 0 v% H_2O. Faradaic efficiency presented for (a) hydrogen, (b) carbon monoxide, (c) methane, and (d) ethylene.

A.7 Scanning Electron Microscopy

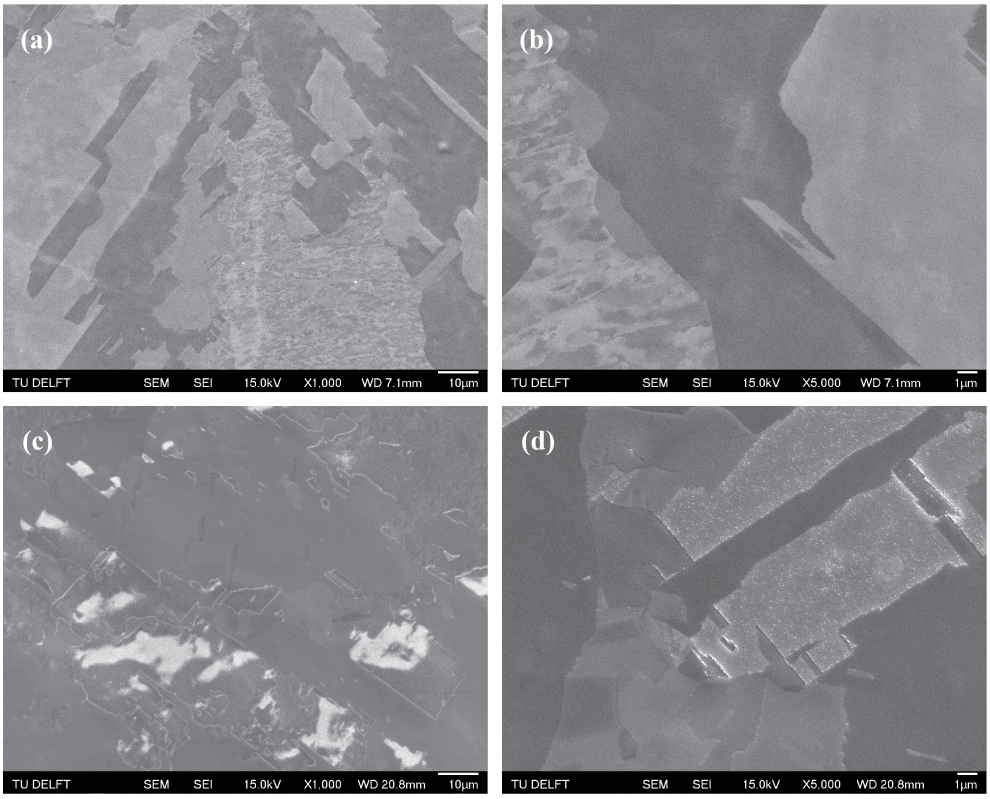

Figure A.8: SEM images of the Cu electrode after (a) and (b) electropolishing, and (c) and (d) after chronoamperometry at -1.8 V for in a 0.7 M in propylene carbonate solution with 0 v% water additions, at 25 °C.

A.8 Energy Dispersive X-ray Spectroscopy

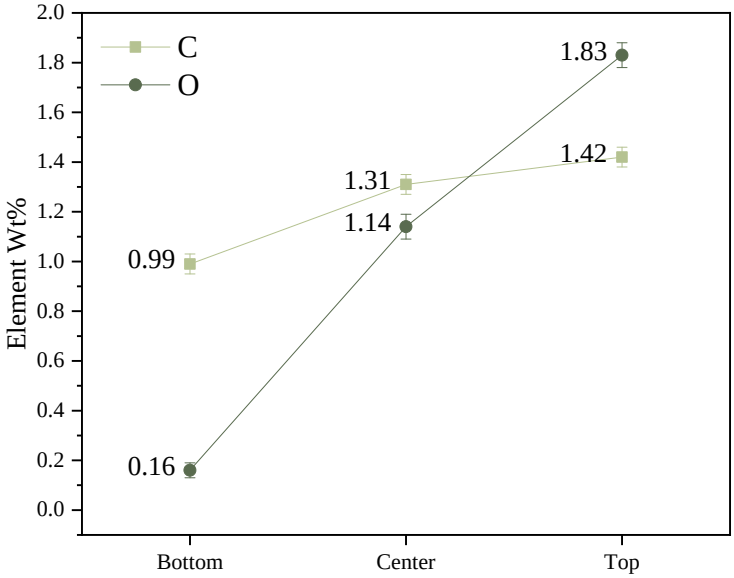

Figure A.9: Elemental weight percentage for C and O at the Cu electrode surface after electrolysis at 60 °C, at different positions on the Cu surface.

Table A.1: EDS results for post mortem Cu foil for electrolysis at 25 °C and 60 °C.

	Post mortem at 25 °C		**Post mortem at 60 °C**	
Element	**Element Wt%**	**Wt% error**	**Element Wt%**	**Wt.% error**
C	1.02	± 0.05	0.99	± 0.04
O	0.07	± 0.04	0.16	± 0.03
Cu	98.91	± 0.73	98.85	± 0.57

A.9 Inductively Coupled Plasma Spectroscopy

Table A.2: Overview of different components measured by ICP in the anolyte and catholyte, before and after electrolysis with 0 v% water in the catholyte, operated at 25 °C. All values are in mg/kg.

Sample	**Al**	**B**	**Ba**	**Ca**	**Cu**	**Fe**	**K**	**Mg**	**Na**	**Zn**	**PO_4**	**Si**
Anolyte blank	1.61	4.16	0.03	0.76	0.05	0.05	0.47	0.03	5.17	0.01	0.34	3.34
Catholyte blank	0.04	0.04	0.01	0.30	0.00	0.25	3.41	0.05	0.18	0.05	21.20	0.0
Anolyte after electrolysis	1.90	5.07	0.04	2.36	0.13	0.09	26.73	0.11	6.51	0.05	1.53	3.77
Catholyte after electrolysis	0.05	0.37	0.01	0.41	7.94	0.12	5.24	0.05	0.40	0.11	22.40	0.0

Appendix B

Supporting Information to Chapter 3

Appendix B

B.1 Experimental Section

B.1.1 Electrochemical Cell

All chronoamperometry experiments were performed using a twocompartment H-cell, based on the design by Lobaccaro et al.[140] The cell was stored in 20% v/v nitric acid to prevent any contamination and rinsed thoroughly with MilliQ water before use. A copper foil (Sigma Aldrich 99.999 1 mm thickness, 2.5 cm x 2.5 cm) was used as working electrode. Initial sanding was performed (up to grain size 2000), followed by mechanical polishing (up to 1 μm grade diamond paste). Before each experiment the copper foil was electropolished using phosphoric acid solution (85 in H_2O, Sigma Aldrich) at 2.1 V versus a graphite rod for 3 min, based on a procedure by Kuhl et al.[40] A platinum counter electrode (MaTeck 99.99 0.1 mm thickness, 2.5 cm x 2.5 cm) and a leak-free Ag/AgCl reference electrode (Innovative Instruments, LF-1-45) were used. A cation exchange membrane (Nafion-117) was used to separate the anolyte and catholyte compartment. The anolyte used was a 0.5 M aqueous H_2SO_4 (Sigma Aldrich) and catholyte were prepared using propylene carbonate (Sigma Aldrich, anhydrous 99.7%) with either 0.7 M TEACl (98%, Sigma Aldrich), TBACl (97%, Sigma Aldrich), THACl (96%, Sigma Aldrich), $TEABF_4$ (99%, Sigma Aldrich), $TBABF_4$ (99%, Sigma Aldrich), $THABF_4$ (97%, Sigma Aldrich), $TEAPF_6$ (99%, Sigma Aldrich), $TBAPF_6$ (98%, Sigma Aldrich) or $THAPF_6$ (98%, Alfa chemistry). A potentiostat (SP-200, BioLogic) was used perform the cyclic voltammetry and chronoamperometry experiments. A continuous CO_2 gas stream of 8 sccm was supplied at the bottom of the cathode compartment. The outlet was connected to an inline gas chromatograph (Compact GC 4.0, Interscience), equipped with two thermal conductivity detectors (TCD) and one flame ionization detector (FID), that measured the gaseous products formed in the cathode compartment with 2 minute intervals. The reported faradaic efficiencies are calculated as the average value of the stable period during the last 15 minutes of the experiment. Liquid samples were taken at the end of the 1 hour experiment for which the product analysis was done by high pressure liquid chromatograph (HPLC,1290 Infinity II, Agilent). For HPLC analysis, 5 μL of the catholyte solution was injected on two Aminex HPX-87H columns (Biorad) placed in series. The columns were heated to 60 °C, using an eluent containing 1 mM H_2SO_4 in ultrapure water and a refractive index detector (RID) for the detection of products. Coulometric Karl Fischer titration (Metrohm 756 KF Coulometer) was used for the water content measurement before and after the experiment.

B.1.2 Fourier Transform Infrared Spectroscopy

The FTIR experiments were performed using a Bruker Vertex 80 V IR spectrometer in combination with an Autolab PGSTAT12 potentiostat. A three electrode spectroelectrochemical cell configuration was used in combination with a 60° CaF_2 prism pressed to the bottom of the cell.[111,188] A polycrystalline Cu foil working electrode (MaTeck 99.99%), platinum coil counter electrode (MaTeck 99.99%), and Ag/Ag^+

reference electrode (Alvatek) were used. Spectra were collected in a thin-film configuration in the wavenumber range 4000 to 900 cm^{-1} by varying the potential from -1.0 V to -2.5 V vs. Ag/AgCl with steps of 0.1 V under Ar and CO_2 saturated conditions (see Figure B.7 and Figure B.8). A reference spectrum was obtained and subtracted from the spectra at the measured potentials. The spectra are presented as absorbance spectra, according to $A = -\log(\frac{R}{R_0})$ where R and R_0 is the reflectance corresponding to the single beam spectra obtained at the sample and reference potential, respectively. Therefore, negative bands correspond to consumed species on the surface, whereas positive bands correspond to the formation of species. Prior to the experiment, the Cu electrode was electropolished using the same method as described in the previous section, except the polishing was done for 15 seconds only.

B.2 Overview of Chronoamperometry Results

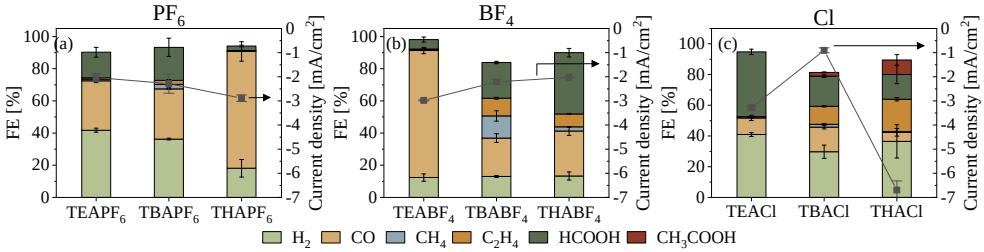

Figure B.1: CO_2 reduction product distribution after 1 hour chronoamperometry (CA) on a Cu electrode using PC solvent with different salts at 0.7 M grouped per cation, at -2.0 V vs. Ag/AgCl. Error bars indicate differences between duplicate measurements.

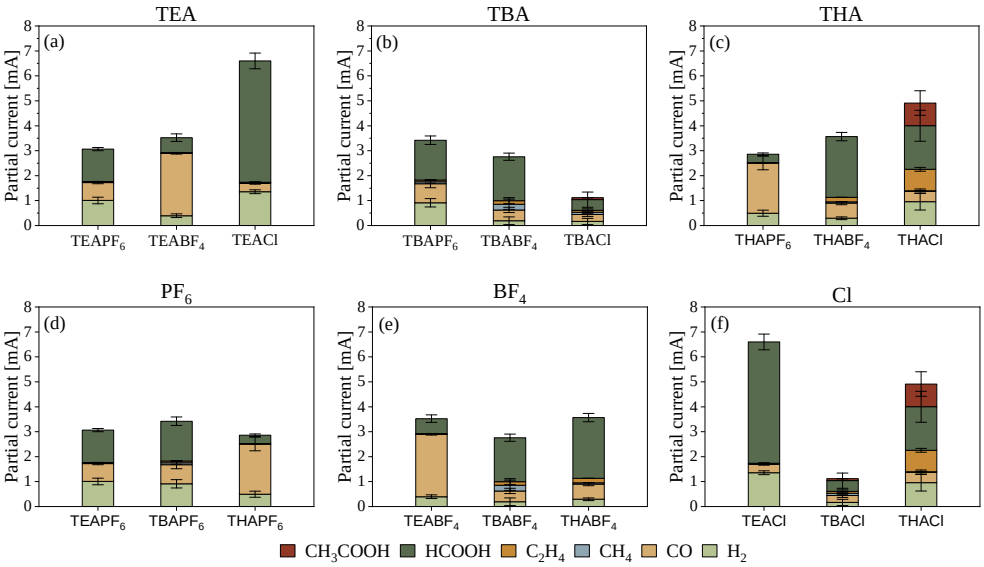

Figure B.2: Partial current densities after 1 hour chronoamperometry (CA) on a Cu electrode using PC solvent with different salts at 0.7 M at -2.0 V vs. Ag/AgCl. Error bars indicate differences between duplicate measurements.

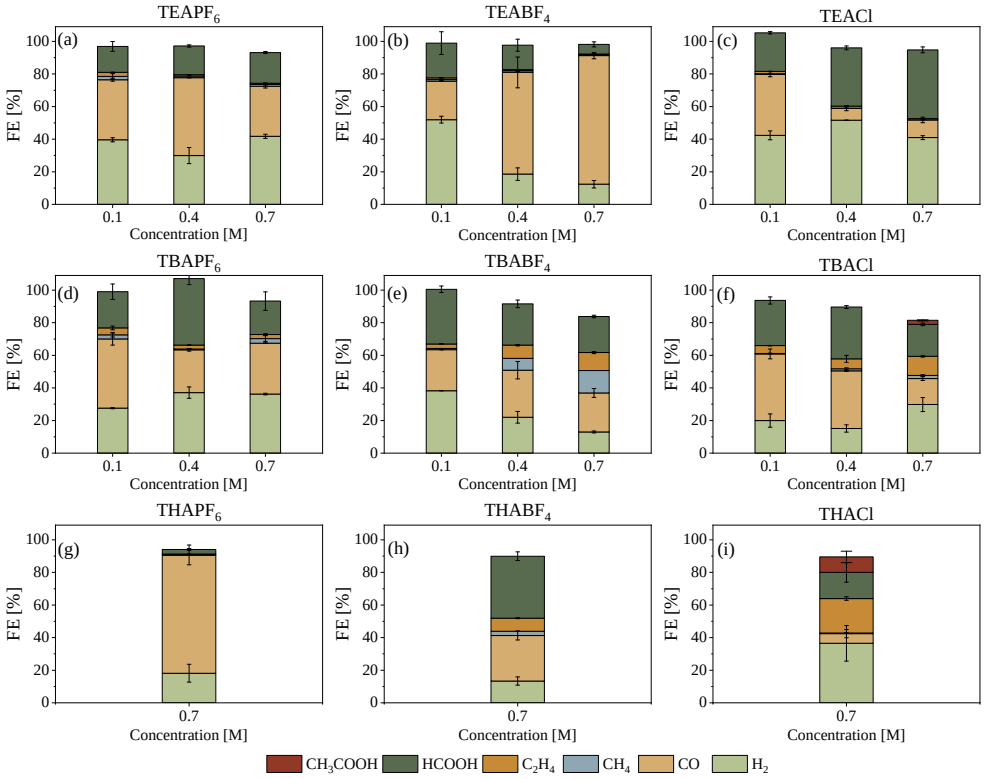

Figure B.3: CO_2 reduction product distribution after 1 hour chronoamperometry (CA) on a Cu electrode using PC solvent with different salts at different concentrations at -2.0 V vs. Ag/AgCl. Error bars indicate differences between duplicate measurements.

B.3 Non-aqueous Anolyte

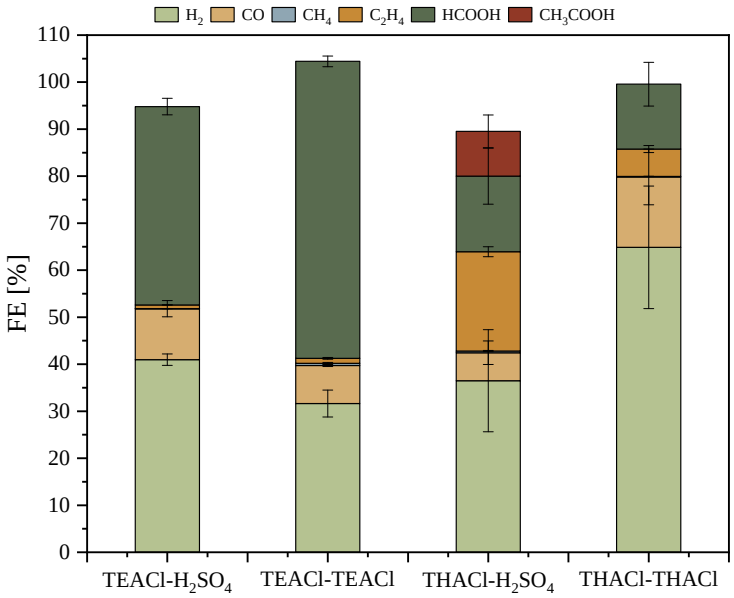

Figure B.4: Faradaic efficiencies of CO_2 reduction products during 1 hour chronoamperometry on a Cu electrode using 0.7 M TEACl in PC and 0.7 M THACl in PC as catholyte combined with either an aqueous 0.5 M H_2SO_4 anolyte or similar PC anolyte. The error bars indicate differences between duplicate measurements.

B.4 Water Concentrations

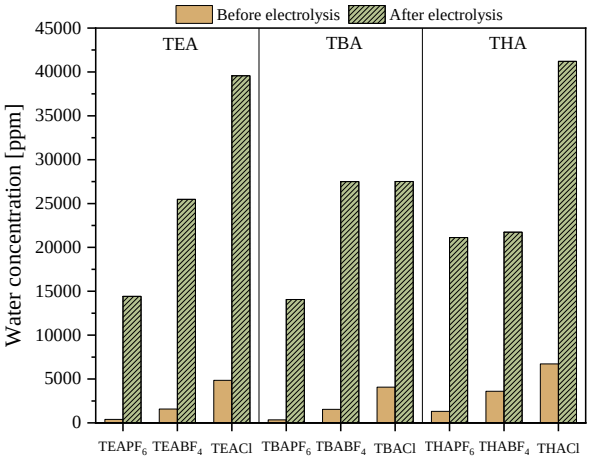

Figure B.5: Water concentrations (ppm) of the different electrolytes used during CO_2 reduction at -2.0 V vs. Ag/AgCl before and after electrolysis.

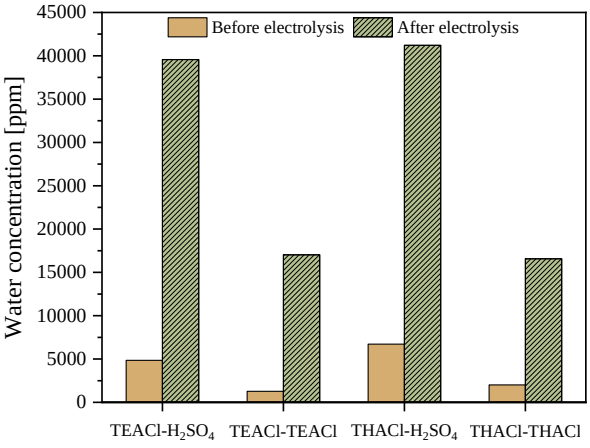

Figure B.6: Water concentration (ppm) of the different electrolytes used during CO_2 reduction at -2.0 V vs. Ag/AgCl before and after electrolysis, comparing an aqueous H_2SO_4 and non-aqueous propylene carbonate anolyte.

B.5 Overview FTIR Data

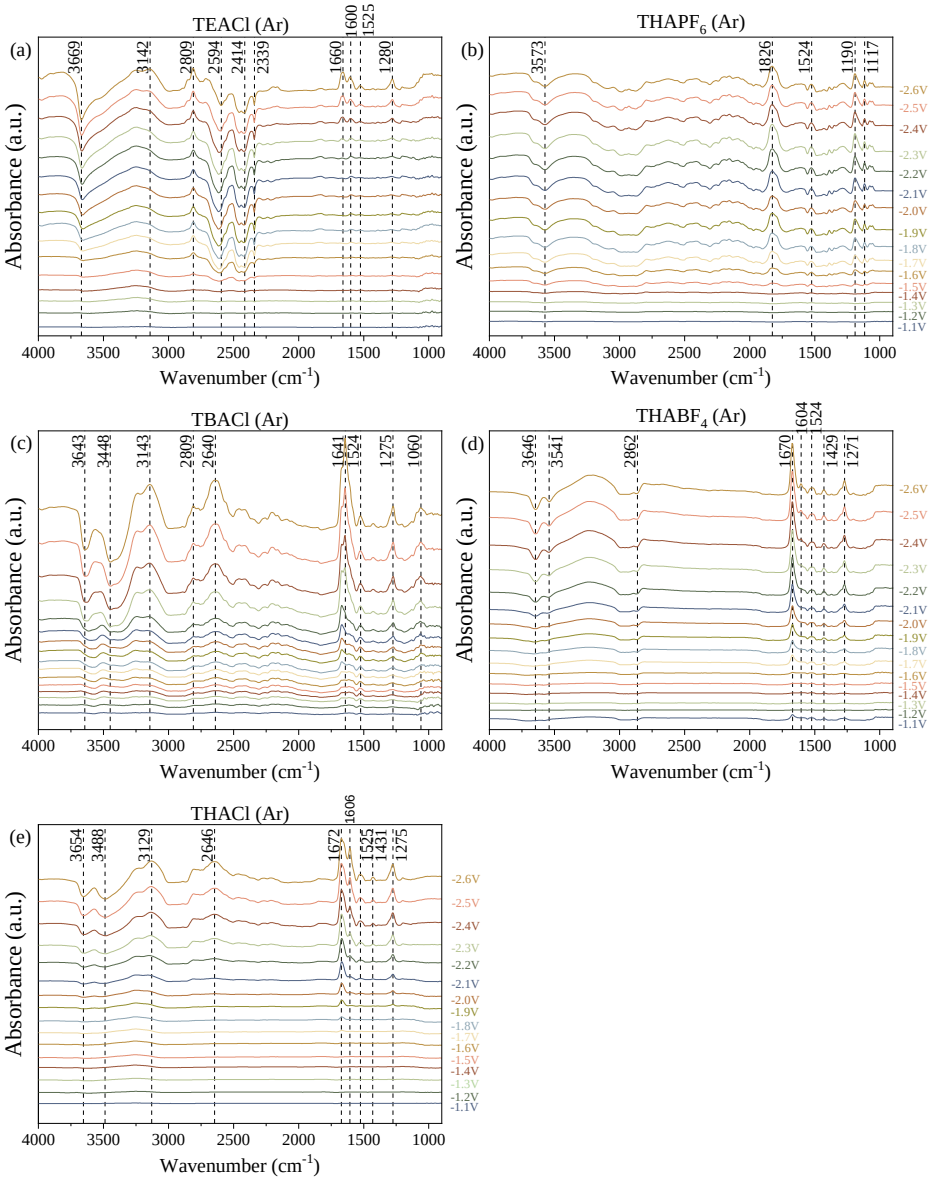

Figure B.7: FTIR spectra from -1.1 V to -2.6 V vs. Ag/AgCl for the different salts (0.7 M) dissolved in PC, for Ar saturated conditions, using a Cu electrode.

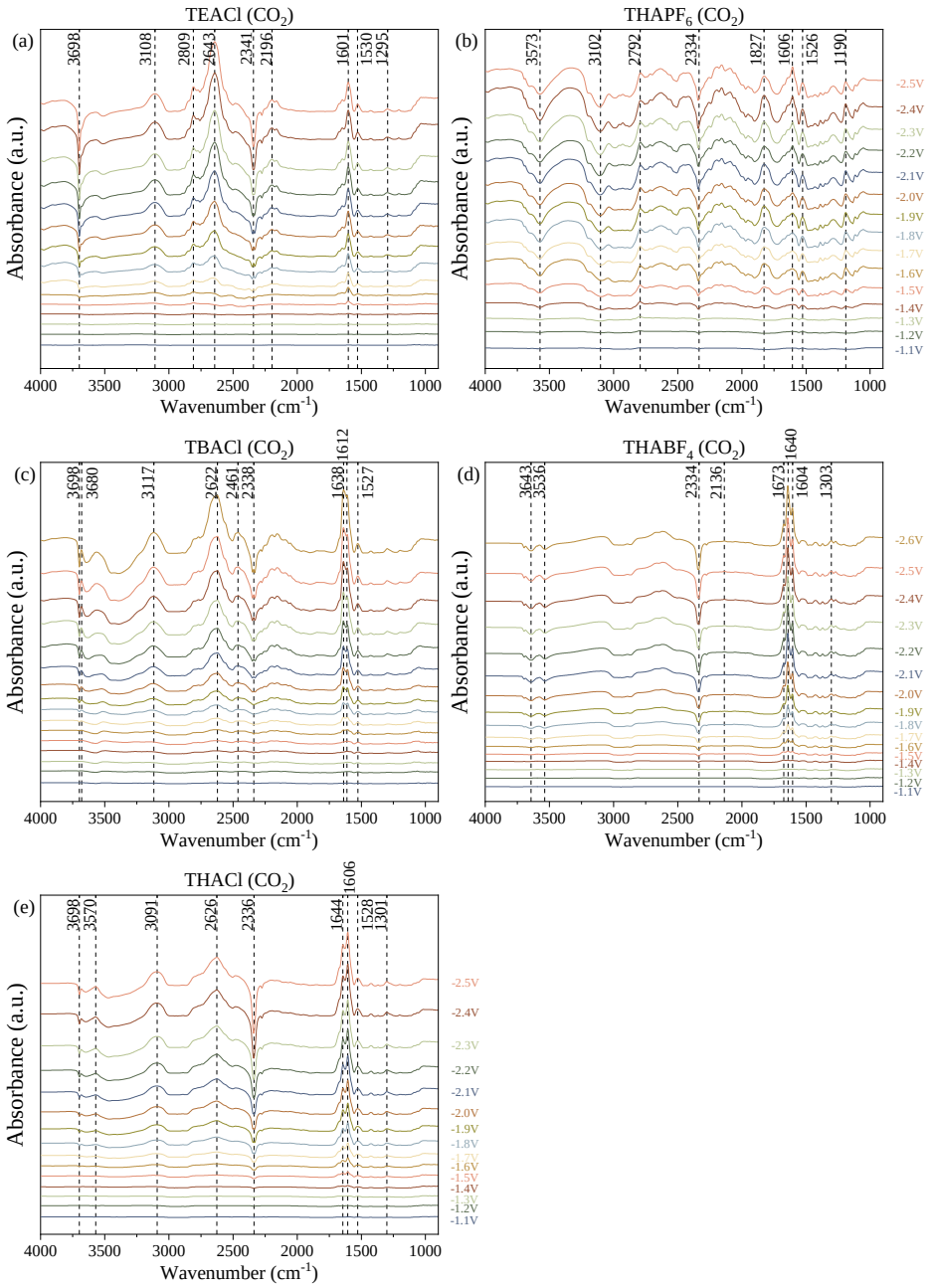

Figure B.8: FTIR spectra from -1.1 V to -2.6 V vs. Ag/AgCl for the different salts (0.7 M) dissolved in PC, for CO_2 saturated conditions, using a Cu electrode.

B.6 Cyclic Voltammetry

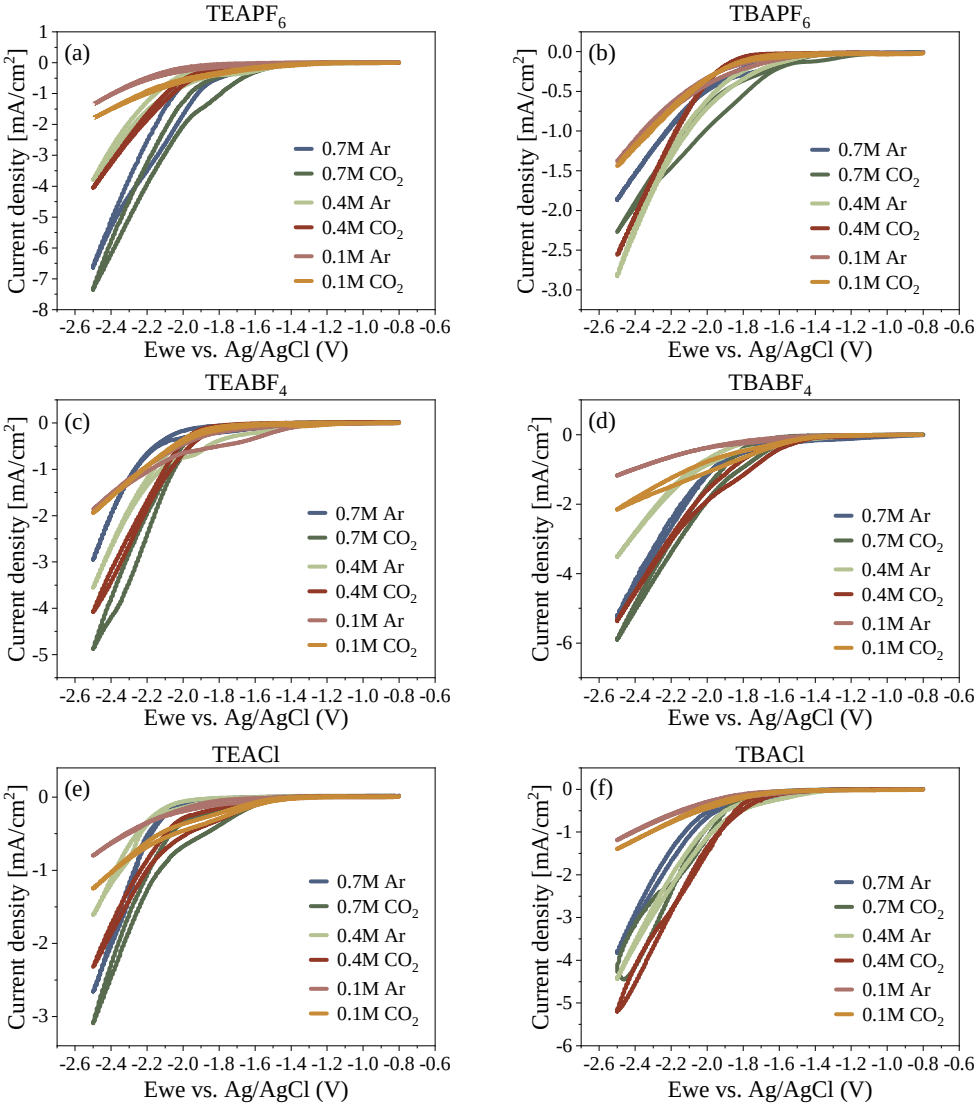

Figure B.9: Cyclic voltammetry for the different TEA and TBA salts at varying concentrations in PC, both for Ar and CO_2 saturated electrolytes.

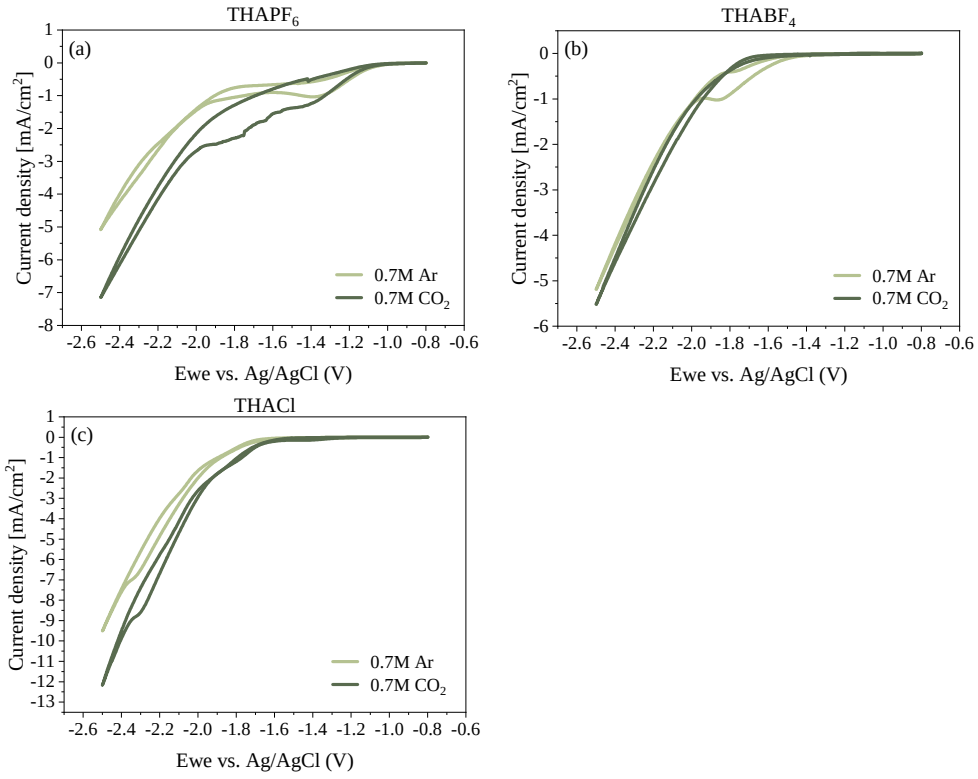

Figure B.10: Cyclic voltammetry for the different THA salts and concentration in PC, for Ar and CO_2 saturated electrolytes.

Appendix C

Supporting Information to Chapter 4

Appendix C

C.1 Experimental Section

C.1.1 Bicarbonate Electrolysis

A commercial ElectroCell flow cell (Micro Flow cell 10 cm^2 MFC30010) was used to perform the bicarbonate electrolysis experiments. An exploded view of the cell and the different components can be seen in Figure C.1. A nickel foam (2 mm thickness, ElectroCell) was used as the anode and a bipolar membrane (Fumasep FBM-PK) was used to separate the cathode and anode. The bipolar membrane (BPM) was stored in 1 M NaCl and reused multiple times, but replaced regularly. The Ni foam was stored in water and sonicated for 5 minutes prior to experiments, and replaced regularly as well. A 3 M $KHCO_3$ (99.97%, Sigma Aldrich) solution was prepared in 1 L stock solutions at a time and the pH measured. For the single-pass pH experiments, different pH buffer solutions of $KHCO_3$ and K_2CO_3 were mixed to obtain the required pH. The anolyte used was 1 M KOH (<85%, Sigma Aldrich). A mixed cellulose ester (MCE, 8 μm pore diatemeter, MF-Millipore) membrane was used as a spacer between the membrane and the cathode. The membrane was wetted with MilliQ water after which it was stored in the catholyte solution for about 5 minutes to ensure full saturation prior to assembling the electrochemical cell. To assemble the cell, the EPDM sealing gaskets supplied by ElectroCell were used, as well as a thinner silicon gasket for the cathode. On the anode side, a Ni current collector was used whereas on the cathode

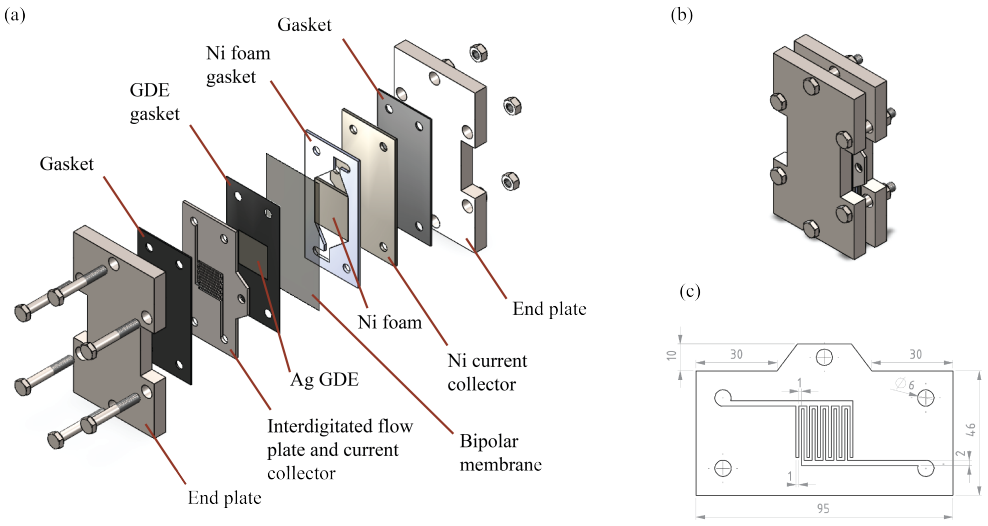

Figure C.1: Schematic of the lab-scale bicarbonate electrolyser. (a) Exploded view of flow cell including all the different components, (b) stacked electrolyser, (c) drawing of the interdigitated flow plate, all dimensions in mm.

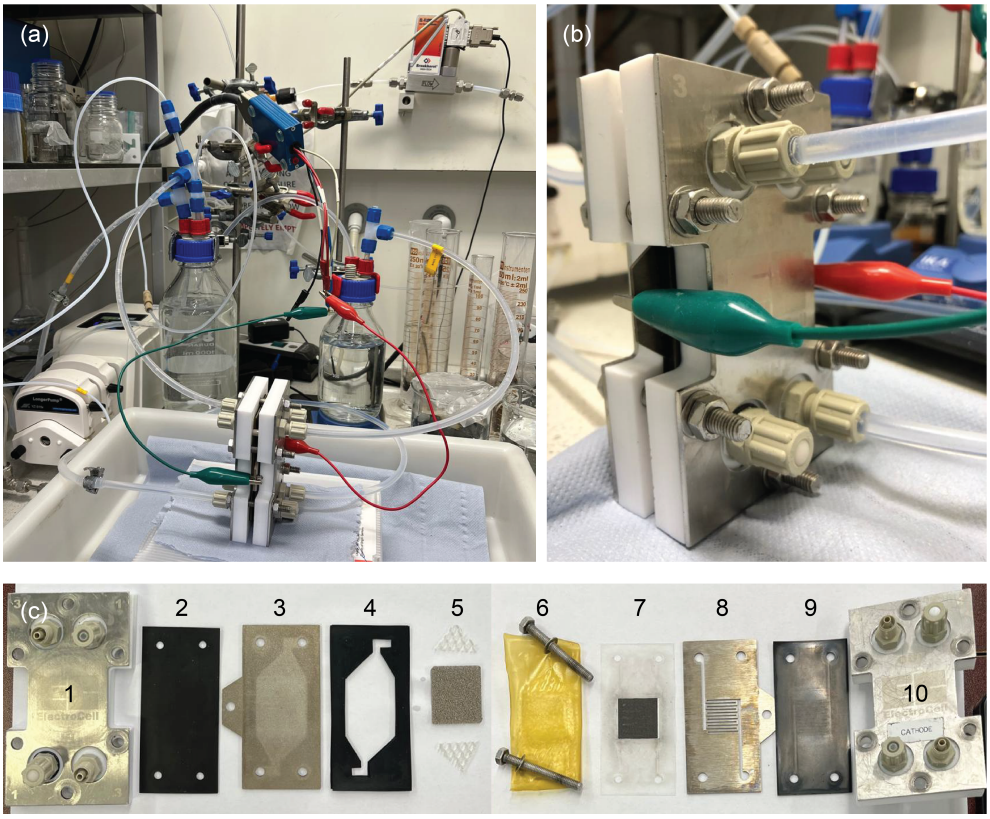

Figure C.2: Lab-scale bicarbonate electrolyser. (a) and (b) commercial flow cell electrolyser, (c) components used in the stack of the electrolyser: 1) End plate, 2) Gasket (1 mm thickness), 3) Ni current collector, 4) Flow pattern gasket (2x 1 mm thickness), 5) Ni foam anode (2 mm thickness) and flow distributors, 6) Bipolar membrane, 7) Gasket (200 μm thickness) and Ag GDE, 8) Titanium interdigitated flow pattern and current collector, 9) Gasket (1 mm thickness), 10) End plate.

side a Ti interdigitated flow plate was used as current collector. The interdigitated flow plate had 1 mm wide flow channels and bridges (see Figure C.1(c)). The electrode stack was closed evenly by 6 bolds, using a torque wrench at 3 Nm. In Figure C.2, all components used in the bicarbonate flow cell are depicted. For the 3 hour experiments, a catholyte volume of 70 mL and anolyte volume of 140 mL were used. The overnight 15 hour runs used 1000 and 500 mL of catholyte and anolyte respectively. For the single-pass experiments, the anolyte volume was kept at 140 mL and the catholyte volume was increased to 5 L. An inline pH probe (InPro3250i with Transmitter M300 Water 2-channel, Mettler) was installed at the outlet of the bicarbonate electrolyser,

to measure the output pH continuously during an experiment. A peristaltic pump (BT100-3J Basic Peristaltic Pump, Darwin Microfluidics) was used in combination with 2 pump heads (YZ1515X-B, Darwin Microfluidics) and silicon tubing (#25, Darwin Microfluidics). A flow rate of 50 mL/min was used for both electrolytes. A potentiostat (SP-200, Biologic) was used as the current supply, using the EC-lab software. A constant current of 500 mA was applied to the cathode, which corresponds to 100 mA/cm^2 as the active area of the cathode is 5 cm^2.

C.1.2 Electrode Preparation

The Ag catalysts were prepared by spray-coating (Custom Micron Absolute Precision, Iwata) a Ag nanoparticle (20-40 nm, Thermo Fisher Scientific) ink onto a carbon support layer (Sigracet 39BB, Fuelcell Store). The carbon support layers were cut into pieces of 25 x 30 mm to allow extra space to hold the electrode in place during spray-coating. An area of 25 x 25 mm was spray-coated and the excess material was cut off post electrode preparation. Prior to spray-coating, the carbon material was sonicated in acetone and MilliQ water subsequently, for 10 minutes each. The electrodes were dried on a hot plate (covered with aluminium foil) at 90 °C for about 10 minutes until completely dry. The dry electrodes were weighed to determine the pre-spray-coating weight. Before spraying, the heat of the hotplate was reduced to 70 °C to ensure rapid evaporation of the isopropanol and curing of the Ag-Nafion layering. For the ink, 84 ± 2 mg of Ag nanoparticles (20-40 nm, Thermo Fischer Scientific) were mixed with 8 mL of isopropanol (VWR Chemicals) and 80 μL of Nafion binder (Nafion 1100W, 5 wt% in water and propanol, Sigma Aldrich). The ink was sonicated for 30 minutes in an ultrasonic bath (2800 Ulstrasonic cleaner 2.8L, Branson) and used within 30 minutes of preparation. Using a spray gun (Custom Micron Absolute Precision, Iwata) connected to a N_2 gas line at a pressure of 0.6 bar, the ink was dispersed onto the carbon papers. Before using the ink, the ink was vortexed for about 10 seconds. A total of 2 mL of ink was pipetted into the cup of the spray gun, which was used to spray the first layer onto 2 electrodes. This was repeated again with 2 mL of ink, to make two electrodes with a loading of 1 ± 0.3 mg Ag/cm^2 and 4 wt% Nafion. The prepared electrodes were kept on the hot plate for 10 more minutes to ensure all isopropanol had evaporated, after which they were weighed again to measure the loading.

C.1.3 Gas Product Analysis

The gas products formed were measured inline using a gas chromatograph (Compact GC 4.0, Interscience). The GC was equipped with two thermal conductivity detectors and one flame ionization detector. Samples were measured at 3 minute intervals during the experiments. Argon was used as flushing gas, which was purged in the head space of the catholyte vessel at a constant flow rate of 100 mL/min using a mass flow controller (Bronkhorst). The outlet gas stream of the catholyte vessel passed through a liquid trap filled with silica beads (Sigma Aldrich) and a mass flow meter

(Bronkhorst), before it entered the GC. The GC was equipped with a pump at the outlet, which pumps in a constant amount of gas into the channels of the GC before a sample is taken, otherwise the gas is vented off. This allows the use of a larger gas flow without building up pressure in the lines. The gas flow going into the GC is a mixture of the products, unreacted CO_2 and the argon carrier gas. The MFC used was calibrated for CO_2, hence the measured flow (Q_m) had to be corrected for the actual flow (Q_r) by using the gas conversion factors (GCF_i) for each separate component.

$$\mathrm{GCF}_i = \frac{\rho_{\mathrm{N}_2} \cdot C_{p_{\mathrm{N}_2}}}{\rho_i \cdot C_{p_i}} \tag{C.1}$$

Then, the GCF for the mixture (GCFmix) was calculated and the actual flow (Qr) can be determined.

$$\mathrm{GCF}_{mix} = \left(\frac{c_i}{\mathrm{GCF}_i} + \frac{c_{i+1}}{\mathrm{GCF}_{i+1}} + \cdots + \frac{c_n}{\mathrm{GCF}_n} + \frac{10^6 - (c_i + c_{i+1} + \cdots + c_n)}{\mathrm{GCF}_{\mathrm{Ar}}} \right)^{-1} \cdot 10^6 \tag{C.2}$$

$$Q_r = Q_m \cdot \frac{\mathrm{GCF}_{\mathrm{mix}}}{\mathrm{GCF}_{\mathrm{CO_2}}} \tag{C.3}$$

The corrected gas flow was used to calculate the faradaic efficiency (FE)

$$\mathrm{FE} = \frac{n \cdot c_i \cdot F \cdot Q_r \cdot p}{R \cdot T \cdot I} \cdot 100\% \tag{C.4}$$

C.1.4 Gas Chromatograph Calibration Method

The gas chromatograph (GC) uses 3 channels and two different detectors. All channels use Helium as carrier gas. The first channel has on main Rtx-1 column (15 m length, 0.32 mm ID) and an flame ionization detector (FID). This channel is used for the detection of hydrocarbons, of which a calibration is available for methane and ethylene. The second channel has a Carboxen 1010 pre-column (3 m length, 0.32 mm ID), a Carboxen 1010 main column (7 m length, 0.32 mm ID), and a thermal conductivity detector (TCD). On this channel, only CO_2 is calibrated. Theoretically, CO can also be detected on this channel. However, due to the use of Argon as flush gas in the electrochemical setup, these peaks are overlapping. The third channels uses

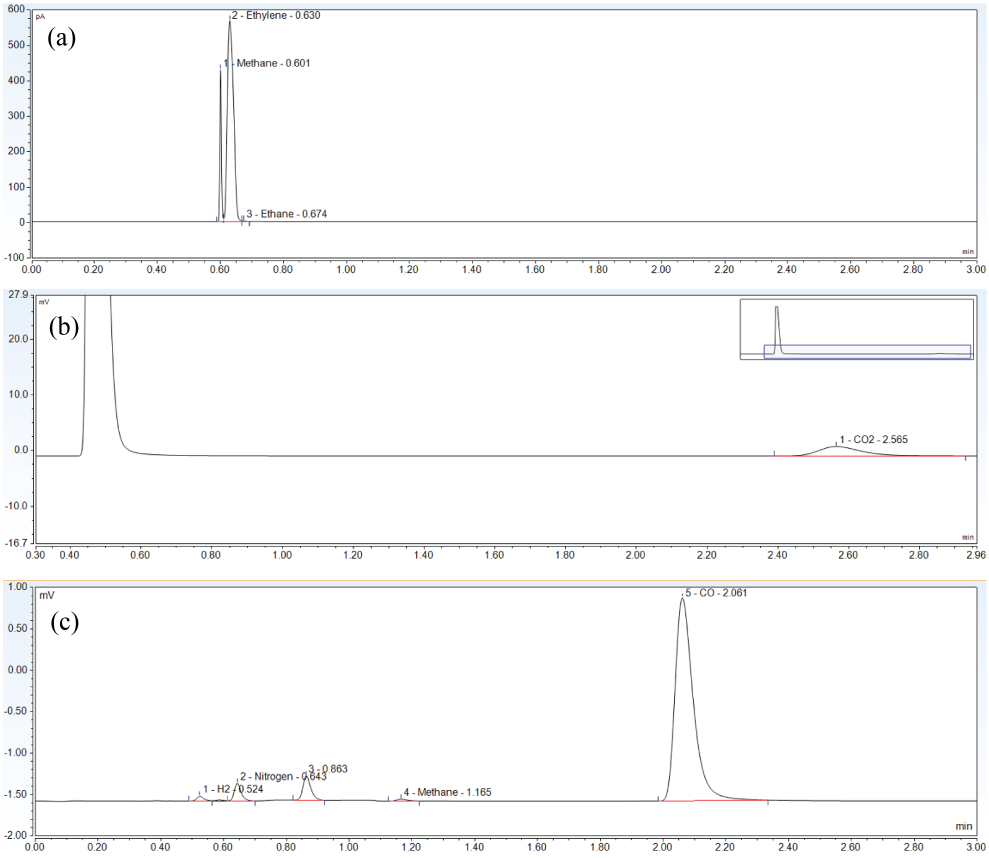

Figure C.3: Chromatograms of (a) the first channel, measuring methane and ethylene, (b) the second channel, measuring CO_2 and (c) the third channel, measuring H_2 and CO.

a Rt-Qbond pre-column (3 m length, 0.32 mm ID), Molsieve 5A main column (7 m length, 0.32 mm ID), and a TCD as well. On this channel, hydrogen and CO are calibrated. The sensitivity for hydrogen is limited, therefore lower concentrations are less accurately detected. The amount of hydrogen that is produced in the electrochemical cell is in higher concentrations and therefore accurate for the measurements needed in this system. The calibration is performed using 5 different gas bottles with fixed amounts of gases mixed in CO_2. The gas mixture is made up of hydrogen, carbon monoxide, methane, and ethylene. Each component is calibrated at a concentration of 50, 100, 1000, 3000, and 8000 ppm. CO_2 is calibrated separately, since this is the bulk gas in the calibration bottles. A back flush is used after the pre-column on the second and third channel to prevent the CO_2 from poisoning the main column. The CO_2 calibration is performed by mixing N_2 and CO_2 in different concentrations using mass flow controllers (Bronkhorst). The chromatograms of for the different channels can be seen in Figure C.3.

C.2 Longer Term Electrolysis

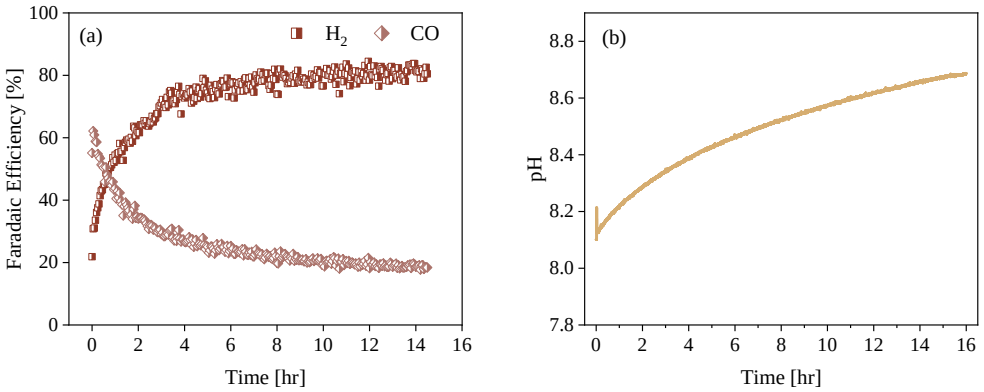

Figure C.4: Longer term stability of zero-gap bicarbonate electrolyser at 100 mA/cm^2 using a Ag spray-coated cathode and recirculating 3 M $KHCO_3$ catholyte (1 L) and 1 M KOH anolyte (0.5 L). (a) Faradaic efficiencies over time towards H_2 and CO for a zero-gap configuration. (b) The change in electrolyte bulk pH over time. All results are average values of duplicate measurements with an average error of ± 3% and total FE of <98%.

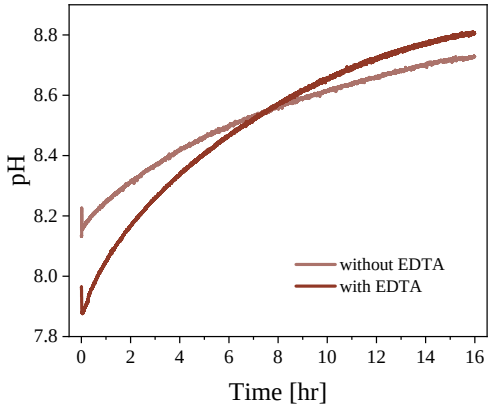

Figure C.5: The change in electrolyte bulk pH over time for the longer term stability experiment of the bicarbonate electrolyser at 100 mA/cm^2 using a Ag spray-coated cathode and recirculating 3 M $KHCO_3$ catholyte (1 L) and 1 M KOH anolyte (0.5 L).

C.3 Scanning Electron Microscopy

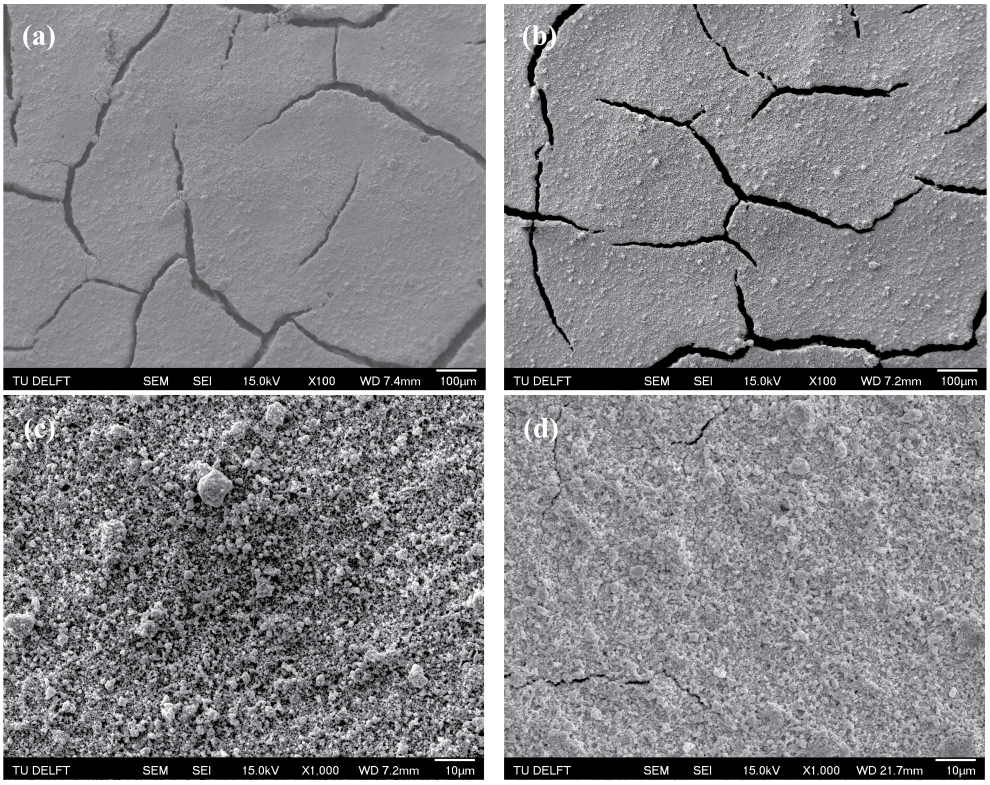

Figure C.6: SEM images (a) and (c) of a fresh electrodes, (b) and (d) of an electrode post-electrolysis. Except for small cracks due to the catholyte flow through the electrode, no visual changes of the surface are visible.

C.4 Inductively Coupled Plasma Spectroscopy

Table C.1: ICP results for the electrolyte of the longer-term electrolysis runs (3 hours and 15 hours), presented in ppm.

Sample		**Ba**	**Ca**	**Fe**	**Na**	**Cl**
Blank		0.07	0.02	0.03	110.06	26.36
3hrs	Zero-gap	0.09	0.23	0.05	161.79	24.26
3hrs	135 μm	0.08	0.08	0.04	156.32	12.36
3hrs	270 μm	0.09	0.08	0.08	144.76	11.18
3hrs	405 μm	0.08	0.14	0.10	146.32	16.32
15hrs	Zero-gap	0.06	0.03	0.04	124.87	18.30
15 hrs	135 μm	0.07	0.03	0.05	108.70	4.95

Table C.2: List of contaminants present in the $KHCO_3$ (batch BCCL2557) and K_2CO_3 (batch BCCL0256) used. [189,190]

Component	**Concentration [mg/kg]**	
	$KHCO_3 \geq 99.7\%$	$K_2CO_3 \geq 99.0\%$
Sodium (Na)	<300	<200
Silicate (as SiO_2)	n.a.	<50
Sulfur as SO_4	<30	<40
Calcium (Ca)	<20	<10
Magnesium (Mg)	<10	<5
Chloride (Cl)	<10	<10
Iron (Fe)	<5	<5
Phosphate (PO_4)	<5	<10
Ammonia (NH_4)	<5	n.a.
Heavy metals (as Pb)	<5	<5

C.5 Potentials

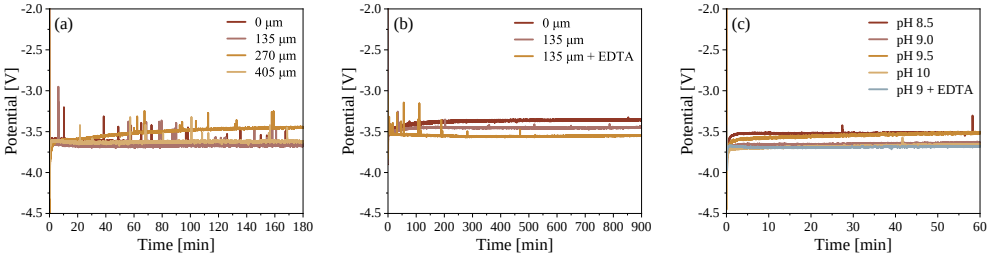

Figure C.7: The measured potential over time for all (a) 3 hour experiments, (b) 15 hour experiments, and (c) single pass experiments.

Appendix D

Supporting Information to Chapter 5

Appendix D

D.1 Experimental Section

D.1.1 Electrode Preparation

The Ag catalysts were made by spray-coating (Custom Micron Absolute Precision, Iwata, connected to CO_2 gas line set to 0.6 bar) the catalyst ink onto a carbon support layer (Sigracet 39BB, Fuelcell Store). The ink composition was a mixture of Ag nanoparticle (20-40 nm, Thermo Fisher Scientific, 84 ± 1 mg), 4 wt% Nafion binder (Nafion 1100W, 5 wt% in water and propanol, Sigma Aldrich, 80 μL) and isopropanol (VWR Chemicals, 8 mL), which was sonicated in an ultrasonic bath (2800 Ulstrasonic cleaner 2.8 L, Branson) for 30 minutes filled with ice to ensure sufficient cooling. The carbon support layer was cut into 25 x 30 mm pieces and subsequently sonicated for 10 minutes in acetone and MilliQ water each. They were then dried on a hotplate at 90 °C for about 10 minutes and their weight measured before spray coating. After, the heat of the hotplate was turned down to 70 °C before spray coating, to ensure rapid evaporation of the isopropanol. The prepared ink was vortexed for 10 seconds before use and pipetted into the cup of the spray gun with 2 mL at a time. After all ink was used, the electrode was kept on the hot plate to fully dry, after which it was weighed again to measure the Ag loading (1 ± 0.3 mg Ag/cm^2). To make the higher Ag loading catalysts, the Ag and Nafion concentrations were increased and multiple extra layers were added, until the desired Ag loading was obtained.

D.1.2 Bicarbonate Electrolyser

The commercial ElectroCell flow cell (Micro Flow cell 10 cm^2 MFC30010) was used in all bicarbonate experiments (see Figure S1-3). A 1.5 M K^+ catholyte was used at varying pH unless specified otherwise ($KHCO_3$ 99.97%, Sigma Aldrich, K_2CO_3 ≥ 99%, Sigma Aldrich) and 1 M KOH anolyte (>85%, Sigma Aldrich). All experiments performed at ambient conditions used 1 L catholyte and 0.5 L anolyte. All experiments performed at different temperatures used 200 mL of catholyte and anolyte each, due to the size of the double-walled reservoirs (custom made by LGS, Assen, the Netherlands). A peristaltic pump (BT100-3J Basic Peristaltic Pump, Darwin Microfluidics) with two pump heads (YZ1515X-B, Darwin Microfluidics) and silicon tubing (#25, Darwin Microfluidics) was used to recirculate the electrolytes, using a flow rate of 50 mL/min. The potentiostat (SP-200, Biologic, using the EC-lab software) supplied a constant current of 500 mA to the cathode, which corresponds to 100 mA/cm^2 at the 5 cm^2 active area of the cathode. A Ni foam (2 mm thickness, ElectroCell) as anode was used and a bipolar membrane (Fumasep FBM-PK). The membrane was stored in 1 M NaCl and rinsed with MilliQ water before use. A mixed cellulose ester (MCE, 8 μm pore diatemeter, MF-Millipore) membrane was used in all experiments as spacer between the Ag GDE and membrane. The EPDM sealing gaskets (supplied by ElectroCell) and a thinner silicon gasket used for the cathode separated the different cell components. A interdigitated flow plate at the cathode

served simultaneously as current collectors (Ti, watercutted, 1 mm wide channels and bridges), whereas a Ni plate current collector was used at the cathode. The cell was closed evenly using 6 bolds at a torque of 3 Nm.

D.1.3 Gas Product Analysis

A compact gas chromatograph (Compact GC 4.0, Interscience) equipped with three channels (using Helium as carrier gas for each channel) and two types of detectors. Channel one has a main Rtx-1 column (15 m length, 0.32 mm ID) and an flame ionization detector (FID) and is used for the detection of hydrocarbons. Channel two has a Carboxen 1010 pre-column (3 m length, 0.32 mm ID), a Carboxen 1010 main column (7 m length, 0.32 mm ID), and a thermal conductivity detector (TCD) to measure the CO_2 concentration. Channel three is equipped with a Rt-Qbond pre-column (3 m length, 0.32 mm ID), Molsieve 5A main column (7 m length, 0.32 mm ID), and a TCD as well to measure the carbon monoxide and hydrogen products. A pump is connected to the outlet of the GC, which pumps in a constant amount of gas (at 30 mL/min) into the sample loops before an injection is taken. This allows for larger gas flow without a pressure building up inside the GC, as all other gas is vented off. The headspace of the catholyte reservoir was continuously flushed with 100 mL/min Ar (mass flow controller, Bronkhorst) to ensure a constant product flow to the gas chromatograph (GC), which measured a sample every three minutes. A liquid trap filled with silica beads (Sigma Aldrich) was installed to remove any moist in the gas stream, before entering the mass flow meter (Bronkhorst) and subsequently the GC.

D.1.4 Experimental Setup

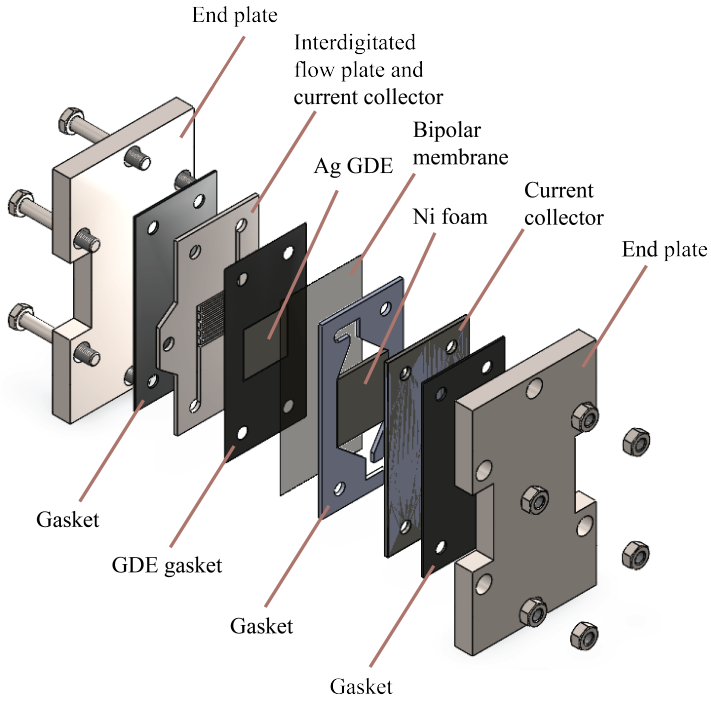

Figure D.1: Exploded view of the lab-scale bicarbonate electrolyser, indicating the different components as used.

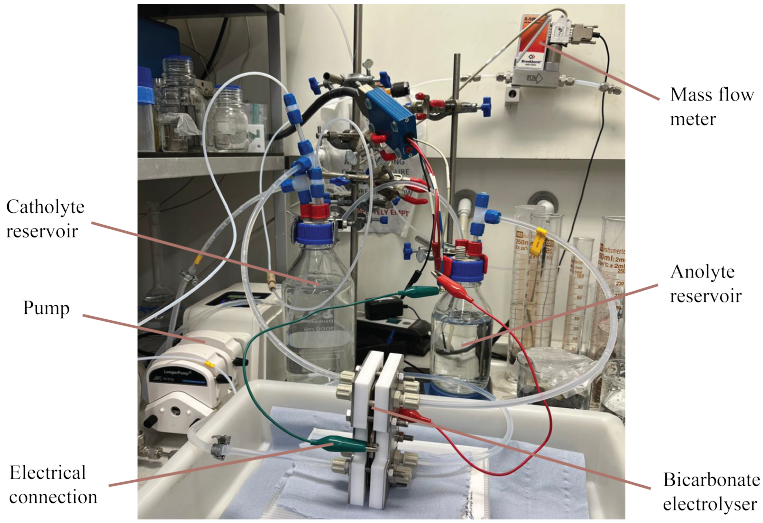

Figure D.2: Lab-scale electrochemical setup for the bicarbonate electrolyser experiments performed in this study.

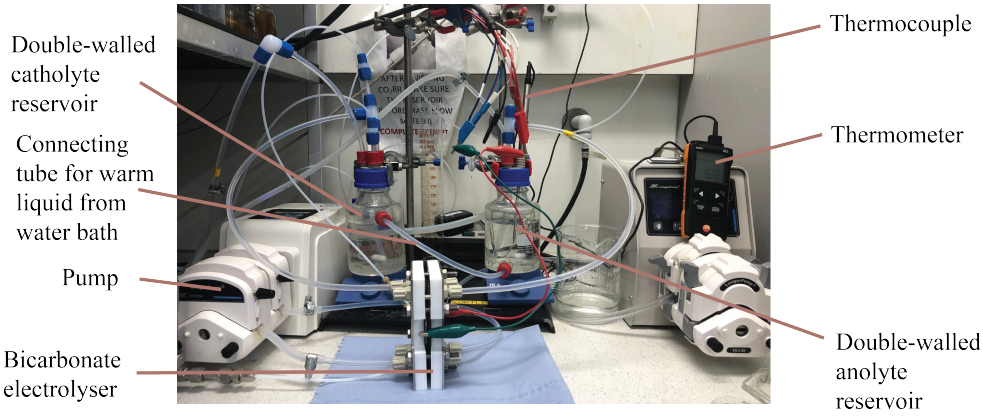

Figure D.3: Lab-scale electrochemical setup for the bicarbonate electrolyser, modified for operation at different operating temperatures. Double-walled electrolyte reservoirs are connected to a water bath supplying the heated liquid for heating of the electrolytes. Temperature is continuously measured in the anolyte compartment with a thermocouple.

D.2 Effect of K^+ Concentration

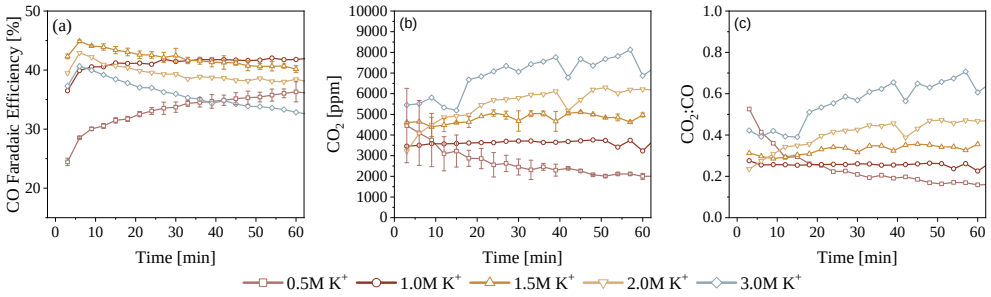

Figure D.4: Bicarbonate electrolysis at constant current of 100 mA/cm^2 showing the effect of the K^+ concentration of the catholyte over time using a constant electrolyte pH of 9 is presented for (a) the FE_{CO}, (b) the unreacted CO_2 concentration in the outlet of the electrolyser, and (c) the CO_2:CO ratio. All experiments used a 1 mg/cm^2 Ag spray coated electrode, Ni foam anode, and 1 M KOH anolyte.

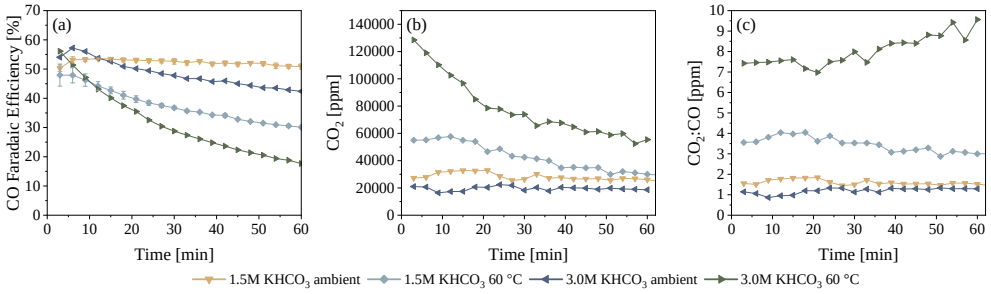

Figure D.5: Bicarbonate electrolysis at constant current of 100 mA/cm^2 showing the difference for 1.5 M and 3.0 M $KHCO_3$ catholyte at ambient temperature and 60 °C over time for (a) the FE_{CO}, (b) the unreacted CO_2 concentration in the outlet of the electrolyser, and (c) the CO_2:CO ratio. All experiments used a 1 mg/cm^2 Ag spray coated electrode, Ni foam anode, and 1 M KOH anolyte.

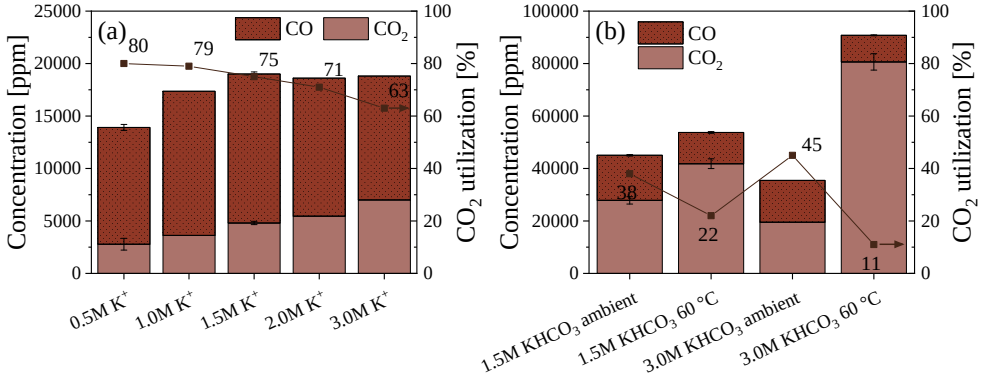

Figure D.6: Measured CO_2 and CO concentration at the outlet of the bicarbonate electrolyser and calculated CO_2 utilization. Results presented at ambient temperature for (a) varying catholyte K^+ concentration, and (b) showing the difference for 1.5 M and 3.0 M $KHCO_3$ catholyte at ambient temperature and 60 °C.

D.3 Additional Results Operating Temperature

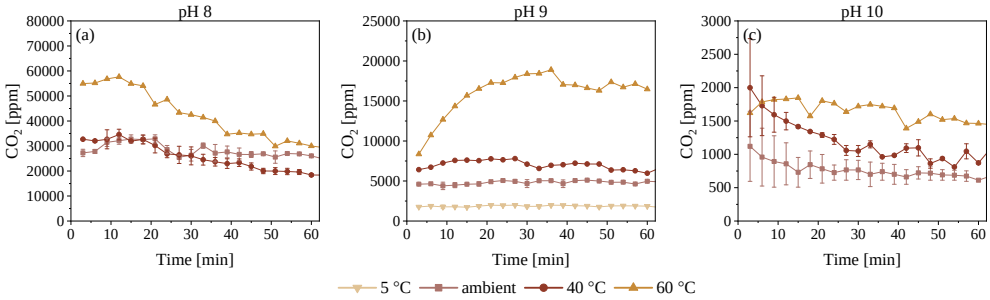

Figure D.7: Bicarbonate electrolysis at constant current of 100 mA/cm^2 and a 1.5 M K^+ catholyte. Showing the measured CO_2 concentrations over time for varying operating temperature at (a) pH 8, (b) pH 9, and (c) pH 10. All experiments used a 1 mg/cm^2 Ag spray coated electrode, Ni foam anode, and 1 M KOH anolyte.

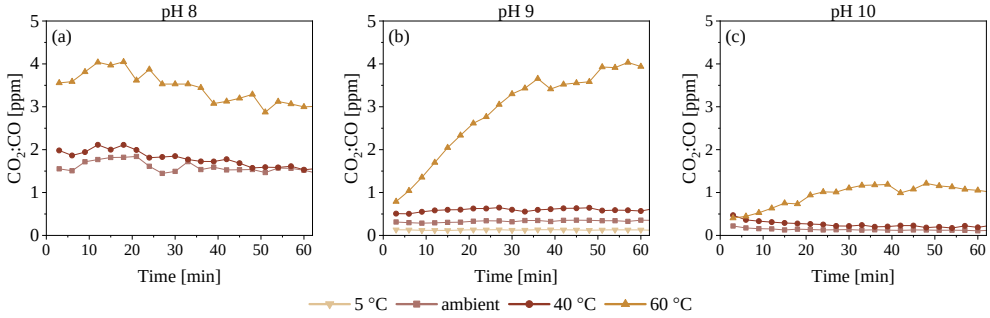

Figure D.8: Bicarbonate electrolysis at constant current of 100 mA/cm^2 and a 1.5 M K^+ catholyte. Showing the CO_2:CO ratio over time for varying operating temperature at (a) pH 8, (b) pH 9, and (c) pH 10. All experiments used a 1 mg/cm^2 Ag spray coated electrode, Ni foam anode, and 1 M KOH anolyte.

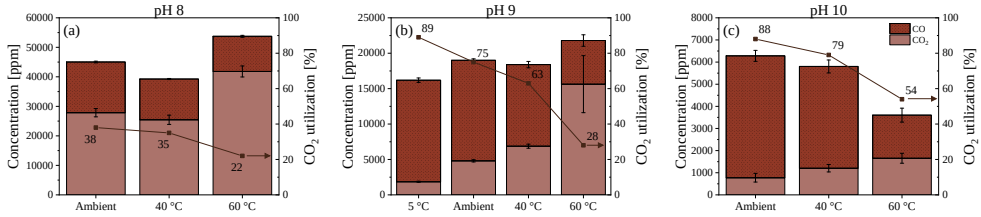

Figure D.9: Measured CO_2 and CO concentration at the outlet of the bicarbonate electrolyser and calculated CO_2 utilization. Results presented for varying operating temperature and electrolyte pH at (a) 8, (b) 9, and (c) 10.

D.4 Additional Results Increased Ag loading and EDTA

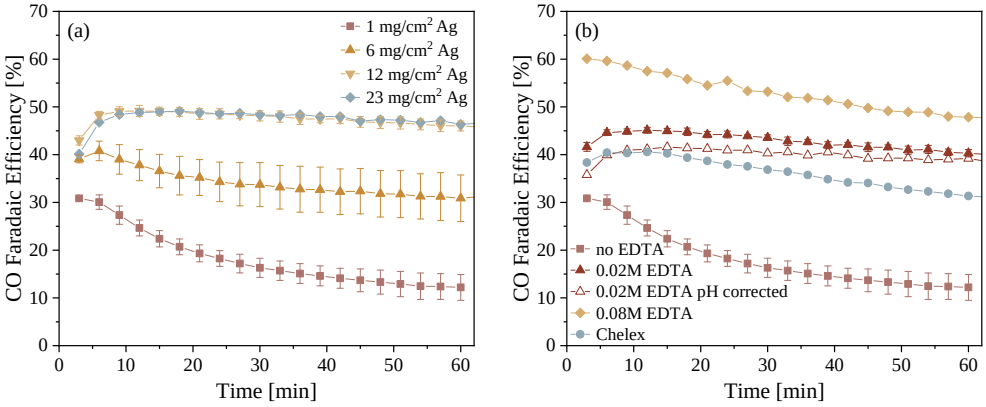

Figure D.10: Performance of bicarbonate electrolysis at constant current of 100 mA/cm^2 and operating temperature of 60 °C using a Ag spray-coated cathode and recirculating 1.5 M K^+ catholyte at pH 9 and 1 M KOH anolyte. FE_{CO} over time for (a) changing catalyst Ag loading of 1, 6, 12, and 23 mg/cm^2 Ag, and (b) increasing concentration of EDTA added to the electrolyte of no EDTA, 0.02 M, and 0.08 M as well as Chelex treated electrolyte. Error bars indicated for duplicate measurements with a maximum error of ± 5% and a total FE of 90 ± 5%.

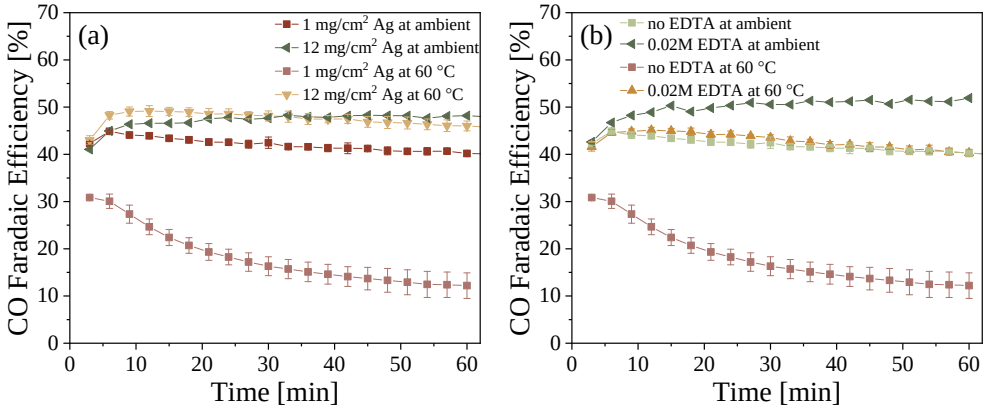

Figure D.11: Performance of bicarbonate electrolysis at constant current of 100 mA/cm^2 and constant electrolyte of 1.5 M K^+ at pH 9 and 1 M KOH anolyte. Comparing results of FE_{CO} over time for ambient temperature and 60 °C for (a) different Ag loadings and (b) increasing concentrations of EDTA added to the electrolyte. Error bars indicated for duplicate measurements with a maximum error of ± 5% and a total FE of 90 ± 5%.

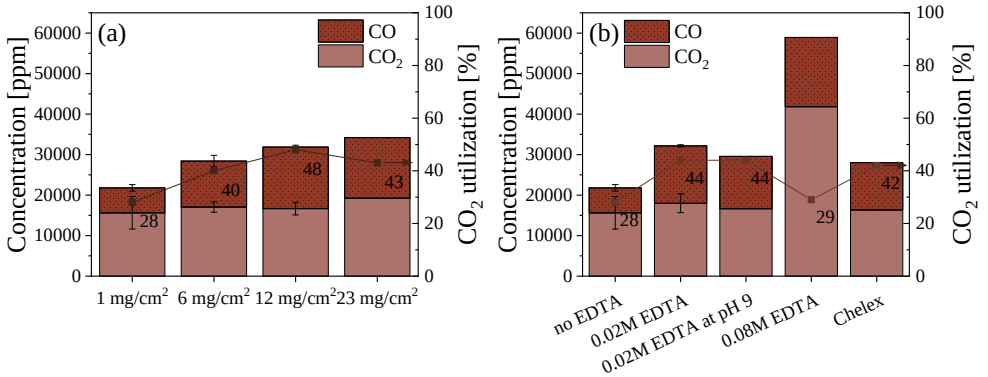

Figure D.12: Measured CO_2 and CO concentration at the outlet of the bicarbonate electrolyser and calculated CO_2 utilization. Results presented at 60 °C for (a) changing catalyst Ag loading of 1, 6, 12, and 23 mg/cm^2 Ag, and (b) increasing concentration of EDTA added to the electrolyte of no EDTA, 0.02 M, and 0.08 M as well as Chelex treated electrolyte.

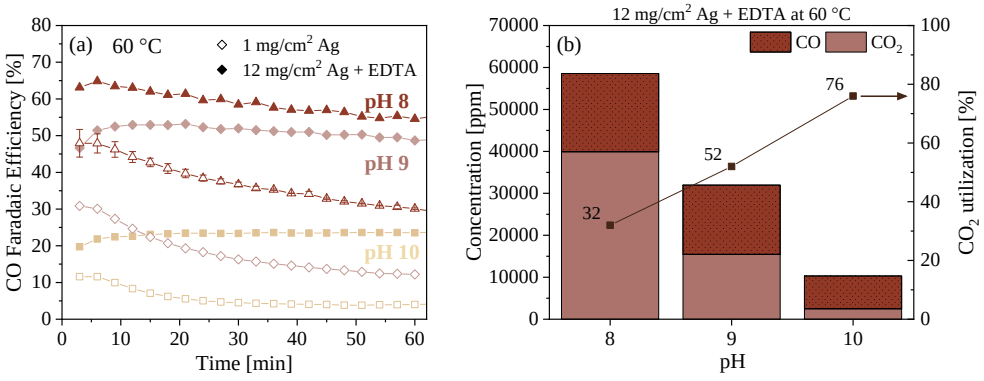

Figure D.13: Performance of bicarbonate electrolysis at constant current of 100 mA/cm^2 and operating temperature of 60 °C using a Ag spray-coated cathode and recirculating 1.5 M K^+ catholyte at varying pH and 1 M KOH anolyte. Comparing results for varying electrolyte pH 8, 9, and 10 for (a) FE_{CO} over time using 1 mg/cm^2 Ag and 12 mg/cm^2 with 0.02 M EDTA addition to the electrolyte (pH corrected) and (b) measured CO_2 and CO concentration at the outlet of the bicarbonate electrolyser and calculated CO_2 utilization for optimized system (12 mg/cm^2 Ag and 0.02 M EDTA).

D.5 Potentials

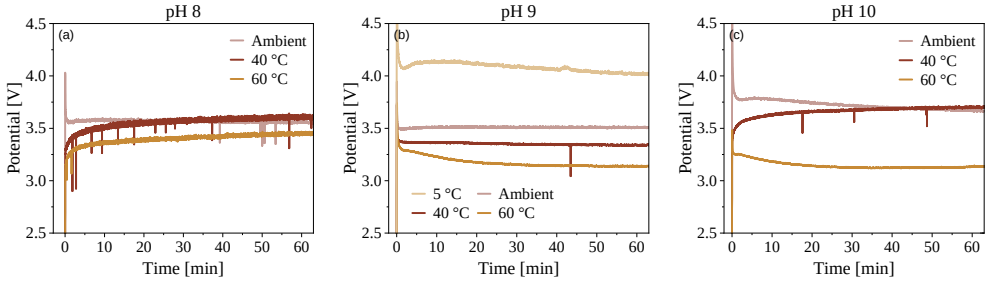

Figure D.14: Measured potential over time for bicarbonate electrolysis experiments at 100 mA/cm^2 at varying operating temperatures for and electrolyte pH at (a) 8, (b) 9, and (c) 10.

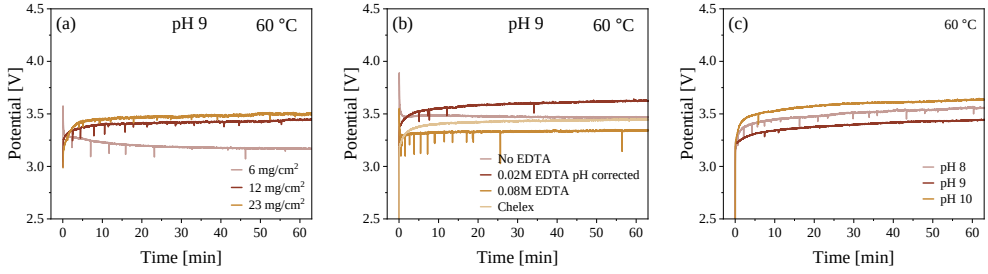

Figure D.15: Measured potential over time for bicarbonate electrolysis experiments at 100 mA/cm^2 at constant electrolyte of 1.5 M K^+ and 60 °C for (a) increasing Ag catalyst loading and constant pH 9, (b) changing EDTA concentration and constant pH 9, and (c) for changing pH and 12 mg/cm^2 Ag loading combined with 0.02 M EDTA addition (pH corrected).

D.6 Inline pH Measurement

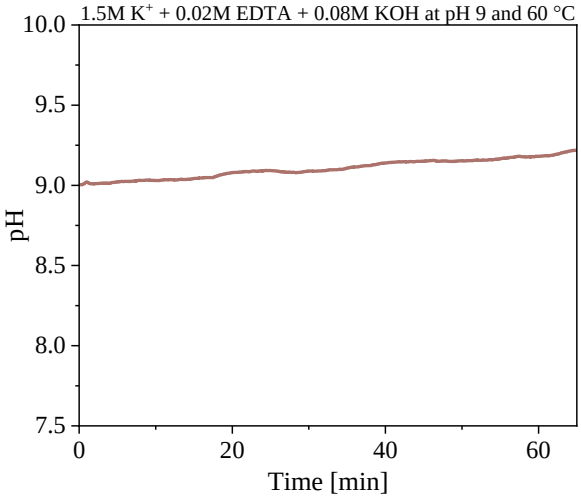

Figure D.16: Measured change in pH over time during the bicarbonate electrolysis experiment at 100 mA/cm^2 when using 1.5 M K^+ at pH 9, operating at 60 °C and 0.02 M EDTA addition (pH corrected) for 1 mg/cm^2 Ag electrode.

D.7 Inductively Coupled Plasma Spectroscopy

Table D.1: Results ICP in ppm [mg/kg].

Sample	**Al**	**B**	**Cu**	**Fe**	**Na**	**Si**
Blank electrolyte	0.79	0.11	0.06	0.15	85.32	0.81
Chelex treated before electrolysis	1.06	0.13	0.06	0.09	111.76	1.38
Chelex treat after electrolysis	0.96	0.23	0.06	0.10	165.64	2.62

D.8 Additional Electrolysis Results

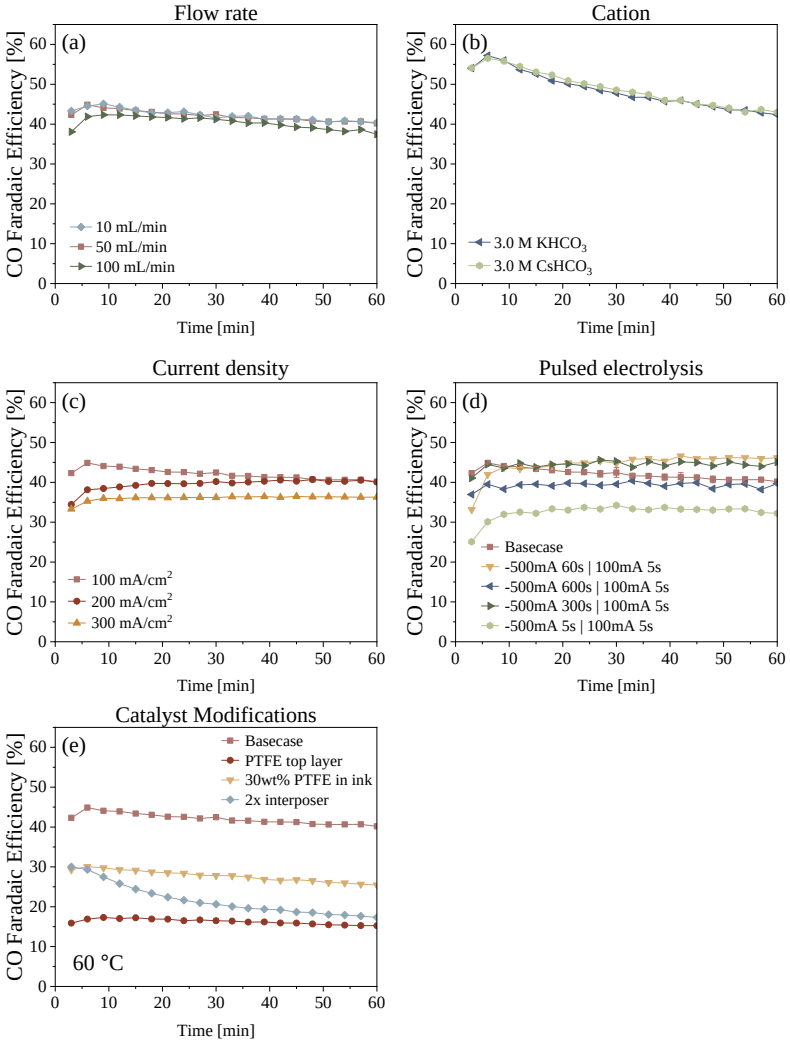

Figure D.17: Bicarbonate electrolysis results for various tested conditions using a 1.5 M K^+ electrolyte at pH 9 showing the FE_{CO} at (a) increasing electrolyte flowrate, (c) increasing applied current density, (d) pulsed electrolysis for different applied reducing and oxidizing currents and time intervals, and (e) for different catalyst modifications at 60 °C. FE_{CO} for a 3 M HCO_3 electrolyte at ambient conditions for (b) different cations.

Appendix E

Supporting Information to Chapter 6

Appendix E

E.1 Experimental Section

E.1.1 Capture Setup

The experimental setup consisted of a custom made double-walled adsorption column with an inner diameter of 30 mm and total height of 640 mm. A set of three mass flow controllers (MFC) (Bronkhorst) were used to simulate air with a concentration of 425 ppm CO_2. A constant humidity of 40% was obtained by flowing part of the N_2 gas (1000 mL/min) through a gas washing bottle filled with MilliQ water. The remaining N_2 stream (3000 mL/min) and CO_2 (1.7 mL/min) were sent directly to a gas mixing bottle. The combined flow was sent through to the adsorption column. The relative humidity was measured before and after the column (Testo 605i). A liquid trap was placed before the infrared CO_2 gas analyser (BINOS 100 2M) to protect the equipment. Furthermore, a peristatic pump (BT100-3J Basic, Darwin Microfluidics) was used to pump the liquid solvent through the column. Both before and after the column, the pH was measured with 2 inline pH probes (InPro3250i with Transmitter M300 Water 2-channel, Mettler).

E.1.2 Adsorption and Desorption

Before each experiment the adsorbent material (20 g LEWATIT® VP OC 1065) was pretreated; first by drying overnight in a vacuum oven at 80 °C, then by purging with N_2 at 80 °C in the double walled column until no remaining CO_2 was detected by the gas analyser. Before starting the adsorption cycle, the column was brought back to ambient temperature, while continuously purging with N_2. At the start of the adsorption cycle, the humidity sensors and the CO_2 analyser were continuously logged (Agilent BenchLink DataLogger 3).

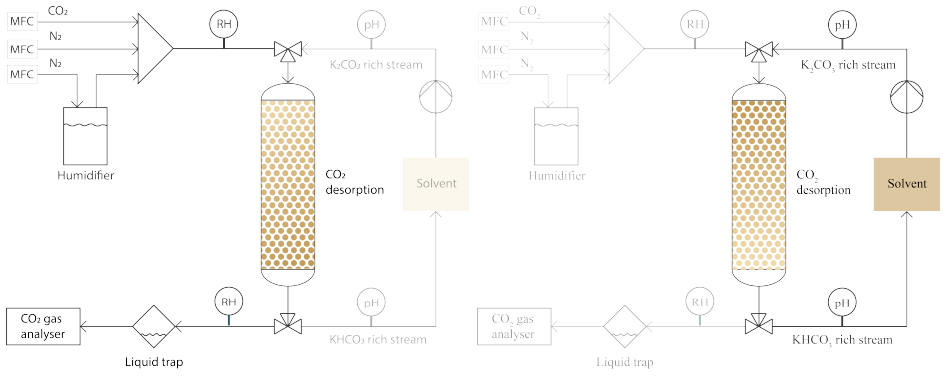

(a) (b)

Figure E.1: (a) Adsorption and (b) desorption process flow diagram.

After breakthrough was observed, the sorbent was rinsed using 200 mL 0.5 M K_2CO_3 solvent. The solvent was recirculated through the column using the pump at a flow rate of 0.63 mL/min. The pH was continuously measured before and after the column. When the pH stabilized, the desorption process was terminated. To confirm the CO_2 loading, FTIR was used for accurate measurement of the $KHCO_3$ and K_2CO_3 concentrations in the solution.

E.1.3 Electrochemical Setup

All electrochemical experiments were performed in a commercial flow cell (Micro Flow cell 10 cm^2 MFC30010, ElectroCell). The system uses a Ni foam anode (2 mm thickness, ElectroCell), bipolar membrane (Fumasep FBM-PK), and Ag spray-coated carbon support layer as cathode (5 cm^2, Ag loading of 1 $\pm$ 0.3 mg/cm^2). A 1 M KOH anolyte (>85%, Sigma Aldrich) and a catholyte of 0.5 M $KHCO_3/K_2CO_3$ (99.97%, Sigma Aldrich) at different pH conditions were used and continuously circulated through the cell using a peristaltic pump (BT100-3J Basic, Darwin Microfluidics) at a flow rate of 50 mL/min. At the cathode, an interdigitated flow plate was used with channel width of 1 mm. An exploded view of the cell and the different components can be seen in Figure E.2.

E.1.4 Electrode Preparation

The cathode was made by spray-coating Ag nanoparticles (20-40 nm, Thermo Fisher Scientific) on a carbon support (Sigracet 39BB, Fuelcell Store). The carbon support was cut into pieces of 25x30mm and sonicated in acetone and water subsequently, for 10 minutes each. The electrodes were dried prior to spray-coating on a hot plate at 90 °C. An ink was prepared using 84 $\pm$ 2 mg of Ag nanoparticles, 80 μL of Nafion binder (Nafion 1100W, 5 wt% in water and propanol, Sigma Aldrich), and 8 mL of isopropanol (IPA, VWR Chemicals). It was sonicated for 30 minutes after which it was deposited on the carbon support using a spray gun (Custom Micron Absolute Precision, Iwata) to make 4 electrodes with a Ag loading of 1 $\pm$ 0.3 mg Ag/cm^2 and 4 wt% Nafion. A hot plate at 70 °C was used to ensure rapid evaporation of the IPA.

E.1.5 Experimental Setup

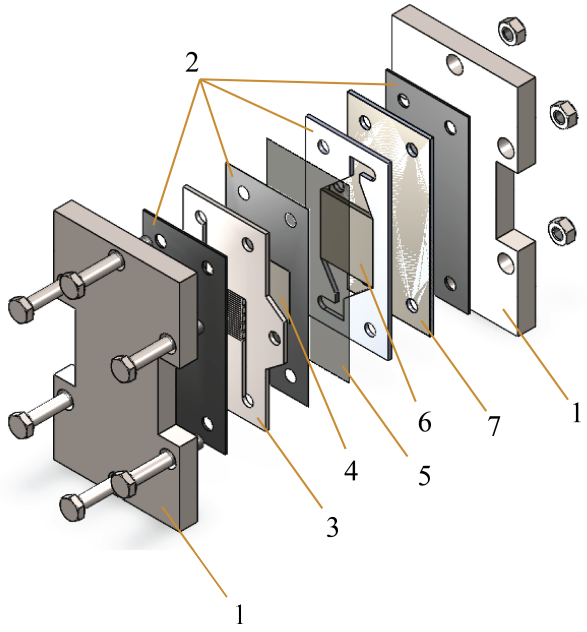

1. End plate
2. Gasket
3. Interdigitate flow plate and current collector
4. Ag GDE
5. Bipolar membrane
6. Ni foam
7. Ni current collector

Figure E.2: Exploded view of the electrochemical cell with list of components.

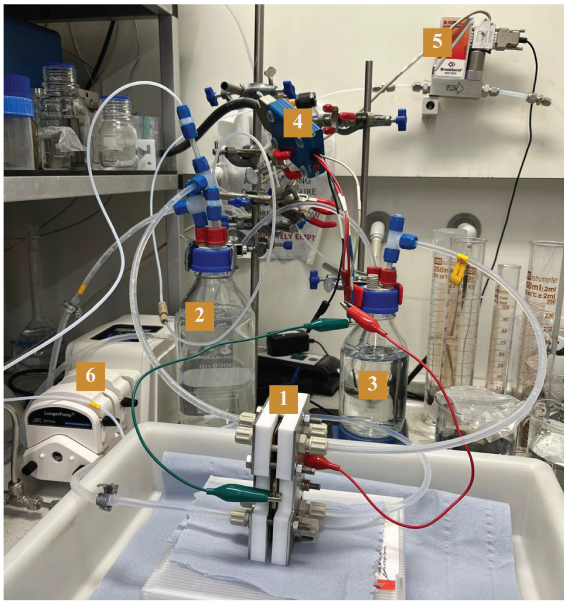

1. Electrolyser
2. Catholyte vessel
3. Anolyte vessel
4. Potentiostat connection
5. Mass flow controller
6. Liquid pump

Figure E.3: Electrochemical lab setup used for the bicarbonate electrolysis experiments.

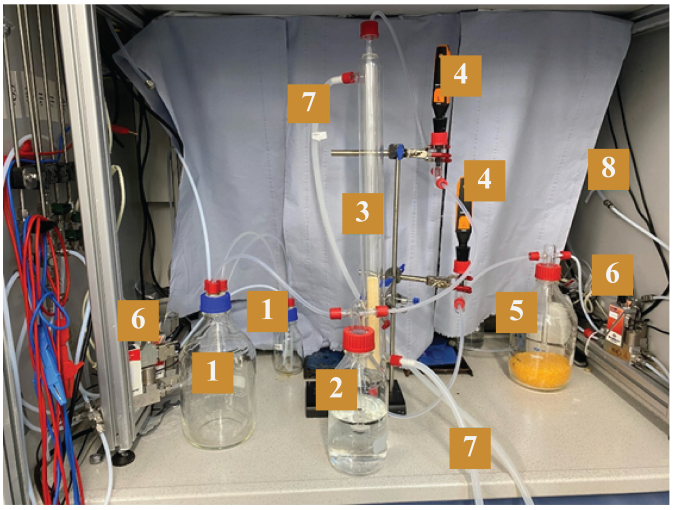

1. Gas mixing
2. Humidifier
3. Adsorber column
4. Humidity and temperature sensor
5. Liquid trap
6. Mass flow controllers
7. Tubing to water bath
8. Tubing to gas analyser

Figure E.4: Experimental lab setup used for the adsorption and desorption experiments.

E.2 Additional Experimental Data

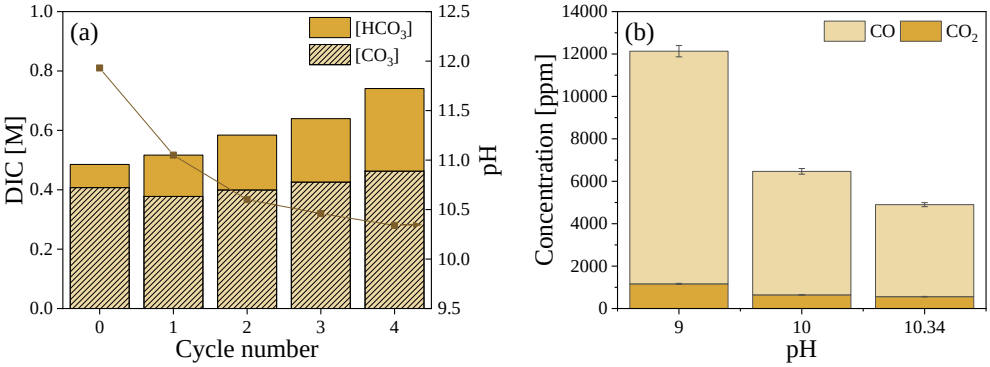

Figure E.5: (a) Dissolved Inorganic Carbon (DIC) in the form of (bi)carbonate for different desorption cycles measured using FTIR (bars), as well as the solvent pH after desorption (symbols). (b) The measured concentrations of the gaseous CO and CO_2 at the outlet of the electrolyser as a function of pH, measured during the 1 hour chronopotentiometry experiment at 100 mA/cm^2. Error bars indicated for duplicate measurement results.

E.3 Energy consumption and voltage efficiency

The energy consumption per mole CO produced is calculated as,

$$E_{\mathrm{CO}} = \frac{n \cdot E \cdot F}{\mathrm{FE_{CO}}} \tag{E.1}$$

where n=2 is the number of electrons involved, E the cell potential, F the faradaic constant (96485 C/mol), and $\mathrm{FE_{CO}}$ the faradaic efficiency towards CO. A cell potential of 3.8-4.0 V was measured during electrolysis. The voltage efficiency of the co-electrolysis of water and CO_2 is calculated as,

$$VE = \mathrm{FE_{CO}} \cdot \frac{E_{\mathrm{tn,CO}}}{E} + \mathrm{FE_{H_2}} \cdot \frac{E_{\mathrm{tn,H_2}}}{E} \tag{E.2}$$

where E_{tn} is the thermoneutral voltage for each reaction, calculated from the enthalpy of reaction for the bicarbonate and water electrolysis reactions. The enthalpy of reaction is obtained from the reaction stoichiometry υ and the enthalpy of formation of the products and reactants (Hess's law), taken from.[68]

$$E_{\mathrm{tn},i} = \frac{\Delta H_{\mathrm{r},i}}{n_i \cdot F} \tag{E.3}$$

$$\Delta H_r = \sum_{i=1}^{n_{\mathrm{prod}}} \nu_i \cdot \Delta H_{\mathrm{f},i} - \sum_{j=1}^{n_{\mathrm{reac}}} \nu_j \cdot \Delta H_{\mathrm{f},j} \tag{E.4}$$

$$\mathrm{HCO_3^-} \rightarrow \mathrm{CO} + \mathrm{OH^-} + \frac{1}{2}\mathrm{O_2} \quad \Delta H_r = 351.46\ \mathrm{kJ/mol} \quad V_{\mathrm{tn,CO}} = 1.82\ \mathrm{V} \tag{E.5}$$

$$\mathrm{H_2O} \rightarrow \mathrm{H_2} + \frac{1}{2}\mathrm{O_2} \quad \Delta H_r = 285.82\ \mathrm{kJ/mol} \quad V_{\mathrm{tn,H_2}} = 1.48\ \mathrm{V} \tag{E.6}$$

E.4 Model Description

E.4.1 Solution Equilibrium

The (bi)carbonate solution is assumed to always be in chemical equilibrium. The composition is calculated through the chemical equilibria of water disassociation (Equation E.7), bicarbonate formation (Equation E.8), and carbonate formation (Equation E.9). Due to high pH ranges, we did not consider the presence of free dissolved CO_2. The total Dissolved Inorganic Carbon (DIC) is calculated as the sum of all carbon species concentrations (Equation E.10).

$$\text{Water dissociation:} \quad pK_w = -\log_{10}\left([H^+]\cdot[\mathrm{OH}^-]\right) \tag{E.7}$$

$$\text{Bicarbonate formation:} \quad pK_1 = -\log_{10}\left(\frac{[\mathrm{HCO}_3^-]\cdot[H^+]}{[\mathrm{H_2CO_3}]}\right) \tag{E.8}$$

$$\text{Carbonate formation:} \quad pK_2 = -\log_{10}\left(\frac{[\mathrm{CO}_3^{2-}]\cdot[H^+]}{[\mathrm{HCO}_3^-]}\right) \tag{E.9}$$

$$\text{Dissolved Inorganic Carbon:} \quad \mathrm{DIC} = [\mathrm{H_2CO_3}] + [\mathrm{HCO}_3^-] + [\mathrm{CO}_3^{2-}] \tag{E.10}$$

E.4.2 Absorber Model

The absorber is modelled as a chemical equilibrium between the (bi)carbonate solution and the amine-functionalised resin. The protonation of the amine group (Equation E.11) is added to the equilibrium calculation. The total amine concentration of the sorbent-solution mixture (Equation E.12) is calculated from the amine loading. Before regeneration, we consider the resin loaded CO_2 in the form of bicarbonate ions (Equation E.13), as any CO_2 in carbamate form would rapidly convert to bicarbonate form when saturated with water. During regeneration, the total DIC is the sum of the DIC present in the lean solution and the adsorbed CO_2 (Equation E.14). When the solution is drained from the column, the bicarbonate remaining on the lean resin is taken equal to the concentration of protonated amines to maintain charge neutrality (Equation E.15). The DIC of the solution produced after regeneration is then the DIC from the sorbent-solution mixture minus any bicarbonate remaining on the resin (Equation E.16). The volume of water lost in one regeneration step is taken equal to the interstitial volume of the adsorber column (Equation E.17). Finally, the adsorption time is determined by the sorbent working capacity and the adsorption rate (Equation E.18).

$$\text{Amine protonation:} \quad pK_a = -\log_{10}\left(\frac{[RNH_2]\cdot[H^+]}{[RNH_3^+]}\right) \tag{E.11}$$

$$\text{Amine concentration:} \quad [RNH_2] + [RNH_3^+] = q_{\text{Am}} \cdot M_s / V_l \tag{E.12}$$

$$\text{Before regeneration:} \quad [RNH_3^+] = [\text{HCO}_3^-]_{\text{ads,rich}} = q_{\text{CO}_2,\text{rich}} \cdot M_s / V_l \tag{E.13}$$

$$\text{During regeneration:} \quad \text{DIC}_{\text{regen}} = \text{DIC}_{\text{in}} + [\text{HCO}_3^-]_{\text{ads}} \tag{E.14}$$

$$\text{After regeneration:} \quad q_{\text{CO}_2,\text{lean}} = [\text{HCO}_3^-]_{\text{ads,lean}} \cdot V_l / M_s = [RNH_3^+] \cdot V_l / M_s \tag{E.15}$$

$$\text{DIC}_{\text{out}} = \text{DIC}_{\text{regen}} - [\text{HCO}_3^-]_{\text{ads,lean}} \tag{E.16}$$

$$\text{Water loss:} \quad V_{\text{WL}} = \varepsilon_b M_s / \rho_b \tag{E.17}$$

$$\text{Adsorption time:} \quad t_{\text{ads}} = q_{\text{CO}_2,\text{rich}} - q_{\text{CO}_2,\text{lean}} / R_{\text{ads}} \tag{E.18}$$

E.4.3 Electrolyser Model

The electrolyser is modelled as a stack of cells, each cell at a constant pH. The production rates of CO, H_2 and unreacted CO_2 in each cell i are calculated from the electrode area, current density, Faradeic efficiency and CO_2 utilisation fraction (Equation E.19-E.21). The latter two are calculated as function of the cell pH by linear interpolation of the experimental results in Figure 6.2)(b). The DIC is reduced by the CO and CO_2 production rates (Equation 16), after which the equilibrium calculation (Equation E.7-E.10) are repeated to find the pH of the next cell. The total gas production rate of compound j is the sum over all cells in the stack (Equation E.23).

$$\text{CO production rate:} \quad R_{\text{CO},i} = \frac{A_i \cdot j_i}{2F} \cdot \text{FE}_{\text{CO}}(\text{pH}_i) \tag{E.19}$$

$$\text{H}_2\text{ production rate:} \quad R_{\text{H}_2,i} = \frac{A_i \cdot j_i}{2F} \cdot (1 - \text{FE}_{\text{CO}}(\text{pH}_i)) \tag{E.20}$$

$$\text{CO}_2\text{ liberation rate:} \quad R_{\text{CO}_2,i} = R_{\text{CO},i} \cdot \frac{1 - \text{Ut}(\text{pH}_i)}{\text{Ut}(\text{pH}_i)} \tag{E.21}$$

$$\text{Dissolved Inorganic Carbon:} \quad \text{DIC}_{\text{out},i} = \text{DIC}_{\text{out},i-1} - (R_{\text{CO},i} + R_{\text{CO}_2,i})/\phi_V \tag{E.22}$$

$$\text{Total gas production rate:} \quad R_j = \sum_{i=1}^{N_{\text{cells}}} R_{j,i} \tag{E.23}$$

E.4.4 Convergence

To simulate the situation in which the adsorber column and electrolyser reach a mutual equilibrium, we looped the models until converged. Starting from an initial potassium bicarbonate solution fed to adsorber, to adsorber output was fed to the

electrolyser model, constituting one iteration. After each iteration, rate of the carbon mass adsorption in the column (Equation E.24) and the rate of carbon mass release in the electrolyser (Equation E.25) were calculated, and the error between them (Equation E.26) compared to a pre-set tolerance. If the convergence criterion (Equation E.27) was met, the simulation was ended, otherwise the electrolyser output composition was fed back to the column model for another iteration. Figure E.6 shows the convergence of the pH (a) and mass error (b) for a typical case.

$$\text{Carbon adsorption rate:} \quad M_{C,\text{in}} = (q_{\text{CO}_2,\text{rich}} - q_{\text{CO}_2,\text{lean}}) \cdot M_s / t_{\text{ads}} \tag{E.24}$$

$$\text{Carbon release rate:} \quad M_{C,\text{out}} = \phi_{m,\text{CO}_2} + \phi_{m,\text{CO}} \tag{E.25}$$

$$\text{Carbon mass error:} \quad \text{Error}_C = |M_{C,\text{in}} - M_{C,\text{out}}| \, / M_{C,\text{in}} \tag{E.26}$$

$$\text{Convergence criterion:} \quad \text{Error}_C \leq \text{Tol} \tag{E.27}$$

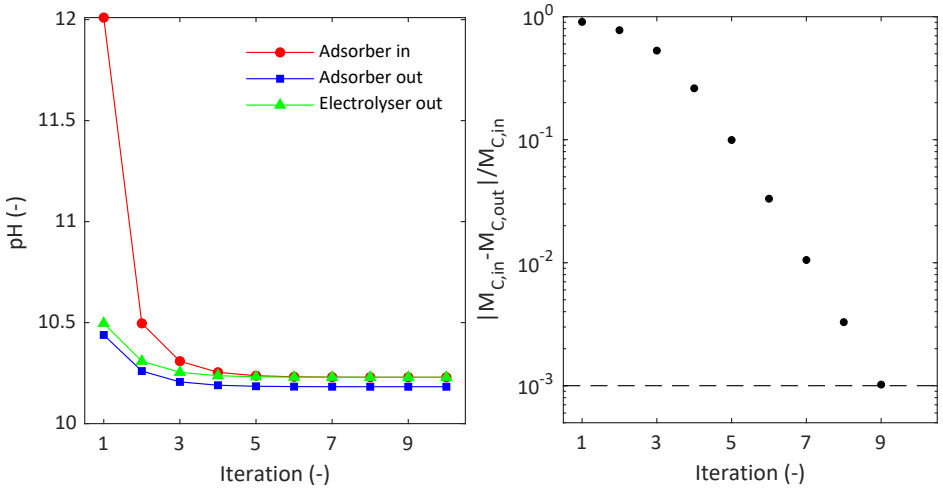

Figure E.6: Convergence of adsorber and electrolyser pH (a) and carbon mass balance (b) as function of iteration number. The adsorber-electrolyser loop is iterated until the mass-error is below the set tolerance (0.1%, indicated by the dashed line in (b)). In this example, convergence is achieved after 15 iterations

E.4.5 Parameters

Table E.1 provides an overview of the constant parameters used in our modelling. The two design parameters used for scaling the system are the total electrode area per volumetric solvent flow rate (A_e/ϕ_V), varied between 1-63 s/mm, and the sorbent mass per solvent volume (M_s/V_l), varied between 10-200 kg/m^3. The base case A_e/ϕ_V = 9 s/mm and M_s/V_l = 100 kg/m^3 corresponds to our experimental conditions.

Table E.1: Constant parameters used in modelling

Water disassociation eq. constant	pK_w	14.0	-	[191]
Bicarbonate formation eq. constant	pK_1	6.35	-	[191]
Carbonate formation eq. constant	pK_2	10.33	-	[191]
Amine protonation eq. constant	pK_a	9.34	-	[171]
Total amine loading	q_{Am}	7.5	mol/kg	[192]
Rich CO_2 loading	$q_{CO_2,rich}$	1.55	mol/kg	[192]
Adsorption rate	R_{ads}	0.093	mol/hr	This work
Bed density	ρ_b	700	kg/m^3	This work
Bed porosity	ϵ_b	0.37	-	
Current density	j	100	mA/cm^2	This work
Number of cells	N_{cells}	20	-	
Solver tolerance	Tol	10-3	-	

E.5 Additional Model Results

Figure E.7 shows the syngas ratio (a) and CO_2 utilisation (b) as function of the normalised electrode area and normalised sorbent mass. Both the faradaic efficiency and CO_2 utilisation fraction are inversely proportional to the electrolyser pH (Figure 6.2(b)). Therefore, both profiles of Figure E.5(b) are of similar shape to the electrolyser inlet pH profile in Figure 6.3(a). The highest syngas quality (high CO content, low CO_2 content) is achieved when the column and electrolyser sizing are carefully balanced.

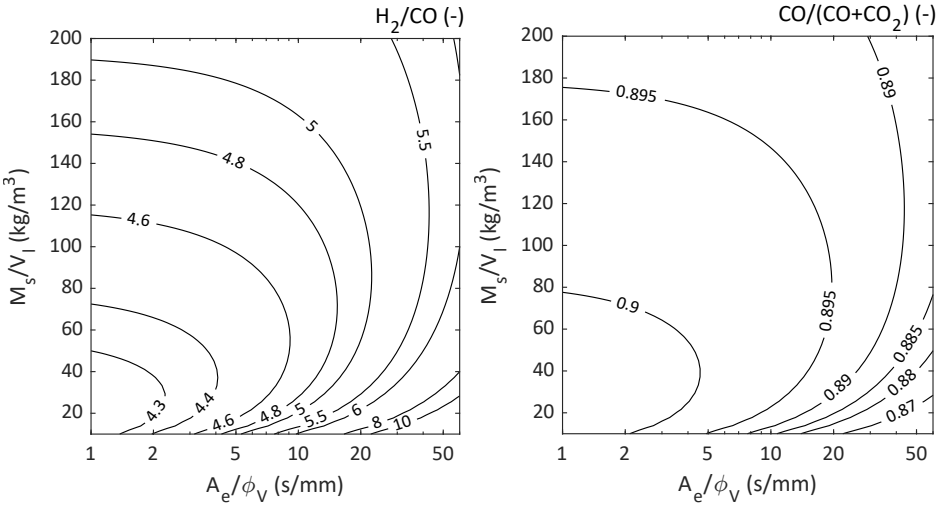

Figure E.7: Calculated results of solvent productivity (M_{CO_2}/M_l, CO_2 capture mass rate per solvent mass flow rate), (a) and water loss (M_{H_2O}/M_{CO_2}, water mass per CO_2 mass), (b) as function of electrolyser size (A_e/ϕ_V, electrode area per volumetric solvent flow rate) and column size (M_s/V_l, sorbent mass per solvent volume). Results were obtained from the model described in Section E.4.

Appendix F

Supporting Information to Chapter 7

Appendix F

F.1 Experimental Section

F.1.1 High Pressure Setup

The high pressure experiments were performed using a commercial ElectroCell flow cell (Micro Flow cell 10 cm^2 MFC30010) in a similar configuration as described previously in Chapter 4, 5, and 6. A Ni foam anode (2 mm thickness, ElectroCell) and hand spray-coated Ag cathode with different loadings were used (see Section C.1.2 and D.1.1). A bipolar membrane (Fumasep FBM-PK) was used to separate the two compartments. The cathode compartment used a Ti interdigitated flow plate and simultaneously current collector. In all experiments, a mixed cellulose ester (MCE, 8 μm pore diatemeter, MF-Millipore) membrane was used as a spacer between the cathode and membrane. At the anode, the anolyte flow was guided through the Ni foam. A 1 M KOH (<85%, Sigma Aldrich) anolyte solution and $KHCO_3/K_2CO_3$ catholyte with varying electrolyte pH was used, keeping the a constant 1.5 M K^+ concentration. A volume of 200 mL was used for both anolyte and catholyte and pumped around using a high pressure pump (Knauer P4.1S 50 mL). Two back pressure regulators (Equilibar) ensured the right pressure inside the electrolyser throughout the experiment. In Figure 1, the experimental setup is shown. For the high temperature experiments, double-walled glass reservoirs were used, in which the electrolyte temperature could be controlled using a warm water bath. A thermometer placed in the anolyte reservoir monitored the liquid temperature continuously.

All experiments were conducted at a constant current of 100 mA/cm^2 using a potentiostat (SP-200, Biologic, using the EC-lab software). A gas chromatograph analysed the products during the experiment, as described previously in Section C.1.3 and D.1.3.

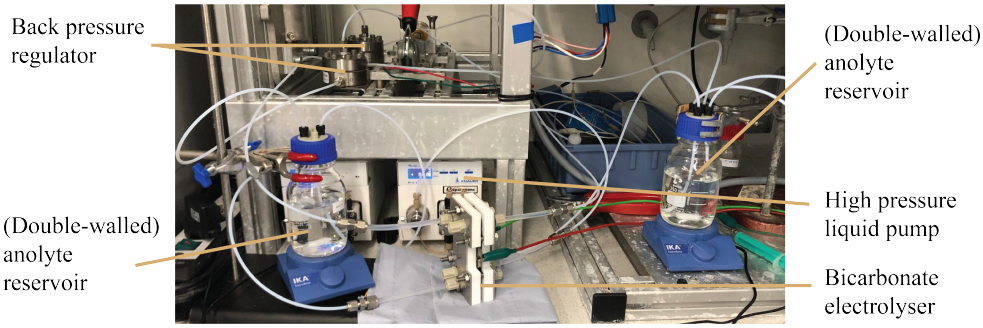

Figure F.1: Lab-scale electrochemical setup for the bicarbonate electrolyser at elevated pressures, which can be modified for operation at different operating temperatures. High pressure liquid pumps and back pressure regulators control the pressure inside the bicarbonate electrolyser.

F.2 Additional Experimental Results

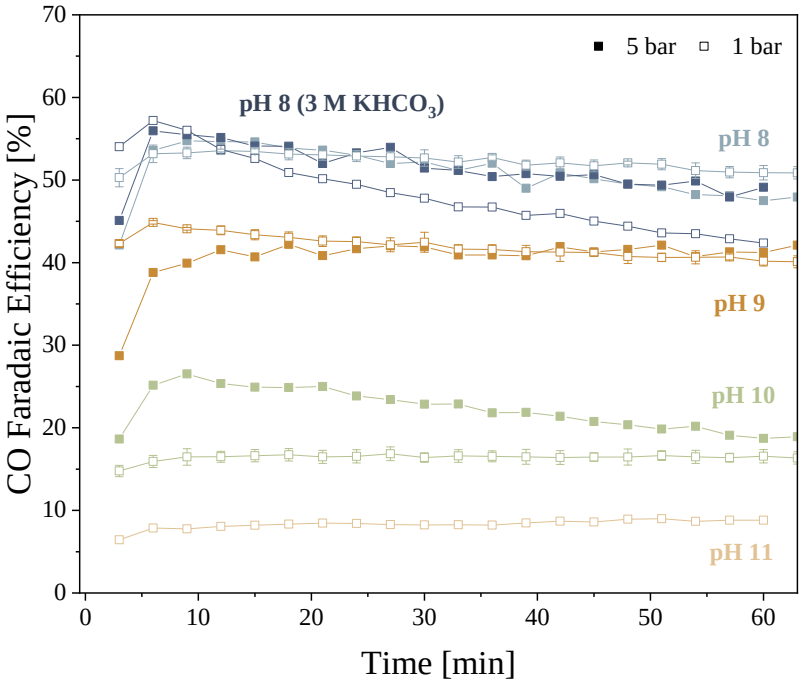

Figure F.2: Faradaic efficiency towards CO measured during the electrolysis of bicarbonate electrolyte at 100 mA/cm^2 using a 1 mg/cm^2 Ag electrode and at ambient temperature and varying for 1 and 5 bar at varying electrolyte pH using a constant 1.5 M K^+ concentration.

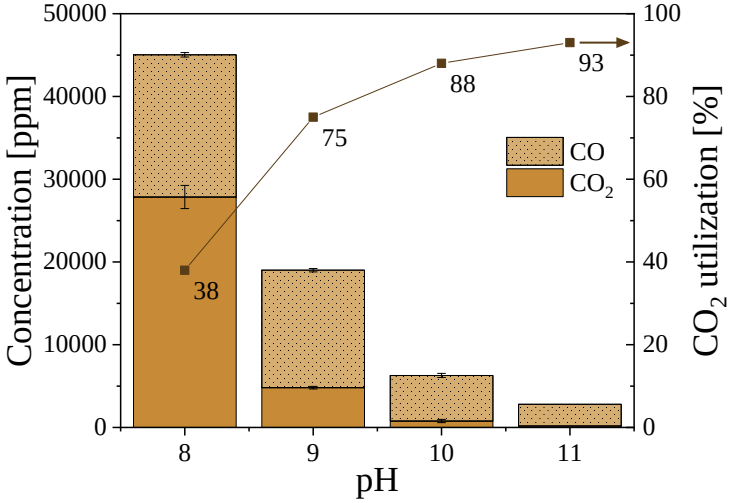

Figure F.3: Concentration of CO and CO_2 at the electrolyser gas outlet measured during the electrolysis of bicarbonate electrolyte and the calculated CO_2 utilization. Experiments performed ambient temperature and pressure using 1.5 M K^+ at varying pH and constant current of 100 mA/cm^2 and using 1 mg/cm^2 Ag electrode.

F.3 Energy consumption and voltage efficiency

The energy consumption per mole CO produced for the different electrolyte pH and operating pressure is calculated as follows,

$$E_{\mathrm{CO}} = \frac{n \cdot E \cdot F}{\mathrm{FE_{CO}}} \tag{F.1}$$

where $n = 2$ is the number of electrons involved, E the measured cell potential, F the Faradaic constant (96485 C/mol), and $\mathrm{FE_{CO}}$ the faradaic efficiency towards CO. The energy consumption per mole of CO is corrected for the co-electrolysis of water by subtracting the energy required for H_2, based on alkaline water electrolysis at 50 kWh/kg[193],

$$E_{\mathrm{CO}} = \frac{n \cdot (\mathrm{E}_{cell} - \mathrm{E_{H_2}}) \cdot F}{\mathrm{FE_{CO}}} \tag{F.2}$$

The energy consumption for the various electrolyte pH and operating pressure is tabulated in Table F.1.

Table F.1: Calculated energy consumption per mole of CO produced based on experimental cell potential and FE.

		Cell pot. [V]	**$\mathrm{FE_{CO}}$ [-]**	**$\mathrm{FE_{H_2}}$ [-]**	**$\mathrm{E_{CO}}$ [kJ/mol CO]**	**$\mathrm{E}_{corrected}$ [kJ/mol CO]**	**EE [-]**
Conventional electrolysis[181]	1 bar	3	90%	10%	643.24	240.03	59.58%
Lees et al.[64]	1 bar	3.65	82%	18%	858.95	416.42	48.22%
pH 8	1 bar	3.5	59%	41%	1144.74	529.69	48.05%
	5 bar	3.37	54%	46%	1204.28	532.28	49.40%
pH 9	1 bar	3.39	51%	49%	1282.69	571.16	48.81%
	5 bar	3.47	51%	49%	1312.96	601.43	47.68%
pH 10	1 bar	3.58	59%	41%	1170.91	555.85	46.98%
	5 bar	3.66	59%	41%	1197.07	582.02	45.95%
pH 11	1 bar	3.71	14%	86%	5113.72	2521.71	41.21%
	5 bar	3.62	8%	92%	8731.92	4195.91	41.67%

Reverse water gas shift reaction:[194]

$$\mathrm{CO_2 + H_2 \rightleftharpoons CO + H_2O} \qquad \Delta \mathrm{H}_R = 42 \text{ kJ/mol} \tag{F.3}$$

References

[1] D. Attenborough and J. Hughes, *A Life on Our Planet: My Witness Statement and a Vision for the Future* (Ebury Publishing) (2020).

[2] K. Abbass, M. Z. Qasim, H. Song, M. Murshed, H. Mahmood, and I. Younis, *A review of the global climate change impacts, adaptation, and sustainable mitigation measures*, Environmental Science and Pollution Research **29**, 42539–42559 (2022), DOI: https://doi.org/10.1007/s11356-022-19718-6.

[3] M. Pathak, R. Slade, P. R. Shukla, J. Skea, R. Pichs-Madruga, and D. Ürge Vorsatz, *Climate Change 2022: Mitigation of Climate Change. Contribution of Working Group III to the Sixth Assessment Report of the Intergovernmental Panel on Climate Change*, (Cambridge University Press) (2022), URL : https://www.cambridge.org/core/services/aop-cambridge-core/content/view/5B255A3E29E6976F492038261E811206/9781009157933pre3_51-148.pdf/technical-summary.pdf, DOI: https://doi.org/10.1017/9781009157926.002.

[4] *Climate Change: Atmospheric Carbon Dioxide*, URL : https://gml.noaa.gov/ccgg/trends/mlo.html.

[5] T. F. Stocker, D. Qin, G.-K. Plattner, M. Tignor, S. K. Allen, J. Boschung, A. Nauels, Y. Xia, V. Bex, and P. M. Midgley, *Climate Change 2013: The Physical Science Basis. Contribution of Working Group I to the Fifth Assessment Report of the Intergovernmental Panel on Climate Change*, (Cambridge University Press) (2013), URL : https://www.ipcc.ch/report/ar5/wg1/.

[6] *Atmospheric Carbon Dioxide*, URL : https://www.globalchange.gov/indicators/atmospheric-carbon-dioxide.

[7] *2023, a year of climate contrasts in Europe*, URL : https://unric.org/en/2023-a-year-of-climate-contrasts-in-europe/.

[8] O. Serdeczny, S. Adams, F. Baarsch, D. Coumou, A. Robinson, W. Hare, M. Schaeffer, M. Perrette, and J. Reinhardt, *Climate change impacts in Sub-Saharan Africa: from physical changes to their social repercussions*, Regional Environmental Change **17**, 1585–1600 (2016), DOI: https://doi.org/10.1007/s10113-015-0910-2.

[9] UNFCCC, *The Paris Agreement*, (2015), URL : https://unfccc.int/sites/default/files/resource/parisagreement_publication.pdf.

[10] *Climate change mitigation: reducing emissions*, URL : https://www.eea.europa.eu/en/topics/in-depth/climate-change-mitigation-reducing-emissions?activeAccordion=4268d9b2-6e3b-409b-8b2a-b624c120090d.

[11] J. D. Schrijver, M. Sporer, H. Förater, S. Gores, V. Graichen, C. Winger, C. Zell-Ziegler, and N. Renders, *Trends and projections in Europe 2023*, (European Environment Agency) (2023), DOI: https://doi.org/10.2800/595102.

[12] A. Bhavsar, D. Hingar, S. Ostwal, I. Thakkar, S. Jadeja, and M. Shah, *The current scope and stand of carbon capture storage and utilization A comprehensive review*, Case Studies in Chemical and Environmental Engineering **8** (2023), DOI: https://doi.org/10.1016/j.cscee.2023.100368.

[13] J. C. M. Pires, F. G. Martins, M. C. M. Alvim-Ferraz, and M. Simões, *Recent developments on carbon capture and storage: An overview*, Chemical Engineering Research and Design **89**, 1446–1460 (2011), DOI: https://doi.org/10.1016/j.cherd.2011.01.028.

[14] E. Koohestanian and F. Shahraki, *Review on principles, recent progress, and future challenges for oxy-fuel combustion CO_2 capture using compression and purification unit*, Journal of Environmental Chemical Engineering **9** (2021), DOI: https://doi.org/10.1016/j.jece.2021.105777.

[15] S.-I. Nakao, K. Yogo, K. Goto, T. Kai, and H. Yamada, *Advanced CO_2 capture technologies. Absorption, Adsorption, and Membrane Separation Methods.* (Springer Nature Switzerland AG) (2019), DOI: https://doi.org/10.1007/978-3-030-18858-0.

[16] P. Feron, *Absorption-Based Post-Combustion Capture of Carbon Dioxide*, 1 edition (Joe Hayton) (2016).

[17] B. Aghel, S. Behaein, S. Wongwises, and M. S. Shadloo, *A review of recent progress in biogas upgrading: With emphasis on carbon capture*, Biomass and Bioenergy **160** (2022), DOI: https://doi.org/10.1016/j.biombioe.2022.106422.

[18] C. B. Peres, P. M. R. Resende, L. J. R. Nunes, and L. C. de Morais, *Advances in Carbon Capture and Use (CCU) Technologies: A Comprehensive Review and CO_2 Mitigation Potential Analysis*, Clean Technologies **4**, 1193–1207 (2022), DOI: https://doi.org/10.3390/cleantechnol4040073.

[19] M. Wang, A. Lawal, P. Stephenson, J. Sidders, and C. Ramshaw, *Post-combustion CO_2 capture with chemical absorption: A state-of-the-art review*, Chemical Engineering Research and Design **89**, 1609–1624 (2011), DOI: https://doi.org/10.1016/j.cherd.2010.11.005.

[20] E. Oko, M. Wang, and A. S. Joel, *Current status and future development of solvent-based carbon capture*, International Journal of Coal Science Technology **4**, 5–14 (2017), DOI: https://doi.org/10.1007/s40789-017-0159-0.

[21] *First tons of CO_2 captured from residual waste supplied to greenhouse horticulture*, URL : https://www.avr.nl/en/first-tons-of-co2-captured-from-residual-waste-supplied-to-greenhouse-horticulture/.

[22] *Technology Centre Mongstad*, URL : https://tcmda.com/.

[23] L. Cozzi, T. Gül, A. Fernández, T. Spencer, S. Bouckaert, C. McGlade, U. Remme, B. Wanner, and D. D'Ambrosio, *Net Zero Roadmap. A Global Pathway to Keep the 1.5 °C Goal in Reach*, (International Energy Agency) (2023), URL : https://www.iea.org/reports/net-zero-roadmap-a-global-pathway-to-keep-the-15-0c-goal-in-reach.

[24] E. S. Sanz-Perez, C. R. Murdock, S. A. Didas, and C. W. Jones, *Direct Capture of CO_2 from Ambient Air*, Chemical Reviews **116**, 11840–11876 (2016), DOI: https://doi.org/10.1021/acs.chemrev.6b00173.

[25] *Orca: the first large-scale plant*, URL : https://climeworks.com/plant-orca.

[26] N. Berghout and S. McCulloch, *Putting CO_2 to Use, Creating value from emissions*, (International Energy Agency) (2019).

[27] A. van Berkel, C. Gee, M. Kaushik, and O. Gamez, *CO_2 Utilization: The Evolution of the Carbon Economy* (Lux Research, Incl.), URL : https://luxresearchinc.com/resources/consumer-products/co2-capture-and-utilization-the-emergence-of-a-carbon-economy/.

[28] M. Yusuf and H. Ibrahim, *A comprehensive review on recent trends in carbon capture, utilization, and storage techniques*, Journal of Environmental Chemical Engineering **11** (2023), DOI: https://doi.org/10.1016/j.jece.2023.111393.

[29] H. B. Goyal, S. Diptendu, and R. C. Saxena, *Bio-fuels from thermochemical conversion of renewable resources: A review*, Renewable and Sustainable Energy Reviews **12**, 504–517 (2008), DOI: https://doi.org/10.1016/j.rser.2006.07.014.

[30] J. Wu, Y. Huang, W. Ye, and Y. Li, *CO_2 Reduction: From the Electrochemical to Photochemical Approach*, Advanced Science **4**, 1700194 (2017), DOI: https://doi.org/10.1002/advs.201700194.

[31] R. A. Tufa, D. Chanda, M. Ma, D. Aili, T. B. Demissie, J. Vaes, Q. Li, S. Liu, and D. Pant, *Towards highly efficient electrochemical CO_2 reduction: Cell designs, membranes and electrocatalysts*, Applied Energy **277** (2020), DOI: https://doi.org/10.1016/j.apenergy.2020.115557.

[32] D. M. Weekes, D. A. Salvatore, A. Reyes, A. Huang, and C. P. Berlinguette, *Electrolytic CO_2 Reduction in a Flow Cell*, Accounts of Chemical Research **51**, 910–918 (2018), DOI: https://doi.org/10.1021/acs.accounts.8b00010.

[33] O. Gutiérrez-Sánchez, Y. Y. Birdja, M. Bulut, J. Vaes, T. Breugelmans, and D. Pant, *Recent advances in industrial CO_2 electroreduction*, Current Opinion in Green and Sustainable Chemistry **16**, 47–56 (2019), DOI: https://doi.org/10.1016/j.cogsc.2019.01.005.

[34] E. V. Kondratenko, G. Mul, J. Baltrusaitis, G. O. Larrazábal, and J. Pérez-Ramírez, *Status and perspectives of CO_2 conversion into fuels and chemicals by catalytic, photocatalytic and electrocatalytic processes*, Energy Environmental Science **6** (2013), DOI: https://doi.org/10.1039/c3ee41272e.

[35] G. Marcandalli, M. C. O. Monteiro, A. Goyal, and M. T. M. Koper, *Electrolyte Effects on CO_2 Electrochemical Reduction to CO*, Accounts of Chemical Research **55**, 1900–1911 (2022), DOI: https://doi.org/10.1021/acs.accounts.2c00080.

[36] S. Nitopi, E. Bertheussen, S. B. Scott, X. Liu, A. K. Engstfeld, S. Horch, B. Seger, I. E. L. Stephens, K. Chan, C. Hahn, J. K. Norskov, T. F. Jaramillo, and I. Chorkendorff, *Progress and Perspectives of Electrochemical CO_2 Reduction on Copper in Aqueous Electrolyte*, Chemical Reviews **119**, 7610–7672 (2019), DOI: https://doi.org/10.1021/acs.chemrev.8b00705.

[37] A. Bagger, W. Ju, A. S. Varela, P. Strasser, and J. Rossmeisl, *Electrochemical CO_2 Reduction: A Classification Problem*, ChemPhysChem **18**, 3266–3273 (2017), DOI: https://doi.org/10.1002/cphc.201700736.

[38] Y. Y. Birdja, E. Pérez-Gallent, M. C. Figueiredo, A. J. Göttle, F. Calle-Vallejo, and M. T. M. Koper, *Advances and challenges in understanding the electrocatalytic conversion of carbon dioxide to fuels*, Nature Energy **4**, 732–745 (2019), DOI: https://doi.org/10.1038/s41560-019-0450-y.

[39] R. Kortlever, J. Shen, K. J. Schouten, F. Calle-Vallejo, and M. T. Koper, *Catalysts and Reaction Pathways for the Electrochemical Reduction of Carbon Dioxide*, Journal of Physical Chemistry Letters **6**, 4073–4082 (2015), DOI: https://doi.org/10.1021/acs.jpclett.5b01559.

[40] K. P. Kuhl, E. R. Cave, D. N. Abram, and T. F. Jaramillo, *New insights into the electrochemical reduction of carbon dioxide on metallic copper surfaces*, Energy Environmental Science **5**, 7050–7059 (2012), DOI: https://doi.org/10.1039/c2ee21234j.

[41] S. Liang, N. Altaf, L. Huang, Y. Gao, and Q. Wang, *Electrolytic cell design for electrochemical CO_2 reduction*, Journal of CO_2 Utilization **35**, 90–105 (2020), DOI: https://doi.org/10.1016/j.jcou.2019.09.007.

[42] W. Zhang, Y. Hu, L. Ma, G. Zhu, Y. Wang, X. Xue, R. Chen, S. Yang, and Z. Jin, *Progress and Perspective of Electrocatalytic CO_2 Reduction for Renewable Carbonaceous Fuels and Chemicals*, Advanced Science **5**, 1700275 (2018), DOI: https://doi.org/10.1002/advs.201700275.

[43] M. M. de Salles Pupo and R. Kortlever, *Electrolyte Effects on the Electrochemical Reduction of CO_2*, ChemPhysChem **20**, 2926–2935 (2019), DOI: https://doi.org/10.1002/cphc.201900680.

[44] M. König, J. Vaes, E. Klemm, and D. Pant, *Solvents and Supporting Electrolytes in the Electrocatalytic Reduction of CO_2*, iScience **19**, 135–160 (2019), DOI: https://doi.org/10.1016/j.isci.2019.07.014.

[45] A. Murata and Y. Hori, *Product Selectivity Affected by Cationic Species in Electrochemical Reduction of CO_2 and CO at a Cu Electrode*, The Chemical Society of Japan **64**, 123–127 (1991), DOI: https://doi.org/10.1246/bcsj.64.123.

[46] A. J. Welch, E. Dunn, J. S. DuChene, and H. A. Atwater, *Bicarbonate or Carbonate Processes for Coupling Carbon Dioxide Capture and Electrochemical Conversion*, ACS Energy Letters **5**, 940–945 (2020), DOI: https://doi.org/10.1021/acsenergylett.0c00234.

[47] Q. Xia, K. Zhang, T. Zheng, L. An, C. Xia, and X. Zhang, *Integration of CO_2 Capture and Electrochemical Conversion*, ACS Energy Letters **8**, 2840–2857 (2023), DOI: https://doi.org/10.1021/acsenergylett.3c00738.

[48] Y. Kim, E. W. Lees, C. Donde, C. E. B. Waizenegger, G. L. Simpson, A. Valji, and C. P. Berlinguette, *Electrochemical capture and conversion of CO_2 into syngas*, ChemRxiv (2023), DOI: https://doi.org/10.26434/chemrxiv-2023-hvjxn.

[49] I. Sullivan, A. Goryachev, I. A. Digdaya, X. Li, H. A. Atwater, D. A. Vermaas, and C. Xiang, *Coupling electrochemical CO_2 conversion with CO_2 capture*, Nature Catalysis **4**, 952–958 (2021), DOI: https://doi.org/10.1038/s41929-021-00699-7.

[50] E. Pérez-Gallent, C. Vankani, C. Sánchez-Martínez, A. Anastasopol, and E. Goetheer, *Integrating CO_2 Capture with Electrochemical Conversion Using Amine-Based Capture Solvents as Electrolytes*, Industrial Engineering Chemistry Research **60**, 4269–4278 (2021), DOI: https://doi.org/10.1021/acs.iecr.0c05848.

[51] A. S. Kumar, M. Pupo, K. V. Petrov, M. Ramdin, J. R. van Ommen, W. de Jong, and R. Kortlever, *A Quantitative Analysis of Electrochemical CO_2 Reduction on Copper in Organic Amide and Nitrile-Based Electrolytes*, The Journal of Physical Chemistry C **127**, 12857–12866 (2023), DOI: https://doi.org/10.1021/acs.jpcc.3c01955.

[52] G. Hu, N. J. Nicholas, K. H. Smith, K. A. Mumford, S. E. Kentish, and G. W. Stevens, *Carbon dioxide absorption into promoted potassium carbonate solutions: A review*, International Journal of Greenhouse Gas Control **53**, 28–40 (2016), DOI: https://doi.org/10.1016/j.ijggc.2016.07.020.

[53] T. N. G. Borhani, A. Azarpour, V. Akbari, S. R. W. Alwi, and Z. A. Manan, *CO_2 capture with potassium carbonate solutions: A state-of-the-art review*, International Journal of Greenhouse Gas Control **41**, 142–162 (2015), DOI: https://doi.org/10.1016/j.ijggc.2015.06.026.

[54] Y. Hori and S. Suzuki, *Electrolytic Reduction of Bicarbonate Ion at a Mercury Electrode*, Journal of The Electrochemical Society **130**, 2387–2390 (1983), DOI: https://doi.org/10.1149/1.2119593.

[55] A. V. Rudnev, U. E. Zhumaev, A. Kuzume, S. Vesztergom, J. Furrer, P. Broekmann, and T. Wandlowski, *The promoting effect of water on the electroreduction of CO_2 in acetonitrile*, Electrochimica Acta **189**, 38–44 (2016), DOI: https://doi.org/10.1016/j.electacta.2015.12.088.

[56] J. Shi, F. Shen, F. Shi, N. Song, Y. Jia, Y. Hu, Q. Li, J. Liu, T. Chen, and Y. Dai, *Electrochemical reduction of CO_2 into CO in tetrabutylammonium perchlorate/propylene carbonate: Water effects and mechanism*, Electrochimica Acta **240**, 114–121 (2017), DOI: https://doi.org/10.1016/j.electacta.2017.04.065.

[57] T. C. Berto, L. Zhang, R. J. Hamers, and J. F. Berry, *Electrolyte Dependence of CO_2 Electroreduction: Tetraalkylammonium Ions Are Not Electrocatalysts*, ACS Catalysis **5**, 703–707 (2014), DOI: https://doi.org/10.1021/cs501641z.

[58] M. König, S. H. Lin, J. Vaes, D. Pant, and E. Klemm, *Integration of aprotic CO_2 reduction to oxalate at a Pb catalyst into a GDE flow cell configuration*, Faraday Discuss **230**, 360–374 (2021), DOI: https://doi.org/10.1039/d0fd00141d.

[59] V. Boor, J. Frijns, E. Perez-Gallent, E. Giling, A. T. Laitinen, E. L. V. Goetheer, L. J. P. van den Broeke, R. Kortlever, W. de Jong, O. A. Moultos, T. J. H. Vlugt, and M. Ramdin, *Electrochemical Reduction of CO_2 to Oxalic Acid: Experiments, Process Modeling, and Economics*, Industrial Engineering Chemistry Research **61**, 14837–14846 (2022), DOI: https://doi.org/10.1021/acs.iecr.2c02647.

[60] E. A. dos Reis, G. da Silva, E. I. Santiago, and C. R. Ribeiro, *Revisiting Electrocatalytic CO_2 Reduction in Nonaqueous Media: Promoting CO_2 Recycling in Organic Molecules by Controlling H_2 Evolution*, Energy Technology **11** (2023), DOI: https://doi.org/10.1002/ente.202201367.

[61] C. Deacon-Price, A. H. M. da Silva, C. S. Santana, M. T. M. Koper, and A. C. Garcia, *Solvent Effect on Electrochemical CO_2 Reduction Reaction on Nanostructured Copper Electrodes*, The Journal of Physical Chemistry C **127**, 14518–14527 (2023), DOI: https://doi.org/10.1021/acs.jpcc.3c03257.

[62] R. J. Gomes, C. Birch, M. M. Cencer, C. Li, S.-B. Son, I. D. Bloom, R. S. Assary, and C. V. Amanchukwu, *Probing Electrolyte Influence on CO_2 Reduction in Aprotic Solvents*, The Journal of Physical Chemistry C **126**, 13595–13606 (2022), DOI: https://doi.org/10.1021/acs.jpcc.2c03321.

[63] T. Li, E. W. Lees, M. Goldman, D. A. Salvatore, D. M. Weekes, and C. P. Berlinguette, *Electrolytic Conversion of Bicarbonate into CO in a Flow Cell*, Joule **3**, 1487–1497 (2019), DOI: https://doi.org/10.1016/j.joule.2019.05.021.

[64] E. W. Lees, M. Goldman, A. G. Fink, D. J. Dvorak, D. A. Salvatore, Z. Zhang, N. W. X. Loo, and C. P. Berlinguette, *Electrodes Designed for Converting Bicarbonate into CO*, ACS Energy Letters **5**, 2165–2173 (2020), DOI: https://doi.org/10.1021/acsenergylett.0c00898.

[65] Z. Zhang, E. W. Lees, F. Habibzadeh, D. A. Salvatore, S. Ren, G. L. Simpson, D. G. Wheeler, A. Liu, and C. P. Berlinguette, *Porous metal electrodes enable efficient electrolysis of carbon capture solutions*, Energy Environmental Science **15**, 705–713 (2022), DOI: https://doi.org/10.1039/d1ee02608a.

[66] Y. C. Li, G. Lee, T. Yuan, Y. Wang, D. H. Nam, Z. Wang, F. P. G. de Arquer, Y. Lum, C. T. Dinh, O. Voznyy, and E. H. Sargent, *CO_2 Electroreduction from Carbonate Electrolyte*, ACS Energy Letters **4**, 1427–1431 (2019), DOI: https://doi.org/10.1021/acsenergylett.9b00975.

[67] Y. C. Xiao, C. M. Gabardo, S. Liu, G. Lee, Y. Zhao, C. P. O'Brien, R. K. Miao, Y. Xu, J. P. Edwards, M. Fan, J. E. Huang, J. Li, P. Papangelakis, T. Alkayyali, A. S. Rasouli, J. Zhang, E. H. Sargent, and D. Sinton, *Direct carbonate electrolysis into pure syngas*, EES Catalysis **1**, 54–61 (2023), DOI: https://doi.org/10.1039/d2ey00046f.

[68] H. M. Almajed, R. Kas, P. Brimley, A. M. Crow, A. Somoza-Tornos, B.-M. Hodge, T. E. Burdyny, and W. A. Smith, *Closing the Loop: Unexamined Performance Trade-Offs of Integrating Direct Air Capture with (Bi)carbonate Electrolysis*, ACS Energy Letters **9**, 2472–2483 (2024), DOI: https://doi.org/10.1021/acsenergylett.4c00807.

[69] M. Jouny, W. Luc, and F. Jiao, *General Techno-Economic Analysis of CO_2 Electrolysis Systems*, Industrial Engineering Chemistry Research **57**, 2165–2177 (2018), DOI: https://doi.org/10.1021/acs.iecr.7b03514.

[70] M. Moreno-Gonzalez, A. Berger, T. Borsboom-Hanson, and W. Mérida, *Carbon-neutral fuels and chemicals: Economic analysis of renewable syngas pathways via CO_2 electrolysis*, Energy Conversion and Management **244** (2021), DOI: https://doi.org/10.1016/j.enconman.2021.114452.

[71] R. J. Detz, C. J. Ferchaud, A. J. Kalkman, C. S. Martínez, M. Saric, and M. V. Shinde, *Techno-Economic Assessment of Electrochemical CO_2 Conversion Technologies*, (IEA Environmental Projects Ltd.) (2023).

[72] R. Xia, S. Overa, and F. Jiao, *Emerging Electrochemical Processes to Decarbonize the Chemical Industry*, Journal of the American Chemical Society Au **2**, 1054–1070 (2022), DOI: https://doi.org/10.1021/jacsau.2c00138.

[73] A. Chandrasekar, D. Flynn, and E. Syron, *Operational challenges for low and high temperature electrolyzers exploiting curtailed wind energy for hydrogen production*, International Journal of Hydrogen Energy **46**, 28900–28911 (2021), DOI: https://doi.org/10.1016/j.ijhydene.2020.12.217.

[74] O. S. Bushuyev, P. D. Luna, C. T. Dinh, L. Tao, G. Saur, J. van de Lagemaat, S. O. Kelley, and E. H. Sargent, *What Should We Make with CO_2 and How Can We Make It?*, Joule **2**, 825–832 (2018), DOI: https://doi.org/10.1016/j.joule.2017.09.003.

[75] Q. Lu and F. Jiao, *Electrochemical CO_2 reduction: Electrocatalyst, reaction mechanism, and process engineering*, Nano Energy **29**, 439–456 (2016), DOI: https://doi.org/10.1016/j.nanoen.2016.04.009.

[76] S. Garg, M. Li, A. Z. Weber, L. Ge, L. Li, V. Rudolph, G. Wang, and T. E. Rufford, *Advances and challenges in electrochemical CO_2 reduction processes: an engineering and design perspective looking beyond new catalyst materials*, Journal of Materials Chemistry A **8**, 1511–1544 (2020), DOI: https://doi.org/10.1039/c9ta13298h.

[77] H. Jhong, S. Ma, and P. J. A. Kenis, *Electrochemical conversion of CO_2 to useful chemicals: current status, remaining challenges, and future opportunities*, Current Opinion in Chemical Engineering **2**, 191–199 (2013), DOI: https://doi.org/10.1016/j.coche.2013.03.005.

[78] E. Sargeant and P. Rodríguez, *Electrochemical conversion of CO_2 in non-conventional electrolytes: Recent achievements and future challenges*, Electrochemical Science Advances (2022), DOI: https://doi.org/10.1002/elsa.202100178.

[79] A. R. Woldu, Z. Huang, P. Zhao, L. Hu, and D. Astruc, *Electrochemical CO_2 reduction (CO_2RR) to multi-carbon products over copper-based catalysts*, Coordination Chemistry Reviews **454**, 214340–214369 (2022), DOI: https://doi.org/10.1016/j.ccr.2021.214340.

[80] F. M. Sapountzi, J. M. Gracia, C. J. Weststrate, H. O. A. Fredriksson, and J. W. Niemantsverdriet, *Electrocatalysts for the generation of hydrogen, oxygen and synthesis gas*, Progress in Energy and Combustion Science **58**, 1–35 (2017), DOI: https://doi.org/10.1016/j.pecs.2016.09.001.

[81] Y. Hori, K. Kikuchi, A. Murata, and S. Suzuki, *Production of Methane and Ethylene in Electrochemical Reduction of Carbon Dioxide at Copper Electrode in Aqueous Hydrocarbonate Solution*, Chemistry Letters **15**, 897–898 (1986), DOI: https://doi.org/https://doi.org/10.1246/cl.1986.897.

[82] D. W. DeWulf, T. Jin, and A. J. Bard, *Electrochemical and Surface Studies of Carbon Dioxide Reduction to Methane and Ethylene at Copper Electrodes in Aqueous Solutions*, Journal of The Electrochemical Society **136**, 1686–1691 (1989), DOI: https://doi.org/https://doi.org/10.1149/1.2096993.

[83] M. Azuma, K. Hashimoto, M. Hiramoto, M. Watanabe, and T. Sakata, *Electrochemical Reduction of Carbon Dioxide on Various Metal electrodes in low-temperature aqueous $KHCO_3$ media*, Journal of The Electrochemical Society **137**, 1772–1778 (1990), DOI: https://doi.org/https://doi.org/10.1149/1.2086796.

[84] E. J. Dufek, T. E. Lister, and M. E. McIlwain, *Bench-scale electrochemical system for generation of CO and syn-gas*, Journal of Applied Electrochemistry **41**, 623–631 (2011), DOI: https://doi.org/10.1007/s10800-011-0271-6.

[85] S. T. Ahn, I. Abu-Baker, and G. T. R. Palmore, *Electroreduction of CO_2 on polycrystalline copper: Effect of temperature on product selectivity*, Catalysis Today **288**, 24–29 (2017), DOI: https://doi.org/10.1016/j.cattod.2016.09.028.

[86] R. E. Vos and M. T. M. Koper, *The Effect of Temperature on the Cation-Promoted Electrochemical CO_2 Reduction on Gold*, ChemElectroChem **9** (2022), DOI: https://doi.org/10.1002/celc.202200239.

[87] F. Scheepers, M. Stähler, A. Stähler, E. Rauls, M. Müller, M. Carmo, and W. Lehnert, *Temperature optimization for improving polymer electrolyte membrane-water electrolysis system efficiency*, Applied Energy **283** (2021), DOI: https://doi.org/10.1016/j.apenergy.2020.116270.

[88] S. Kaneco, K. Iiba, S. Suzuki, K. Ohta, and T. Mizuno, *Electrochemical reduction of carbon dioxide to hydrocarbons with high faradaic efficiency in LiOH-methanol*, The Journal of Physical Chemistry B **103**, 7456–7460 (1999), DOI: https://doi.org/10.1021/jp990021j.

[89] S. Ohya, S. Kaneco, H. Katsumata, T. Suzuki, and K. Ohta, *Electrochemical reduction of CO_2 in methanol with aid of CuO and Cu_2O*, Catalysis Today **148**, 329–334 (2009), DOI: https://doi.org/10.1016/j.cattod.2009.07.077.

[90] A. Naitoh, K. Ohta, T. Mizuno, H. Yoshida, M. Sakai, and H. Noda, *Electrochemical reduction of carbon dioxide in methanol at low temperature*, Electrochimica Acta **38**, 2177–2179 (1993), DOI: https://doi.org/10.1016/0013-4686(93)80095-H.

[91] S. Kaneco, K. Iiba, H. Katsumata, T. Suzuki, and K. Ohta, *Effect of sodium cation on the electrochemical reduction of CO_2 at a copper electrode in methanol*, Journal of Solid State Electrochemistry **11**, 490–495 (2006), DOI: https://doi.org/10.1007/s10008-006-0185-0.

[92] Y. Oh, H. Vrubel, S. Guidoux, and X. Hu, *Electrochemical reduction of CO_2 in organic solvents catalyzed by MoO_2*, Chemical Communications **50**, 3878–3881 (2014), DOI: https://doi.org/10.1039/c3cc49262a.

[93] M. Murugananthan, M. Kumaravel, H. Katsumata, T. Suzuki, and S. Kaneco, *Electrochemical reduction of CO_2 using Cu electrode in methanol/$LiClO4$ electrolyte*, International Journal of Hydrogen Energy **40**, 6740–6744 (2015), DOI: https://doi.org/10.1016/j.ijhydene.2015.04.006.

[94] M. J. Cheah, I. G. Kevrekidis, and J. Benziger, *Effect of Interfacial Water Transport Resistance on Coupled Proton and Water Transport Across Nafion*, The Journal of Physical Chemistry B **115**, 10239–10250 (2011), DOI: https://doi.org/10.1021/jp204785t.

[95] Y. Hori, A. Murata, and R. Takahash, *Formation of Hydrocarbons in the Electrochemical Reduction of Carbon Dioxide at a Copper Electrode in Aqueous Solution*, Journal of the Chemical Society 2309–2326 (1989), DOI: https://doi.org/10.1039/F19898502309.

[96] S. Asperti, R. Hendrikx, Y. Gonzalez-Garcia, and R. Kortlever, *Benchmarking the Electrochemical CO_2 Reduction on Polycrystalline Copper Foils: The Importance of Microstructure Versus Applied Potential*, ChemCatChem **14** (2022), DOI: https://doi.org/10.1002/cctc.202200540.

[97] M. S. Shaharun, H. Mukhtar, and B. K. Dutta, *Solubility of carbon monoxide and hydrogen in propylene carbonate and thermomorphic multicomponent hydroformylation solvent*, Chemical Engineering Science **63**, 3024–3035 (2008), DOI: https://doi.org/10.1016/j.ces.2008.02.035.

[98] U. J. Jáuregui-Haza, E. J. Pardillo-Fontdevila, A. M. Wilhelm, and H. Delmas, *Solubility of hydrogen and carbon monoxide in water and some organic solvents*, Latin American Applied Research **34**, 71–74 (2004).

[99] A. R. T. Morrison, M. Ramdin, L. J. P. van der Broeke, W. de Jong, T. J. H. Vlugt, and R. Kortlever, *Surface Coverage as an Important Parameter for Predicting Selectivity Trends in Electrochemical CO_2 Reduction*, Journal of Physical Chemistry C **126**, 11927–11936 (2022), DOI: https://doi.org/10.1021/acs.jpcc.2c00520.

[100] E. Perez-Gallent, G. Marcandalli, M. C. Figueiredo, F. Calle-Vallejo, and M. T. M. Koper, *Structure- and Potential-Dependent Cation Effects on CO Reduction at Copper Single-Crystal Electrodes*, Journal of the American Chemical Society **139**, 16412–16419 (2017), DOI: https://doi.org/10.1021/jacs.7b10142.

[101] S. G. Avramov, E. Lefterova, H. Penchev, V. Sinigersky, and E. Slavcheva, *Comparative study on the proton conductivity of perfluorosulfonic and polybenzimidazole based polymer electrolyte membranes*, Bulgarian Chemical Communications **48**, 43–50 (2016).

[102] S. Popovic, M. Smiljanic, P. Jovanovic, J. Vavra, R. Buonsanti, and N. Hodnik, *Stability and Degradation Mechanisms of Copper-Based Catalysts for Electrochemical CO_2 Reduction*, Angewante Chemie **59**, 14736–14746 (2020), DOI: https://doi.org/10.1002/anie.202000617.

[103] C. Li, J. Shi, J. Liu, Y. Duan, Y. Hua, S. Wu, J. Zhang, X. Zhang, B. Yang, and Y. Dai, *Electrochemical reduction of CO_2 to CO in organic electrolyte with HCl oxidized to Cl_2 on anode for phosgene synthesis*, Electrochimica Acta **389** (2021), DOI: https://doi.org/10.1016/j.electacta.2021.138728.

[104] I. Burgers, E. Pérez-Gallent, E. L. V. Goetheer, and R. Kortlever, *Electrochemical CO_2 Reduction on Copper in Propylene Carbonate: Influence of Water Content and Temperature on the Product Distribution*, Energy Technology **11** (2023), DOI: https://doi.org/10.1002/ente.202201465.

[105] A. T. Chu and Y. Surendranath, *Aprotic Solvent Exposes an Altered Mechanism for Copper-Catalyzed Ethylene Electrosynthesis*, Journal of the American Chemical Society **144**, 5359–5365 (2022), DOI: https://doi.org/10.1021/jacs.1c12595.

[106] J. Resasco, L. D. Chen, E. Clark, C. Tsai, C. Hahn, T. F. Jaramillo, K. Chan, and A. T. Bell, *Promoter Effects of Alkali Metal Cations on the Electrochemical Reduction of Carbon Dioxide*, Journal of the American Chemical Society **139**, 11277–11287 (2017), DOI: https://doi.org/10.1021/jacs.7b06765.

[107] M. R. Thorson, K. I. Siil, and P. J. A. Kenis, *Effect of Cations on the Electrochemical Conversion of CO_2 to CO*, Journal of The Electrochemical Society **160**, F69–F74 (2012), DOI: https://doi.org/10.1149/2.052301jes.

[108] M. R. Singh, Y. Kwon, Y. Lum, J. W. A. 3rd, and A. T. Bell, *Hydrolysis of Electrolyte Cations Enhances the Electrochemical Reduction of CO_2 over Ag and Cu*, Journal of the American Chemical Society **138**, 13006–13012 (2016), DOI: https://doi.org/10.1021/jacs.6b07612.

[109] A. S. Varela, W. Ju, T. Reier, and P. Strasser, *Tuning the Catalytic Activity and Selectivity of Cu for CO_2 Electroreduction in the Presence of Halides*, ACS Catalysis **6**, 2136–2144 (2016), DOI: https://doi.org/10.1021/acscatal.5b02550.

[110] M. König, J. Vaes, D. Pant, and E. Klemm, *Effect of Solvents on Aprotic CO_2 Reduction: A Study on the Role of CO_2 Mass Transport in the Product Selectivity between Oxalate and Carbon Monoxide*, The Journal of Physical Chemistry C **127**, 18159–18166 (2023), DOI: https://doi.org/10.1021/acs.jpcc.3c03992.

[111] M. C. Figueiredo, I. Ledezma-Yanez, and M. T. M. Koper, *In Situ Spectroscopic Study of CO_2 Electroreduction at Copper Electrodes in Acetonitrile*, ACS Catalysis **6**, 2382–2392 (2016), DOI: https://doi.org/10.1021/acscatal.5b02543.

[112] E. R. Corson, R. Kas, R. Kostecki, J. J. Urban, W. A. Smith, B. D. McCloskey, and R. Kortlever, *In Situ ATR-SEIRAS of Carbon Dioxide Reduction at a Plasmonic Silver Cathode*, Journal of the American Chemical Society (2020), DOI: https://doi.org/10.1021/jacs.0c01953.

[113] B. Rieger, A. Künkel, G. W. Coates, R. Reichardt, E. Dinjus, and T. A. Zevaco, *Synthetic Biodegradable Polymers* (Springer) (2012), DOI: https://doi.org/10.1007/978-3-642-27154-0.

[114] J. A. Gauthier, Z. Lin, M. Head-Gordon, and A. T. Bell, *Pathways for the Formation of C_{2+} Products under Alkaline Conditions during the Electrochemical Reduction of CO_2*, ACS Energy Letters **7**, 1679–1686 (2022), DOI: https://doi.org/10.1021/acsenergylett.2c00167.

[115] F. Calle-Vallejo and M. T. Koper, *Theoretical Considerations on the Electroreduction of CO to C_2 Species on Cu(100) Electrodes*, Angewante Chemie **125**, 7423–7426 (2013), DOI: https://doi.org/10.1002/ange.201301470.

[116] P. D. Luna, C. Hahn, D. Higgins, S. A. Jaffer, T. F. Jaramillo, and E. H. Sargent, *What would it take for renewably powered electrosynthesis to displace petrochemical processes?*, Science **364** (2019), DOI: https://doi.org/10.1126/science.aav3506.

[117] C. T. Dinh, F. P. G. de Arquer, D. Sinton, and E. H. Sargent, *High Rate, Selective, and Stable Electroreduction of CO_2 to CO in Basic and Neutral Media*, ACS Energy Letters **3**, 2835–2840 (2018), DOI: https://doi.org/10.1021/acsenergylett.8b01734.

[118] J. P. Edwards, Y. Xu, C. M. Gabardo, C. T. Dinh, J. Li, Z. Qi, A. Ozden, E. H. Sargent, and D. Sinton, *Efficient electrocatalytic conversion of carbon dioxide in a low-resistance pressurized alkaline electrolyzer*, Applied Energy **261** (2020), DOI: https://doi.org/10.1016/j.apenergy.2019.114305.

[119] B. Endrődi, E. Kecsenovity, A. Samu, F. Darvas, R. V. Jones, V. Török, A. Danyi, and C. Janáky, *Multilayer Electrolyzer Stack Converts Carbon Dioxide to Gas Products at High Pressure with High Efficiency*, ACS Energy Letters **4**, 1770–1777 (2019), DOI: https://doi.org/10.1021/acsenergylett.9b01142.

[120] M. Erans, E. S. Sanz-Pérez, D. P. Hanak, Z. Clulow, D. M. Reiner, and G. A. Mutch, *Direct air capture: process technology, techno-economic and socio-political challenges*, Energy Environmental Science **15**, 1360–1405 (2022), DOI: https://doi.org/10.1039/d1ee03523a.

[121] X. He, H. He, F. Barzagli, M. W. Amer, C. Li, and R. Zhang, *Analysis of the energy consumption in solvent regeneration processes using binary amine blends for CO_2 capture*, Energy **270** (2023), DOI: https://doi.org/10.1016/j.energy.2023.126903.

[122] J. B. Greenblatt, D. J. Miller, J. W. Ager, F. A. Houle, and I. D. Sharp, *The Technical and Energetic Challenges of Separating (Photo)Electrochemical Carbon Dioxide Reduction Products*, Joule **2**, 381–420 (2018), DOI: https://doi.org/10.1016/j.joule.2018.01.014.

[123] S. Kar, A. Goeppert, and G. K. S. Prakash, *Integrated CO_2 Capture and Conversion to Formate and Methanol: Connecting Two Threads*, Accounts of Chemical Research **52**, 2892–2903 (2019), DOI: https://doi.org/10.1021/acs.accounts.9b00324.

[124] T. Li, E. W. Lees, Z. Zhang, and C. P. Berlinguette, *Conversion of Bicarbonate to Formate in an Electrochemical Flow Reactor*, ACS Energy Letters 2624–2630 (2020), DOI: https://doi.org/10.1021/acsenergylett.0c01291.

[125] Y. Kim, *Re: Bicarbonate electrolysis queries*, (2024), email communication.

[126] G. Lee, A. S. Rasouli, B. H. Lee, J. Zhang, D. H. Won, Y. C. Xiao, J. P. Edwards, M. G. Lee, E. D. Jung, F. Arabyarmohammadi, H. Liu, I. Grigioni, J. Abed, T. Alkayyali, S. Liu, K. Xie, R. K. Miao, S. Park, R. Dorakhan, Y. Zhao, C. P. O'Brien, Z. Chen, D. Sinton, and E. H. Sargent, *CO_2 electroreduction to multicarbon products from carbonate capture liquid*, Joule **7**, 1277–1288 (2023), DOI: https://doi.org/10.1016/j.joule.2023.05.003.

[127] Y. Hori, H. Konishi, T. Futamura, A. Murata, O. Koga, H. Sakurai, and K. Oguma, *Deactivation of copper electrode in electrochemical reduction of CO_2*, Electrochimica Acta **50**, 5354–5369 (2005), DOI: https://doi.org/10.1016/j.electacta.2005.03.015.

[128] C. G. Vayenas, R. E. White, and M. E. Gambo-Aldeco, *Modern aspects of electrochemistry* (Springer Science+Business Media) (2008), DOI: https://doi.org/10.1007/978-0-387-49489-0.

[129] A. Wuttig and Y. Surendranath, *Impurity Ion Complexation Enhances Carbon Dioxide Reduction Catalysis*, ACS Catalysis **5**, 4479–4484 (2015), DOI: https://doi.org/10.1021/acscatal.5b00808.

[130] Q. Pan, P. Zhao, L. Gao, H. Liu, H. Hu, and L. Dong, *In-Depth Study on the Effects of Impurity Ions in Saline Wastewater Electrolysis*, Molecules **28** (2023), DOI: https://doi.org/10.3390/molecules28124576.

[131] H. Becker, J. Murawski, D. V. Shinde, I. E. L. Stephens, G. Hinds, and G. Smith, *Impact of impurities on water electrolysis: a review*, Sustainable Energy Fuels **7**, 1565–1603 (2023), DOI: https://doi.org/10.1039/D2SE01517J.

[132] R. Yoshimura, S. Wai, Y. Ota, K. Nishioka, and Y. Suzuki, *Effects of Artificial River Water on PEM Water Electrolysis Performance*, Catalysts **12**, 934 (2022), DOI: https://doi.org/10.3390/catal12090934.

[133] W. Lai, Y. Qiao, Y. Wang, and H. Huang, *Stability Issues in Electrochemical CO_2 Reduction: Recent Advances in Fundamental Understanding and Design Strategies*, Advanced Materials **35**, e2306288 (2023), DOI: https://doi.org/10.1002/adma.202306288.

[134] J. M. Álvarez Gómez and A. S. Varela, *Review on Long-Term Stability of Electrochemical CO_2 Reduction*, Energy Fuels **37**, 15283–15308 (2023), DOI: https://doi.org/10.1021/acs.energyfuels.3c01847.

[135] E. S. Fernandez, E. L. V. Goetheer, G. Manzolini, E. Macchi, S. Rezvani, and T. J. H. Vlugt, *Thermodynamic assessment of amine based CO_2 capture technologies in power plants based on European Benchmarking Task Force methodology*, Fuel **129**, 318–329 (2014), DOI: https://doi.org/10.1016/j.fuel.2014.03.042.

[136] G. Manzolini, E. S. Fernandez, S. Rezvani, E. Macchi, E. L. V. Goetheer, and T. J. H. Vlugt, *Economic assessment of novel amine based CO_2 capture technologies integrated in power plants based on European Benchmarking Task Force methodology*, Applied Energy **138**, 546–558 (2015), DOI: https://doi.org/10.1016/j.apenergy.2014.04.066.

[137] D. J. D. Pimlott, Y. Kim, and C. P. Berlinguette, *Reactive Carbon Capture Enables CO_2 Electrolysis with Liquid Feedstocks*, Accounts of Chemical Research **57**, 1007–1018 (2024), DOI: https://doi.org/10.1021/acs.accounts.3c00571.

[138] I. Burgers, J. Jonasson, E. Goetheer, and R. Kortlever, *The Effect of Electrolyte pH and Impurities on the Stability of Electrolytic Bicarbonate Conversion*, ChemSusChem e202401631 (2024), DOI: https://doi.org/10.1002/cssc.202401631.

[139] H. Thee, Y. A. Suryaputradinata, K. A. Mumford, K. H. Smith, G. da Silva, S. E. Kentish, and G. W. Stevens, *A kinetic and process modeling study of CO_2 capture with MEA-promoted potassium carbonate solutions*, Chemical Engineering Journal **210**, 271–279 (2012), DOI: https://doi.org/10.1016/j.cej.2012.08.092.

[140] P. Lobaccaro, M. R. Singh, E. L. Clark, Y. Kwon, A. T. Bell, and J. W. Ager, *Effects of temperature and gas-liquid mass transfer on the operation of small electrochemical cells for the quantitative evaluation of CO_2 reduction electrocatalysts*, Physical Chemistry Chemical Physics **18**, 26777–26785 (2016), DOI: https://doi.org/10.1039/c6cp05287h.

[141] IPCC, *Climate Change 2023 synthesis report*, (2023), DOI: https://doi.org/10.59327/ipcc/ar6-9789291691647.

[142] *Trends in CO_2*, URL : https://gml.noaa.gov/ccgg/trends/.

[143] K. S. Lackner, P. Grimes, and H. J. Ziock, *Carbon dioxide extraction from air: is it an option?*, (Los Alamos Nationa Laboratory) (1999).

[144] C. Gebald, J. A. Wurzbacher, P. Tingaut, T. Zimmermann, and A. Steinfeld, *Amine-based nanofibrillated cellulose as adsorbent for CO_2 capture from air*, Environmental Science Technology **45**, 9101–9108 (2011), DOI: https://doi.org/10.1021/es202223p.

[145] J. A. Wurzbacher, C. Gebald, and A. Steinfeld, *Separation of CO_2 from air by temperature-vacuum swing adsorption using diamine-functionalized silica gel*, Energy Environmental Science **4** (2011), DOI: https://doi.org/10.1039/c1ee01681d.

[146] *Remove to zero*, URL : www.climeworks.com.

[147] *The Air Carbon Solution*, URL : https://www.globalthermostat.com/.

[148] D. W. Keith, G. Holmes, D. S. Angelo, and K. Heidel, *A Process for Capturing CO_2 from the Atmosphere*, Joule **2**, 1573–1594 (2018), DOI: https://doi.org/10.1016/j.joule.2018.05.006.

[149] *We believe humanity can*, URL : https://carbonengineering.com/.

[150] *Support the scale-up of carbon removal*, URL : https://climeworks.com/subscriptions.

[151] F. Sabatino, A. Grimm, F. Gallucci, M. van Sint Annaland, G. J. Kramer, and M. Gazzani, *A comparative energy and costs assessment and optimization for direct air capture technologies*, Joule **5**, 2047–2076 (2021), DOI: https://doi.org/10.1016/j.joule.2021.05.023.

[152] C. J. E. Bajamundi, J. Koponen, V. Ruuskanen, J. Elfving, A. Kosonen, J. Kauppinen, and J. Ahola, *Capturing CO_2 from air: Technical performance and process control improvement*, Journal of CO_2 Utilization **30**, 232–239 (2019), DOI: https://doi.org/10.1016/j.jcou.2019.02.002.

[153] H. Azarabadi and K. S. Lackner, *A sorbent-focused techno-economic analysis of direct air capture*, Applied Energy **250**, 959–975 (2019), DOI: https://doi.org/10.1016/j.apenergy.2019.04.012.

[154] K. An, A. Farooqui, and S. T. McCoy, *The impact of climate on solvent-based direct air capture systems*, Applied Energy **325** (2022), DOI: https://doi.org/10.1016/j.apenergy.2022.119895.

[155] UNEP, *Options for decoupling economic growth from water use and water pollution*, (International Resource Panel Working Group on Sustainable Water Management) (2015), URL : https://www.resourcepanel.org/reports/options-decoupling-economic-growth-water-use-and-water-pollution.

[156] Q. Shu, L. Legrand, P. Kuntke, M. Tedesco, and H. V. M. Hamelers, *Electrochemical Regeneration of Spent Alkaline Absorbent from Direct Air Capture*, Environmental Science Technology **54**, 8990–8998 (2020), DOI: https://doi.org/10.1021/acs.est.0c01977.

[157] F. Sabatino, M. Mehta, A. Grimm, M. Gazzani, F. Gallucci, G. J. Kramer, and M. van Sint Annaland, *Evaluation of a Direct Air Capture Process Combining Wet Scrubbing and Bipolar Membrane Electrodialysis*, Industrial Engineering Chemistry Research **59**, 7007–7020 (2020), DOI: https://doi.org/10.1021/acs.iecr.9b05641.

[158] M. D. Eisaman, L. Alvarado, D. Larner, P. Wang, B. Garg, and K. A. Littau, *CO_2 separation using bipolar membrane electrodialysis*, Energy Environmental Science **4**, 1319–1328 (2011), DOI: https://doi.org/10.1039/c0ee00303d.

[159] O. Gutiérrez-Sánchez, B. de Mot, N. Daems, M. Bulut, J. Vaes, D. Pant, and T. Breugelmans, *Electrochemical Conversion of CO_2 from Direct Air Capture Solutions*, Energy Fuels **36**, 13115–13123 (2022), DOI: https://doi.org/10.1021/acs.energyfuels.2c02623.

[160] E. García-Bordejé and R. González-Olmos, *Advances in process intensification of direct air CO_2 capture with chemical conversion*, Progress in Energy and Combustion Science **100** (2024), DOI: https://doi.org/10.1016/j.pecs.2023.101132.

[161] C. M. Jens, L. Müller, K. Leonhard, and A. Bardow, *To Integrate or Not to Integrate—Techno-Economic and Life Cycle Assessment of CO_2 Capture and Conversion to Methyl Formate Using Methanol*, ACS Sustainable Chemistry Engineering (2019), DOI: https://doi.org/10.1021/acssuschemeng.9b01603.

[162] Q. Shu, M. Haug, M. Tedesco, P. Kuntke, and H. V. M. Hamelers, *Direct Air Capture Using Electrochemically Regenerated Anion Exchange Resins*, Environmental Science Technology **56**, 11559–11566 (2022), DOI: https://doi.org/10.1021/acs.est.2c01944.

[163] E. E. Ünveren, B. Özmen Monkul, Şerife Sarıoğlan, N. Karademir, and E. Alper, *Solid amine sorbents for CO_2 capture by chemical adsorption: A review*, Petroleum **3**, 37–50 (2017), DOI: https://doi.org/10.1016/j.petlm.2016.11.001.

[164] F. M. Chimani, A. A. Bhandari, A. Wallmüller, G. Schöny, S. Müller, and J. Fuchs, *Evaluation of CO_2/H_2O Co-Adsorption Models for the Anion Exchange Resin Lewatit VPOC 1065 under Direct Air Capture Conditions Using a Novel Lab Setup*, Separations **11** (2024), DOI: https://doi.org/10.3390/separations11060160.

[165] R. B. Said, J. M. Kolle, K. Essalah, B. Tangour, and A. Sayari, *A Unified Approach to CO_2-Amine Reaction Mechanisms*, ACS Omega **5**, 26125–26133 (2020), DOI: https://doi.org/10.1021/acsomega.0c03727.

[166] Y. Matsuzaki, H. Yamada, F. A. Chowdhury, T. Higashii, and M. Onoda, *Ab initio study of CO_2 capture mechanisms in aqueous monoethanolamine: reaction pathways for the direct interconversion of carbamate and bicarbonate*, J Phys Chem A **117**, 9274–81 (2013), DOI: https://doi.org/10.1021/jp406636a.

[167] Y. Lu and T. Lee, *Influence of the Feed Gas Composition on the Fischer-Tropsch Synthesis in Commercial Operations*, Journal of Natural Gas Chemistry **16**, 329–341 (2007), DOI: https://doi.org/10.1016/s1003-9953(08)60001-8.

[168] *Energizing Chemistry*, URL : https://lanxess.com/en.

[169] G. Holmes and D. W. Keith, *An air-liquid contactor for large-scale capture of CO_2 from air*, Philosophical Transactions of the Royal Society **370**, 4380–4403 (2012), DOI: https://doi.org/10.1098/rsta.2012.0137.

[170] P. Suess and L. Spiegel, *Hold-up of mellapak structured packings*, Chemical Engineering and Processing **31** (1992), DOI: https://doi.org/10.1016/0255-2701(92)85005-M.

[171] H. K. Hall, *Correlation of the base strengths of amines*, Journal of the American Chemical Society **79** (1957).

[172] Y. Kim, E. W. Lees, C. Donde, A. M. L. Jewlal, C. E. B. Waizenegger, B. M. W. de Hepcée, G. L. Simpson, A. Valji, and C. P. Berlinguette, *Integrated CO_2 capture and conversion to form syngas*, Joule **8**, 3106–3125 (2024), DOI: https://doi.org/10.1016/j.joule.2024.10.010.

[173] F. K. Ayittey, A. Saptoro, P. Kumar, and M. K. Wong, *Rate-based simulation study of boric acid promoted potassium carbontate capture system*, (IOP Conf. Series: Materials Science and Engineering) (2020), DOI: https://doi.org/10.1088/1757-899X/778/1/012082.

[174] T. N. G. Borhani, V. Akbari, M. K. A. Hamid, and Z. A. Manan, *Rate-based simulation and comparison of various promoters for CO_2 capture in industrial DEA-promoted potassium carbonate absorption unit*, Journal of Industrial and Engineering Chemistry **22**, 306–316 (2015), DOI: https://doi.org/10.1016/j.jiec.2014.07.024.

[175] K. H. Smith, C. J. Anderson, W. Tao, K. Endo, K. A. Mumford, S. E. Kentish, A. Qader, B. Hooper, and G. W. Stevens, *Pre-combustion capture of CO_2 - Results from solvent absorption pilot plant trials using 30wt% potassium carbonate and boric acid promoted potassium carbonate solvent*, International Journal of Greenhouse Gas Control **10**, 64–73 (2012), DOI: https://doi.org/10.1016/j.ijggc.2012.05.018.

[176] A. C. Pierre, *Enzymatic Carbon Dioxide Capture*, ISRN Chemical Engineering **2012**, 1–22 (2012), DOI: https://doi.org/10.5402/2012/753687.

[177] A. G. Fink, E. W. Lees, J. Gingras, E. Madore, S. Fradette, S. A. Jaffer, M. Goldman, D. J. Dvorak, and C. P. Berlinguette, *Electrolytic conversion of carbon capture solutions containing carbonic anhydrase*, Journal of Inorganic Biochemistry **231**, 111782 (2022), DOI: https://doi.org/10.1016/j.jinorgbio.2022.111782.

[178] Y. H. Ro, K. Y. Kim, S. K. Jeong, G. B. Rhim, D. H. Moon, J. Eo, H. S. Lee, G. W. Lee, B. Y. Lim, D. H. Chun, J. Park, and M. H. Youn, *Membrane-separated reactor for an integrated CO_2 capture-mineralization process using carbonic anhydrase*, Chemical Engineering Journal **477** (2023), DOI: https://doi.org/10.1016/j.cej.2023.146847.

[179] *Carbon capture and heat recovery system in one for superior efficiency with the proven and safe HPC solvent*, URL : https://www.capsoltechnologies.com/.

[180] S. Hamrin, *Method and Plant for CO_2 Capture*, (CAPSOL-EOP AS) (2019), patent.

[181] H. Lee, S. Kwon, N. Park, S. G. Cha, E. Lee, T. H. Kong, J. Cha, and Y. Kwon, *Scalable Low-Temperature CO_2 Electrolysis: Current Status and Outlook*, (American Chemical Society) (2024), DOI: https://doi.org/10.1021/jacsau.4c00583.

[182] A. P. Muroyama and L. Gubler, *Carbonate Regeneration Using a Membrane Electrochemical Cell for Efficient CO_2 Capture*, ACS Sustain Chem Eng **10**, 16113–16117 (2022), DOI: https://doi.org/10.1021/acssuschemeng.2c04175.

[183] A. Venkataraman, H. Song, V. D. Brandão, C. Ma, M. S. Casajus, C. A. F. Otero, C. Sievers, M. C. Hatzell, S. S. Bhargava, S. S. Arora, C. Villa, S. Dhingra, and S. Nair, *Process and techno-economic analyses of ethylene production by electrochemical reduction of aqueous alkaline carbonates*, Nature Chemical Engineering **1**, 710–723 (2024), DOI: https://doi.org/10.1038/s44286-024-00137-y.

[184] M. Kannangara, J. Shadbahr, M. Vasudev, J. Yang, L. Zhang, F. Bensebaa, E. Lees, G. Simpson, C. Berlinguette, J. Cai, E. Nishikawa, S. McCoy, H. MacLean, and J. Bergerson, *A standardized methodology for economic and carbon footprint assessment of CO_2 to transport fuels: Comparison of novel bicarbonate electrolysis with competing pathways*, Applied Energy **325** (2022), DOI: https://doi.org/10.1016/j.apenergy.2022.119897.

[185] P. Yue, Z. Kang, Q. Fu, J. Li, L. Zhang, X. Zhu, and Q. Liao, *Life cycle and economic analysis of chemicals production via electrolytic (bi)carbonate and gaseous CO_2 conversion*, Applied Energy **304** (2021), DOI: https://doi.org/10.1016/j.apenergy.2021.117768.

[186] T. Gao, B. Xia, K. Yang, D. Li, T. Shao, S. Chen, Q. Li, and J. Duan, *Techno-economic Analysis and Carbon Footprint Accounting for Industrial CO_2 Electrolysis Systems*, Energy Fuels **37**, 17997–18008 (2023), DOI: https://doi.org/10.1021/acs.energyfuels.3c01581.

[187] D. Salvatore and C. P. Berlinguette, *Voltage Matters When Reducing CO_2 in an Electrochemical Flow Cell*, ACS Energy Letters **5**, 215–220 (2019), DOI: https://doi.org/10.1021/acsenergylett.9b02356.

[188] G. Garcia, P. Rodriguez, V. Rosca, and M. T. Koper, *Fourier transform infrared spectroscopy study of CO electro-oxidation on Pt(111) in alkaline media*, Langmuir **25**, 13661–13666 (2009), DOI: https://doi.org/10.1021/la902251z.

[189] R. Schwenninger, *Certificate of Analysis Potassium Bicarbonate*, (2024).

[190] R. Schwenninger, *Certificate of Analysis Potassium Carbonate*, (2024).

[191] J. J. Middelburg, *Marine Carbon Biogeochemistry* (Springer Nature) (2019), DOI: https://doi.org/10.1007/978-3-030-10822-9.

[192] W. R. Alesi and J. R. Kitchin, *Evaluation of a Primary Amine-Functionalized Ion-Exchange Resin for CO_2 Capture*, Industrial Engineering Chemistry Research **51**, 6907–6915 (2012), DOI: https://doi.org/10.1021/ie300452c.

[193] E. Taibi, H. Blanco, R. Miranda, and M. Carmon, *Green Hydrogen Cost Reduction Scaling Up Electrolysers to meet the 1.5°C Climate Goal* (International Renewable Energy Agency) (2020), URL : www.irena.org/publications.

[194] E. Rezaei and S. Dzuryk, *Techno-economic comparison of reverse water gas shift reaction to steam and dry methane reforming reactions for syngas production*, Chemical Engineering Research and Design **144**, 354–369 (2019), DOI: https://doi.org/10.1016/j.cherd.2019.02.005.

Acknowledgements

Although a PhD may often feel like a solitary journey, it is a journey that is never undertaken alone. I have had the privilege to work with so many wonderful people and I am deeply grateful for those who have inspired me, guided me, and supported me throughout this process. It is with heartfelt appreciation that I acknowledge all the people who have been part of this journey.

First of all, I would like to express my heartfelt gratitude to **Earl Goetheer** and **Ruud Kortlever**. Thank you for giving me the opportunity to start with this PhD journey and for seeing my potential before I did. Earl, your enthusiasm and passion for the work you do have been and will always be truly inspiring to me. I never even considered doing a PhD before you asked me to! I am very grateful I have had the opportunity to work together with you and to learn so much from you as a scientist and as a supervisor. Thank you for always being optimistic and providing invaluable insights whenever I felt stuck.

Ruud, thank you so much for your guidance and support. Just like Earl, you have provided me invaluable freedom and trust from the start. I feel fortunate to have carried out my PhD in your group. Thank you for your thoughtful and critical questions, it has helped me to refine my ideas and improve the quality of my work. Next to that, I am also grateful for all the fun times we have had together during the conference in Lyon, playing padel, and during the many dinners with the group!

Furthermore, I would like to express my sincere thanks to **Elena Pérez-Gallent** for supervising and mentoring me during my PhD. I don't think you realise how much your mentoring has helped me in becoming the researcher that I am today. I was sad to see you go, but happy we are still in touch! Thanks also to **Michele Tedesco** for taking over the role of Elena without hesitation. I wish we could have worked together more!

I would like to sincerely thank the members of my thesis committee, **Wiebren de Jong**, **Wim Brilman**, **Amanda Garcia**, and **David Vermaas** for taking the time to read my dissertation and for participating in the defence.

This PhD project was part of the large national consortium **RELEASE**. I would like to express my gratitude to all the partners and fellow PhD candidates. Thank you for all the scientific discussions during our many consortium meetings and for all

the fun we had during the archery and fending workshop, the pub quiz, and the many dinners!

During my PhD I had the privilege to collaborate with multiple other researchers. Thank you **Amanda Garcia** and **Connor Deacon-Price** for the fruitful collaboration. I really enjoyed our discussions and learned a lot from both of you. Furthermore, thank you to **Peter van den Broeke** for supervising the MSc thesis project of Jonas together. Thanks for sharing your knowledge and expertise with me. **Tim Nijssen**, it has been such a pleasure to work with you! What started as supervising Saartje's MSc thesis project evolved into co-authoring a publication. I think this shows how well we work together and combine our mutual interests. Next to that, I have many fond memories of our time in Calgary during the GHGT conference. Seeing the Calgary flames was definitely a highlight!

The countless hours I have spent in the lab or the office during my PhD were absolutely made more enjoyable thanks to my dear colleagues! I would like to start with thanking **Michel** for his technical support in the lab. Thank you for always listening to my many questions and support requests and for all the ICP measurements you have done for me. Everyone from the DEMO workshop, **Daniël**, **Martijn**, **Bart**, thank you for always letting me borrow your tools and helping me where possible. **Eveline** and **Caroline**, thanks for your support and assistance with all the administrative hurdles within the TU Delft.

Thank you to **Katie** and **Sohan** for being my paranymphs and supporting me from the very beginning all the way through to my PhD defence! Katie, it has been a pleasure to work with you, both as a colleague and a friend. Your willingness to help and brainstorm together has been invaluable to me. And thanks for always saying yes when I asked you to join me for *good coffee*! Sohan, thank you for all the chats over coffee, during lunch, or in the office. Thanks for always being a listening ear when I needed to vent about my struggles in the lab and for always showing interest. Initially, you were the only representative of your group in our office, but over the years you have steadily turned the tide. Thanks for making me feel part of your group as much as you were part of ours!

Daniël, you were always so positive and highly motivated in doing your research. You truly inspired me to keep on going whenever I felt discouraged. Thank you for always turning on the radio in the lab first thing in the morning, it has been very quiet since you finished your PhD! **Boaz**, thanks for all the nice chats during our numerous lunch breaks and the fun times we had in Lyon. You are a very thoughtful researcher and I admire your aspiration to continue in academia. **Henga**, I don't think I have ever seen you without a smile on your face! Your positive energy spreads to everyone around you, so thank you for sharing that with all of us. **Shilong**, I admire your work ethics and precision in the research you do. Thanks for sharing your knowledge and for the lovely dumplings you made for us for Chinese new year! **Katherine**, you are such a warm and welcoming person! I really appreciate the fresh energy that you brought with you to the group. Ever since your arrival, lab cleanings have reached an entire new level. **Asvin**, every time I came to you with a question,

I could count on a thorough and detailed answer. Your willingness to help others is really admirable, and I have greatly enjoyed to work together with you in the lab! I also want to thank you for sharing our love for soccer and for organising the soccer matches with our colleagues, they were always great fun! **Nandalal**, your creative mind is really inspiring. I really enjoyed our brainstorm sessions together, they always sparked so many new exciting ideas to explore. Thank you also for the good times playing soccer together. **Shahid**, you are such a kind person and I enjoyed our many shared lunch and coffee breaks. Thank you for your help and patience in getting my experiments up and running in the high pressure setup. **Ahmed**, thank you for sharing your invaluable fundamental electrochemistry knowledge and for enriching my understanding of Egyptian culture. **Kevin**, although you only arrived a few months ago, you have already found your place in the group. I wish you all the best in your research!

Suriya, you are such a social butterfly! I truly appreciate your efforts in connecting our colleagues and establishing the P&E PhD board together. Without your active role and determination this would not have been possible. **Jelmer**, **Gilles**, and **Wouter**, your group slowly took over our office. Thanks for making me feel part of your group and for all the nice chats over coffee and lunch. **Cheng**, I never thought I would meet you again as a colleague! Unfortunately, my journey has already come to an end whereas yours only just started. I wish you all the best in your research and am confident that you will do well!

Svenja, you are such a wonderful person! Thanks for all the good chats over lunch and coffee and the fun we had during the RELEASE meetings. **Thijmen**, I had such a good time with you, Tim, Marieke, and Luuk in Calgary at the GHGT conference. Thanks for making that trip so enjoyable and for sharing the many travel tips for the Rocky Mountains. **Josephine**, you are a force to be reckoned with! Thank you for the thoughtful conversations we had about our career paths after completing our PhD. It has been invaluable in helping me navigate my own journey.

Next, I want to express my sincere gratitude to all the students that worked together with me during their theses. **Fathaah**, **Boris**, **Elodie**, **Jón**, **Saartje**, **Jonas**, thank you for your hard work and all the scientific discussions we had. I really enjoyed having you work with me, challenge my perspectives, and listen to your thoughts!

Furthermore, during my PhD I was part of the Sustainable Process & Energy Systems group at **TNO**. I would like to thank **Susan Turk** and **Saskia Bubberman** for being so supportive in the early stages of my PhD and explaining me the ins and outs of experimental electrochemistry work in the lab at TNO. Thanks to **Paul Haesakkers** for helping me setup in the lab and to **Paul Gravesteijn** for running the VLE experiments. A special thanks to **Arjen Huizinga**, you are such a positive and helpful colleague! You have helped me countless times with your expertise and knowledge. Thanks for borrowing the different equipments and helping me setting them up. Thank you to **Bastian**, **Peter**, **Juliana**, **Marco**, **Roberta**, **Georgiana**, **Jessica**, **Simone**, **Jasper**, **Melvin**, **Mark**, **Eirini**, **Didjay** and all the other colleagues for making me feel so welcome whenever I was at TNO.

I am so grateful to have been able to be part of the PhD Council during my PhD and to have met so many inspiring and driven colleagues! I want to thank **José**, **Jette**, **Robin**, **Anna**, **Annabel**, **Vasu**, **Suriya**, **Niharika**, **Bob**, **Paulina**, **Pieter**, **Mariano**, **Gilles**, and all the other members of the **ME PhD council**. The work you do together with **Paul** and **Mascha** is so valuable and I am very proud of all the things we have achieved in recent years.

In addition, I had the opportunity to join the PhD Honours program AMBITION. I am grateful to **Claire**, **Fay**, **Roberto**, and the entire **AMBITION team** for organising the multiple summer schools and providing me with the opportunity to learn so many new things. Thank you to my dear colleagues from TU Delft, **Siva**, **Vincent**, **Yizhao**, and **Ravi** and all the other colleagues from Gothenburg, Aachen, Zürich, Milan, Nairobi, and Kumasi for your kindness and making this program truly amazing.

And of course, a heartfelt thank you to my wonderful extended **family** and **friends** for surrounding me with so much love and for all the cherished memories we have together. Thank you for your genuine interest in my work, but mostly for helping me unwind and enjoy life!

Above all, I would like to thank my parents. You have encouraged me every step of the way and I cannot be more grateful. You have always shown so much interest in my work. **Pap**, thanks for sharing all the news articles you encountered that mentioned projects on CO_2. Although most were totally unrelated to my research, I really appreciate your interest in trying to understand my work and your curiosity to learn new things. **Mam**, from as far back as I can remember, you have encouraged me to be an independent woman. Thank you so much for making me believe in myself and my abilities to achieve my dreams. Most of all, thank you for being such a caring mum and role model.

Finally, I would like to express my deepest gratitude to **Luuk**. Thank you so much for your unwavering love, support, and encouragements. I could not have completed this PhD without you. Thank you for always being there to listen to me and to help me see things more clearly again. I feel so incredibly lucky to have you by my side and I am very excited for our future together.

Iris Burgers
Amsterdam, April 2025

About the author

Iris Burgers was born in Eindhoven, the Netherlands. She started her Bachelor of Science in Mechanical Engineering at Delft University of Technology in 2013. After graduation, she continued with a Master of Science in Mechanical Engineering, pursuing the Process & Energy track. For her Master thesis, she worked at the University of Melbourne, Australia, focusing on the separation of hydrogen from natural gas using pressure swing adsorption.

After completing her Master degree, she started her PhD at Delft University of Technology in the Process & Energy department under the supervision of Prof. Dr. Ir. Earl Goetheer and Dr. Ruud Kortlever. Her PhD project focused on the integration of CO_2 capture with electrochemical conversion towards value-added chemicals. Her project was part of the reversible large-scale energy storage (RELEASE) consortium and in collaboration with TNO. During her PhD thesis she followed the PhD honours program ambassadors for sustainable transition (AMBITION).

Education

2013 - 2017	Bachelor of Science in Mechanical Engineering Delft University of Technology
2018 - 2020	Master of Science in Mechanical Engineering Delft University of Technology & University of Melbourne *Thesis:* Novel Technology for Hydrogen Separation from Natural Gas using Pressure Swing Adsorption *Supervisors:* Prof. dr. ir. E.L.V. Goetheer (Delft University of Technology) Prof. dr. ir. P.A. Webley (University of Melbourne)
2021 - 2025	PhD in Mechanical Engineering Delft University of Technology *Thesis:* Integrated CO_2 Capture and Electrochemical Conversion *Promotors:* Prof. dr. ir. E.L.V. Goetheer Dr. R. Kortlever

Conferences

2023	Poster at Netherlands Process Technology Symposium (NPS) Enschede, the Netherlands. Poster at 74^{th} Annual Meeting of the International Society of Electrochemistry (ISE). Lyon, France.
2024	Oral presentation at Netherlands Process Technology Symposium (NPS). Groningen, the Netherlands. Oral presentation at 17^{th} Greenhouse Gas Control Technologies Conference (GHGT-17). Calgary, Canada.

List of Publications

Journal Publications (within the scope of this dissertation)

1. Burgers, I., Kortlever, R., Goetheer, E. (2025). Perspective on Integrated Carbon Capture and Conversion Systems. *(in preparation)*

2. Burgers, I., Kortlever, R., Goetheer, E. (2025). Enhancing Bicarbonate Electrolysis at Increased Alkaline Conditions for Effective Integration with CO_2 Capture. *(submitted)*

3. Burgers, I., Nijssen, T., Feith, S., Kortlever, R., Goetheer, E. (2025). Direct Air Capture with Integrated Electrochemical Conversion through Combined Solid and Liquid Sorbents. *(sumbitted)*

4. Burgers, I., Jónasson, J., Goetheer, E., & Kortlever, R. (2024). The Effect of Electrolyte pH and Impurities on the Stability of Electrolytic Bicarbonate Conversion. *ChemSusChem*, DOI: 10.1002/cssc.202401631.

5. Burgers, I., Wortmann, B., Garcia, A. C., Deacon-Price, C., Pérez-Gallent, E., Goetheer, E., & Kortlever, R. (2024). The Effect of Salts on the CO_2 Reduction Product Distribution in an Aprotic Electrolyte. *ChemPhysChem*, DOI: 10.1002/cphc.202400589.

6. Burgers, I., Pérez-Gallent, E., Goetheer, E., & Kortlever, R. (2023). Electrochemical CO_2 Reduction on Copper in Propylene Carbonate: Influence of Water Content and Temperature on the Product Distribution. *Energy Technology, 11(8)*, DOI: 10.1002/ente.202201465.

Journal Publications (outside the scope of this dissertation)

7. Burgers, I., Dehdari, L., Xiao, P., Li, K. G., Goetheer, E., & Webley, P. (2022). Techno-economic analysis of PSA separation for hydrogen/natural gas mixtures at hydrogen refuelling stations. *International Journal of Hydrogen Energy, 47(85)*, DOI: 10.1016/j.ijhydene.2022.08.175.

8. Dehdari, L., Burgers, I., Xiao, P., Li, K. G., Singh, R., & Webley, P. A. (2022). Purification of hydrogen from natural gas/hydrogen pipeline mixtures. *Separation and Purification Technology, 282*, DOI: 10.1016/j.seppur.2021.120094.

Conference Proceedings

9. Burgers, I., Kortlever, R., & Goetheer, E. (2024). Integrated CO_2 Capture and Electrochemical Conversion to Value Added Chemicals: An Evaluation. *Available at SSRN 5024205*, DOI: 10.2139/ssrn.5024205.